

**Rapid astrocyte morphology changes  
during epileptogenesis in the rodent hippocampus**

**Dissertation**

zur

Erlangung des Doktorgrades (Dr. rer. nat.)

der

Mathematisch-Naturwissenschaftlichen Fakultät

der

Rheinischen Friedrich-Wilhelms-Universität Bonn

vorgelegt von

**Stefanie Anders**

aus

Rochlitz

Bonn, Oktober 2016

Angefertigt mit Genehmigung der Mathematisch-Naturwissenschaftlichen Fakultät der  
Rheinischen Friedrich-Wilhelms-Universität Bonn

**1. Gutachter:**           **Professor Dr. Christian Henneberger**  
Institut für Zelluläre Neurowissenschaften  
Universität Bonn

**2. Gutachter:**           **Professor Dr. Gerhard von der Emde**  
Institut für Zoologie  
Universität Bonn

Tag der Promotion: 29.03.2017

Erscheinungsjahr: 2017

---

## Table of contents

1.	Introduction .....	1
1.1	The hippocampus .....	1
1.1.1	Anatomy of the hippocampus.....	2
1.1.2	Physiological role of hippocampus.....	4
1.2	Development of epilepsy .....	6
1.2.1	Mesial temporal lobe epilepsy in humans .....	6
1.2.2	Animal models of epilepsy .....	9
1.3	Astrocytes.....	11
1.3.1	Physiological role of astrocytes in brain function .....	12
1.3.2	Role of astrocytes in the pathophysiological condition of epilepsy .....	16
1.3.3	Astrocyte morphology in the healthy and epileptic brain .....	18
2.	Aim of the study.....	21
3.	Animal models and materials .....	23
3.1	Animal models.....	23
3.1.1	Wistar rats .....	23
3.1.2	Transgenic mouse line containing EGFP expressing astrocytes.....	23
3.1.3	Transgenic mouse line containing EGFP expressing astrocytes and YFP expressing CA1 pyramidal cells .....	23
3.1.4	FVB mice .....	24
3.2	Materials.....	24
3.2.1	Chemicals .....	24
3.2.2	Recipes .....	27
4.	Methods.....	28
4.1	Electrophysiology .....	28
4.1.1	Preparing of acute hippocampal slices .....	28
4.1.2	Stereotaxic injection of the glutamate sensor iGluSnFR.....	28

---

4.1.3	Electrophysiological setup.....	30
4.1.4	Recording of evoked and spontaneous field potentials .....	31
4.1.5	Analysis of evoked and spontaneous synaptic responses .....	33
4.1.6	Whole-cell patch clamp recordings of astrocytes.....	35
4.1.7	Analysis of passive membrane properties .....	37
4.1.8	Analysis of resting and transient K <sup>+</sup> concentrations .....	37
4.2	Imaging .....	39
4.2.1	Two-photon excitation fluorescence microscopy setup.....	39
4.2.2	Monitoring astrocyte morphology .....	40
4.2.3	Analysis of astrocyte volume fraction .....	41
4.2.4	Characterization of astrocyte morphology changes .....	42
4.2.6	Visualisation of astrocyte dye coupling.....	44
4.2.7	Analysis of astrocyte dye coupling .....	45
4.2.8	Fluorescence recovery after photobleaching .....	45
4.2.9	Imaging of neuronal morphology.....	47
4.2.10	Linear unmixing .....	47
4.2.11	Calculation of the slice volume .....	48
4.2.12	Imaging of extracellular glutamate levels using the glutamate sensor iGluSnFR .....	50
4.3	Statistics .....	51
5.	Results .....	52
5.1	Induction of epileptiform activity leads to astrocyte morphology changes	52
5.1.1	Induction of epileptiform activity in acute rat hippocampal slices .....	52
5.1.2	Astrocyte morphology changes during epileptiform activity in acute rat hippocampal slices .....	54
5.1.3	Induction of epileptiform activity in mouse hippocampal slices .....	58
5.1.4	Astrocyte morphology changes during epileptiform activity in acute mouse hippocampal slices .....	63
5.2	Characterisation of astrocyte morphology changes induced by epileptiform activity .....	65

---

5.2.1	Persistence of epileptiform activity and astrocyte morphology changes .....	65
5.2.2	Characterisation of astrocyte morphology changes .....	68
5.2.3	Neuronal morphology changes during induction of epileptiform activity ....	72
5.3	Functional consequences of altered astrocyte morphology .....	74
5.3.1	Intracellular diffusion in astrocytes during epileptiform activity .....	74
5.3.2	Astrocyte dye coupling in different rat hippocampal regions .....	76
5.3.3	Effect of epileptiform activity on astrocyte dye coupling.....	79
5.4	Mechanism of astrocyte morphology changes.....	81
5.4.1	Effects of Rho Kinase inhibitor Y27632 on astrocyte morphology and epileptiform activity .....	81
5.4.2	Involved signalling cascade of astrocyte morphology changes .....	88
5.4.3	Proconvulsive effects of astrocyte morphology changes .....	90
5.5	Mechanism linking astrocyte morphology changes to epileptiform activity	92
5.5.1	Effect on synaptic transmission .....	92
5.5.2	Excitability of hippocampal neurons.....	96
5.5.3	Effect of astrocyte morphology changes on long-term potentiation .....	98
5.5.4	Effect on K <sup>+</sup> buffering .....	99
5.5.5	Effect of astrocyte morphology changes on extracellular glutamate levels	103
6.	Discussion.....	106
6.1	Astrocyte morphology changes rapidly during the onset of epileptiform activity .....	106
6.1.1	Effects in vitro.....	106
6.1.2	Astrocyte morphology changes in an <i>in vivo</i> epilepsy model.....	111
6.1.3	Persistence of astrocyte morphology changes .....	113
6.1.4	Characterization of astrocyte morphology changes .....	115
6.2	Mechanism of astrocyte morphology changes and its effect on epileptiform activity .....	117
6.2.1	Restructuring of the actin cytoskeleton.....	117
6.2.2	Proconvulsive effect of astrocyte morphology changes.....	120

---

6.3	Physiological and pathophysiological consequences of altered astrocyte morphology .....	121
6.3.1	Effects on intracellular and intercellular diffusion.....	122
6.3.2	Synaptic transmission.....	126
6.3.3	K <sup>+</sup> buffering during induction of epileptiform activity .....	128
6.3.4	Extracellular glutamate levels after induction of astrocyte morphology changes.....	131
6.4	Conclusion .....	134
7.	Summary .....	136
8.	Perspectives .....	137
9.	References.....	139
	List of Figures.....	162
	List of Tables .....	165
	Abbreviations.....	166
	Acknowledgements .....	169
	Erklärung.....	170

# 1. Introduction

The brain is the most complex organ in the human being. Already around 3000 BC humans tried to understand the basal mechanisms of this complex structure. The first recorded reference of the brain is the Edwin Smith Surgical Papyrus from the 17<sup>th</sup> century BC describing the “symptomes, diagnosis and prognosis of two patients with compound fractures in the skull” (Kandel and Schwartz, 2013). By developing an increasing number of new methods, scientific research from the 18<sup>th</sup> century until today had a significant contribution to get insights into the cellular mechanisms of the brain underlying behaviour, although understanding the brain in its whole complexity will probably require decades of further research and development of new tools. For instance, due to the intense research on synaptic transmission and plasticity, the cellular and molecular basis of neuronal communication is very well understood.

By understanding cellular mechanisms underlying brain function, also new and important insights were gained concerning neural mechanisms underlying neurological diseases, like for instance epilepsy. This disease affect a high number of the world population. Although many treatment therapies have been developed, the contribution of different cellular mechanisms to the development of this neurological disorder remains an open question. Thus, ongoing basal scientific research on molecular, cellular and behavioural levels is required to target novel strategies aiming to cure epilepsy. In the last decades the focus of neuroscientific research was shifted towards non-neuronal cells, like glia cells. One type of these glia cells are the astrocytes, which derived their name from their star-like structure. Their morphology allows them to build a close contact with neurons. It has been demonstrated that these cells play an important role in neuronal activity and may contribute to the development of neurological disorders.

This work aims to understand, how structural and functional interactions between astrocytes and neurons potentially contribute to epileptogenesis. The investigations will be conducted in the hippocampus, since this is a well-studied model of cellular mechanisms underlying physiological and pathophysiological brain processes.

## 1.1 The hippocampus

The hippocampus belongs to the limbic system and plays an important role in long-term memory consolidation and spatial navigation (Andersen et al., 2006). This brain region is located in the temporal lobe and belongs evolutionary to one of the oldest structures (Bingman et al., 2009). Due to a number of features, the hippocampus was not only studied in its unique properties, but it was also used for the investigation of general neuronal phenomenons. For instance, it has a highly organized architecture with a single cell layer and laminar inputs. Furthermore, the synapses of the principle cells were shown to be

highly plastic. These properties allowed the investigation of basic principles of neuroscience, like the neuron doctrine, but also synaptic transmission and plasticity. Another advantage of the hippocampus is that acute or cultured slices surviving for prolonged time periods *in vitro* can be used. This allows a broad variety of possible experiments using this brain structure.

### **1.1.1 Anatomy of the hippocampus**

The hippocampus is located in the medial temporal lobe of the mammalian brain and consists of a unique neuronal network. It derived its name from its sea-horse like structure. The hippocampus is a paired structure and part of the hippocampal formation together with the dentate gyrus (DG), subiculum, presubiculum, parasubiculum and entorhinal cortex (EC) (Andersen et al., 2006). Due to its form, the hippocampus is also called cornu ammonis (CA) and can be subdivided into 3 fields, CA1, CA2 and CA3 (Lorente de Nó, 1934). Together with the dentate gyrus, the hippocampus is the most studied part of the hippocampal formation. A characteristic feature of the hippocampus is the mainly unilateral information transmission. The dentate gyrus, CA3 and CA1 together build the so-called trisynaptic circuit (Figure 1), which was already described by Ramon Cajal (Cajal y Ramón, 1909). It starts with the excitatory input from layer II of the entorhinal cortex to the DG via the perforant path. The DG is a trilaminar cortical structure with a characteristic U or V shape (Amaral et al., 2007). It is connected to the CA3 region via mossy fibres (MF). From the CA3 region Schaffer collaterals (SC) build the third connection with the CA1 region. The three hippocampal regions (CA1 – CA3) are structured in 4 different layers. The most prominent visualised structure is the pyramidal cell layer containing mainly the somata of the glutamatergic pyramidal cells, which are the principle cell type of the CA. It is tightly packed in the CA1 region and more loosely in the CA2 and CA3 fields. The basal dendrites of these cells are located in the narrow layer located deep in the pyramidal cell layer, the so-called stratum oriens. The apical dendrites on the opposite are located superficial to the pyramidal layer in the stratum radiatum and the stratum lacunosum moleculare. In the latter layer, fibres from the entorhinal cortex terminate.

The Schaffer collaterals from CA3 pyramidal cells projecting to CA1 pyramidal cells run through the stratum oriens and stratum radiatum thereby forming contacts with the apical and basal dendrites of CA1 pyramidal cells. The CA2 region can be found between CA3 and CA1 region. It receives direct innervation by DG granule cells via longitudinal MF projections (Kohara et al., 2014). The dendritic length and organisation of pyramidal cells in CA3 and CA2 are very variable. Also the distribution of the dendritic trees of CA3 pyramidal cells depend on where the cell body is located (Ishizuka et al., 1995). In contrast, the CA1

pyramidal cells possess homogeneous dendritic trees with the same length and configuration independent of the position of the cell soma (Pyapali et al., 1998).

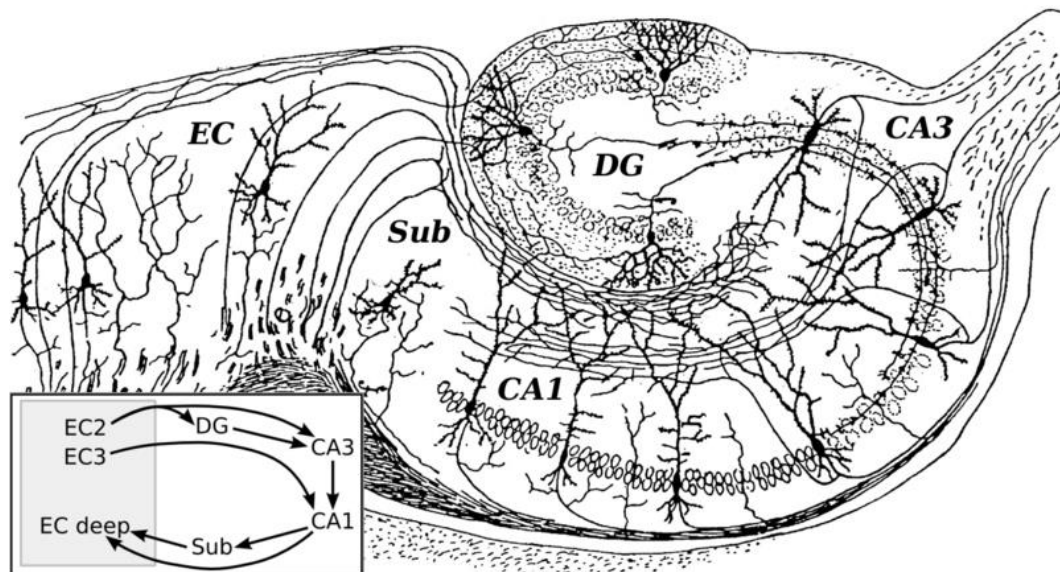


**Figure 1 Schematic of hippocampal slice and its intrinsic connections.** The image shows the single parts of the hippocampal formation. The major input of the dentate gyrus (DG) is the entorhinal cortex layer 2 and 3 (EC2, 3). The hippocampus contains the cornu ammonis (CA) divided into 3 parts (1-3). The CA3 region is innervated by axons of the granular cells of the DG. Schaffer collaterals from CA3 pyramidal cells build synapses with the dendrites of CA1 pyramidal cells. The output of CA1 goes either via the subiculum (Sub) or directly to the deep entorhinal cortex (EC deep; adopted from Cajal y Ramón, 1909).

The three hippocampal regions can not only be differentiated by the morphology of their cells, but they are also defined based on the expression of the molecular markers. CA1 pyramidal cells in adult animals express SCIP, Tyro3 and NGFIA (Tole et al., 1997), CA2 pyramidal cells can be identified by the expression of RGS14, STEP, MAP3K15 (Kohara et al., 2014) and PCP4 (Lein et al., 2005). In the CA3 region, pyramidal cells express KA1 and Py (Tole et al., 1997). In addition to glutamatergic pyramidal cells, also a high number of GABAergic interneurons of different types can be found in the hippocampus (Freund and Buzsáki, 1996). These are not that densely organised like pyramidal cells and are located also in the stratum oriens, stratum pyramidale and stratum radiatum (Maccaferri and Lacaille, 2003).

The hippocampus does not only consists of neuronal cells. Also glia cells are distributed through the whole hippocampus (Ogata and Kosaka, 2002; Savchenko et al., 1997). A very abundant type of glia cells are astrocytes. They are distributed rather evenly in the hippocampus and have their own territories, which are not penetrated by adjacent

astrocytes (Bushong et al., 2002; Ogata and Kosaka, 2002). Scientific research in the last decades have demonstrated that astrocyte-neuron interaction plays an important role in brain function. For instance, astrocytes have been shown to maintain appropriate levels of neuronal activity by clearance of neurotransmitters like  $K^+$  or glutamate (for review Anderson and Swanson, 2000; for review Kofuji and Newman, 2004). Furthermore, experimental research revealed that these cells are able to modulate synaptic activity and its plasticity by gliotransmitter supply (Fellin et al., 2006; Henneberger et al., 2010; Panatier et al., 2006; Zhang et al., 2003).

Since there is increasing evidence that astrocytes are able to regulate neuronal activity, the contribution of astrocytes to physiological and pathophysiological neuronal activity in the hippocampus will be investigated in this project. To understand the relevance of this work, the physiological and pathophysiological role of the hippocampus will be explained in the following subchapters. This is followed by a detailed overview of the astrocyte involvement in physiological and pathophysiological cellular mechanisms.

### **1.1.2 Physiological role of hippocampus**

The hippocampus plays an important role in long-term memory consolidation and spatial navigating. First evidence for the physiological role of the hippocampus was found in 1957. The patient H. M., suffering from epilepsy, was treated by a surgical bilateral removal of the hippocampus. This treatment resulted in anterograde amnesia, which identified the hippocampus as important structure for memory consolidation. His working memory was intact, but his explicit memory was impaired (Scoville and Milner, 1957). Since then, a vast number of studies have confirmed the role of the hippocampus in memory formation. It was shown that this brain structure is involved in episodic memory (O'Keefe and Nadel, 1978), which can be described as memory of personally experienced events in a spatio-temporal context (Burgess et al., 2002; Kentros, 2006; Ryan et al., 2008).

The underlying cellular mechanisms of learning and memory was first hypothesized by Cajal, who believed that information storage depends on changes in the strength of active neuronal synaptic connections (Cajal y Ramón, 1909). This hypothesis was supported by Donald Hebb, who postulated that the synaptic efficacy of two neurons is increased, if they were active simultaneously (Donald O. Hebb, 1949). These theories could be confirmed on a cellular level by discovering the mechanism of long-term potentiation (LTP) (Bliss and Lømo, 1973). They showed that trains of high frequency stimulation in distinct pathways of the hippocampus resulted in a sustained increase of the postsynaptic response. By stimulating the perforant path they were able to potentiate the response of the granule cells of the dentate gyrus. The same phenomenon could be found in the CA1 region. High frequency stimulation of the Schaffer collaterals (SC) caused a long-term potentiation of

the excitatory postsynaptic potentials (EPSPs) of CA1 pyramidal cells (Andersen et al., 1977). Using this protocol a widely used model to study synaptic plasticity in the hippocampus was established.

In the CA1 region of the hippocampus, LTP depends on the activation of ionotropic N-methyl-D-aspartate (NMDA) receptors (Collingridge et al., 1983). This receptor type is located on the pre and postsynapse and contains a glutamate and coagonist binding site. Its pore is blocked by a  $Mg^{2+}$  block (Mayer et al., 1984; Nowak et al., 1984). Activation of the postsynaptic NMDA receptor requires glutamate release from the presynapse, the binding of a coagonist and a depolarisation of the postsynapse to release the  $Mg^{2+}$  block. Thus, the NMDAR receptor acts as a coincidence detector (Bear, 1995; Seeburg et al., 1995). Glycine was found to act as a coagonist of NMDA receptors (Johnson and Ascher, 1987), but research in the last decades discovered D-serine as second potential NMDA receptor coagonist (Mothet et al., 2000). Further research revealed that D-serine is synthesized in astrocytes (Stevens et al., 2003; Wolosker et al., 1999) and its release by this cell type modulates synaptic transmission and plasticity (Henneberger et al., 2010, 2012; Panatier et al., 2006).

Opening the pore of the NMDA receptor results in calcium influx into the postsynaptic cell (Schiller et al., 1998). This calcium rise triggers calcium dependent kinases as the calcium/calmodulin-dependent protein kinase II (CaMKII; (Fukunaga et al., 1993; Ouyang et al., 1997) and the protein kinase C (PKC; (Sweatt, 1999). These kinases can increase the conductance of NMDA receptors and  $\alpha$ -amino-3-hydroxy-5-methyl-4-isoxazolepropionic acid (AMPA) receptors (Derkach et al., 1999; Lau and Zukin, 2007; Malenka and Bear, 2004), a second type of ionotropic glutamate receptors. It is widely believed that also the number of available AMPA and NMDA receptors in the postsynaptic membrane is increased, controlled by the CaMKII and PKC (Lau and Zukin, 2007; Malenka and Bear, 2004; Shi et al., 1999). The increase in conductance and number of synaptic glutamate receptors generate larger postsynaptic responses to synaptic stimulation und thus long-term potentiation. In contrast, there is also evidence that LTP is mainly mediated by presynaptic mechanisms. (Enoki et al., 2009).

Also the opposite effect can occur at hippocampal synapses, namely long-term depression (LTD) (Bear and Abraham, 1996). During LTD synapses are weakened and this process is also NMDA receptor and calcium-dependent (for review Lüscher and Malenka, 2012). Low frequency stimulation of Schaffer collaterals results in a depression of EPSPs. LTD is also suggested to play an important role during learning and memory (Mulkey and Malenka, 1992; Dong et al., 2013; Nabavi et al., 2014).

Beside its importance during memory consolidation, its additional essential role in spatial learning and navigating could be identified by behavioural tests but also experiments on a

cellular level. The Morris water maze test was established as a model for hippocampal spatial learning (Morris et al., 1982). With this behavioural paradigm the capacity of an animal to remember spatial cues to find a hidden platform was tested. Hippocampal lesions resulted in an impairment of spatial navigating during this test (Morris, 1984; Morris et al., 1982). Hippocampal pyramidal cells have been identified as so-called place cells, since they start firing, when the animal is located at a particular location in a room (O'Keefe, 1976, 1979). The idea that place cells form a map of the room was completed by experiments investigating another type of cells, called grid cells. They are located in the mesial entorhinal cortex and form a circuit with place cells, thereby generating a coordinate system underlying precise positioning and pathfinding (Fyhn et al., 2004; Hafting et al., 2005).

However, the hippocampus is not only an important brain region in the context of physiological brain function. Dysfunction of the hippocampal networks are involved in many neurodegenerative diseases like Alzheimer's disease (Allen G et al., 2007; Mu and Gage, 2011) or epilepsy (Jefferys, 1999; Schwartzkroin, 1994). The hippocampus, for instance, is considered to be the origin of temporal lobe epilepsy (TLE), which will be explained further in the following chapters.

## **1.2 Development of epilepsy**

Epilepsy is one of the most common neurological disorders affecting up to 1 % of the world's population (Sander and Shorvon, 1996). Patients suffering from epilepsy develop spontaneous seizures starting at a focal point, which can be subdivided into partial seizures and generalized seizures, occurring throughout the cortex. Seizures are generated by an abnormal firing of neurons (Andersen et al., 2006). An increased neuronal excitability can be caused by different cellular mechanisms. A long time, an imbalance between excitation and inhibition was believed to be the underlying reason for epileptic seizures. But research in the past decades revealed a more complex view on this topic (Engel, 1996). For instance, it could be demonstrated that activation of GABA<sub>A</sub> receptors results in epileptic seizures in absence epilepsy (Cope et al., 2009). Epileptogenesis is described to occur in three phases: acute brain damage as initiator, a latent period without seizures and eventual epilepsy. Until now the molecular and cellular mechanisms causing the alterations in neuronal excitability until the development of chronic epilepsy are not clear.

### **1.2.1 Mesial temporal lobe epilepsy in humans**

Mesial temporal lobe epilepsy (MTLE) occur in approximately 60% of all partial epilepsies and the electrographic origin of seizures was shown to be in the hippocampal formation (King and Spencer, 1995). The clinical development of MTLE often begins with an initial

event like febrile seizures during the childhood, trauma, hypoxia, brain infections or status epilepticus (Kharatishvili and Pitkänen, 2010; Yang et al., 2010) followed by a seizure-free latent phase of years before seizures begin to develop many years later (Wieser and ILAE Commission on Neurosurgery of Epilepsy, 2004). In many cases this form of epilepsy is accompanied by the occurrence of psychiatric disorders, increased mortality and neuropsychology deficits. 25 to 30% of patients are resistant to pharmacological treatments (Schmidt and Löscher, 2005). In this case, neurosurgery is often used as treatment.

Mesial temporal lobe seizures usually are complex partial seizures with disturbed consciousness (Englot and Blumenfeld, 2009) and thus belong to the first group of classified seizures, which is partial seizures (Andersen et al., 2006; Sharma et al., 2007). This group can be divided into simple and complex partial seizures. The second group of seizures are the generalized seizures, which are subdivided into tonic, clonic, tonic-clonic, absence seizures and status epilepticus. The third group are the unclassified seizures (Akdogan and Yonguc, 2011). MTLE seizures can last two to ten minutes. Often a seizure is preceded by a warning, the so-called “aura”, which can be perceived as pain from gastrointestinal origin but can also consist of hallucinations, disturbances of memory or illusions. The aura is followed by early stages of a seizure, like motor arrest or absence, which is subsequently followed by automatisms like chewing, undressing or walking. After a seizure, patients show confusion, headache or postictal psychosis (Andersen et al., 2006).

The seizures itself can be recorded using scalp electroencephalography (EEG) recordings. These showed that the epileptic activity of MTLE consists of ictal and interictal activity (Javidan and Javidan, 2012). Ictal and interictal discharges are different forms of epileptiform activity (Figure 2; Smith, 2005). Interictal epileptiform activity occurs between seizures and is defined by spikes lasting less than 80 ms and sharp waves lasting 80 to 120 ms (Curtis de and Avanzini, 2001). They occur bilaterally or independently in both temporal regions (Williamson et al., 1993). They are believed to be pathophysiological, since they are rarely occurring in a healthy brain and they are strongly associated with epilepsy (Gregory et al., 1993; Marsan and Zivin, 1970). The generation of an interictal spike depends on two mechanisms. The burst properties of the neurons and the synchronisation of neuronal populations (Andersen et al., 2006). Ictal epileptiform discharges are the seizure itself and usually consist of  $\theta$  activity at 5 to 10 Hz in the mid temporal region followed by several afterdischarges. Ictal discharges remain at their focal point or spread involving surrounding regions and the contralateral temporal lobe (Andersen et al., 2006).

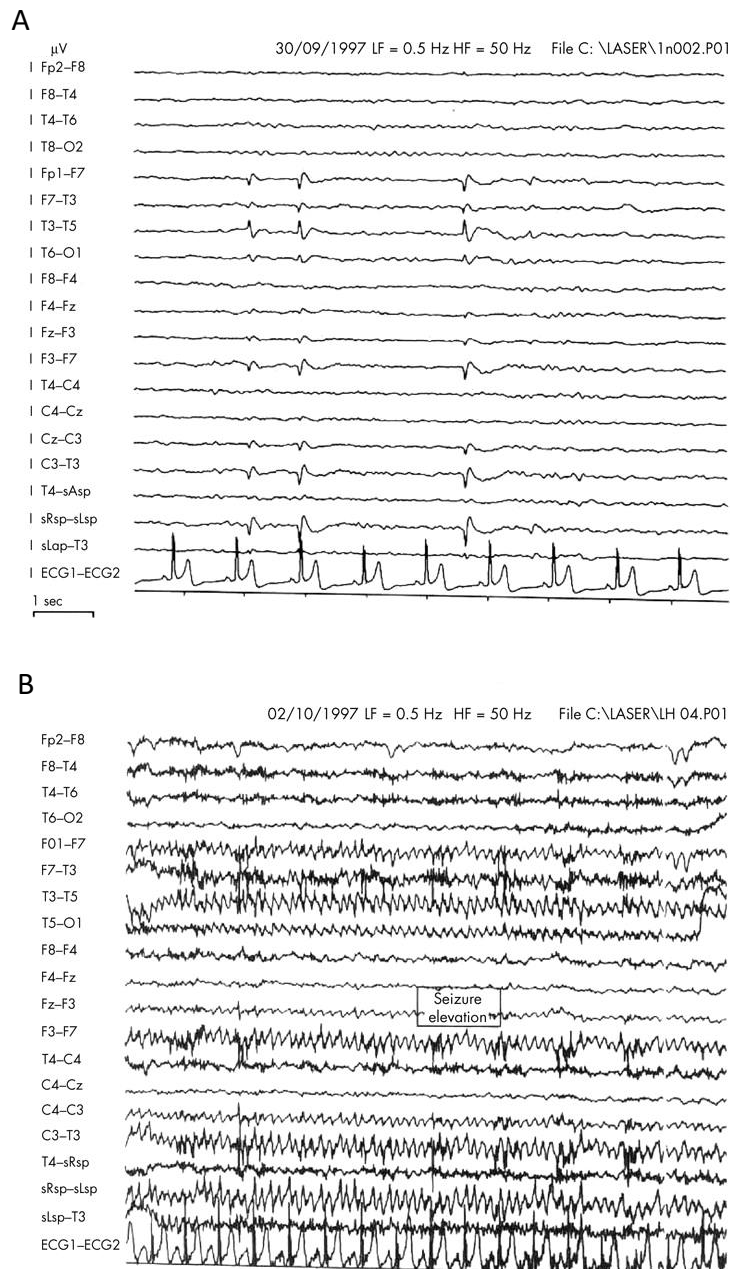


**Figure 2** Interictal and ictal activity recorded using EEG recordings from a patient suffering from left MTLE. (A) Interictal focal temporal discharges, which are defined by sharp waves and spikes. (B) Ictal rhythmic  $\theta$  discharge in left MTLE caused by hippocampal sclerosis (adopted from Smith, 2005).

Since a high number of patients is resistant to pharmacological treatment of the MTLE, hippocampal resection is used to cure epilepsy, which helps the patients to become seizure-free (Arruda et al., 1996). Despite successful surgery, patients often are dependent on antiepileptic drugs, suggesting an involvement of further structures in this disease. One characteristic of MTLE is the development of hippocampal sclerosis (HS) (Cavanagh and

Meyer, 1956; Meyer and Beck, 1955; Thom, 2014). HS is characterised by degeneration and functional loss of pyramidal neurons, granule cell dispersion in the dentate gyrus, mossy fibre sprouting and astrogliosis (Blümcke et al., 2013).

Astrogliosis is defined by alterations in astrocyte function and morphology. The long-lasting changes include changes in  $K^+$  and glutamate uptake, which possibly can contribute to the development of epileptiform activity (for review Carmignoto and Haydon, 2012; Coulter and Steinhäuser, 2015). There is also evidence that astrogliosis plays a causal role during epileptogenesis (chapter 1.3.3).

Related to this pathophysiological change, patients show verbal memory deficits. The exact reasons for development of HS are not clear yet. Retrospective studies of patients with HS reported in 30-50% of the cases an initial cerebral injury in the early life of these patients (French et al., 1993). Febrile seizures during early childhood were believed to induce hippocampal sclerosis and seizures in later years (VanLandingham et al., 1998). Animal studies were used to mimic the effect of febrile seizures using hot air or water to induce hyperthermic seizures. But prolonged hyperthermic seizures did not evoke spontaneous seizures in adult rats. They lowered the threshold for seizure development upon pharmacological treatment with a convulsant (Dube et al., 2000). Also in humans only 2% to 7% of children with febrile seizures develop seizures during their adulthood, indicating that febrile seizures alone do not cause epilepsy. Until today it is still under debate whether HS is a cause or consequence of MTLE (Jefferys, 1999; Walker, 2015). Hippocampal surgery is always performed in the late states of epilepsy. Thus, the investigation of the development of human MTLE and identifying its causes and consequences remains a complicated issue.

### **1.2.2 Animal models of epilepsy**

Investigating epilepsy in humans gave important insights into the development and progression of this disease. However, epilepsy research in human tissue is limited due to a number of disadvantages. Often, these patients have been already treated and there is a lack of control tissue. When obtaining human tissue, the patients are already in the chronic state of epilepsy and thus cause and consequence cannot be differentiated (Andersen et al., 2006). To solve this problem, animal models of mesial temporal lobe epilepsy, but also other forms of epilepsy were developed. The two most prominent *in vivo* models for MTLE are the kindling model and the post status epilepticus. For the kindling model, trains of tetanic stimuli are repeated *in vivo*, which evoke after-discharges (Goddard, 1967; McNamara, 1984). Repetition of these stimuli trains result in lengthening of the after-discharges thereby leading to more severe seizures. After kindling, spontaneous seizures can occur (McNamara, 1984). It was shown that kindling leads to a potentiation of the

NMDA receptor mediated responses. However, kindling itself does not result in hippocampal damage and sclerosis (Tuunanen and Pitkänen, 2000), but the occurring spontaneous seizures after kindling do result in neuronal loss and structural and functional changes in the hippocampus (Cavazos et al., 1994).

The second most frequently used *in vivo* model for MTLE is the induction of status epilepticus by systemic or local administration of kainate or pilocarpine (Ben-Ari and Lagowska, 1978; Turski et al., 1984). Status epilepticus can be the indicator of chronic epilepsy and often occurs due to a central nervous system infection induced by a cerebral vascular accident, alcohol or hypoxia (Andersen et al., 2006). In the mentioned animal models the induced status epilepticus leads to hippocampal damage as observed in humans (Bedner et al., 2015; Curia et al., 2008). These models are useful to study chronic aspects of epileptiform activity. To understand functional mechanisms underlying the acute phases of epileptogenesis, often pharmacological treatment in acute brain slices is used. These epilepsy models induce acute simple partial seizures (Akdogan and Yonguc, 2011). Thus, only epileptiform activity in form of neuronal hyperexcitability is investigated rather than the disease epilepsy. But to understand cellular alterations in a simplified model in acute brain slices or in culture can be helpful before studying epilepsy in a living animal or even humans. Although, experiments in culture or acute brain slices only allow the investigation of particular details of a complex mechanism, the degrees of freedom are very high in these models. These model systems can be controlled and modulated easily, which allow conclusive experiments in a short time scale.

The pharmacological treatment can either target the inhibition of  $\gamma$ -aminobutyric acid (GABA<sub>A</sub>) receptors using picrotoxin, bicuculline or penicillin, thereby leading to a shift towards neuronal excitation. But also an enhancement of excitation can be induced by using low Mg<sup>2+</sup> to activate NMDA receptors or by activation of kainate receptors using bath application of kainate. Whereas inhibition of GABA<sub>A</sub> receptors alone mostly induces interictal activity (Curtis et al., 2012), a combination of low Mg<sup>2+</sup> and bicuculline for instance results in ictal and interictal activity (Gomez-Gonzalo et al., 2011; Köhling et al., 2000). In this work, epileptiform activity will be induced by bath application of penicillin or the combination of low Mg<sup>2+</sup> and bicuculline. Penicillin G sodium salt inhibits the chloride flux through GABA<sub>A</sub> receptors (Tsuda et al., 1994) and thus has a proepileptic effect. Its proconvulsive action was discovered during the 2<sup>nd</sup> world war. Patients with injuries on the head were treated with direct application of penicillin to wounds of the cerebral cortex, when they did not respond to parenteral or intravenous application. These patients generated convulsive seizures following intraventricular injection of the drug (Walker et al., 1945). The proconvulsive action of penicillin was confirmed in monkeys and cats (Walker et al., 1945). Later on it was established as a classical *in vivo* and *in vitro* model for

epileptiform activity (Chen et al., 1986; Dichter M. and Spencer A., 1969; Schwartzkroin and Prince, 1977). The effect of penicillin on hippocampal *in vitro* preparations of guinea pigs were firstly investigated by in 1977 (Schwartzkroin and Prince, 1977). Penicillin can be applied directly to brain slices, but it can also be applied by intraperitoneal, intravenous and intracortical injections, which makes it useful for *in vivo* studies (Chen et al., 1986). Bicuculline methiodide is also a GABA<sub>A</sub> receptor antagonist and is also widely used as model for epileptiform activity (Khalilov et al., 1997; Straughan et al., 1971). Bicuculline alone was shown to induce both spontaneous interictal and ictal epileptiform activity (Cooper et al., 2009), whereas low Mg<sup>2+</sup> concentrations in hippocampal slices were described to induce prolonged periods of hyperexcitability and epileptiform activity (Gloveli et al., 1995; Mody et al., 1987). These *in vitro* models for epileptiform activity reproduce the variable form of discharges occurring in epilepsy and thus have been crucial in the past to understand the cellular mechanism underlying the development of epileptiform activity.

### **1.3 Astrocytes**

Besides neurons other classes of cells exist in the central nervous system, like brain endothelial cells forming the blood brain barrier or glia cells. This work is focussed on the glia cells. This group consists of different cell types which can be distinguished by their morphological and functional characteristics. Glia cells were firstly described in 1858 as cells, which binds neurons together. They derived their name from the Greek word for glue (Virchow, 1858). Glia cells can be divided into the subgroups of microglia and macroglia, whereas astrocytes, oligodendrocytes, NG2 cells and ependymal cells belong to the latter group. In the last decades, research revealed the relevant role of glia cells for brain function, since they were described to be involved in cellular mechanisms underlying behaviour, learning and memory, sensory perception, but also the development of neurodegenerative and psychiatric diseases (Coulter and Steinhäuser, 2015; Lee et al., 2014; Moraga-Amaro et al., 2014; Nave and Ehrenreich, 2014; Perez-Alvarez et al., 2014a; Scolding, 1999).

In this work the role of astrocytes during epileptogenesis will be investigated. Astrocytes derived their name from their star-like morphology. They are divided into two main types, protoplasmic and fibrous astrocytes (Cajal y Ramón, 1909). Protoplasmic astrocytes can be found in the grey matter, whereas fibrous astrocytes are located in the white matter. Protoplasmic astrocytes possess some stem branches with a high number of fine processes. Fibrous astrocytes have many fibre-like processes which contact nodes of Ranvier (Cajal y Ramón, 1909; Sofroniew and Vinters, 2010). Both types of astrocytes are extensively coupled via gap junctions (Sofroniew and Vinters, 2010). A typical marker for identifying

astrocytes is the glial fibrillary acid protein (GFAP). GFAP-labelled brain sections do not show the entire astrocyte morphology, but the astrocyte intermediate filament system (Figure 3A; Wilhelmsson et al., 2004). Astrocytes can be found throughout the brain. They are organized in non-overlapping domains in a manner (Bushong et al., 2002), that only the distal 10% of their processes are overlapping with the processes of their neighbour (Halassa et al., 2007). With their fine processes, protoplasmic astrocytes enwrap thousands of synapses in the hippocampus (Halassa et al., 2007; Ogata and Kosaka, 2002) allowing them to modulate neuronal signalling and contribute to brain function.

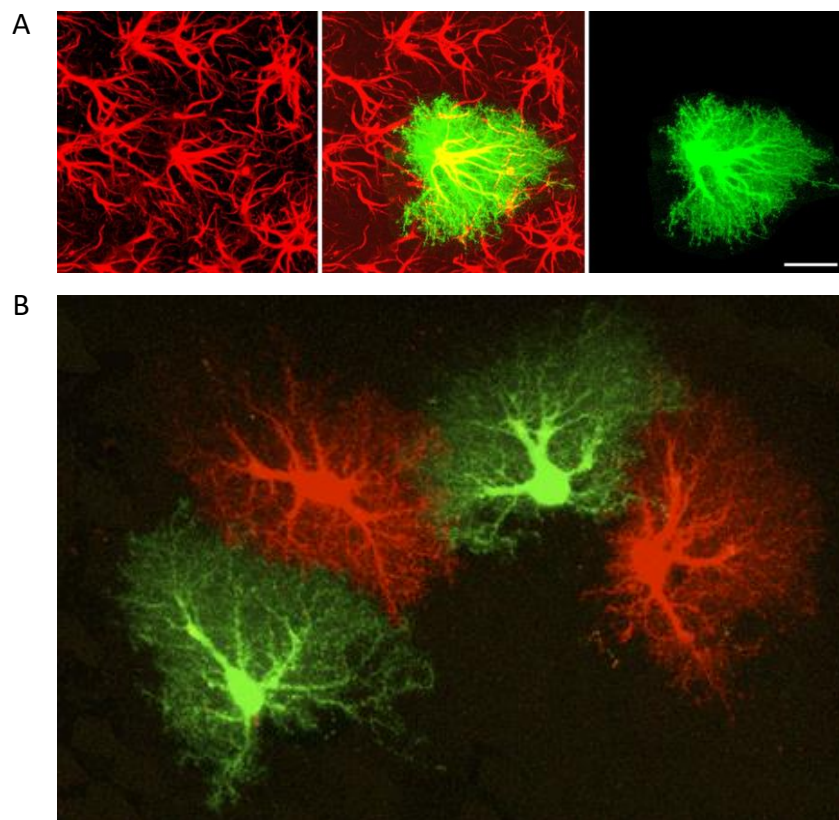


**Figure 3 Astrocyte structure in the mouse hippocampus.** Astrocytes are visualised with antibodies against GFAP, which labels the intermediate filament system (red). Dye filling of the astrocyte reveals the actual morphology, shown as three-dimensional reconstruction (green, middle and right panel, adopted from (Wilhelmsson et al., 2004)). (B) Three-dimensional reconstruction of adjacent astrocytes in the adult mouse hippocampus. Astrocytes were filled with two different dyes (Alexa 568 and Lucifer yellow). They are organised in non-overlapping domains (Pekny and Pekna, 2014).

### 1.3.1 Physiological role of astrocytes in brain function

Research in the last decades have shown that astrocytes play an important role in physiological brain function as they are able to modulate neuronal activity and synaptic transmission by various mechanisms. Astrocytes are considered as active partners of the

tripartite synapse consisting of the presynaptic terminal, the postsynapse and the astrocyte protrusion enwrapping the synapse (Araque et al., 1999). Due to this close contact to neurons, astrocytes are thought to modulate synaptic transmission and neuronal signalling via various functions. One well described function is their ability to regulate the extracellular  $K^+$  concentrations by  $K^+$  uptake and spatial buffering. Under resting conditions the extracellular  $K^+$  concentration is very low (ca. 3 mM; for review Katzman, 1976; Somjen, 1979) compared to the presumed intracellular  $K^+$  concentration of ca. 120 mM (Kettenmann and Ransom, 2013). It was shown that transient increases in the extracellular  $K^+$  concentration ( $[K^+]_{ex}$ ) results in increases in neuronal synaptic transmission and neuronal excitability (Balestrino and Somjen, 1986; Walz, 2000). Under the pathophysiological condition of epilepsy an increased  $[K^+]_{ex}$  up to 12 mM was measured (Heinemann and Dieter Lux, 1977). Thus, neuronal activity strongly depends on the regulation of the  $[K^+]_{ex}$ . Astrocytes are thought to be the key regulators of the extracellular  $K^+$  levels, as they are characterised by a very negative resting membrane potential and a high permeability for  $K^+$ . These properties are mainly controlled by inwardly rectifying Kir 4.1 channels (Seifert et al., 2009). It is postulated that astrocytes can regulate  $[K^+]_{ex}$  by two mechanisms (Steinhäuser et al., 2012), although this topic is still under debate (Larsen et al., 2014; Olsen and Sontheimer, 2008). The  $K^+$  uptake is mediated by the  $Na^+/K^+/Cl^-$  cotransporters and  $Na^+/K^+$  pumps (D'Ambrosio et al., 2002; Kofuji and Newman, 2004; Ransom et al., 2000). The spatial buffering was first suggested by Orkand (1986). In this model, the idea is that astrocytes take up  $K^+$  from sites with high extracellular  $K^+$  concentrations and redistribute it through their gap junction-coupled network and release it at sites with low extracellular  $K^+$  concentrations. This passive mechanism works due to the difference in resting membrane and  $K^+$  equilibrium potential of the astrocytes, which leads to an electrical driving force of  $K^+$  into the cell (Orkand, 1986; Walz, 2000) and is partially mediated by Kir4.1 channels (Ransom and Sontheimer, 1995). The exact mechanism of spatial  $K^+$  buffering still remain unclear. Kir4.1 mediated buffering contributes to the clearance of  $K^+$  from the extracellular space during neuronal activity, but there was evidence that glial and neuronal  $Na^+/K^+$  pumps mediate the recovery of basal  $K^+$  levels, whereas  $Na^+/K^+/Cl^-$  cotransporters appeared not to be involved in this process (Larsen et al., 2014). For an efficient buffering, the astrocyte gap junction-coupled network is essential, as an altered  $[K^+]_{ex}$  was shown using  $K^+$ -sensitive microelectrodes in hippocampal slices obtained from mice lacking connexin (Cx) 43 and 30 (Wallraff et al., 2006). The extensive gap junction coupling of astrocytes throughout the brain is one prominent hallmark of astrocytes. They build a so-called astrocyte syncytium. The coupling is mediated by gap junction channels, which are composed of two types of connexins, namely Cx 43 and Cx 30 (Nagy and Dermietzel, 2000; Nagy et al., 1999). These channels allow the exchange of metabolites for

energy supply to neurons (Giaume et al., 1997), ions and second messengers between neighbouring astrocytes, but also volume regulation (Scemes and Spray, 1998). In the hippocampus, astrocyte gap junctions are mainly composed of Cx 43 and only to small extent on Cx 30 (Gosejacob et al., 2011), while in the thalamus astrocytes predominantly express Cx 30 (Griemsmann et al., 2015). Cx 43 is highly regulated by phosphorylation via different protein kinases like protein kinase A, C and mitogen-activated protein kinases (MAPK; Solan and Lampe, 2014).

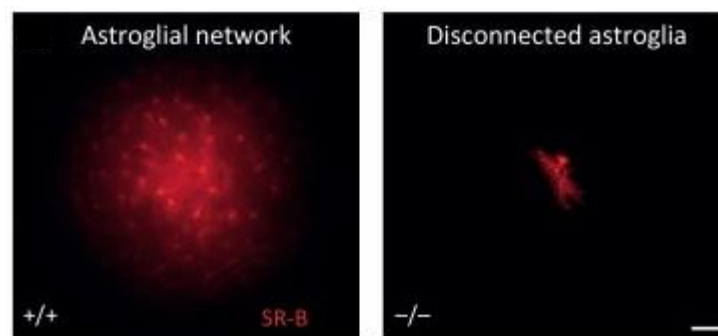


**Figure 4 Astrocytes are extensively coupled via gap junctions.** Astrocyte gap junction network in hippocampal slices is visualized by the diffusion of sulforhodamine B (SR-B), initially dialyzed in a single astrocyte from wild type (+/+) and Cx43/ Cx30 knockout mice (-/-; Pannasch and Rouach, 2013).

Astrocytes express aquaporin 4 (AQP4) channels (Satoh et al., 2007), which are highly abundant water channels in the brain. They are located at the perivascular endfeet and at the peripheral processes of astrocytes (Bedner and Steinhäuser, 2014). They allow bidirectional water flux across the membrane, thereby regulating the extracellular space volume and osmolarity. Their main function is the water flux across the blood-brain barrier. These channels are coexpressed with Kir4.1 in the hippocampus with high expression levels in the CA1 stratum lacunosum moleculare (Hsu et al., 2011; Hubbard et al., 2015). Another important function of astrocytes, by which they are able to modulate synaptic transmission and neuronal excitability, is their fast clearance of glutamate out of the extrasynaptic space via the glutamate transporters GLT1 and GLAST (Perego et al., 2000). GLT1 was described to be highly mobile (Murphy-Royal et al., 2015). The fast activity dependent diffusion of this transporter on the astrocyte membrane between the synaptic and extrasynaptic regions was suggested as possible mechanism for modulating synaptic transmission (Murphy-Royal et al., 2015). Moreover, there was evidence that astrocytes are able to shape synaptic transmission via movement of astrocyte protrusions into the synaptic cleft thereby increasing the availability of glutamate transporters within the synaptic cleft (Pannasch et al., 2014).

Astrocytes contain the enzyme glutamine synthetase (GS) converting glutamate to glutamine (Martinez-Hernandez et al., 1977), which is transported back to neurons (Chaudhry et al., 2002). After hydrolysing it to glutamate via the mitochondrial phosphate-activated glutaminase (PAG), it can be repacked into neuronal vesicles (Fremeau et al., 2004) and released into the synaptic cleft (McKenna, 2007). The astrocyte glutamate uptake occurs in a Na<sup>+</sup> dependent manner (Rose and Ransom, 1997). Together with one glutamate molecule three Na<sup>+</sup> ions and 1 H<sup>+</sup> ion are taken up by the glutamate transporters (Levy et al., 1998; Zerangue and Kavanaugh, 1996).

Besides controlling glutamatergic synaptic transmission, astrocytes were described to be involved in the uptake and recycling of gamma-aminobutyric acid (GABA). They express the GABA transporter GAT3 on their peripheral processes with close contact to neurons (Minelli et al., 1996). After uptake, GABA is metabolized to glutamine via the tricarboxylic acid (TCA) and the glutamate dehydrogenase (GDH; Schousboe et al., 2013). As described before, glutamine is transported back to neurons and converted to glutamate.

It was shown that astrocytes respond to glutamate with intracellular Ca<sup>2+</sup> elevations (Porter and McCarthy, 1996), which can propagate through the astrocyte network via gap junctions. Using sensory stimulation these intracellular Ca<sup>2+</sup> transients could be also observed *in vivo* (Navarrete et al., 2012; Petzold et al., 2008). Astrocytic Ca<sup>2+</sup> elevations in response to neuronal activation occur in most brain regions (for review Halassa and Haydon, 2010) and could be also shown in human brain tissue (Figure 5, Navarrete et al., 2013). It was demonstrated that astrocyte Ca<sup>2+</sup> transients are generated by activation of astrocyte G protein-coupled receptors (GPCRs), which trigger the inositol-1,4,5-trisphosphate (IP3) production and Ca<sup>2+</sup> release from the endoplasmic reticulum (Nash et al., 2002; Volterra et al., 2014). Since astrocytes show Ca<sup>2+</sup> responses due to synaptic stimulation, but also spontaneous fluctuations (Parri et al., 2001) and a wide range of oscillatory Ca<sup>2+</sup> signals (Pasti et al., 1997), it was believed that astrocyte Ca<sup>2+</sup> responses are mainly used for astrocyte intracellular communication modulating a number of signalling cascades. Astrocyte intracellular Ca<sup>2+</sup> signalling can result in the release of gliotransmitters like glutamate, D-Serine or ATP (Halassa et al., 2007; Henneberger et al., 2010; Malarkey and Parpura, 2008), which in turn modulates synaptic transmission. In summary, astrocytes provide a high variety of functions allowing them to modulate synaptic transmission and neuronal network activity.

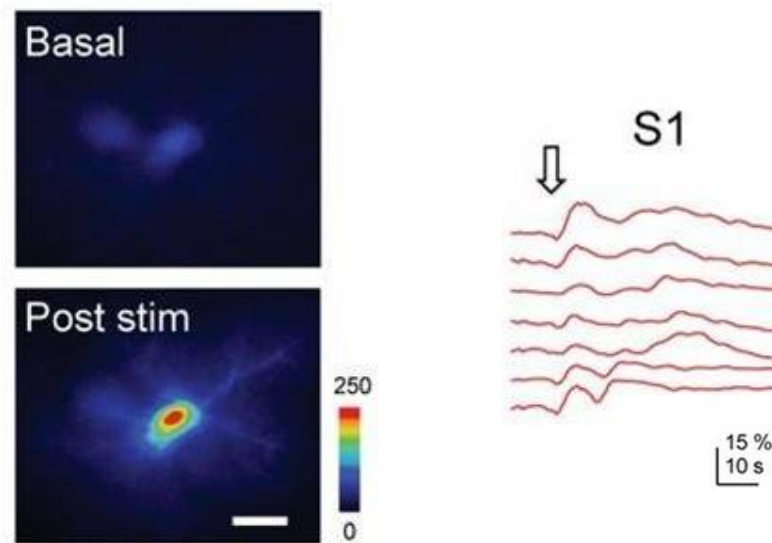


**Figure 5 Calcium transients of hippocampal human astrocyte.** (A) Representative fluorescence images of  $\text{Ca}^{2+}$  levels of a patch-clamped astrocyte filled with the calcium-sensitive dye Fluo4 before and after a train (30 Hz, 5 s) of axonal stimulation (Scale bar 10  $\mu\text{m}$ ). (B) Astrocyte  $\text{Ca}^{2+}$  responses in seven astrocytes elicited by a train of electrical stimulation (30 Hz, 5 s; S1, adapted from Navarrete et al., 2013).

### 1.3.2 Role of astrocytes in the pathophysiological condition of epilepsy

For decades epilepsy research has been focussed on neuronal targets when investigating possible treatment strategies. However, one third of patients suffering from epilepsy are resistant to this neuron-specific drugs. As mentioned previously, one hallmark of mesial temporal lobe epilepsy is the development of astrogliosis (Seifert et al., 2010). Together with the findings in the last decades about astrocyte contribution to physiological brain function (chapter 1.3.1), an involvement of astrocyte function in the pathogenesis of epilepsy has emerged.

Neuronal network activity depends on the extracellular  $\text{K}^+$  ( $[\text{K}^+]_{\text{ex}}$ ) concentration. Increased  $[\text{K}^+]_{\text{ex}}$  was associated with the pathophysiology of epilepsy (Lothman and Somjen, 1975; Moody Jr. et al., 1974) and even in turn, high  $[\text{K}^+]_{\text{ex}}$  were sufficient to induce epileptiform activity *in vitro* (Traynelis and Dingledine, 1988). Increases in  $[\text{K}^+]_{\text{ex}}$  lead to depolarised membrane potentials of neurons, which potentially result in increased firing. During epileptic seizures an increase of  $[\text{K}^+]_{\text{ex}}$  up to 12 mM could be measured *in vivo* (Heinemann and Dieter Lux, 1977). As described before, astrocytes are thought to regulate the  $[\text{K}^+]_{\text{ex}}$  by two mechanisms:  $\text{K}^+$  uptake and spatial  $\text{K}^+$  buffering (Kofuji and Newman, 2004; Orkand, 1986). Whereas it is not clear if alterations in  $\text{K}^+$  uptake contribute to epileptiform activity, there is evidence that spatial  $\text{K}^+$  buffering could play an important role during epileptiform seizures. Investigation of astrocytic Kir channels, which are thought to play an important role in  $\text{K}^+$  buffering, suggested an involvement of these channels in the development of

epilepsy. In animal epilepsy models as well as in human epilepsy these studies revealed an impaired Kir channel expression causing a reduced  $K^+$  buffering in sclerotic human hippocampus (Seifert et al., 2009) as well as decreased Kir currents in MTLE patients (Bordey and Sontheimer, 1998; Hinterkeuser et al., 2000). The protein levels of the astrocyte Kir subunit Kir 4.1 were also significantly reduced in human MTLE-HS (Heuser et al., 2012). Until now it is still not clear, whether changes in the Kir channels are the cause or the consequence of epileptogenesis. Since Kir4.1 channels were shown to be co-expressed with AQP4 (Hsu et al., 2011), it suggests that these water channels are involved in  $K^+$  homeostasis and thus may contribute to epileptiform activity (Binder et al., 2012). Until today, the mechanism linking AQP4 expression and function to  $K^+$  homeostasis is poorly understood. AQP4 knockout mice (AQP4<sup>-/-</sup>) exhibited prolonged seizure duration and enhanced seizure frequency (Binder et al., 2006). Experiments using  $K^+$  sensitive microelectrodes revealed an impaired  $K^+$  clearance from the extracellular space in these mice (Binder and Steinhäuser, 2006; Strohschein et al., 2011), although spatial buffering of  $K^+$  was increased (Strohschein et al., 2011).

One important factor for the hypothesis of  $K^+$  buffering is the extensively coupled astrocyte network. There is evidence that alterations in the astrocyte syncytium may affect spatial  $K^+$  buffering. Mice lacking Cx 43 and 30 and thus lacking astrocyte coupling, showed an impaired  $K^+$  buffering in the CA1 stratum lacunosum-moleculare, although this result could not be observed in CA1 stratum radiatum (Wallraff et al., 2006). However, the important potential role of astrocyte coupling in  $K^+$  buffering was investigated using an *in vivo* kainate model of epilepsy (Bedner et al., 2015). The authors developed a mouse model that reproduced key features of human MTLE. In this model, astrocytes showed a significant decrease in coupling already 4 hours after induction of status epilepticus, which was accompanied by an impaired  $K^+$  buffering. Inconsistent results were found regarding the pro- or antiepileptic effect of astrocyte coupling during epileptogenesis. In sclerotic tissue obtained from patients suffering from human MTLE, astrocytes were completely uncoupled (Bedner et al., 2015). In combination with the results obtained from their used mouse model, that astrocyte uncoupling occurs already on a very early time point, the authors suggested a causative role of astrocyte uncoupling for epileptogenesis. But there is also evidence that the intact astrocyte syncytium acts proepileptic. Astrocyte gap-junctions mediate the metabolic support of neurons by transporting metabolites from blood vessels to neurons, which is suggested to be an essential process for maintaining synaptic transmission during epilepsy (Rouach et al., 2008).

An additional role of the astrocyte gap junction-coupled network is the propagation of  $Ca^{2+}$  waves acting proconvulsive, since it was shown that they synchronize neuronal activity (Gomez-Gonzalo et al., 2011). Epileptiform activity was shown to induce time related  $Ca^{2+}$

transients (Fellin et al., 2006) and spontaneous  $\text{Ca}^{2+}$  were also observed to occur with higher probability during ictal activity induced in hippocampal slices (Gomez-Gonzalo et al., 2011). Another important function of astrocytes is their fast binding of glutamate via the glutamate transporter GLT1, by which they are thought to accomplish more than 80% of the glutamate clearance (Anderson and Swanson, 2000). Alterations in the glutamate metabolism were shown to contribute to the development of epilepsy, which supports the potential crucial role of astrocytes in the development of epilepsy. High levels of glutamate induced seizures and neuronal loss during epilepsy (Chapman, 1998; Meldrum, 1994). GLT1 knockout mice developed spontaneous seizures (Tanaka et al., 1997) and pharmacological inhibition of GLT1 reduced the threshold for epileptiform discharges (Demarque et al., 2004). Moreover, increased glutamate levels and stronger glutamate transients could be observed in hippocampi of MTLE patients (Cavus et al., 2005; During and Spencer, 1993). A causative role of astrogliosis in epileptogenesis was suggested (Ortinski et al., 2010; Robel and Sontheimer, 2016). After uptake of glutamate by astrocytes it is converted into glutamine via the glutamine synthetase (GS), which was also shown to play a role in epileptogenesis. Although its contribution is still under debate, it was demonstrated that experimental induction of reactive astrogliosis resulted in a decreased expression of the glutamine synthetase. This led to a reduced synaptic inhibition and consequently to neuronal hyperexcitability (Ortinski et al., 2010). Additionally, induction of astrogliosis was found to reduce glutamate uptake and the development of epilepsy (Robel and Sontheimer, 2016). Intrahippocampal perfusion with a GS inhibitor induced recurrent seizures (Perez et al., 2012) and in MTLE patients with hippocampal sclerosis a reduced GS protein activity was found (Eid et al., 2004).

Taken together, alterations in astrocyte biochemical processes have significant functional consequences contributing to neuronal network hyperexcitability. Thus, the role of astrocytes in physiological brain function extends to the pathophysiological condition of epilepsy, but also other neurodegenerative diseases like Alzheimer's disease, Parkinson disease or multiple sclerosis (Correale and Farez, 2015; Rappold and Tieu, 2010; Verkhratsky et al., 2010).

### **1.3.3 Astrocyte morphology in the healthy and epileptic brain**

As described before, astrocytes have a very characteristic morphology with a high number of fine processes surrounding neuronal synapses. Studies in rodent hippocampus showed that astrocytes in the CA1 region of the hippocampus develop a homogenous morphology with their high number of fine peripheral processes around postnatal day 14 (Bushong et al., 2004). During development astrocytes possess long and little ramified branches, followed by the formation of spongiform processes until all branches contain fine

processes. After one month, astrocytes build their non-overlapping territories (Bushong et al., 2004; Halassa et al., 2007). With its fine protrusions one single astrocyte can cover thousands of neuronal synapses (Bushong et al., 2002; Oberheim et al., 2006, 2009). The distance between fine astrocyte processes and synaptic compartments can vary between close contact and more than 100 nm (Medvedev et al., 2014; Ventura and Harris, 1999; Witcher et al., 2010). The number of synapses covered in the hippocampus vary from 62% to 90% (Heller and Rusakov, 2015; Ventura and Harris, 1999; Witcher et al., 2007). There is evidence that astrocytes cover rather synapses of thin dendritic spines than synapses of thicker dendritic spines (Medvedev et al., 2014). Since the signalling between neuronal synapses and nearby astrocyte processes is mainly mediated by transmitter diffusion, alterations in the spatial relationship could have a direct effect on the neuron-astrocyte communication (Bernardinelli et al., 2014a; Heller and Rusakov, 2015). One important function of astroglial coverage of synapses is to prevent glutamate spillout from the synaptic cleft thereby avoiding unspecific synaptic crosstalk (Lehre and Rusakov, 2002). There is experimental evidence that the astrocyte coverage of synapses is highly dynamic and activity-dependent (Oliet et al., 2001; Pannasch et al., 2014; Perez-Alvarez et al., 2014a). Neuronal stimulation was shown to result in restructuring of the fine peripheral astrocyte processes in a time scale of minutes (Bernardinelli et al., 2014b; Perez-Alvarez et al., 2014a).

These fast alterations in structure in turn could have an impact on the astrocyte-neuronal signalling and thus on neuronal function. It was shown that astrocyte processes move into the synaptic cleft due to neuronal activation, suggesting an increased number of astrocyte glutamate transporters (GLT1) in the synaptic cleft, which shapes synaptic transmission (Pannasch et al., 2014). Astrocyte structural changes could also be shown during lactation in the supraoptic nucleus, which resulted in alterations of glutamate uptake and synaptic plasticity (Oliet et al., 2001; Panatier and Oliet, 2006). Alterations in astrocyte morphology and their consequences for neuronal activity may also play a role in the development of the pathophysiological state of epilepsy. As mentioned above mesial temporal lobe epilepsy (MTLE) is accompanied by hippocampal sclerosis (HS), which is characterised by a strong astrogliosis. This implicates not only a change in astrocyte function, but also in astrocyte morphology. During the chronic phase of epilepsy using animal models it was shown that astrocytes lose their domain organisation and possessed a 10 fold increase in overlap of processes (Oberheim et al., 2008). Also astrocyte volume was increased in rodents one month after induction of status epilepticus using pilocarpine (Arisi et al., 2011). However, the mechanism linking astrocyte morphology changes to epileptiform activity is not clear yet. As described before astrocytes express a high number of aquaporin 4 channels (AQP4), which regulate the water flux over the membrane, thereby controlling

the astrocyte volume and in consequence the extracellular space (ECS) volume. Several studies have shown that a reduction in ECS volume result in neuronal hyperexcitability (Dudek et al., 1990; Pan and Stringer, 1996), suggesting a potential role of astrocyte swelling in the development of epileptiform activity. The findings that experimentally induced astrogliosis can cause epileptic seizures (Ortinski et al., 2010; Robel and Sontheimer, 2016) suggest a potential involvement of astrocyte morphology changes in epileptogenesis.

Structural changes in astrocyte morphology are not only controlled by passive water fluxes but also by changes in the actin cytoskeleton. Astrocytes express the small Rho GTPases RhoA, Rac1 and CDC42 (Chen et al., 2006; Höltje et al., 2005; Rosso et al., 2007). Further investigations have shown that the Rho associated protein kinase (ROCK) is a central player controlling astrocyte structure, since inhibition of this RhoA downstream effector induced stellation of astrocytes (Höltje et al., 2005; Racchetti et al., 2012). RhoA activation on the other hand was found to inhibit astrocyte stellation (Kalman et al., 1999; Perez et al., 2005; Ramakers and Moolenaar, 1998). Antiepileptic effects could have been shown by intraperitoneal application of the ROCK inhibitors fasudil or Y27632 in an kindling model of epilepsy (İnan and Büyükafşar, 2008).

Controversial results were found, when rats were treated with the ROCK inhibitor Y27632 after induction of status epilepticus (SE) using pilocarpine. Neuronal loss and mossy fibre sprouting was increased in Y27632 treated rats, whereas astrogliosis was decreased compared to control rats treated with the same drug, but without induction of SE (Kourdougli et al., 2015). These findings indicate a potential role of astrocyte cytoskeletal changes in the development of epileptiform activity. However, the contribution of astrocyte morphology changes during the acute onset of epileptiform activity and its potential contribution to epileptogenesis has not been investigated yet. One could speculate that not only physiological activity, but also epileptiform activity induces a fast restructuring of peripheral astrocyte processes. This in turn could affect glutamate uptake. As previously described, glutamate transporters are highly mobile on the astrocyte membrane (Murphy-Royal et al., 2015). Morphology changes of astrocyte processes could affect this mobility and in turn impair glutamate uptake, which could have a proepileptic effect. Also various other mechanisms like the  $K^+$  clearance may be affected by rapid astrocyte morphology changes thereby supporting epileptiform activity. An altered astrocyte morphology could also affect the intracellular diffusivity, which could also modify the intercellular astrocyte communication via gap junctions. Thus, rapid structural changes of astrocytes may result in a feedback loop acting on neuronal activity in a time scale of minutes. This in turn could have long-term consequences concerning the pathophysiological development of epilepsy.

## 2. Aim of the study

Astrocytes have a very characteristic morphology, which allows them a close contact to neuronal synapses. They have been demonstrated to play an important role in physiological and pathophysiological brain function. In the pathophysiological state of epilepsy an altered astrocyte morphology was observed in former studies in the late states of this disease. How early these astrocyte morphology changes occur and to what degree they may contribute to the development of epilepsy is yet unknown. The present study aimed to understand the potential role of astrocyte morphology changes during early epileptogenesis. To this end, three main aspects were investigated in detail.

- *Does epileptiform activity induce astrocyte morphology changes on a rapid time scale of minutes?*

Astrocyte morphology changes have been found in the late states of epilepsy (Oberheim et al., 2008; for review Sofroniew and Vinters, 2010). These structural changes are often accompanied by an altered astrocyte function, which could promote epileptic seizures (Bordey and Sontheimer, 1998; Hinterkeuser et al., 2000; Seifert et al., 2010). Until now it was not shown at which time point of epileptogenesis astrocyte morphology changes occur. Alterations in astrocyte morphology in response to neuronal activity on a time scale of minutes have been shown under physiological conditions (Bernardinelli et al., 2014b; Haber et al., 2006; Perez-Alvarez et al., 2014a). Virally induced astrogliosis caused an increased neuronal excitability (Robel and Sontheimer, 2016). Since neuron-astrocyte interaction depends on the diffusion of molecules through the extracellular space, alterations in the spatial relationship between neurons and astrocytes may also have consequences during the very early onset of epileptogenesis.

- *Which mechanism mediates astrocyte morphology changes?*

Astrocyte morphology changes can be mediated by different pathways. Astrocyte volume can be regulated via AQP4 channels, which regulate the water flux across the membrane. By this passive mechanism the extracellular space volume is controlled simultaneously (Binder et al., 2012; Hsu et al., 2011; Hubbard et al., 2015; Satoh et al., 2007). Additionally, there is evidence that astrocyte morphology is regulated by the actin cytoskeleton since they express the small Rho GTPases (Chen et al., 2006; Höltje et al., 2005; Rosso et al., 2007). Both mechanisms for regulating astrocyte morphology have been associated with epileptiform activity (Dudek et al., 1990; Pan and Stringer, 1996). Understanding the mechanism of potential rapid astrocyte morphology changes due to induction of epileptiform activity would also give the opportunity to modulate

astrocyte morphology and investigate the possible consequences for epileptiform activity.

- *What are the functional consequences of rapid astrocyte morphology changes?*

As explained, changes in astrocyte structure may result in alterations in the spatial relationship of astrocyte protrusions and neuronal synapses. This in turn could alter neuronal activity, since astrocytes were shown to modulate synaptic transmission and neuronal activity via neurotransmitter clearance (Kofuji and Newman, 2004; Orkand, 1986) and neurotransmitter supply (Halassa et al., 2007; Henneberger et al., 2010; Malarkey and Parpura, 2008). If rapid astrocyte morphology changes could be observed after induction of epileptiform activity, it would be interesting to understand the functional consequences of these morphology changes. Additionally, it should be investigated if these structural alterations have a potential pro- or antiepileptic effect and this should help to clarify the potential role of rapid astrocyte morphology changes during early epileptogenesis.

### **3. Animal models and materials**

#### **3.1 Animal models**

All animals used for this project were handled in accordance to the European and national government regulations and all experiments were designed and planned to minimize the number of animals required for this project. The animals were held in the “Haus für experimentelle Tiermedizin” (HET) under standard housing conditions with a 12h / 12h dark-light cycle. Food and water were always present. For this project male Wistar rats as well as transgenic male and female mice with FVB (Friend leukemia virus B) background were used.

##### **3.1.1 Wistar rats**

Male Wistar rats were obtained from Charles River at the age of p21 and used until p35. This rat type is an outbred albino rat strain and was the first strain developed for biological and medical research in the Wistar Institute in 1906. This strain was also used for the developing of other rat strains like Sprague-Dawley and Long-Evans rats, which were derived from Wistar rats.

##### **3.1.2 Transgenic mouse line containing EGFP expressing astrocytes**

In this mouse line, astrocytes are labelled with the enhanced green fluorescent protein (EGFP), which is expressed under the human glial fibrillary acidic protein (hGFAP) promoter (Nolte et al., 2001). It is expressed in all regions of the mouse brain including the cortex, cerebellum, hippocampus, retina and the spinal cord. The transgenic mice were generated by microinjection of FVB/N oocytes with a plasmid construct of a 2.2 kb DNA fragment of the hGFAP promoter inserted into the multiple cloning site of pEGFP-1 (Nolte et al., 2001). This mouse strain was used to image fluorescent astrocytes without requirement of whole-cell patch-clamp recordings. They were used at the age of p21 to p42.

##### **3.1.3 Transgenic mouse line containing EGFP expressing astrocytes and YFP expressing CA1 pyramidal cells**

This mouse line was used to monitor astrocyte and neuronal morphology in parallel. Thy-1-YFP mice express the yellow fluorescent protein (YFP) under the Thy-1 promoter. They were kindly provided by the laboratory of Professor Heneka, University of Bonn, medical school. Additionally to motor and sensory neurons, also central neurons like hippocampal pyramidal cells are labelled on a high level. In non-neural cells no expression of YFP was

detectable. In general, fluorescence starts to appear brightly in young adult mice (Feng et al., 2000). The genetic background of this mouse strain is C57BL6. For this project, these mice were crossed with hGFAP-EGFP mice to obtain mice, where CA1 hippocampal neurons and astrocytes were endogenous fluorescent labelled, which allowed performing of imaging experiments without filling cells with morphological dyes through whole-cell patch-clamp recordings. These mice were heterozygous for Thy-1 YFP and homozygous for GFAP-EGFP.

### 3.1.4 FVB mice

Friend leukemia virus B (FVB) mice are an inbred albino mouse strain, which was established at the National Institute of Health in 1966. This strain is very suitable for transgenic experiments since it is characterized by a good reproductive performance and consistent large litters (Taketo et al., 1991). FVB mice at the age of p23 to p28 were obtained from Charles River and used for stereotaxic injections of AAV.GFAP.iGluSnFR (chapter 4.1.2). Since the genetic background of animals used for epilepsy models seems to be important factor for the success of induction of epileptiform activity (Leclercq and Kaminski, 2015; McKhann II et al., 2003; Schauwecker, 2011), this mouse strain was used because it has the same genetic background like the hGFAP-EGFP mice used for imaging experiments in acute hippocampal slices.

## 3.2 Materials

### 3.2.1 Chemicals

Table 1: Chemicals

Compound	Company
Alexa 594 Hydrazide	Invitrogen (now Thermo Fisher Scientific), Waltham, US
Antisedan®	Vetoquinol GmbH, Ravensburg, Germany
Ascorbic acid	AppliChem GmbH, Darmstadt, Germany
ATP (disodium salt)	AppliChem GmbH, Darmstadt, Germany

CaCl <sub>2</sub> 1M solution	Sigma Aldrich, St. Louis, US
Cepetor	CP Pharma Handelsgesellschaft mbH, Burgdorf, Germany
D-AP5	Abcam, Cambridge, UK
di(Tris)-Phosphocreatine	Sigma Aldrich, St. Louis, US
DMSO	Sigma Aldrich, St. Louis, US
Ethanol 99 %	AppliChem GmbH, Darmstadt, Germany
Ethanol absolut pa.	AppliChem GmbH, Darmstadt, Germany
Glucose	AppliChem GmbH, Darmstadt, Germany
GTP (sodium salt)	Sigma Aldrich, St. Louis, US
HEPES	AppliChem GmbH, Darmstadt, Germany
Isofluran (Forene®)	AbbVie Deutschland GmbH & Co. KG, Mainz, Germany
Kainic acid	Abcam, Cambridge, UK
KCl	Sigma Aldrich, St. Louis, US
Ketamin 10%	betapharm Arzneimittel GmbH, Augsburg, Germany
KMS	Sigma Aldrich, St. Louis, US
LY341495	Tocris, Bristol, UK

Methanesulfonic acid	Sigma Aldrich, St. Louis, US
MgCl <sub>2</sub> (6 H <sub>2</sub> O)	AppliChem GmbH, Darmstadt, Germany
MgSO <sub>4</sub> (7x H <sub>2</sub> O)	Sigma Aldrich, St. Louis, US
NaCl	AppliChem GmbH, Darmstadt, Germany
NaH <sub>2</sub> PO <sub>4</sub>	AppliChem GmbH, Darmstadt, Germany
NaHCO <sub>3</sub>	AppliChem GmbH, Darmstadt, Germany
NBQX Disodium salt	Abcam, Cambridge, UK
Penicillin G sodium salt	Sigma Aldrich, St. Louis, US
Potassium hydroxide	Sigma Aldrich, St. Louis, US
Refobacin®	Almirall, Barcelona, Spain
Rimadyl®	Zoetis, New Jersey, US
Sodium pyruvate	AppliChem GmbH, Darmstadt, Germany
Sucrose	AppliChem GmbH, Darmstadt, Germany
TTX citrate	Abcam, Cambridge, UK
Xylocain	Astra Zeneca, Wedel, Germany
Y27632 dihydrochloride	Abcam, Cambridge, UK

### 3.2.2 Recipes

#### Slicing solution

	<b>Conc (mM)</b>	<b>Osmolarity</b>	<b>MW</b>	<b>g (2 l)</b>
<b>Sucrose</b>	105.00	105	342.30	71.883
<b>NaCl</b>	60.00	120	58.44	7.013
<b>KCl</b>	2.50	5	74.56	0.373
<b>MgCl<sub>2</sub> 6H<sub>2</sub>O</b>	7.00	21	203.30	2.846
<b>NaH<sub>2</sub>PO<sub>4</sub></b>	1.25	2.5	119.98	0.300
<b>Ascorbic acid</b>	1.30	1.3	176.12	0.458
<b>Sodium pyruvate</b>	3.00	6	110.00	0.660
<b>NaHCO<sub>3</sub></b>	26.00	52	84.01	4.369
<b>Glucose</b>	10.00	10	180.16	3.603

+ 0.5 mM CaCl<sub>2</sub> from 1M CaCl<sub>2</sub> stock solution, osmolarity 300 -310

#### Artificial cerebral spinal fluid (ACSF)

	<b>Conc (mM)</b>	<b>Osmolarity</b>	<b>MW</b>	<b>g (1 l)</b>
<b>NaCl</b>	131.00	262	58.44	7.656
<b>KCl</b>	2.50	5	74.56	0.186
<b>MgSO<sub>4</sub> 7H<sub>2</sub>O</b>	1.30	2.6	246.48	0.320
<b>NaH<sub>2</sub>PO<sub>4</sub></b>	1.25	2.5	119.98	0.150
<b>NaHCO<sub>3</sub></b>	21.00	42	84.01	1.764
<b>Glucose</b>	10.00	10	180.16	1.802

+ 2 mM CaCl<sub>2</sub> from 1M CaCl<sub>2</sub> stock solution, pH 7.4, osmolarity 297-303

#### Intracellular solution KMS (IC)

	<b>Conc (mM)</b>	<b>Osmolarity</b>	<b>MW</b>	<b>g (50 ml)</b>
<b>Methanosulfonic acid</b>	135.00	135		
<b>KOH</b>	135.00	135		
<b>HEPES</b>	10.00	10	238.3	0.1192
<b>Di(Tris)-Phosphocreatine</b>	10.00	30	453.4	0.2267
<b>MgCl<sub>2</sub> 6 H<sub>2</sub>O</b>	4.00	12	203.3	0.0407
<b>Na<sub>2</sub>-ATP</b>	4.00	12	551.1	0.1102
<b>NaX-GTP</b>	0.40	1.6	523.2	0.0105

438 µl Methanosulfonic acid were mixed with 30 ml dd H<sub>2</sub>O. pH were adjusted with 1 M KOH, pH 7.2, osmolarity 290

## 4. Methods

### 4.1 Electrophysiology

#### 4.1.1 Preparing of acute hippocampal slices

Acute hippocampal slices were prepared from 21 to 35 days old Wistar rats or from p21 to p42 mice with different transgenic backgrounds (chapter 3.1). Animals were transferred in a 10 l glass cylinder. 1 ml of Isoflurane was dropped on a tissue inside the cylinder to anaesthetise the animal. After three to five minutes the depth of anaesthesia was checked by pinching the hind paws. When no motor reaction could be observed, animals were deeply anesthetized. They were quickly decapitated either with a guillotine (rats) or a pair of scissors (mice) and the head was directly put into ice-cold slicing solution (chapter 3.2.2). To receive healthy brain slices it was important to perform the following steps quickly. The brain was removed out of the skull and transferred into ice-cold sucrose solution which was bubbled 15 minutes with 95% O<sub>2</sub> / 5% CO<sub>2</sub> before using. The cerebellum and forebrain were removed using a steel blade (Ted Pella Inc., US). The remaining brain was separated into the two hemispheres. Two cuts were made on each hemisphere, one on the dorsal and one on the ventral part of each hemisphere. The dorsal cut was made to create an even plane, which was glued onto a metal platform. The ventral cut was used to remove brain tissue covering the hippocampus. This allowed to directly start slicing the hippocampus and thus, saved time during slicing. The glued brain hemispheres were brought into the slicing chamber also filled with ice-cold sucrose solution bubbled with 95% O<sub>2</sub>/ 5% CO<sub>2</sub>. The brain tissue was orientated without any angle and in a manner that it could be sliced in a defined direction, starting from CA1 region through the dentate gyrus towards CA3 region. It turned out that this orientation of brain slicing was the best to obtain healthy brain slices with a high number of intact cells. Horizontal slices of 300 to 350 µm were cut starting from the ventral hippocampus and moving towards the dorsal hippocampus using a vibratome (Campden Instruments, UK). For slicing ceramic blades (Campden Instruments, UK) were used. After slicing was completed, all slices were transferred into sucrose solution at 34 °C water bath (Grant Instruments, UK) for 15 min before they were stored in artificial cerebrospinal fluid (ACSF, chapter 3.2.2) for one hour at room temperature.

#### 4.1.2 Stereotaxic injection of the glutamate sensor iGluSnFR

To investigate if induction of epileptiform activity leads to an altered glutamate uptake the glutamate sensor iGluSnFR (Marvin et al., 2013) was brought into astrocytes by virus injections. Hippocampi of FVB mice (chapter 3.1.4) at p23 to p28 were injected bilaterally

with the adeno-associated virus (AAV) under the GFAP promotor (AAV1.GFAP.iGluSnFR.WPRE.SV40; Vector Core, University of Pennsylvania, USA) to drive expression in astrocytes. Mice were weighted and anesthetised by intraperitoneal (i.p.) injection of a mixture of ketamin/medetomidine using Ketamin with a concentration of 100 g/1 kg body weight (bw) and Cepetor (1 mg/ml). The injection volume for the induction of anaesthesia was 0.1 ml/10 g bw. Mice were constantly placed on a heating plate at 36 °C to hold them on body temperature. The toe pinch test was used to test, whether mice were deeply anesthetized. If this was the case, the hair of the head was removed until the skin was free. Mice were head-fixed in a stereotaxic frame (Model 901, David Kopf Instruments, US). It was important to ensure that the skull was positioned straight in the anterior/posterior and in the lateral direction. The eyes were protected from drying with Bepanthen® eye unguent and the skin was anesthetized locally using Xylocaine. The skin was cut to uncover the skull. Pieces of skin tissue on the skull were removed properly and the skull was dried with cotton bud. The injection needle was positioned on bregma and on lambda and ventral positions were compared to ensure that the skull was positioned straight. Beside the ventral position of bregma also the anterior/posterior as well as the lateral position was measured using the scale of the stereotaxic frame. From these positions the coordinates for the injections sites on each hemisphere were calculated for injections into the CA1 region of the hippocampus.

**Table 2:** Coordinates for stereotactic injections

	Position from bregma
Anterior/posterior	- 0.35
Lateral	+/- 0.3
Ventral	- 0.25

The injection needle (World Precision Instruments, WPI, US) was positioned on the skull accordingly to the calculated coordinates for the first injection. The point, where the skull has to be opened was marked with a permanent marker and a hole was drilled into the skull subsequently. After opening of the skull, the injection needle was dipped into the brain to overcome the meninx and removed again. To avoid any blockage of the tip, 50 nl of the virus were injected into the air. The appearing drop at the tip of the needle ensured that the injection needle was unblocked and could be moved down to the calculated ventral position. After reaching the position, the needle stayed in position for two to three minutes to let the surrounding tissue adapt to the mechanical disturbance. Subsequently, 1000 nl of AAV.GFAP.iGluSnFR were injected with a speed of 100 nl/min using a micro

syringe pump controller (WPI, US). Two minutes after finishing the injection, the needle was removed slowly and moved to the calculated coordinates for the injection of the right hemisphere, which was the same procedure as described for the left side. After all, the injection needle was removed and the mouse was released from the stereotaxic frame. The skin was sutured using absorbable thread (Ethicon, US) and covered again with Xylocaine as well as the antibiotic Refobacin containing the active component Gentamicin (1mg / g). For analgesia Rimadyl® was injected with a dose of 5 mg/kg bw and an injecting volume of 0.05 ml/10g bw and anaesthesia was stopped by i. p. injection of antisedan (0.1 ml / 10 g bw). Mice were put back into their cages, which were left on a heating plate overnight. Animals were controlled daily for further four days and subsequently every second day. Experiments were performed three to four weeks after virus injections. To ensure analgesia, Rimadyl® i. p. injection was repeated after 24 and 48 hours.

#### **4.1.3 Electrophysiological setup**

Experiments were performed at two electrophysiological setups (Scientifica, UK). They were used in combination with two different imaging systems (Chapter 4.2.1). The microscope (Scientifica, UK and Olympus, Japan) equipped with a motorized focus as well as the submerged recording chamber were placed on a antivibration table surrounded by a faraday cage to reduce mechanical disturbance and the noise level during the recordings. The grounding pellet (WPI, US) was fixed in the bath and connected to a grounding point, with which also the headstages (Molecular Devices, US) were connected. Two headstages including pipette holders (G23 Instruments, UK) controlled by electrically driven micromanipulators (Scientifica, UK) were placed on each side of the recording chamber. For recording of electrical signals a teflon-coated silver wire (WPI, US) with a chloride tip was put into a glass pipette (Science Products, Germany) filled with 5µl artificial cerebrospinal fluid (ACSF) for extracellular recordings or with intracellular solution (IC, chapter 3.2.2). A concentric bipolar stimulation electrode (FHC, US) was also placed at one side of the recording chamber. The stimulation electrode was controlled by a stimulus isolator (Digitimer, US), which was triggered by the Clampex software (pClamp version 10, Molecular Devices, US). The headstages were connected to the amplifier (Multiclamp 700b, Molecular Devices, US) and the incoming signals were transmitted through a humbug (Quest Scientific, Canada) for noise reduction to the analogue digital converter (Digidata 1440A, Molecular Devices, US). The AD converter was connected to the computer (Dell, US). As recording and stimulation software Clampex was used. To ensure a physiological temperature a sensor was fixed in the bath next to the grounding pellet and temperature was monitored and controlled by a heater (Warner Instruments, US) throughout the experiments. The microscopes were equipped with a Dodt contrast (Dodt and

Zieglgänsberger, 1990) or differential interference contrast (DIC). The light microscopy pictures of the tissue were displayed on a monitor (Dell, US; Benq, China) using a camera (Watec Incorporated, US).

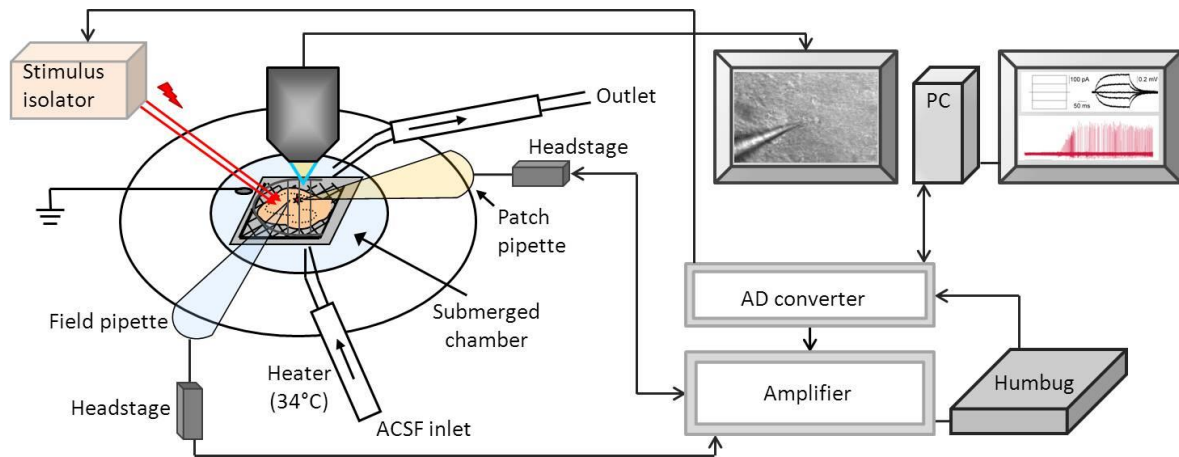


**Figure 6 Electrophysiological setup.** The hippocampal slice was located in a submerged chamber on a grid and was fixed with a nylon harp. The slice was perfused with ACSF at 34 °C. Electrical signals were recorded from single cells via the patch pipette or from a population of neurons via the field pipette. The signals were preamplified by the headstages and sent to the amplifier. From there, electrical signals were transmitted to the PC via the AD converter. A humbug was used for noise reduction. For stimulation the stimulus isolator was triggered by Clampex software. Light microscopy pictures were displayed on a monitor.

#### 4.1.4 Recording of evoked and spontaneous field potentials

For electrophysiological recordings one slice was transferred into the submerged recording chamber and placed on a self-made nylon grid to ensure a fast and proper perfusion of the slice (Ivan Pavlov, UCL London). It was fixed with a harp built out of platinum wire (neoLab, Germany) and polyamide thread from tights and perfused with artificial cerebrospinal fluid (ACSF). Throughout the experiment the ACSF was bubbled with 95% O<sub>2</sub> / 5% CO<sub>2</sub> and it was heated to 34°C. Spontaneous and evoked field potentials were recorded in the CA1 stratum pyramidale and / or stratum radiatum using a chloride silver wire in a glass pipette filled with 5 µl of ACSF. Glass pipettes were produced using a micropipette puller (Model P-1000, Sutter Instruments, US) and resistances of the field pipettes ranged between 3 and 5 MΩ. The tip size of the glass pipettes was 1 to 3 µm.

Spontaneous epileptiform discharges were recorded in CA1 stratum pyramidale in rat and mouse hippocampal slices. After obtaining 10 to 20 minutes baseline recordings, slices were either recorded under control or epileptiform conditions. Epileptiform activity was induced by bath application of 4 mM penicillin for 30 minutes (Schwartzkroin and Prince, 1977). In control recordings no penicillin was applied. The extracellular K<sup>+</sup> concentration

was increased to 5 mM or 4 mM for experiments in rats or mice, respectively. This was necessary to induce epileptiform discharges. To rule out any side effect of higher extracellular  $K^+$  levels on epileptiform activity and astrocyte morphology, this concentration was also used in baseline and control recordings. In a subset of experiments the persistence of epileptiform activity combined with monitoring astrocyte morphology changes was investigated in hGFAP-EGFP mice, which contain astrocytes expressing EGFP under the GFAP promotor (Nolte et al., 2001; chapter 3.1.2). This allowed stable electrophysiological recordings and imaging over this long time scale. To examine the persistence of epileptiform activity, penicillin was washed out for 40 to 50 minutes and spontaneous epileptiform discharges were recorded throughout the experiment. After each experiment the extracellular solution was renewed and after bath application of drugs the tubes and the chamber were washed properly before starting a new experiment.

Evoked field excitatory postsynaptic potentials (fEPSPs) were recorded in parallel to the spontaneous fEPSPs described before. To this end, a bipolar stimulation electrode was placed in CA3 / CA2 stratum radiatum to stimulate the Schaffer collaterals (SCs) which project to CA1 pyramidal cells. For subsequent analysis it was important to record the fEPSP and the population spike in the stratum pyramidale. Therefore, the tip of the recording electrode was placed in the CA1 stratum oriens close to the stratum pyramidale to ensure both a fEPSP and a population spike after stimulation which was required to analyse the spike/slope coupling (Chapter 4.1.5). SCs were stimulated in mice every 20 to 30 seconds either with a single 100  $\mu$ s pulse or with a paired pulse 50 ms apart. In a subset of experiments another field electrode was placed in the stratum radiatum at the same lateral distance to the stimulation electrode like the field electrode placed in stratum oriens. Stimulation intensity ranged from 30  $\mu$ A to 150  $\mu$ A.

The stimulation and recording was triggered by Clampex software. Each episode lasted 30 seconds and the episode interval was set to minimum so that there were nearly no gaps between the episodes to ensure that all spontaneous epileptiform discharges were detected and recorded. In rat experiments SCs were stimulated three times every five minutes and in between spontaneous epileptiform discharges were recorded in gap free mode.

Long-term potentiation (LTP) of CA1 synapses was induced in a subset of experiments after washout of penicillin. In these experiments LTP was explored after control recordings and respectively after induction of epileptiform activity. To this end, penicillin was bath-applied after a 20 minutes baseline for 30 minutes. Afterwards it was washed out for 40 minutes followed by the LTP protocol. LTP was induced by high-frequent stimulation (HFS, 100 pulses, 100 Hz, 1 s, 3 repeats, 60 s delay between pulse trains) after a 10 minutes baseline

was recorded with a single stimulation pulse every 30 s. After the HFS, single stimulation was repeated for 30 minutes.

#### 4.1.5 Analysis of evoked and spontaneous synaptic responses

Different parameters of the evoked and spontaneous field potentials were analysed using Clampfit (pClamp, version 10, Molecular Devices, US) and Microsoft Excel (Microsoft, version 2010, US).

To investigate if synaptic transmission is altered in epileptiform conditions compared to control recordings, the slope of the evoked fEPSPs recorded in CA1 stratum pyramidale and stratum radiatum were analysed. The slope was used as parameter since it is proportional to the synaptic current induced by SC stimulation. To this end, 2 cursors were set 100 ms apart to determine the baseline 100 ms before the stimulus artefact occurred. Another time window was used to estimate the slope of the first 50% of the rising (stratum pyramidale) or falling (stratum radiatum) fEPSP were used. The slope was calculated by the software Clampfit, normalized to baseline and plotted versus the time.

$$\text{slope}_{fEPSP} = \frac{dV}{dt}$$

Another important parameter to investigate synaptic transmission is the paired pulse ratio (PPR). Its calculation reveals changes of the presynaptic release probability of neurotransmitters. To this end, 2 stimuli (100  $\mu$ s) were given with 50 ms delay and the ratio of the slope of the second response versus the slope of the first response was calculated.

$$PPR = \frac{\text{slope}2}{\text{slope}1}$$

A PPR > 1 indicates paired pulse facilitation whereas a PPR < 1 indicates paired-pulse depression. Paired pulse facilitation is caused by a higher vesicular neurotransmitter release during the second pulse. This indicates that the synapse has a low release probability. Paired pulse depression is induced by a high vesicular neurotransmitter release during the first pulse at synapses with a high release probability. Because of the lower number of remaining vesicles, less vesicles can be released during the second pulse, which results in a decreased response (Debanne et al., 1996).

To test whether induction of epileptiform activity leads to a persistent alteration in neuronal excitability, the spike/slope coupling was analysed. The spike-slope coupling is a measurement to describe the excitability of a cell. The amplitude of the population spike (spike) was normalised to the slope of a fEPSP (slope) in response to electrical stimulation.

With this analysis the excitability of a neuronal population in different conditions can be compared independent of the strength of the synaptic stimulation. For this analysis the fEPSPs recorded in CA1 stratum pyramidale were used. The slope was determined as described before and normalized to the amplitude of the fibre volley, which represents the axonal response and thus number of stimulated axons. This allowed a comparison between experiments, where the stimulation intensity could differ. Additionally, the amplitude of the population spike ( $A_{ps}$ ) representing the synchronous firing of stimulated neurons was calculated (Figure 7).

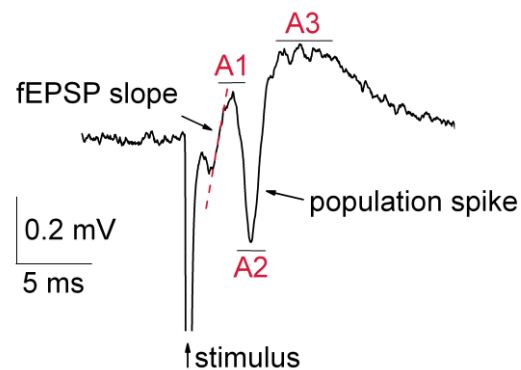


**Figure 7 Analysis of spike slope coupling.** Typical fEPSP response to SC stimulation recorded in the CA1 stratum pyramidale. The amplitude of the population spike was calculated from the three potential values compared to baseline (A1-A3) and then normalised to the fEPSP slope.

$$A_{ps} = \frac{A1 + A3}{2} - A2$$

The amplitude of the population spike was normalized to the calculated slope, which resulted in the value for the spike/slope coupling. This analysis was again performed for control and penicillin conditions.

Spontaneous epileptiform activity was defined as occurrence of typical epileptiform discharges induced by bath-application of penicillin. Slices, which were exposed to penicillin but did not show spontaneously these discharges, were excluded. To characterize the induced epileptiform activity the frequency of the occurring spontaneous discharges per minute was calculated. To this end, events were detected using the event-detection tool of Clampfit. A template was created out of several recorded discharges and events were detected by template matching. All traces were checked for correctness of the automatic event-detection. As additional parameter, the discharge probability was calculated. It was defined as probability, by which a slice developed spontaneous

epileptiform discharges at a distinct time point. Also, the mean peak amplitude was calculated with Clampfit, whereas the peak amplitude was averaged out of 5 signal points at the maximal response in a 0.5 ms time window. The mean amplitude was calculated from all single epileptiform discharges in one experiment and the means of the single recordings were compared statistically.

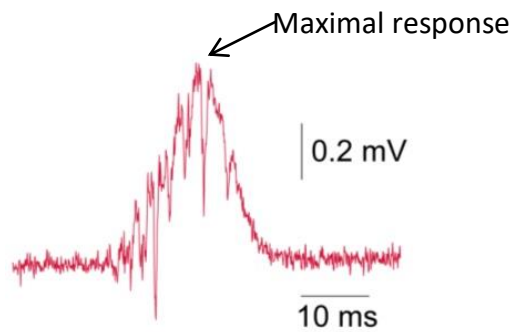


**Figure 8 Typical epileptiform discharge induced by bath application of penicillin.** The peak amplitude was measured at the maximum of the response, where five amplitude values were averaged in a 0.5 ms time window.

#### 4.1.6 Whole-cell patch clamp recordings of astrocytes

Whole-cell patch-clamp recordings were performed in rat hippocampal slices in parallel to field recordings as described by (Neher and Sakmann, 1976). This technique was mainly used to fill astrocytes with morphological dyes for imaging experiments (chapter 4.2.2) but also to capture changes in  $K^+$  buffering upon induction of epileptiform activity (chapter 4.1.8). Putative astrocytes were identified using either differential interfering contrast (DIC) optics (Olympus, Japan; chapter 4.2.1) or Dodt optics (Scientifica, UK, chapter 4.2.1). For patch-clamp recordings, patch pipettes with a resistance of 2.5 to 3.5 M $\Omega$  were used and filled with 5  $\mu$ l intracellular solution (IC, chapter 3.2.2). IC contained morphological dyes depending on the experiment (chapter 4.2). The pipette was fixed in the pipette holder of the headstage. To avoid contamination of the pipette tip an overpressure was applied using a 1 ml syringe which was connected to the patch pipette via a silicone tube. The pipette was then placed under the objective in the bath and brought down to the hippocampal slice. The headstage was controlled by the software Multiclamp (pClamp, Molecular Devices, US).

Patch-clamp recordings can be performed in two different modes, voltage-clamp and current-clamp mode. In voltage-clamp mode, the resting membrane potential of a cell is compared with the selected holding potential. Differences are compensated via current injections by the amplifier. In current-clamp mode, the voltage of a cell is clamped and the

net current flowing over the cell membrane is recorded by the amplifier. In current-clamp mode, the net current flowing over the membrane is clamped and the patched cell is at its physiological membrane resting potential. In this mode, changes in resting potential can be measured.

Voltage steps of 5 mV with a duration of 100 ms were applied via the patch pipette to determine the pipette resistance. The resulting recorded current was used to calculate the pipette resistance using the Ohm's law by Clampex software. The prior identified astrocyte was approached with the pipette using the micromanipulator until the tip was placed directly next to the cell membrane such that the overpressure produced a dimple in the cell membrane which could be recognized as light reflex on the cell. The overpressure was removed, which pulled the cell membrane towards the pipette and a seal with a resistance of several 100 M $\Omega$  was established. The holding potential was switched from 0 mV to -70 mV. By using gentle negative pressure the cell was sucked towards the tip of the pipette building a very tight connection between pipette and cell with a resistance higher than 1 G $\Omega$ . Fast capacitive artefacts were compensated. This configuration is known as cell-attached configuration.

To induce the whole-cell configuration, the membrane was ruptured by a strong negative pressure which was accompanied with a decrease in resistance. After opening the cell it was held in voltage-clamp mode and 10 mV steps were repeated 3 times to determine the access resistance  $R_s$  (Figure 19). To monitor the membrane potential the configuration was switched to current clamp. To determine the input resistance of the patched astrocyte, 100 pA current steps were injected five times starting from -200 pA and ending at +200 pA with three repetitions (Figure 19). To measure the exact input resistance of the cell, it was necessary to monitor the exact membrane potential of the cell. Therefore, the bridge balance control of Clampex was required. A current is injected through the microelectrode results in a voltage drop across the electrode, which is dependent on the product of the injected current and the pipette resistance. This voltage drop affects the recorded membrane potential. Using the bridge balance, this voltage drop is balanced and the exact membrane potential can be recorded. During the experiments astrocytes were mainly held in current clamp mode to observe the resting membrane potential. Astrocytes with an initial membrane potential above -75 mV or an access resistance > 30 M $\Omega$  were discarded. The liquid junction potential was calculated using Clampex (-8.4 mV). Data were not liquid junction potential corrected. Resting membrane potential and access resistance were checked throughout the entire experiments and cells which show a depolarisation of more than 5 mV or a change in access resistance > 20% of initial access resistance were also excluded. Signals were filtered at 3 kHz and sampled at 40 kHz.

#### 4.1.7 Analysis of passive membrane properties

Different membrane properties of the patched astrocytes were determined during whole-cell patch-clamp recordings. The first step was the calculation of the access resistance  $R_s$ , which ensured a proper connection between pipette and cytoplasm and consequently led to a constant dye filling of the cell for imaging experiments. The access resistance is defined as the resistance between silver wire and cell soma. It can be calculated from the current responses of the cell to the applied 10 mV steps using the Ohm's law. Since the cell membrane has capacitive and resistive properties, a voltage step leads to a charging of the membrane surface, the capacitor ( $C_m$ ). At the onset of the voltage step ( $\Delta V$ ) the peak of the current ( $I_{\text{peak}}$ ) is limited to  $R_s$ .

$$R_s = \frac{\Delta V}{I_{\text{peak}}}$$

Other important parameters are the input resistance  $R_i$  of the cell and its membrane potential. To analyse these, the protocol performed in current clamp was used. Since the membrane resistance of astrocytes are very low, it cannot be simply calculated out of  $I_{\text{offset}}$ . The basic assumption for the relationship between  $C_m$ ,  $R_i$  and  $R_s$ , as described in Numberger and Draguhn (1996), is that  $R_i \gg R_s$ . This is not the case in astrocytes, which have a membrane resistance of 3 to 5 M $\Omega$ .  $R_i$  was calculated out of the current step and the resulting plateau offset amplitude of the voltage response using Ohm's law:

$$R_i = \frac{V_{\text{offset}}}{\Delta I}$$

The recordings in current mode were also used to capture the membrane potential of the patched cell simply by measuring a baseline region before the current steps occurred. All values were measured using Clampfit.

#### 4.1.8 Analysis of resting and transient $K^+$ concentrations

To analyse if induction of epileptiform activity alter the extracellular resting or transient  $K^+$  concentrations in the acute rat hippocampal slices, whole-cell patch-clamp recordings were used. The astrocyte membrane potential is very sensitive to the extracellular  $K^+$  concentration since its membrane potential is mainly caused by  $K^+$  currents (Kuffler et al., 1966; Orkand et al., 1966). Increases in the extracellular  $K^+$  concentration results in a depolarisation of the astrocyte resting membrane potential. This can be calculated by the Nernst equation.

$$P_{\text{cell}} = \frac{RT}{z_e F} \lg \frac{[K^+]_{\text{extracellular}}}{[K^+]_{\text{intracellular}}}$$

$P_{\text{cell}}$  = potential of the cell;  $R$  = universal gas constant;  $T$  = temperature;  $z_e$  = number of electrons transferred;  $F$  = Faraday constant

Astrocytes were held in whole-cell configuration in current clamp mode, which allowed to measure the astrocyte membrane potential (chapter 4.1.6). To capture changes in the resting potassium concentration the membrane potential of astrocytes at distinct time points was measured in gap-free recordings. The first time point was during baseline recordings and the second time point was in the last 10 minutes of control or penicillin recordings, respectively. Spontaneous epileptiform discharges during application of penicillin led to transient depolarisations of the astrocyte membrane potential. To ensure that the membrane potential under resting conditions is captured, the time constant of the transient depolarisations was measured using the fit-function of Clampfit. A time window twice the time constant away from the peak of the transient depolarisation was used to measure the astrocyte membrane potential.

To examine whether the transient  $K^+$ -buffering is altered, the amplitude and decay of the  $K^+$ -dependent component of astrocyte field excitatory postsynaptic potentials (afEPSP, (Henneberger and Rusakov, 2012a) due to SC stimulation was analysed. This component was analysed during baseline recordings and under control and penicillin conditions as described before. Paired pulse stimulation was used and the peak amplitude was analysed 30 ms after the second pulse using Clampfit (Figure 9). The time constant  $\tau$  of the signal was estimated by positioning the first cursor 200 ms after the second stimulation artefact and the second one at the end of the signal (Figure 9). A monoexponential fit was used with the fitting method Levenberg-Marquardt using Clampfit.

$$f(t) = \sum_{i=1}^n A_i e^{-t/\tau_i} + C$$

Before fitting, the baseline of all signals was set to zero and thus the offset  $C$  was always fixed to zero. The time constants were normalized to baseline using Excel and control and penicillin values were compared.

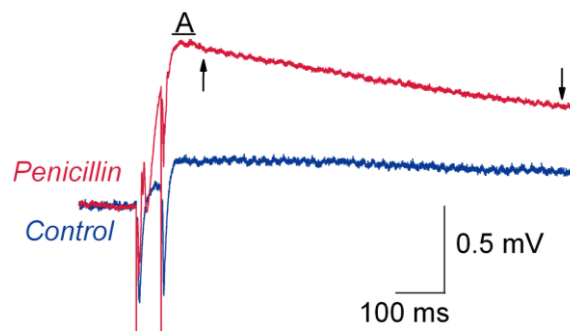


**Figure 9** Example traces of astrocyte field potentials recorded after paired pulse stimulation. A shows the time window, where the amplitude of the signal was measured (30 ms after stimulus artefact). The arrows indicate the used time window for calculating the time constant  $\tau$  of the signal.

## 4.2 Imaging

### 4.2.1 Two-photon excitation fluorescence microscopy setup

For imaging experiments a Scientifica two-photon system (Scientifica UK) and a FV10MP system (Olympus, Japan) optically linked to a femtosecond Ti:sapphire pulse laser Vision S (Coherent, US, 73 fs pulse width) was used. Wavelengths of 800 nm were used for imaging of astrocytes filled with Texas red dextran (3kDa) and astrocyte expressing EGFP under the human GFAP promoter (Nolte et al., 2001). Both setups were integrated with the electrophysiological setups for whole-cell patch-clamp and field potential recordings. The Olympus setup was equipped with a 25x (NA 1.05) objective (Olympus, Japan) whereas the Scientifica setup was equipped with a 40x (NA 0.8) or 60x (NA 1.0) objective (Olympus, Japan). Each system was equipped with a dichroic mirror and filter cubes for a selective separating of the fluorescent signals. At the Scientifica setup the dichroic mirror reflected light with wavelengths lower than 565 nm to the green filter with a range from 500 to 550 nm and light with wavelengths higher than 565 nm were transmitted to the red filter with a range from 600 to 660 nm. In the Olympus setup fluorescent light was either reflected (<570 nm) by the dichroic mirror towards the bandpass green filter (515–560 nm) or transmitted (>570 nm) to the bandpass red filter (575–630 nm). For a subset of experiments a bandpass CFP/YFP filter was used (CFP: 460–500 nm, YFP 520–560 nm). In this case an additional filter (600 – 675 nm) allowed the transmission of long-wave wavelengths > 635 nm. The fluorescent signals were then detected with photomultiplier tubes (PMTs).

### 4.2.2 Monitoring astrocyte morphology

Astrocyte morphology was monitored in parallel to electrophysiological recordings using time-lapse imaging. For experiments with Wistar rats, astrocytes were visualized by filling them with the morphological dye Texas Red dextran 3kDa (300  $\mu$ M, Figure 10) using whole-cell patch-clamp recording. This morphology dye does not diffuse through gap junctions due to its size, since gap junctions are only permeable for molecules with a size < 1kDa. This was necessary for the analysis of astrocyte morphology changes, since alterations in soma fluorescence intensity would artificially affect the calculated astrocyte volume fraction (chapter 4.2.3). The cell was filled 10 to 15 minutes before the actual experiment started to ensure a stable baseline fluorescence, which was important to capture possible effects of astrocyte morphology changes. Astrocytes were imaged with a resolution of nominal 0.1  $\mu$ m/pixel and 3 to 5 frames were obtained every 5 minutes. With the depth of the tissue fluorescence intensity is decreasing. To ensure a constant laser power at the imaged cell, the laser power under the objective was adapted to the depth of the imaged astrocyte (4 to 10 mW) to adjust the laser power to 2 mW at the imaged cell. This was necessary to avoid photo damage. The z-position of each cell was adjusted in a manner that the cell soma, thick and fine branches as well as part of the patch pipette were visible (Figure 10) and was corrected very carefully before taking pictures to ensure that the focal plane of the imaged astrocyte was kept stable over the entire time of one experiment.

In hGFAP-EGFP mice (chapter 3.1.2) astrocytes expressed EGFP under the GFAP promotor (Figure 10) and thus patch-clamp recordings were not required for imaging experiments. Astrocytes in a depth of 30 to 90  $\mu$ m with a moderate fluorescence intensity were chosen to image astrocytes with a similar EGFP expression patterns and avoid outliers with very low or very high EGFP expression. Again three to five frames were obtained every 5 minutes with the same settings used in whole-cell patch-clamp recording experiments.

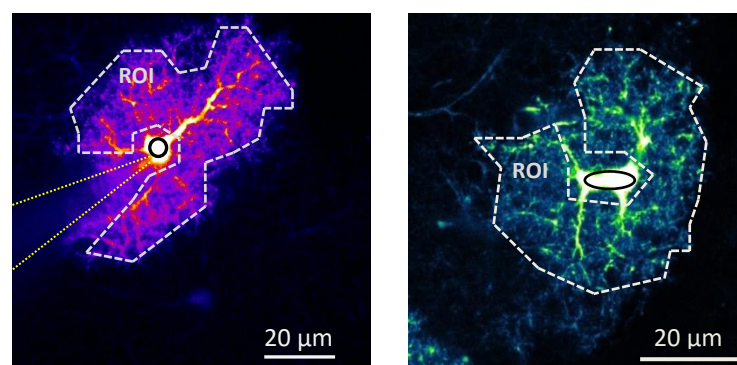


**Figure 10 Examples of fluorescent astrocytes.** (A) Astrocyte filled with Texas red dextran (TR, 3 kDa) using whole-cell patch-clamp configuration. Dotted lines indicate patch pipette. ROI (region of interest) includes fine and thick branches of patched astrocyte. Fluorescence intensity was normalized to soma fluorescence (black circle), where 100% of the tissue is occupied by the astrocyte. (B) Astrocyte expressing EGFP under the GFAP promotor. The analysis was performed as described for astrocytes filled with TR.

### 4.2.3 Analysis of astrocyte volume fraction

Monitoring of astrocyte morphology was used to capture changes in the fine branches of the single astrocytes. Peripheral astrocyte processes are often smaller than  $1 \mu\text{m}^3$  (Medvedev et al., 2014). Thus, morphology changes could also occur at this spatial range. Since these morphology changes are smaller than the diffraction limit of two-photon microscopy, an indirect read-out was required to capture astrocyte morphology changes. The astrocyte volume fraction (Medvedev et al., 2014) was used as this indirect read-out. Figure 11 visualises astrocyte segments (red parts) in a focal plane of an electron microscopy section (EM, done by Nikolai Medvedev). By isolating the astrocyte segments, two parameters can be distinguished, which define the volume fraction of an astrocyte. One parameter is the number of the astrocyte segments and the second parameter is their size. Astrocyte morphology changes, for instance, astrocyte retraction or swelling should lead to changes in either one or both parameters. Thus, the astrocyte volume fraction should be sensitive to astrocyte morphology changes. The assumption for the calculation of the astrocyte volume fraction was that the fluorescence intensity  $F$  at defined pixel coordinates  $(i, j)$  in the  $x - y$  plane is proportional to the local volume of the fluorescent astrocyte branches.

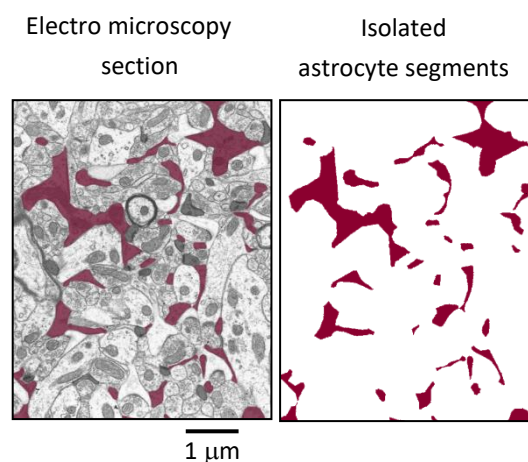


**Figure 11 Definition of the astrocyte volume fraction.** Astrocyte segments in an electron microscopy section (left panel, red parts) were isolated (right panel, red parts). The astrocyte volume fraction can be defined by two parameters, which are the size and number of astrocyte segments. These parameters should be sensitive to astrocyte morphology changes, which can be captured by the calculation of the astrocyte volume fraction (figure adopted from C. Henneberger).

For analysis, a region of interest (ROI) was defined which includes all the thick and fine processes of the imaged astrocytes (Figure 10). The averaged fluorescence  $F(i, j)$  in this ROI was corrected for background fluorescence  $F_0$  and normalized to the soma fluorescence  $F_{\text{soma}}$  where 100% of the tissue is occupied by the astrocyte. The analysis was performed for each time point to generate a time course of astrocyte volume fraction over the entire experiment using Matlab.

$$A_{vf}(i, j) = \frac{F(i, j) - F_0}{F_{\text{soma}} - F_0}$$

$A_{vf}$  = astrocyte volume fraction;  $i, j$  = pixel coordinates in the x – y plane;  $F$  = fluorescence intensity;  $F_0$  = background fluorescence;  $F_{\text{soma}}$  = fluorescence inside the soma

#### 4.2.4 Characterization of astrocyte morphology changes

For further characterization of astrocyte morphology changes, the localization as well as the type of astrocyte morphology changes were analysed. To investigate where the astrocyte morphology changes occur, the strength of the observed volume fraction changes was calculated depending on the initial volume fraction of the processes. An initial volume fraction of 100 % represents the soma, whereas 10 % initial volume fraction represents a fine astrocyte process. To investigate the type of astrocyte morphology change, the segmentation was analysed. Pictures of a focal plane were taken for analysis. In this focal plane, parts of astrocyte processes are visible as different segments. The segmentation reflects the number of detectable astrocyte processes in this focal plane. Figure 12 visualises how this parameter can be analysed. The left panel shows astrocyte segments (Figure 11) in the resolution of diffraction-limited microscopy (Figure 12, left panel). It was binarised by setting an intensity threshold at the value of the volume fraction (Figure 12, right panel). The number of resolvable segments were counted and analysed for the different experimental conditions.

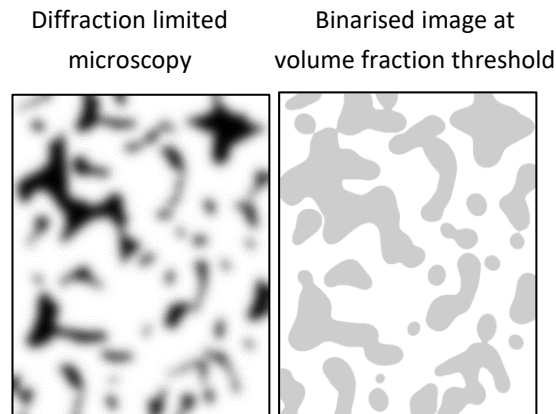


**Figure 12 Image processing for segmentation analysis.** The left panel shows astrocytic processes obtained from EM pictures (Figure 10) with the resolution of diffraction-limited microscopy. This image was then binarised by setting an intensity threshold at the value of the volume fraction. The resulting segments were counted and analysed in different experimental conditions (images adopted from C. Henneberger).

#### 4.2.5 Investigation of the underlying mechanism of astrocyte morphology changes

To investigate the underlying mechanism, which controls the astrocyte morphology changes, pharmacological studies were performed in hGFAP-EGFP mice containing astrocytes expressing EGFP under the GFAP promotor (Nolte et al., 2001). To this end, different drugs, which affect the adenylyl cyclase (AC) either directly or indirectly over a receptor were bath applied for 30 minutes after a 10 minutes baseline. For activation of AC, 10  $\mu\text{M}$  S1P or 50  $\mu\text{M}$  NKH477 and for inhibition of AC 20  $\mu\text{M}$  LPA or SQ 22536 were applied. Baseline and control recordings were performed in the presence of ethanol, Dimethylsulfoxid (DMSO) or normal ACSF respectively to which of these substances were required for diluting the used drug. To inhibit the Rho-associated protein kinase (ROCK), a downstream effector of AC and a regulator of the cytoskeleton, 20 or 5  $\mu\text{M}$  Y27632 were bath applied to hippocampal slices. For selectively targeting ROCK in astrocytes, 10  $\mu\text{M}$  Y27632 were added to the intracellular solution and brought into rat hippocampal astrocytes via whole-cell patch-clamp configuration. In the presence of this inhibitor, either in the bath or intracellularly, penicillin and control experiments were conducted as mentioned before. Images of astrocytes were obtained every 5 minutes during the entire experiment and volume fraction analysis was performed as described before (chapter 4.2.2 -4.2.3). Additionally, spontaneous epileptiform activity was investigated in these slices. To this end, the discharge frequency per minute and the discharge probability were calculated. The discharge probability was defined as probability, by which slices developed epileptiform discharges at a distinct time point.

#### 4.2.6 Visualisation of astrocyte dye coupling

Astrocyte networks were visualised by filling these with a fluorescent dye using whole-cell patch-clamp configuration in Wistar rats. Astrocytes were patched in the hippocampal CA1 stratum radiatum and in the molecular layer of the dentate gyrus to compare astrocyte dye-coupling in different brain regions (Anders et al., 2014). Gap junctions were described to be temperature-dependent (Bukauskas and Weingart, 1993). To investigate the sensitivity of the analysis of astrocyte dye-coupling (chapter 4.2.7), experiments were performed in room temperature (RT, experiments performed by D. Minge) and at 34°C. Astrocytes were filled with the morphology dye Alexa 594 (40  $\mu\text{M}$ ) using whole-cell patch-clamp configuration. Due to its size, this dye can diffuse through gap junctions and thus into neighbouring coupled astrocytes (Figure 13). This allowed to measure the dye-coupled network of astrocytes. The laser power was adjusted to 4 to 10 mW under the objective dependent on the depth of the initial cell, aiming a maximal laser power of 2 mW at the patched cell. Single image stacks (512 x 512 pixel, 0.65  $\mu\text{m}/\text{px}$ ) were obtained 20 minutes after opening the initial patched cell, which allowed the dye to diffuse into the gap-junction coupled astrocyte network. To capture the whole dye-coupled astrocyte network, the image stack was started in a depth, where the last fluorescent-coupled astrocyte was visible (max. 100  $\mu\text{m}$  in depth) towards the surface of the slice. Images were taken with a distance of 2  $\mu\text{m}$  in z-direction. Recording with an initial access resistance ( $R_s$ ) above 20  $\text{M}\Omega$  were discarded.

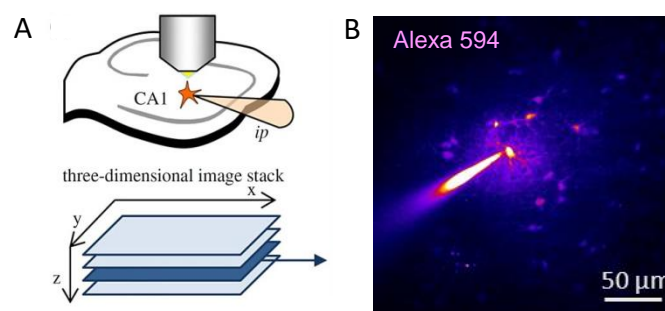


**Figure 13 Visualisation of astrocyte coupling in the CA1 stratum radiatum of the hippocampus.** (A) Astrocytes were filled with the morphology dye Alexa 594 using whole-cell patch-clamp configuration (upper panel). X-y-z image stacks were obtained 20 and 40 minutes after opening the initial cell (adopted from Anders et al., 2014). (B) Sample slice of an image stack with the initial cell in whole-cell configuration and the dye-coupled neighbouring astrocytes.

Furthermore, astrocyte dye coupling was observed under control and under epileptiform conditions. To this end, the described protocol for induction of epileptiform activity was

used. These data were obtained in parallel to monitoring astrocyte morphology. Since the morphology dye TR is a red fluorescent dye, the green fluorescent dye Alexa 488 (40  $\mu\text{M}$ ) was used to investigate astrocyte dye coupling in parallel. This allowed a separation of the two fluorescent signals. The first image stack 20 minutes after break in was used as baseline, whereas a second one was obtained 20 minutes later either in control or in penicillin conditions. To ensure a stable filling, in all experiments the access resistance ( $R_s$ ) was monitored during the entire experiment. Experiments with an initial  $R_s$  value higher than 30  $\text{M}\Omega$  were excluded.

#### 4.2.7 Analysis of astrocyte dye coupling

The analysis of astrocyte dye coupling was performed with Image J (Schindelin et al., 2015), Excel and Origin (version 9, OriginLab, US). The coupled cells were identified manually, their x-y-z position was measured and their mean maximal soma fluorescence intensity was determined in a region of interest of  $5 \times 5 \mu\text{m}^2$  in x-y plane centred on the soma. The fluorescence intensities depended monoexponentially on depth from the slice surface.

$$I_{\text{depth}} = I_0 \exp^{-z/\tau}$$

$I_{\text{depth}}$  = intensity in a certain depth,  $I_0$  = intensity on the surface,  $\tau$  = time constant,  $z$  = z-position

The measured soma intensities were corrected for the depth and for the background. The distance  $D_{\text{cell}}$  of each coupled cell relative to the initial patched cell was calculated from their x-y-z position according to the Pythagoras' theorem.

$$D_{\text{cell}} = \sqrt{(X_{\text{cell}} - X_0)^2 + (Y_{\text{cell}} - Y_0)^2 + (Z_{\text{cell}} - Z_0)^2}$$

The soma intensities were normalised to the soma intensity of the patched cell and plotted against the distance of each cell to the initial cell (Anders et al., 2014). The fluorescence decays from the initial cell monoexponentially. All plots were fitted with a monoexponential function using Origin and the time constant  $\tau$  of the decay was calculated and defined as the coupling length constant (Anders et al., 2014). This was used as parameter to investigate the coupling strength in different conditions.

#### 4.2.8 Fluorescence recovery after photobleaching

Fluorescence recovery after photobleaching (FRAP) was used to investigate the intracellular diffusivity in different conditions. On the one hand, the temperature dependence of astrocyte intracellular diffusivity was determined. On the other hand, the intracellular diffusivity under control and penicillin conditions was investigated. For these

experiments mice were used, which contain astrocytes expressing EGFP under the GFAP promotor (Nolte et al., 2001). EGFP is freely diffusing in the cytosol and does not escape through gap junctions or hemichannels. Thus, this fluorescent molecule can be used for intracellular diffusion measurements. A region of interest, in this case a line scan through the astrocyte soma and its thick and fine branches, was bleached for 500 ms (Figure 14). To bleach the region of interest the laser power under the objective was increased to 20-25 mW. After that, the shutter was closed for 1 sec and intact fluorescent molecules could diffuse into the bleached region of interest. When the shutter was opened again a recovery fluorescence could be detected (Figure 14). FRAP was performed under baseline conditions and 30 minutes later either under control or penicillin conditions to compare the intracellular diffusion under healthy and epileptiform conditions. During the entire time evoked and spontaneous fEPSPs were recorded to ensure epileptiform activity under penicillin conditions but also an intact slice until the end of the experiment. To quantify FRAP, the bleached fluorescence  $F_B$  and the recovery fluorescence  $F_R$  was measured and FRAP was calculated as follows:

$$FRAP = \frac{\Delta F_R}{\Delta F_B}$$

An increase in FRAP indicates an increase in the recovery fluorescence  $F_R$ , which would suggest that more intact fluorescent EGFP molecules diffused into the ROI after bleaching resulting in a higher recovery fluorescence  $F_R$ . Thus, an increase in FRAP would suggest an increase in intracellular diffusivity.

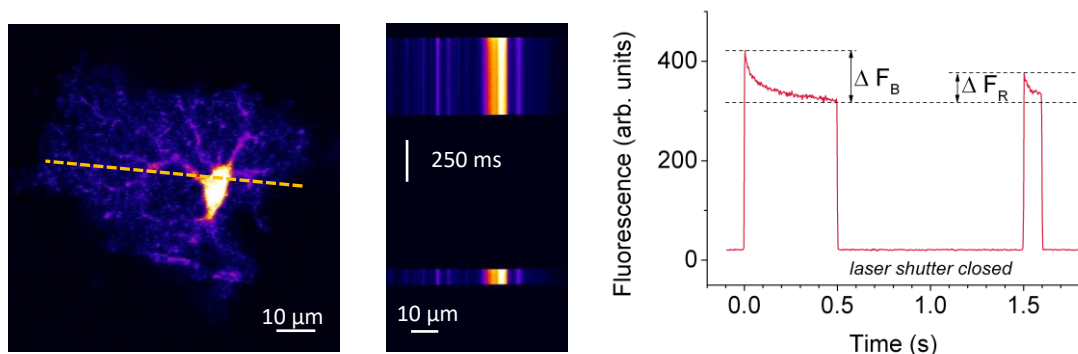


**Figure 14 FRAP experiments.** A line through an EGFP expressing astrocyte was bleached for 500 ms followed by laser shutting and reopening to capture recovery fluorescence. The middle panel shows an example of the corresponding line scan. The mean fluorescence intensity of the line scan was plotted (right panel). FRAP could be calculated by the ratio of  $F_R$  over  $F_B$ . A higher intracellular diffusivity would result in more intact fluorescent EGFP molecules diffusing into the bleached ROI and thus in a higher FRAP.

### 4.2.9 Imaging of neuronal morphology

To examine how neuronal morphology is affected by induction of epileptiform activity slices from mice were used, which contain neurons expressing YFP under the Thy1 promoter and astrocytes expressing EGFP under the GFAP promoter (chapter 3.1.3). This allowed to monitor neuronal morphology and astrocyte morphology in parallel. Epileptiform activity was induced as described before. For imaging, the Olympus two-photon setup was used with filters for YFP/CFP. Frame scans of 512 x 512 pixel were obtained every 5 minutes throughout the experiment and the z-position was carefully controlled in both channels. Since the wavelengths of GFP and YFP are very close to each other, linear unmixing (Tsurui et al., 2000; Zimmermann, 2005) was necessary before analysing the morphology changes in neurons and astrocytes. For this image processing a background region was required. To this end, the image area chosen always included an astrocyte with soma and processes, neuronal dendrites and a background region which could be a blood vessel for instance. Linear unmixing was done to separate the signals of the two fluorophores YFP and EGFP by an in house written analysis using Matlab. After separating the signals, the volume fraction of astrocytes was calculated as described before. To check whether neuronal morphology was altered after induction of epileptiform activity, also the neuronal volume fraction was calculated. To this end, a big dendrite of a neuron was defined as reference region (like soma region in astrocytes) and surrounding dendrites were chosen as region of interest. Using the same Matlab script as used for astrocyte volume fraction, the morphology changes of neurons were captured using the same analysis method.

### 4.2.10 Linear unmixing

Multichannel fluorescence imaging, in this case with YFP and EGFP, results in an overlapping emission spectra of the two fluorophores. Thus, in pictures, where the EGFP expressing astrocyte processes and the YFP expressing neuronal dendrites co-localize, it is not clear, which part of a pixel belongs to which structure. But for the separate analysis of morphological changes in neurons and astrocytes this information is required.

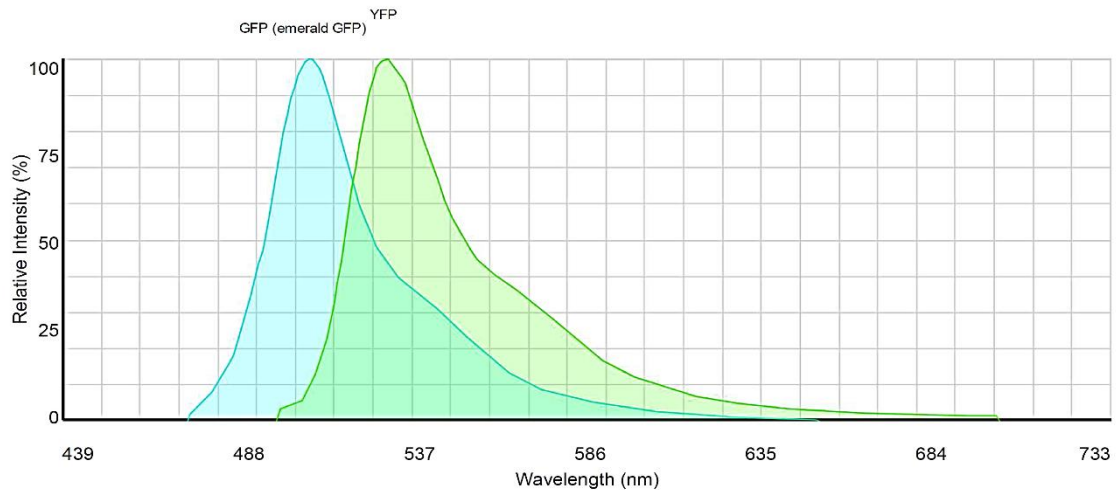


**Figure 15 Emission spectra of GFP and YFP.** The 2 emission spectra of GFP and YFP overlap, which requires a separating of the fluorescent signals using linear unmixing (adopted from Thermo Fisher Fluorescence Spectra Viewer).

Linear unmixing allows to analyse mixed contributions of the two fluorophores to a pixel (Lansford et al., 2001). The basic assumption for linear unmixing is that the detected fluorescent signal  $S$  for every channel is a linear combination of the contributing reference spectra of the fluorophores  $F$  with a defined weight  $A$  (Zimmermann, 2005).

$$S_1 = A_1 * F_1 + A_2 * F_2 \dots A_i * F_i$$

$$S_2 = A_1 * F_1 + A_2 * F_2 \dots A_i * F_i$$

To perform the linear unmixing using Matlab, first the background region was defined. Then, weights for the single fluorophores were obtained in each fluorescent channel. Several regions of interest were marked, which belonged either to the astrocyte structure (GFP) or to neuronal structures (YFP), respectively. Depending on the contribution of each fluorophore different summed spectra could be measured for each pixel. After the contribution for each fluorophore was calculated, the astrocyte and neuronal structures could be separated into two individual images, with which volume fraction analysis could be performed. For volume fraction analysis of dendrites a thick dendrite was used as reference region (soma region in astrocytes) and as region of interest a field including several dendrites with spines was chosen (Figure 28). Only slices, where astrocytes showed a significant morphology response were analysed for neuronal morphology changes.

#### 4.2.11 Calculation of the slice volume

To analyse whether induction of epileptiform activity leads to a change in slice volume, this parameter was calculated (analysis done by C. Henneberger). For calculation the known

imaging depth, which was automatically saved during imaging at the Olympus setup, and the slice thickness were used. The recorded z-position was measured at the beginning of a recording and 40 minutes later in control or penicillin conditions, respectively. With the assumption that the slice would swell or shrink with a distinct factor (expansion factor  $\alpha$ ), the measured z position would change with the same factor like the whole slice would shrink or expand (Figure 16). This factor was calculated for estimation how the slice volume changes over time.

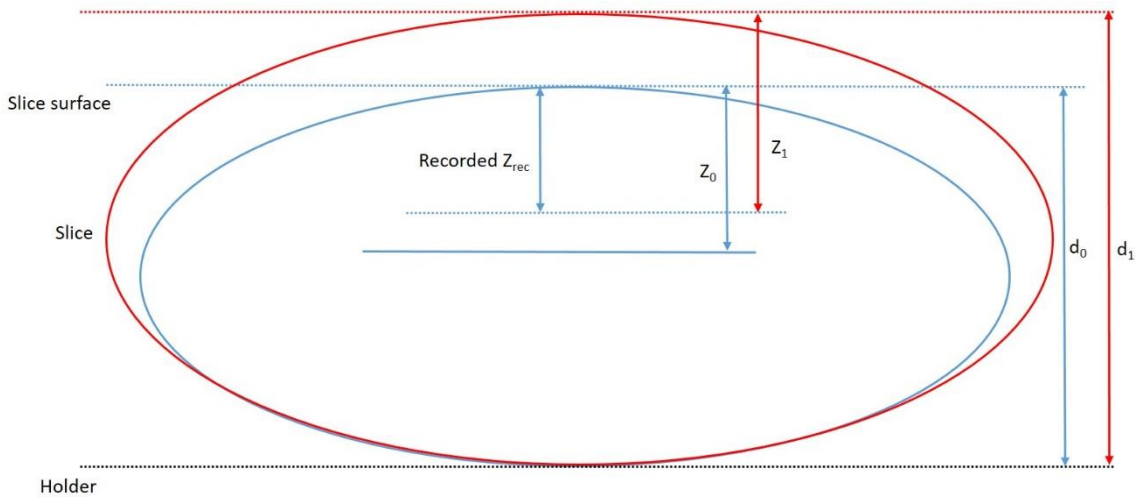


**Figure 16 Schematic for calculation of possible slice volume changes.** Blue indicates the slice volume at the beginning of the recordings. The recorded z-position of the imaged cell at the beginning ( $z_0$ ) would change with changes in slice volume. Red indicates the slice after possible swelling. The slice thickness ( $d$ ) and the recorded z-position would increase.

$$d_1 = \alpha * d_0, z_1 = \alpha * z_0$$

$d_0$  = slice thickness at timepoint zero,  $d_1$  = slice thickness at time point 40 minutes,

$z_0$  = recorded z-position at time point zero,  $z_1$  = recorded z-position at timepoint 40 minutes

The slice thickness at the beginning of the recording ( $d_0$ ) was known. Also the z-position of the focal plane of the cell at the beginning of the recording ( $z_0$ ) and at the end of a recording are measured ( $z_{rec}$ ). The expansion factor was calculated as follows for control and penicillin recordings and the averaged values for each group were compared statistically.

$$\alpha = \frac{z_1}{z_0} = \frac{z_{rec} - d_0}{z_0 - d_0}$$

#### 4.2.12 Imaging of extracellular glutamate levels using the glutamate sensor iGluSnFR

To investigate the extracellular glutamate levels after induction of epileptiform activity, the glutamate sensor iGluSnFR (Marvin et al., 2013) was expressed in astrocytes to visualise glutamate (chapter 4.1.2). To investigate if the extracellular glutamate levels are altered after induction of epileptiform activity, glutamate imaging was performed after a complete experiment. After a 10 minutes baseline recording, penicillin was bath applied for 30 minutes or control recordings were performed, respectively. Subsequently, synaptic transmission and neuronal activity was inhibited, by blocking voltage gated  $\text{Na}^+$  channels (TTX, 1  $\mu\text{M}$ ), NMDA receptors (APV, 50  $\mu\text{M}$ ), AMPA receptors (NBQX, 20  $\mu\text{M}$ ) and metabotropic glutamate receptors (mGluRs, Ly341495, 100  $\mu\text{M}$ ). For imaging glutamate levels, an astrocyte expressing iGluSnFR in the CA1 stratum radiatum was chosen. A region of interest (ROI) for a line scan in the periphery of the astrocyte was chosen randomly. The iontophoresis pipette had a resistance of ca. 80  $\text{M}\Omega$ , which was checked always before using. It was filled with L-glutamate (150 mM, pH adjusted to 7) and Alexa633 (40  $\mu\text{M}$ ) to visualise the position of the pipette. L-glutamate was applied with iontophoresis (MVCS-02C, npi, Germany) for 250 ms and line scans were performed at a frequency of 300 to 1000 Hz close to the middle of the scanned line with a distance  $< 1\mu\text{m}$  (Figure 17). The iGluSnFR fluorescence signal was captured using a wavelength of 910 nm. Two different amplitudes were used for iontophoretic injections of glutamate. 100 nA were used to reach a rapid and saturated iGluSnFR fluorescence. This was used as maximum fluorescence ( $F_{\text{max}}$ ).

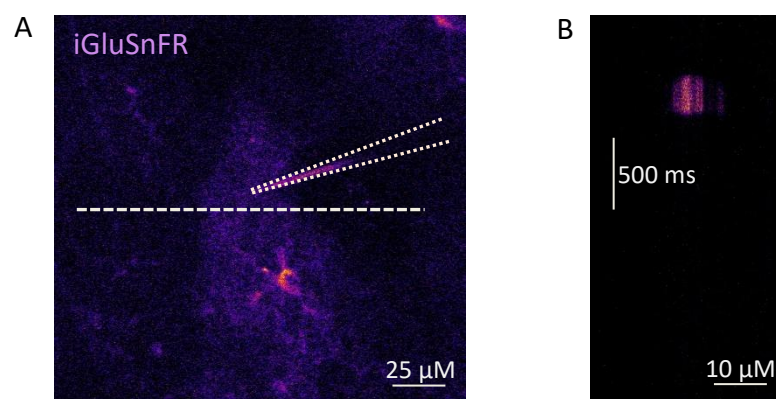


**Figure 17** Example of glutamate imaging using the glutamate sensor iGluSnFR. (A) Astrocyte expressing iGluSnFR. Glutamate was applied using iontophoresis (pipette, puncted lines) in the periphery of an astrocyte. Linescans were performed 1  $\mu\text{m}$  away from glutamate application. (B) Corresponding line scan with iGluSnFR response to a 10 nA pulse.

A pulse of 10 nA was used to translate the glutamate fluorescence transients ( $F$ ) into glutamate concentrations (Figure 46). Both line scans were background-corrected. The background-corrected resting fluorescence was used as fluorescence without glutamate bound ( $F_0$ ). Each image was binned by 30 pixels on the x-axis and 3 lines on the y-axis. The dissociation constant ( $K_d$ ) of iGluSnFR was determined before (4.3  $\mu$ M).

$$[Glu] = K_D * \frac{F - F_0}{F_{\max} - F}$$

Each translated glutamate concentrations profile was fitted to obtain the time constant  $\tau$  of glutamate accumulation (Figure 46).

$$[Glu] = A(1 - e^{-\frac{t}{\tau}})$$

The time constants of the glutamate profile of each cell was averaged in control or penicillin recordings, respectively, and the averaged values were compared statistically.

### 4.3 Statistics

All statistical analyses were done with Excel (Microsoft Excel 2010, US) and Origin (OriginLab, version 9, US). All data were tested for normality using the Shapiro-Wilk test. When datasets were distributed normally, unpaired data points were compared using the two-sample t-test. These datasets were tested for variance using the two-sample test for variance and Welch correction was used, when variances showed significant differences between the groups. Paired data were analysed using the paired-sample t-test, if these datasets were normally distributed. When datasets were not normally distributed, non-parametric tests were used, which will be indicated in the text and the figures.

## 5. Results

### 5.1 Induction of epileptiform activity leads to astrocyte morphology changes

The first aim of this study was to find out, if induction of epileptiform activity in acute hippocampal slices is accompanied by astrocyte morphology changes and if so, at which timescale these morphology changes occur. This question was addressed by performing the experiments described in the following chapters. In parallel to the induction of epileptiform activity in acute hippocampal slices, astrocyte morphology was monitored simultaneously with two-photon excitation microscopy.

#### 5.1.1 Induction of epileptiform activity in acute rat hippocampal slices

To investigate the role of acute astrocyte morphology changes during epileptiform activity a protocol for induction of mild epileptiform activity in acute hippocampal slices was established. It was necessary to find a suitable protocol that allowed electrophysiological recordings and imaging of the astrocytes together. Different *in vitro* models were tested under interface and submerged conditions. For imaging experiments slices needed to be used in a submerged chamber, thus, it was important to induce reliable epileptiform activity under this conditions. Increasing the extracellular  $K^+$  concentration ( $[K^+]_{ex}$ ) to 12 mM resulted in epileptiform activity in both conditions, which was not reliable when used in a submerged chamber. Reduction of the extracellular  $Mg^{2+}$  concentration also led to epileptiform discharges under both conditions, but they occurred with low frequency. For further analysis a model inducing a higher number in discharges was more suitable, because this allows to capture possible changes in epileptiform activity. The best suited *in vitro* model for epileptiform activity was bath application of penicillin for 30 minutes in a submerged chamber. Using this model reliable epileptiform discharges in a high number could be evoked. This model was firstly described by Walker et al., 1945. Penicillin blocks the chloride channel of the  $GABA_A$  receptors which leads to a disinhibition and thus a higher excitability of the neurons (Tsuda et al., 1994). As described in chapter 4.2.2, visualisation of astrocytes was either performed by filling them with a morphological dye via whole-cell patch-clamp recordings, done in adult Wistar rats, or by genetic expression of the enhanced green fluorescent protein (EGFP) in astrocytes under the GFAP promotor in hGFAP-EGFP mice (Nolte et al., 2001). Epileptiform activity was induced in rat hippocampal slices (Figure 18) as well as in mouse hippocampal slices (Figure 22) under submerged conditions. Slices were placed on a grid (original idea by Ivan Pavlov, UCL London) in the submerged chamber to ensure a proper perfusion (Figure 18A, see also 4.1.4). For stable induction of

epileptiform activity it was necessary to slightly increase the extracellular K<sup>+</sup> concentration, which was held constant during baseline-, control- and penicillin recordings. In rat hippocampal slices the extracellular K<sup>+</sup> concentration of the ACSF was 5 mM whereas in mouse hippocampal slices 4 mM of extracellular K<sup>+</sup> were used, as higher extracellular K<sup>+</sup> concentrations led to unstable baseline- and control recordings. Epileptiform discharges were recorded in the CA1 stratum pyramidale using a field electrode (Figure 18). Slices, which had no stable baseline activity or showed a neuronal hyperexcitability were discarded. This was important to ensure that the later analysed morphology changes of astrocytes are comparable between baseline-, control- and penicillin conditions. Figure 18A shows the recording configuration in rat hippocampal slices. Under control conditions, the neuronal network activity stayed stable and no spontaneous epileptiform discharges could be observed (Figure 18B, C). Application of penicillin after 10 minutes baseline recording reliably induced mild interictal epileptiform discharges (Figure 18B). The right panel shows an example of a typical epileptiform discharge, which had a mean amplitude of  $0.59 \pm 0.08$  mV ( $n = 12$ , Figure 18E). The mean amplitude was calculated from all single epileptiform discharges in one recording and the means of the single recordings were compared statistically (chapter 4.1.5). Epileptiform discharges typically occurred within 5 minutes after application of penicillin. The frequency of epileptiform discharges was calculated by counting the number of discharges per minute. It reached a plateau level 10 to 15 minutes after induction (Figure 18C). They occurred with a mean frequency of  $8.12 \pm 1.80 \text{ min}^{-1}$  ( $n = 12$ , Figure 18D).

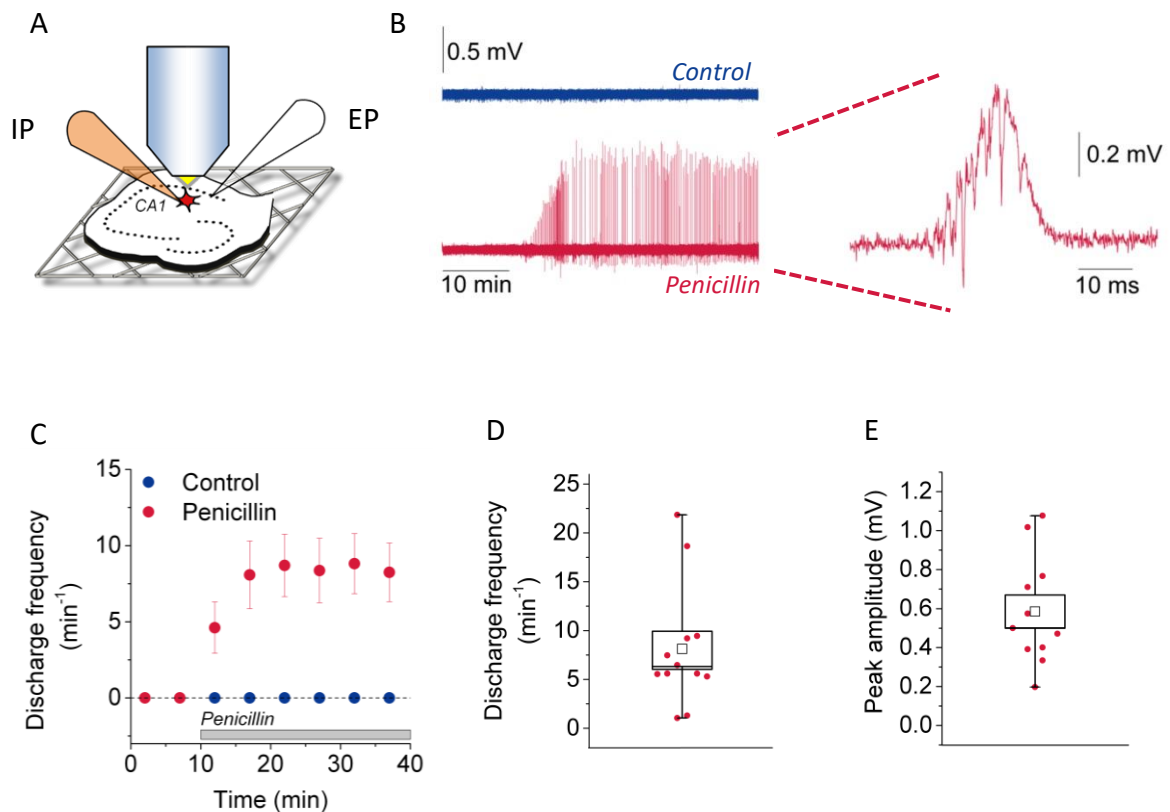


**Figure 18 Induction of epileptiform activity in the CA1 region of rat hippocampal slices.** (A) Recording configuration in the CA1 region of the hippocampus. Ep: extracellular pipette for field potential recordings in the stratum pyramidale, ip: intracellular pipette for visualisation of astrocytes in whole-cell patch-clamp configuration. (B) 40 minute-traces of control (blue) and penicillin (red) recordings. Application of 4 mM penicillin led reliably to epileptiform activity with typical discharges (right panel), (C) Discharge frequency per minute reached a stable level 10 to 15 minutes within application of penicillin activity with a mean frequency of  $8.12 \pm 1.80 \text{ min}^{-1}$  (D,  $n = 12$ ) and a mean amplitude of the  $0.59 \pm 0.08 \text{ mV}$  (E,  $n = 12$ ).

### 5.1.2 Astrocyte morphology changes during epileptiform activity in acute rat hippocampal slices

In parallel to the induction of epileptiform activity in rat hippocampal slices astrocyte morphology was monitored online using two-photon excitation microscopy. For visualisation of astrocyte morphology the astrocyte was held in whole-cell configuration and filled with the morphology dye Texas red dextran (TR, 3kDa). Due to its size this dye does not diffuse through astrocyte gap junctions. It was important to ensure a stable soma intensity, because the calculation of the astrocyte volume fraction depends on the soma dye intensity. Alterations in the soma intensity would artificially change the measured astrocyte volume fraction (see also 4.2.3). Figure 19A shows a patched astrocyte in differential interference contrast (DIC) microscopy and in the red fluorescent channel filled with TR. Astrocytes were identified by their low membrane resistance which was

calculated from somatic voltage responses to current steps (see also chapter 4.1.7). Figure 19B shows a typical voltage response due to current steps applied to the soma via the patch pipette. The left panel shows the current steps from -200 pA to + 200 pA in 100 pA steps. On the right panel an example of the typical somatic voltage response to the single current steps is shown. Due to the capacitance of the cell membrane the voltage response is rather a curve than a square. When the response reaches the plateau the membrane is recharged completely. This plateau phase was then used to calculate the membrane resistance via Ohm's law (chapter 4.1.7). The membrane resistance of the recorded astrocyte was  $3.65 \pm 0.30 \text{ M}\Omega$  ( $n = 13$ ). For successful imaging over the entire experiment cells needed to be held in whole-cell configuration with stable access resistance ( $R_s$ ) for more than 1 hour at 34°C. The access resistance was calculated from somatic current responses to voltage steps also applied via the patch pipette (Figure 19C). As described in more detail in chapter 4.1.7 the initial peak of the response was used for the calculation of the access resistance using also Ohm's law. The mean baseline  $R_s$  of all recorded astrocytes was  $10.02 \pm 0.98 \text{ M}\Omega$  ( $n = 13$ ) whereby statistical analysis revealed that, neither during baseline recordings nor at the end of control or penicillin recordings, the access resistance was significantly different between control and penicillin group (baseline recordings,  $p = 0.47$ , control  $R_s = 10.1 \pm 1.0$ , penicillin  $R_s = 13.4 \pm 3.7$ ; control/penicillin recordings,  $p = 0.93$ , control  $R_s = 20.7 \pm 2.1$ , penicillin  $R_s = 20.3 \pm 3.5$ , unpaired two-sample t-test, not illustrated).

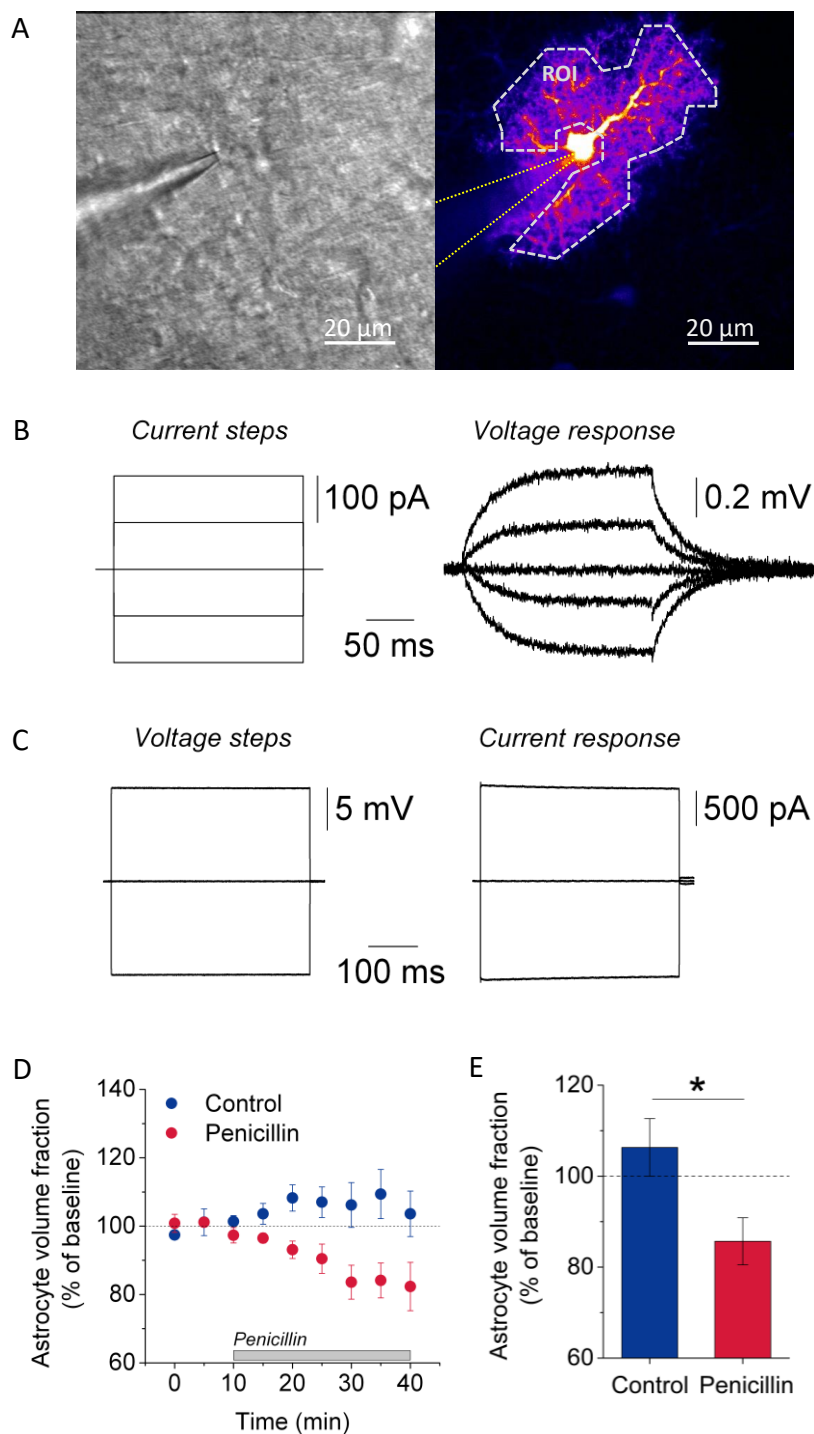


**Figure 19 Astrocyte volume fraction decreases upon induction of epileptiform activity in rat hippocampal slices.** (A) left picture shows the patched cell in the slice with DIC optics, right panel shows the patched astrocyte filled with the morphology dye TR. (B) example traces of somatic current stimulation (left panel) and the corresponding somatic voltage response (right panel) used to estimate the membrane resistance. (C) Example traces of 10 mV voltage steps (left panel) and the corresponding current responses (right panel) used to calculate the access resistance (D) time course of astrocyte volume fraction, induction of epileptiform (red) activity leads to a significant decrease of astrocyte volume fraction compared to control (E, blue,  $p = 0.027$ ,  $n = 6$  for each group, unpaired two-sample t-test).

In addition to the stable access to the astrocyte, also the z-position of was carefully adjusted to always image the same focal plane to allow a proper analysis of astrocyte morphology changes which are not caused by changes in the focal plane. Images were taken every 5 minutes and as an indirect read-out for astrocyte morphology changes the volume fraction in the indicated region of interest (ROI, Figure 19A, right panel) of a single astrocyte was estimated for each time point (see also chapter 4.2.3). The aim was to capture astrocyte morphology changes in the periphery, where all fine and fuzzy astrocyte processes are located. These fine processes often have sizes smaller than 1 nm as shown in Figure 20. Since changes in this scale cannot be resolved by diffraction limited microscopy, an indirect read out was required. This indirect readout was the astrocyte volume fraction (Medvedev et al., 2014). The baseline mean volume fraction of all monitored astrocytes was  $4.3 \pm 0.3$  %. In rat hippocampal slices astrocyte volume fraction stayed stable over 40 minutes of control recordings with a volume fraction of  $106.3 \pm 6.3$  % of baseline during the last 10 minutes of recording (Figure 19D, E, n = 6, indicated in blue). However, induction of epileptiform activity by using penicillin led to a significant decrease of the astrocyte volume fraction by  $15.2 \pm 5.3$  % compared to baseline and 21.5 % compared to control recordings during the last 10 minutes ( $p = 0.027$ ,  $n = 6$ , unpaired two-sample t-test, Figure 19D, E, indicated in red). The decrease in astrocyte volume fraction started within 10 minutes of penicillin application and reached a stable level after further 10 minutes (Figure 19D).

Taken together, these results show that bath application of penicillin induces stable epileptiform activity in rat hippocampal slices under submerged conditions. More importantly, the induction of epileptiform activity is accompanied by a rapid decrease of astrocyte volume fraction on a timescale of minutes.

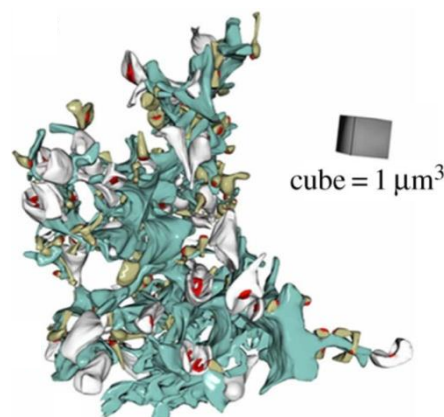


**Figure 20 Three-dimensional reconstruction of astrocyte fragments with adjacent synapses.** Green shows an astrocyte reconstructed in 3 dimensions together with dendritic spines (grey and dark yellow), equipped with postsynaptic densities (red). The cube is used as scale (Medvedev et al., 2014).

### 5.1.3 Induction of epileptiform activity in mouse hippocampal slices

The role of acute astrocyte morphology changes during epileptogenesis was also investigated in hGFAP-EGFP mice (chapter 3.1.2). The advantage of this animal model was that astrocytes could be visualised by genetic expression of the enhanced green fluorescent protein (EGFP) and did not require whole-cell patch-clamp configuration. The advantage of patching the cell is the possibility to control the inner cell milieu and to ensure that the cell is healthy and alive during the entire experiment. The disadvantage of patching the cell is that the astrocyte cytosol is diluted by the intracellular solution of the pipette, which may lead to a washout of important factors responsible for cell morphology. Thus, the morphology response to epileptiform activity in rat hippocampal slices could have been artificially altered by patching the cell. To this end, genetically altered mice were used containing EGFP-expressing astrocytes under the human GFAP promoter (Nolte et al., 2001). EGFP diffuses freely in the cytosol and does not escape through gap junctions. For this reasons, these astrocytes could be used for imaging experiments and analysis of the astrocyte volume fraction. To ensure that the endogenous expressed EGFP is comparable to using Texas red dextran, a subset of experiments was performed in collaboration with Daniel Minge and Christian Henneberger (Figure 21). EGFP-expressing astrocytes were held in cell-attached modus and 5 pictures of the astrocyte were obtained. Subsequently, the patch configuration was switched to whole-cell configuration and the astrocyte was filled with Texas red dextran. 15 minutes after opening the cell again 5 pictures were obtained with two-photon excitation microscopy. The volume fraction of the labelled astrocyte was analysed for the EGFP signal as well as for the Texas red dextran signal. Comparison revealed that astrocyte volume fractions monitored using either genetically expressed EGFP or gap-junction impermeable Texas red dextran showed a perfect match and a linear positive correlation (Figure 21,  $n = 13$ ,  $R^2 = 0.978$ ,  $p < 0.001$ , analysis done by C. Henneberger). This verified that EGFP expressing astrocytes were a useful tool to investigate astrocyte morphology changes during epileptiform activity.

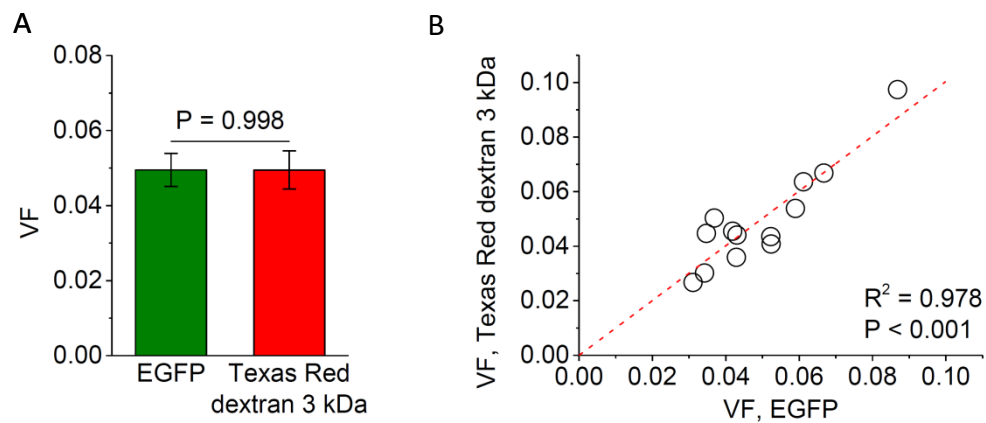


**Figure 21 Astrocyte volume fractions of EGFP labelled astrocytes and subsequently filled with Texas red dextran.** (A) Average astrocyte volume fraction values of EGFP labelled astrocytes and subsequently patched and filled with Texas red dextran (data obtained in collaboration with D. Minge). (B) Volume fraction values of EGFP labelled astrocytes are plotted against volume fraction values measured with Texas red dextran, red line: linear regression ( $n = 13$ ,  $R^2 = 0.978$ ,  $p < 0.001$ , analysis done by C. Henneberger, figure adopted from C. Henneberger).

Epileptiform activity was induced in acute hippocampal slices of mice containing EGFP expressing astrocytes. The used protocol was the same as used for recordings from rat hippocampal slices, but the extracellular  $K^+$  concentration was 4 mM instead of 5 mM used for rat slices, because higher extracellular  $K^+$  concentrations led to unstable baseline- and control recordings. Bath application of penicillin induced mild ictal epileptiform discharges (Figure 22A) with the characteristic shape (Figure 22A, right panel). In contrast to rat hippocampal slices, where epileptiform activity occurred in 100% of the slices exposed to penicillin, the slices of mouse hippocampi showed a higher failure rate in developing epileptiform activity. This means that in slices from some animals no epileptiform activity at all could be induced after bath application of penicillin. Control recordings were only used for analysis when slices from the same animals were able to develop epileptiform discharges after application of penicillin. Female and male mice were used. Male mice showed a success rate of 75% for developing epileptiform discharges whereas female mice only displayed a success rate of 50%. This means that in 75% or 50% of the animals respectively, at least one slice developed epileptiform seizures on an experimental day. The first epileptiform discharges occurred within 5 minutes and a stable level was reached within 15 to 20 minutes of penicillin application (figure 8B,  $n = 10$ ) with a plateau frequency of  $6.78 \pm 1.38 \text{ min}^{-1}$  (Figure 22C,  $n = 10$ ). The mean discharge amplitude was  $0.50 \pm 0.08 \text{ mV}$  (Figure 22D,  $n = 10$ ). Compared to the observed epileptiform discharges in rat, epileptiform discharges in mouse hippocampal slices had a non-significant trend towards

lower amplitude and plateau frequency compared to rat hippocampal slices (Figure 22E, F, frequency:  $p = 0.77$ ,  $n = 12$  for rat,  $n = 10$  for mouse, Mann-Whitney-U test; amplitude:  $p = 0.47$ , unpaired two-sample t-test).

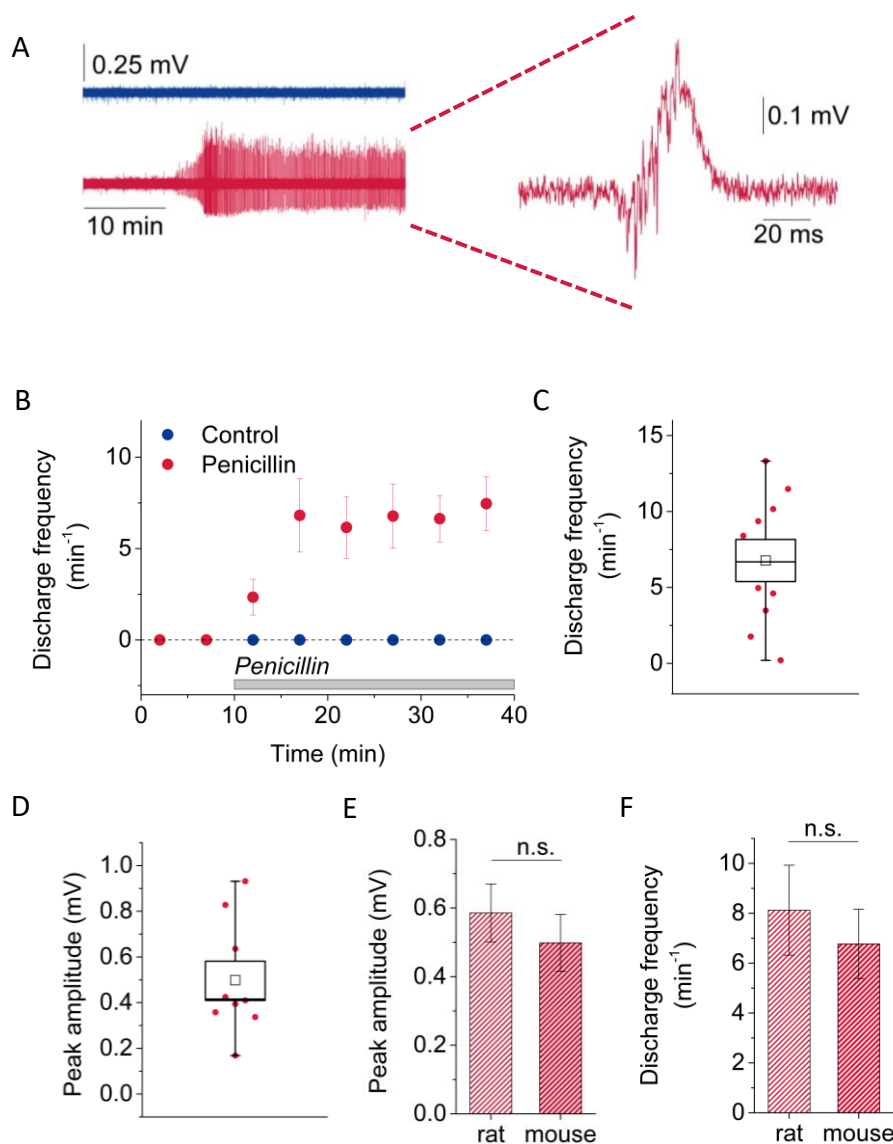


**Figure 22 Induction of epileptiform activity in mouse hippocampal slices.** (A) 40 minute-traces of control (blue) and penicillin (red) recordings. Application of 4mM penicillin led to reliable epileptiform activity, right panel shows a typical single discharge. (B) Discharge frequency per minute reached a stable level 10 minutes after induction of epileptiform activity. The discharges occurred with a mean peak frequency of  $6.78 \pm 1.38 \text{ min}^{-1}$  (C,  $n = 10$ ). The mean amplitude of the recorded discharges was  $0.50 \pm 0.08 \text{ mV}$  (D). No significant changes could be observed concerning amplitude (E,  $p = 0.47$ , unpaired two-sample t-test) and frequency (F,  $p = 0.77$ , Mann-Whitney-U test) of discharges between rat ( $n = 12$ ) and mice ( $n = 10$ ) hippocampal slices.

To investigate if the observed results in epileptiform activity as well as in astrocyte morphology changes (Chapter 5.2) are not only induced by the penicillin model, experiments were repeated with another well-established model for induction of epileptiform activity in acute hippocampal slices of hGFAP-EGFP mice (Nolte et al., 2001). The penicillin model was described to produce interictal activity *in vitro* (Schwartzkroin and Prince, 1977). Epileptiform activity *in vivo* has been categorized as ictal, meaning during a seizure, postictal, meaning after a seizure and interictal, meaning between seizures (Fisher et al., 2014). Interictal activity is defined by spikes lasting less than 80 ms and sharp waves lasting 80 to 120 ms (Curtis de and Avanzini, 2001). Since epileptiform activity also consists of ictal discharges, a model described to develop both ictal and interictal events was chosen (Traub et al., 1994). To this end, zero  $Mg^{2+}$  and bicuculline were applied to the slice ( $n = 8$ , chapter 4.1.4). This procedure also led to reliable epileptiform activity although with different types of epileptiform discharges in 100% of the animals. Ictal and interictal components could be observed (Figure 23A) whereas between big ictal components (Figure 23B) also interictal events occurred (Figure 23C). Ictal discharges could be characterized by a big initial discharge followed by a burst of afterdischarges with smaller amplitudes (Figure 23B). The mean amplitude of the initial discharges was  $0.76 \pm 0.09$  mV (Figure 23G) and they occurred with a frequency of  $0.425 \pm 0.15$   $min^{-1}$  (Figure 23D, F). The interictal discharges (Figure 23C) recorded in between of ictal events had a similar waveform like the ones recorded in penicillin treated slices (Figure 23A). They occurred with a mean frequency of  $0.58 \pm 0.07$   $min^{-1}$  (Figure 23E, F) and a mean amplitude of  $0.47 \pm 0.07$  mV (Figure 23G). Although the amplitude was comparable to the amplitude of epileptiform discharges induced by application of penicillin, the frequency was 10 fold smaller in the 0  $Mg^{2+}$  / Bicuculline model. Both, interictal and ictal discharges, did not reach a frequency plateau but increased over time (Figure 23D, E) and did not differ significantly in their mean frequencies over the last 10 minutes of recording ( $n = 6$  for both groups,  $p = 0.38$ , unpaired two-sample t-test, figure 23F). Taken together, in this model fewer epileptiform discharges could be observed, but within ictal activity more epileptic bursts were produced. Thus, epileptiform discharges did not occur equally distributed over time like observed after application of penicillin, but rather occurred in bundles at distinct time points. Beside their waveform interictal and ictal activity could be clearly distinguished by their mean peak amplitude, which was significantly lower in interictal discharges than in ictal discharges ( $n = 8$  for both groups,  $p = 0.0302$ , unpaired two-sample t-test, figure 23G).

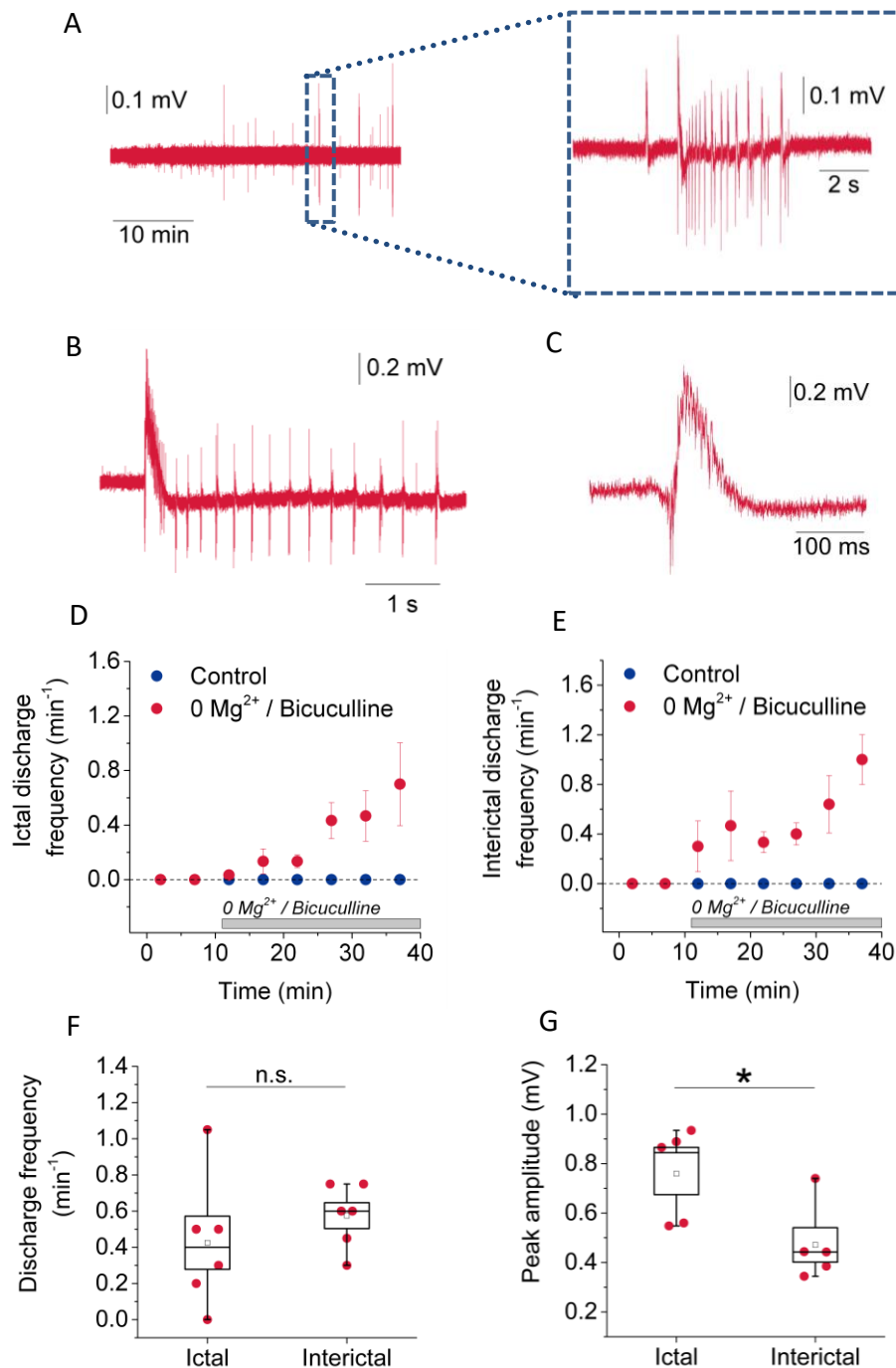


**Figure 23 Induction of epileptiform activity by bath application of 0  $\text{Mg}^{2+}$  and bicuculline.** This protocol led to ictal and interictal discharges (A); Ictal discharges consisted of one initial great discharge followed by a burst of afterdischarges (B). Interictal discharges (C) occurred in between of ictal discharges with a similar frequency 5 to 10 minutes after drug application (D, E). The frequency by which both types of discharges occurred was not significantly different (F,  $n = 8$ ,  $p = 0.38$ , unpaired two-sample t-test). In contrast, the initial discharges of ictal events occurred with a significant higher amplitude compared to interictal events (G,  $n = 8$ ,  $p = 0.0302$ , unpaired two-sample t-test).

#### 5.1.4 Astrocyte morphology changes during epileptiform activity in acute mouse hippocampal slices

As done for rat hippocampal slices astrocyte morphology in mouse hippocampal slices was monitored in parallel to the induction of epileptiform activity. Pictures were taken every 5 or 10 minutes, when using the penicillin or 0 Mg<sup>2+</sup>/ bicuculline model, respectively. The astrocyte volume fraction was calculated for each time point (see also chapter 4.2.2). Figure 24A shows an astrocyte genetically expressing EGFP and astrocyte morphology changes were analysed in the indicated region of interest (ROI). The baseline mean volume fraction of all used EGFP-expressing astrocytes was  $5.8 \pm 0.6 \%$  ( $n = 31$ ). After induction of epileptiform activity using bath application of penicillin the astrocyte volume fraction decreased significantly by  $14.1 \pm 2.2\%$  compared to baseline and  $14.2 \%$  compared to control ( $p = 0.00037$ , control  $n = 13$ , penicillin  $n = 18$ , unpaired two-sample t-test, figure 24B, D). Under control conditions no changes in astrocyte volume fraction could be observed (Figure 24B, D). The astrocyte volume fraction was  $100.2 \pm 2.9 \%$  of baseline during the last 10 minutes of recording. To rule out any direct effect of penicillin on astrocyte morphology, the volume fraction was monitored in presence of the voltage gated sodium channel blocker TTX, the NMDA receptor blocker APV and the AMPA receptor blocker NBQX to silence neuronal activity and synaptic transmission. Under this condition penicillin alone had no effect on astrocyte volume fraction (Figure 24C, D, grey bar,  $p = 0.82$  compared to control,  $n = 4$ , unpaired two-sample t-test). This shows, that astrocyte morphology changes required neuronal activity and penicillin alone does not affect astrocyte morphology.

Astrocyte morphology was also monitored when epileptiform activity was induced using 0 Mg<sup>2+</sup> and bicuculline. Also using this model, epileptiform activity could be induced reliably. Like observed in experiments with penicillin, the astrocyte volume fraction significantly decreased by  $9.7 \% \pm 2.9 \%$  during epileptiform activity compared to control conditions ( $p = 0.042$ , unpaired two-sample t-test, control  $n = 13$ , 0 Mg<sup>2+</sup> / Bicuculline  $n = 8$ , figure 24E, F).

Taken together, the data indicate that epileptiform activity was reliably induced in acute rat and mouse hippocampal slices using penicillin, in the mouse hippocampal slices also with 0 Mg<sup>2+</sup> and bicuculline. In both species and with both *in vitro* epilepsy models, induction of epileptiform activity was accompanied by a significant decrease of astrocyte volume fraction within the timescale of minutes.

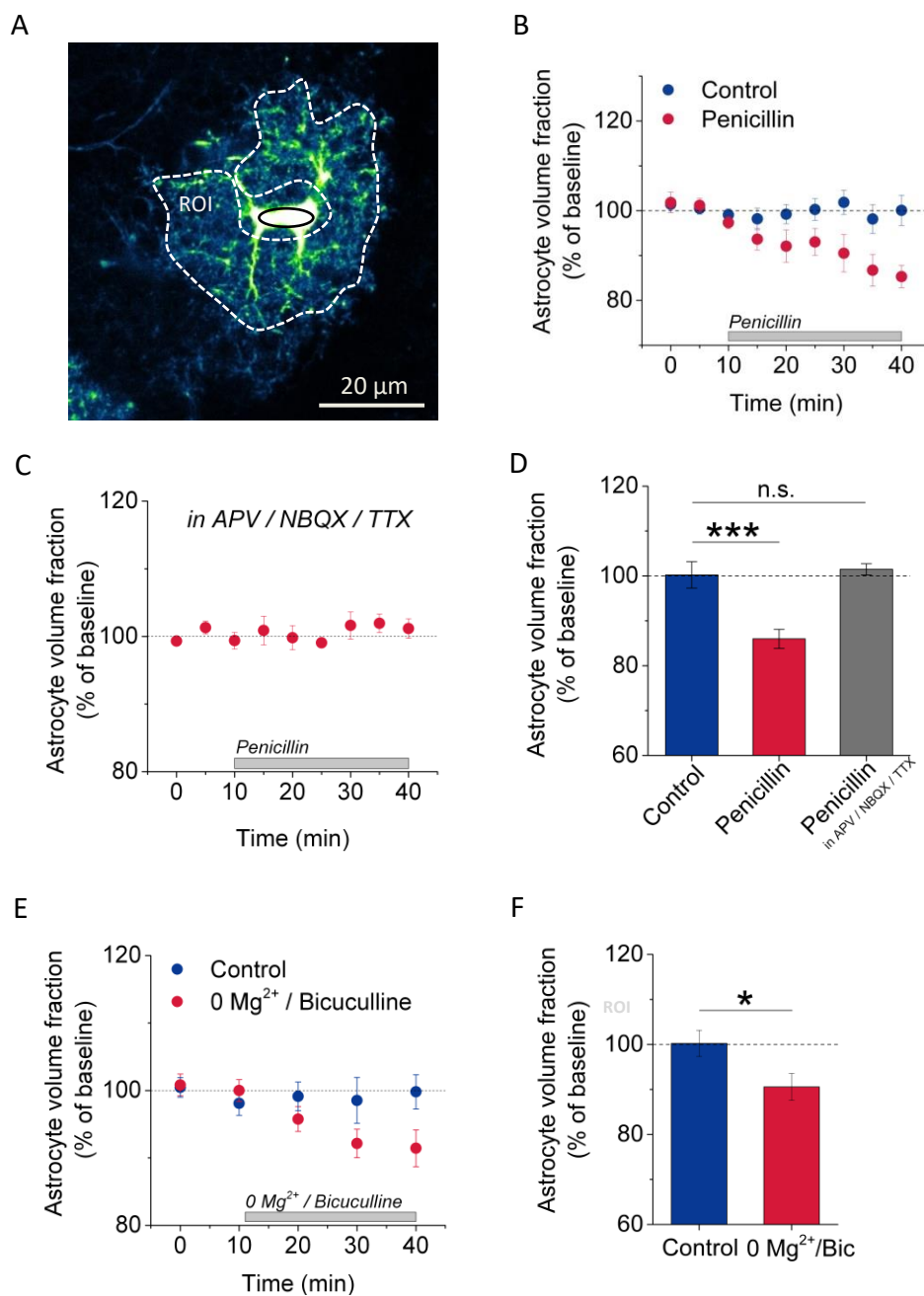


**Figure 24 Astrocyte volume fraction changes upon induction of epileptiform activity with penicillin.** (A) Example of EGFP-expressing astrocytes with analysed ROI. (B) time course of astrocyte volume fraction normalized to baseline in mouse hippocampal slices, 30 minutes after application of penicillin astrocyte volume fraction shows a significant decrease of  $13.4 \pm 2.4 \%$  (D,  $n = 13$  for control,  $n = 18$  for penicillin,  $p = 0.00079$ , unpaired two-sample t-test). Penicillin alone with inhibited neuronal activity and synaptic transmission had no effect on astrocyte volume fraction (C, D, grey bar). Repeating experiments with  $0 \text{ Mg}^{2+}$  and bicuculline as model for epileptiform activity also led to a significant decrease of astrocyte volume fraction (E, F,  $n = 8$  for  $0 \text{ Mg}^{2+}$  and bicuculline,  $p = 0.042$ , unpaired two-sample t-test). Control recordings were pooled with control recordings from penicillin experiments.

## 5.2 Characterisation of astrocyte morphology changes induced by epileptiform activity

The experiments presented so far uncovered that indeed astrocyte morphology changes occur in the acute phase of induction of epileptiform activity on a time scale of minutes. In the following subchapters the observed astrocyte morphology changes will be characterized in more detail. The aim is to clarify, how long these morphology changes persist, what type of morphology changes can be observed and if neuronal morphology is also affected by induction of epileptiform activity *in vitro*.

### 5.2.1 Persistence of epileptiform activity and astrocyte morphology changes

To investigate how astrocyte morphology and epileptiform activity develop after removing penicillin as stimulus for epileptiform activity, penicillin was washed out after 30 minutes of application and electrophysiological recordings as well as imaging of astrocyte morphology were continued for another 40 minutes in hGFAP-EGFP mice. After washout epileptiform activity decreased and finally persisted with a lower frequency of  $0.79 \pm 0.29$  discharges per minute in mouse hippocampal slices (Figure 25A). As an additional parameter, the discharge probability was analysed (see chapter 4.1.5). It describes the probability by which a slice showed epileptiform discharges at a given time point. For each time point the percentage of slices displaying epileptiform discharges were counted and normalized to all measured slices. Although the frequency was reduced during penicillin washout the discharge probability stayed overall constant after washout with a decrease from 93% to 66% at time point 80 minutes (Figure 25B). In parallel to the epileptiform activity, astrocyte morphology was monitored during washout of penicillin. The time course (Figure 25C) illustrates that astrocyte volume fraction stayed on the formerly acquired decreased level during the 40 minutes washout with a stable significant difference compared to control recordings ( $n = 6$  for both groups,  $p = 0.047$ , unpaired two-sample t-test, Figure 25D). Thus, these experiments revealed that epileptiform activity as well as astrocyte morphology changes persisted after washout of penicillin. It remained unclear, if the remaining epileptiform activity causes the persistent decrease in astrocyte volume fraction or if these morphology changes maintain the ongoing epileptiform activity. To address this question, astrocyte morphology was measured when neuronal activity was inhibited during washout of penicillin using TTX (Figure 25E). Epileptiform discharges immediately stopped when TTX was applied, but interestingly, the decrease of astrocyte volume fraction stayed stable during washout of penicillin with inhibited neuronal activity (Figure 25G, H,  $p = 0.047$ ,  $n = 9$  for penicillin, unpaired two-sample t-test). Additionally, the

persistence of epileptiform activity was NMDAR dependent since bath application of D-AP5 immediately abolished epileptiform discharges during the washout of penicillin (Figure 25F, n = 4 for control, n = 5 for penicillin recordings).

In summary these experiments show that induction of epileptiform activity triggers a persistent decrease of astrocyte volume fraction which does not require ongoing epileptiform activity.

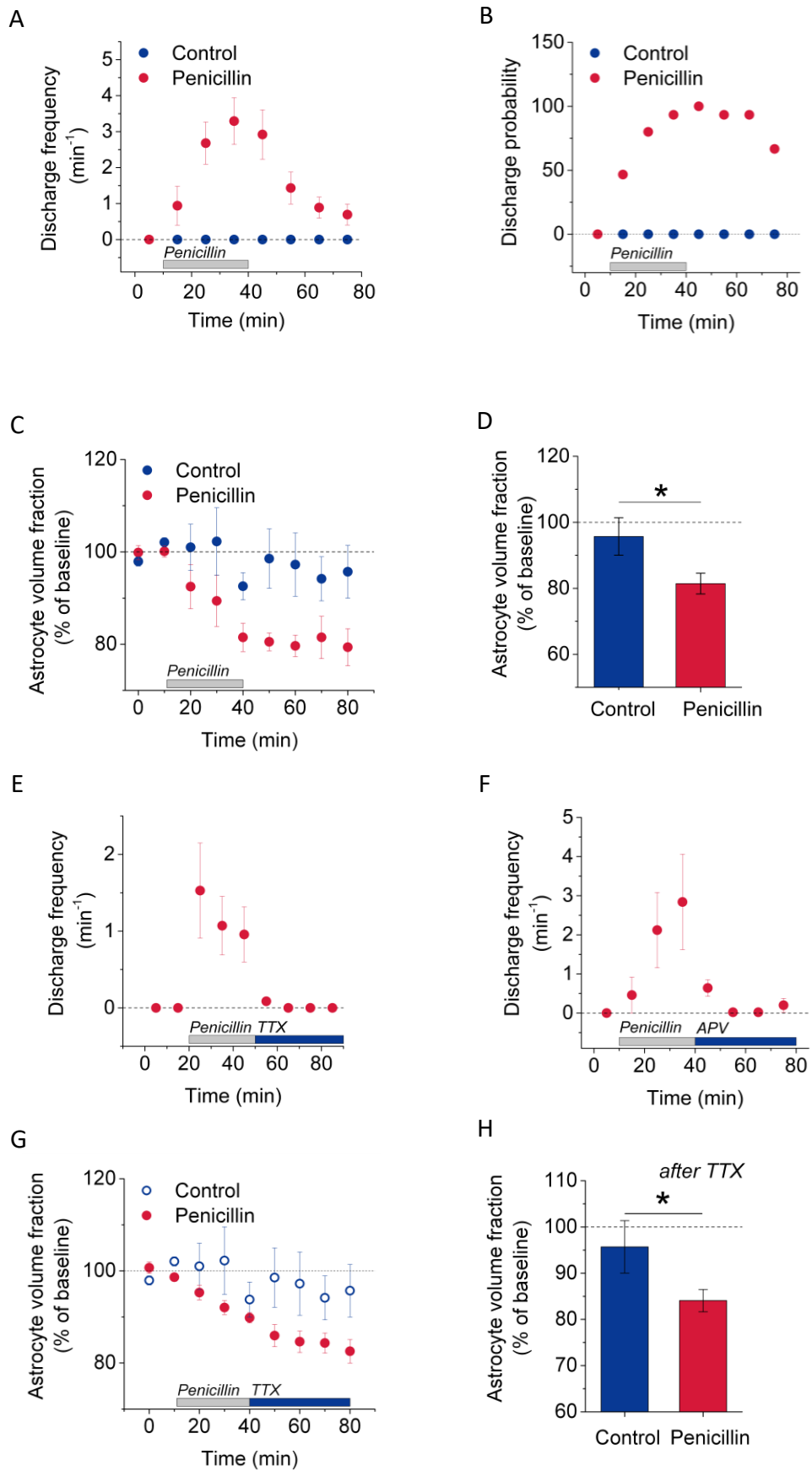


**Figure 25 Persistence of epileptiform activity and morphology changes.** (A) After washout of penicillin epileptiform activity persisted with a lower frequency (red). (B) Discharge probability stayed constant after washout with a little decrease at timepoint 80 (40 minutes after washout). (C) Astrocyte volume fraction decrease persisted and was still significantly decreased compared to control (blue) at the end of recording (D,  $p = 0.047$ , unpaired two-sample t-test). (E) Epileptiform discharges disappeared immediately in the presence of TTX during penicillin washout as well as in the presence of APV (F). (G) Astrocyte volume fraction remained decreased when neuronal activity was blocked (H,  $p = 0.047$ , unpaired two-sample t-test). The volume fraction values under control conditions are taken from the control recordings in figure 25C.

### 5.2.2 Characterisation of astrocyte morphology changes

To assess possible functional consequences of the observed astrocyte morphology changes, the localisation and the type of the morphology changes was further characterized. To determine where in the astrocyte the main volume fraction reduction occur, the images of EGFP expressing astrocytes of slices treated with penicillin and control slices were further analysed. Figure 26A shows an example of an overlap of an EGFP expressing astrocyte before and after penicillin treatment. The color coding represents the magnitude of the volume fraction decrease. Red indicates a 100 % decrease and green indicates 0 % volume change. The image shows that the main change in astrocyte volume fraction occurs in the periphery. The brightness reflects the initial volume fraction, thus, very bright reflects a 100 % initial volume fraction representing the soma and the darker parts represent a lower initial volume fraction like fine processes in the periphery. The peripheral fine branches with a low initial volume fraction undergo the highest change in volume fraction upon induction of epileptiform activity. This was also quantified statistically (Figure 26B). The change in astrocyte volume fraction was plotted against the initial volume fraction of the respective astrocyte segment. Astrocyte segments with a very small initial volume fraction of 10 – 20 % correspond to fine astrocyte processes whereas segments with high initial volume fraction of 80 - 90 % belong to thick astrocyte branches. The soma has an initial volume fraction of 100 %. The analysis revealed that the highest changes in astrocyte volume occur in astrocyte segments with an initial volume fraction of 10 to 50 %, which represent small and medium sized astrocyte processes ( $n = 10$  for control,  $n = 11$  for penicillin, unpaired two-sample t-test,  $p$ -value compared to control measurements see table 3). The visualisation of the example astrocyte (Figure 26A) and the statistical quantification thus revealed, that astrocyte morphology changes occur in the periphery in the fine and medium sized processes of astrocytes which are believed to form the close contact with neurons.

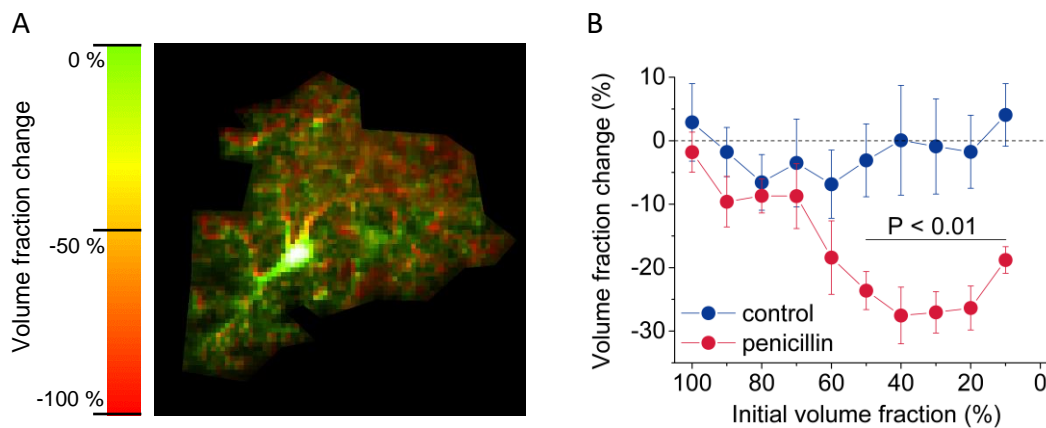


**Figure 26 Astrocyte morphology changes induced by induction of epileptiform activity occur in the periphery in thin and medium-sized processes.** (A) Color- and brightness-coded image of an astrocyte. The brightness reflects the initial volume fraction, the color represents the % of volume fraction change (B) Quantification of the observed changes in the periphery. The volume fraction change is plotted against the initial volume fraction. The significant decrease in astrocyte volume fraction occurs in small- and medium-sized astrocyte branches with an initial volume fraction of 0 to 50% ( $p < 0.01$ , unpaired two-sample t-test).

**Table 3:** p-values of the volume fraction change of astrocyte segments dependent on their initial volume fraction.

Initial VF	10%	20%	30%	40%	50%	60%	70%	80%	90%	100%
p-value	0.0003	0.0014	0.0037	0.0089	0.0042	0.1674	0.5445	0.6784	0.1816	0.6491

Additionally, the type of astrocyte morphology changes occurring upon induction of epileptiform activity was investigated. Two scenarios could explain the decrease in astrocyte volume fraction. The astrocyte volume fraction is defined as the fraction of tissue occupied by the peripheral astrocyte processes (chapter 4.2.3). Figure 27A, left panel shows an image, where astrocyte segments were isolated from electron microscopy (EM) sections (done by Nikolai Medvedev). These images illustrate that the astrocyte volume fraction depends on two parameters: the numbers and the size of these astrocyte segments. These parameters can be used to understand in which manner astrocyte processes are changing when the astrocyte volume fraction is decreasing. On one hand, a volume fraction decrease could be induced by a retraction of astrocyte processes whereas on the other hand it could also be due to a shrinkage of these processes. To differentiate between the two scenarios, the segmentation of the astrocyte processes was analysed (chapter 4.2.4). For a better understanding the shrinkage of astrocyte processes was simulated. Astrocyte segments, isolated from electron microscopy sections, were filtered with a Gaussian filter with the resolution of diffraction limited microscopy (Figure 27A, middle panels). These images were binarised with the threshold at astrocyte volume fraction, which resulted in images, where

astrocyte segments could be counted. A shrinkage by 15 % of astrocyte processes was simulated and images were edited as described before. A shrinkage of astrocyte processes leads to a reduced overlapping of astrocyte segments (red circles, simulation done by C. Henneberger). Thus, the number of resolvable astrocyte processes would increase if the observed reduction in astrocyte volume fraction was caused by a shrinkage of processes. If the astrocyte processes retracted, the number of resolvable segments in turn should decrease (not illustrated). Therefore, the number of resolvable astrocyte segments was analysed (chapter 4.2.4) in control and penicillin conditions at the beginning and the end of the recordings (30 minutes after penicillin application). In control conditions this parameter stayed stable over time (Figure 27B, left panel,  $n = 8$ ,  $p = 0.10$ , paired-sample t-test). In contrast, under penicillin conditions the number of resolvable astrocyte segments increased significantly compared to baseline after penicillin treatment (Figure 27B, second panel,  $n = 10$ ,  $p = 0.005$ , paired-sample t-test) but also compared to control recordings (Figure 27C,  $p = 0.019$ , one-way ANOVA, red bar). The results could be reproduced using hyperosmolar ACSF (400 mOsm) inducing an expected shrinkage of cells. Bath application of hyperosmolar ACSF also led to a significant increase in resolvable astrocyte segments compared to baseline (Figure 27B,  $n = 8$ ,  $p = 0.008$ , paired-sample t-test, third panel) and compared to control (Figure 27C,  $p = 0.003$ , one-way ANOVA, grey bar). Together these results indicate that the observed reduction in periphery astrocyte volume fraction is caused by an overall shrinkage of astrocyte processes.

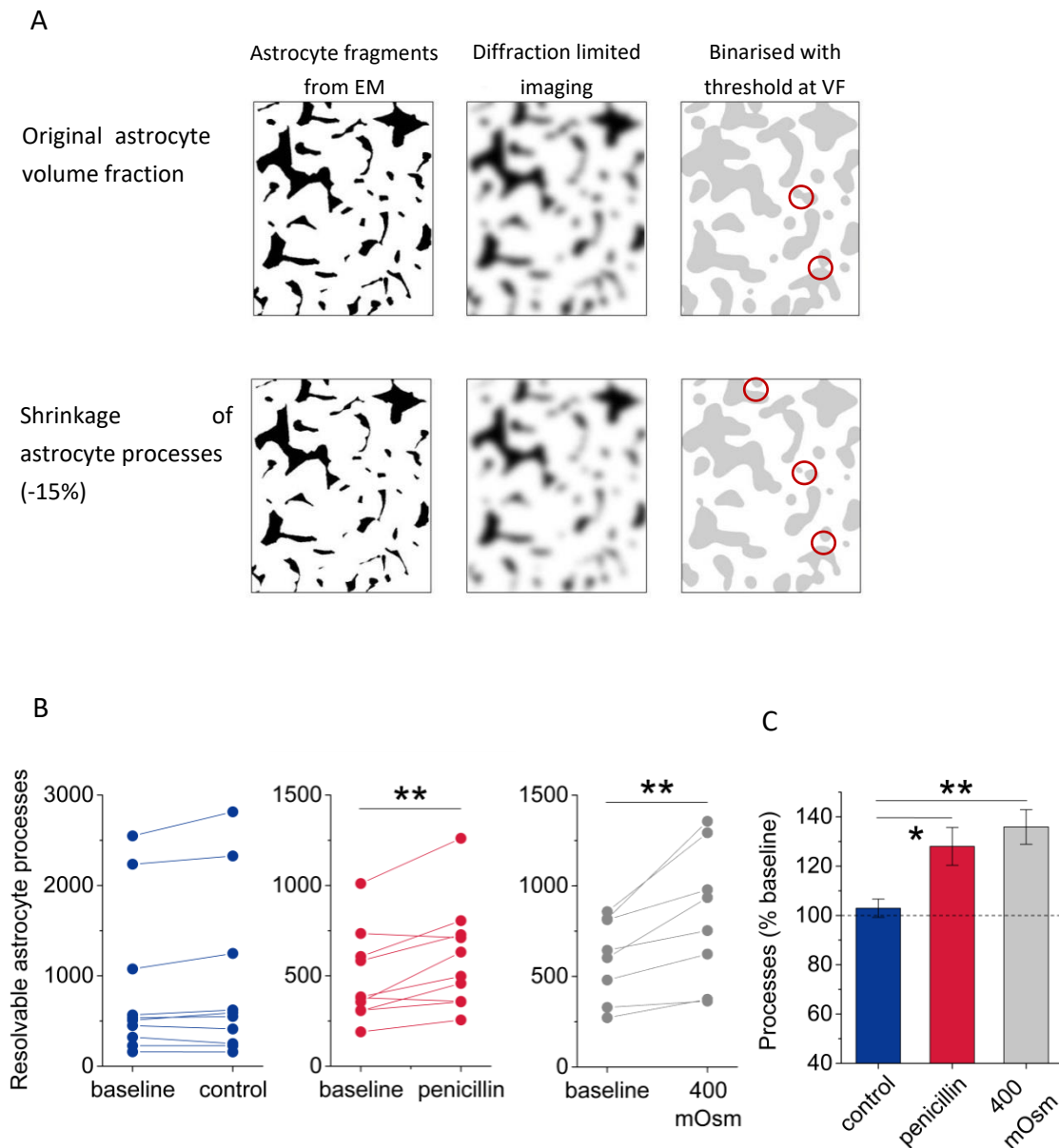


**Figure 27 Segmentation analysis of astrocyte processes under control and penicillin conditions.** (A) The left panels show astrocyte fragments isolated from electron microscopy (EM) sections (obtained by N. Medvedev). These images were filtered with a gaussian noise with the resolution of diffraction-limited microscopy and binarised at the threshold of astrocyte volume fraction. The binarised images show a simulation of astrocyte segments under normal conditions and when astrocyte processes were thinned by 15%. This image processing leads to a less overlapping of astrocyte segments and thus, an increasing number of resolvable astrocyte segments. (B) Under control conditions the number of resolvable astrocyte processes stayed stable (left panel), whereas under penicillin conditions the astrocyte segmentation increased significantly (second panel,  $p = 0.005$ , paired-sample t-test). Results could be mimicked by using hyperosmolar ACSF (third panel). (C) Quantification revealed a significant increase in resolvable astrocyte segments under penicillin conditions ( $p = 0.019$ , one-way ANOVA) and under hyperosmolar conditions ( $p = 0.003$ , one-way ANOVA, analysis done by C. Henneberger).

### 5.2.3 Neuronal morphology changes during induction of epileptiform activity

In parallel to astrocytic volume fraction changes during induction of epileptiform activity, also neuronal morphology could change. The observed astrocyte morphology changes could be due to a swelling of neurons in the same range. This would suggest that the extracellular space does not change upon induction of epileptiform activity, but also that the spatial distance between neuronal and astrocyte compartments is not altered. The other possible scenario is that neuronal morphology is unaltered in this early state of epileptogenesis which might lead to an increased extracellular space. Both scenarios would give relevant hints for possible functional consequences of the induced astrocyte morphology changes during acute epileptiform activity. To investigate this in detail, neuronal morphology was analysed during induction of epileptiform activity. To this end, the volume fraction of neurons expressing YFP under the Thy-1 promotor (chapter 3.1.4) was analysed as done before for astrocyte analysis (chapter 4.2.12). Dendritic volume was only analysed in slices where astrocytes showed a significant decrease in astrocyte volume fraction to be able to observe clear effects on neuronal morphology. A critical issue for this analysis was that the calculation of the volume fraction strongly depended on a stable reference region, where 100 % of the tissue is occupied by the dendrite. The region of interest (ROI) included many dendrites with spines from different CA1 pyramidal cells. Since a thick dendrite was used as a reference region, very small movements had already strong effects on the calculated dendritic volume fraction. Thus, only images with stable reference regions could be used for the analysis, which resulted in a low number of penicillin recordings ( $n = 3$ ). Figure 28A and B show images of YFP labelled dendrites in the CA1 stratum radiatum of the hippocampus under baseline (Figure 28A) and under penicillin conditions (Figure 28B). As shown in the time course (Figure 28C) the dendritic volume fraction did not change over time in control and penicillin recordings ( $n = 7$  for control,  $n = 3$  for penicillin recordings). Comparing the dendrite volume fraction as % of baseline of the last 10 minutes of the experiments revealed no significant differences between control and penicillin conditions (Figure 28D,  $p = 0.18$ , unpaired two-sample t-test). These results suggest that the neuronal volume is not changing in the acute phase of epileptiform activity in this model.

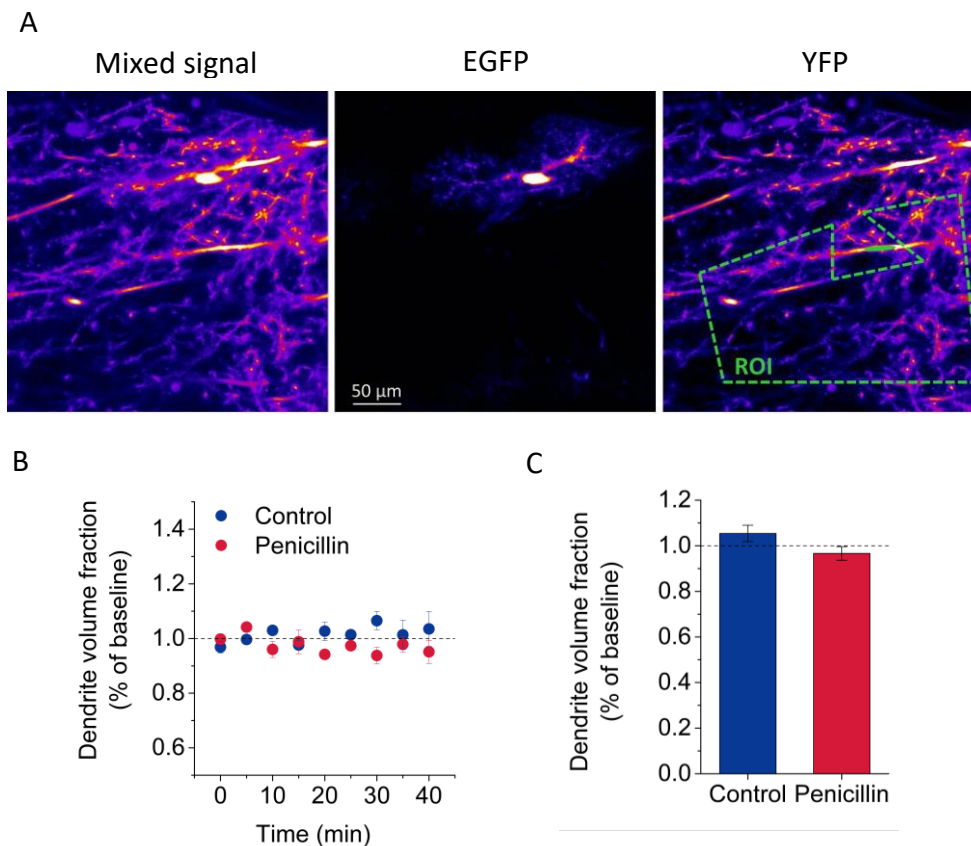


**Figure 28 Neuronal morphology changes during induction of epileptiform activity.** (A) Example images of YFP expressing dendrites under the Thy1 promoter and EGFP expressing astrocytes under the hGFAP promoter. After linear unmixing the EGFP signal (middle panel) could be separated from the YFP signal. (B) Volume fraction of neuronal dendrites stays stable also during induction of epileptiform activity and no significant difference compared to control could be found (C,  $n = 7$  for control,  $n = 3$  for penicillin,  $p = 0.18$ , unpaired two-sample t-test).

The experiments revealed that neuronal morphology is not changing during the induction of epileptiform activity. This suggested that the extracellular space is increasing. To rule out that the slice volume itself is altered after induction of epileptiform activity, it was calculated under baseline conditions and under control or penicillin conditions, respectively (chapter 4.2.11). For calculation the z-position of the cell was used (for the formula see appendix). The calculated slice volume normalised to baseline did not change over time (Figure 29A) neither under control conditions ( $n = 4$ ) nor under penicillin conditions ( $n = 7$ ). Comparing the average normalised slice volume of the last 10 minutes of control or penicillin recordings did not reveal significant differences between these two groups (Figure 29B,  $p = 0.27$ , unpaired two-sample t-test). Taken together, these results show that, although astrocyte volume fraction is decreasing, neuronal morphology was not changing and the overall slice volume stayed constant after induction of epileptiform

activity. This indicates that the extracellular space increases during epileptiform activity. This suggests that the spatial relationship between neuronal compartment and astrocyte processes is altered after induction of epileptiform activity, which may implement modulations of the astrocyte-neuron signalling.

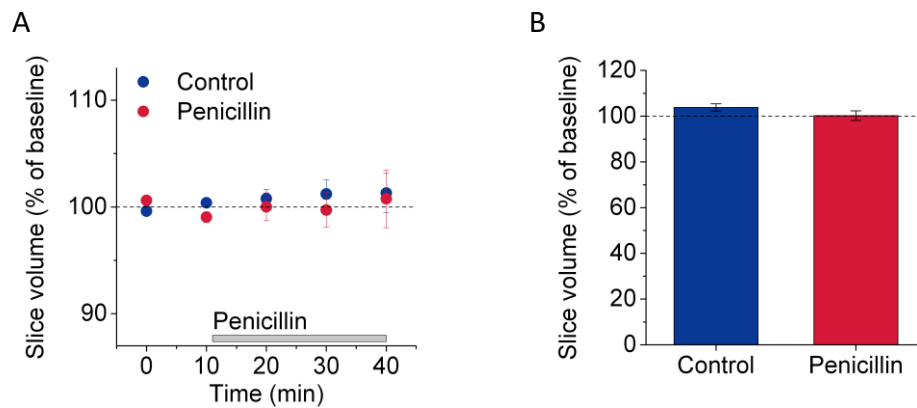


**Figure 29 Slice volume under control and penicillin conditions.**(A) Neither under control conditions nor under penicillin conditions the slice volume was changing over time. (B) Comparing the normalised slice volume in the last 10 minutes of control or penicillin recordings did not reveal significant differences ( $n = 4$  for control,  $n = 7$  for penicillin,  $p = 0.27$ , unpaired two-sample t-test).

## 5.3 Functional consequences of altered astrocyte morphology

### 5.3.1 Intracellular diffusion in astrocytes during epileptiform activity

The results in chapter 5.2 indicate that astrocyte processes are shrinking within 30 minutes of induction of epileptiform activity. This might lead to a decrease in intracellular space which in turn could have consequences for the intracellular diffusion. To investigate if the intracellular diffusion was altered during epileptiform activity compared to control recordings fluorescence recovery after photo bleaching (FRAP) experiments were performed in mice expressing EGFP in astrocytes under the hGFAP promotor (Nolte et al., 2001, chapter 4.2.8). In an EGFP-expressing astrocyte a region of interest was bleached (Figure 30A, dashed line) including the soma and both thick and fine astrocyte processes using high laser power. Closing the shutter allowed intact fluorescent EGFP-molecules to diffuse back into the bleached region. By reopening the shutter a recovered fluorescence could be measured. Figure 30B (left panel) shows the corresponding line scan with the initial bleaching and the fluorescence trace after reopening the shutter. The fluorescence arbitrary units of the corresponding line scan (Figure 30B, left panel) were plotted and the values of the initial bleached fluorescence  $\Delta F_B$  and the recovery fluorescence  $\Delta F_R$  (Figure

30B, right panel) after reopening the laser shutter were used to calculate FRAP as described in chapter 4.2.8. The higher the diffusion of intact molecules is, the higher is the intensity of the recovered fluorescence. FRAP is calculated by the ratio of the recovered fluorescence  $\Delta F_R$  and the bleached fluorescence  $\Delta F_B$  ( $\Delta F_R / \Delta F_B$ ). Thus a higher FRAP value indicates a higher diffusion. FRAP was calculated for control and penicillin recordings and was used to capture changes in intracellular diffusion of astrocytes. Under control conditions FRAP showed a slight, but not significant increase (Figure 30C,  $n = 10$ ,  $p = 0.07$ , paired-sample t-test) compared to baseline whereas after induction of epileptiform activity using penicillin FRAP was significantly decreased by  $9.55 \pm 3.2\%$  compared to baseline (Figure 30D,  $n = 10$ ,  $p = 0.016$ , paired-sample t-test) and  $17.8\%$  to control (Figure 30E,  $p = 0.003$ , unpaired two-sample t-test). These experiments indicate that the induced astrocyte morphology changes during epileptiform activity affect the intracellular diffusion. This could be caused by changes in astrocyte tortuosity.

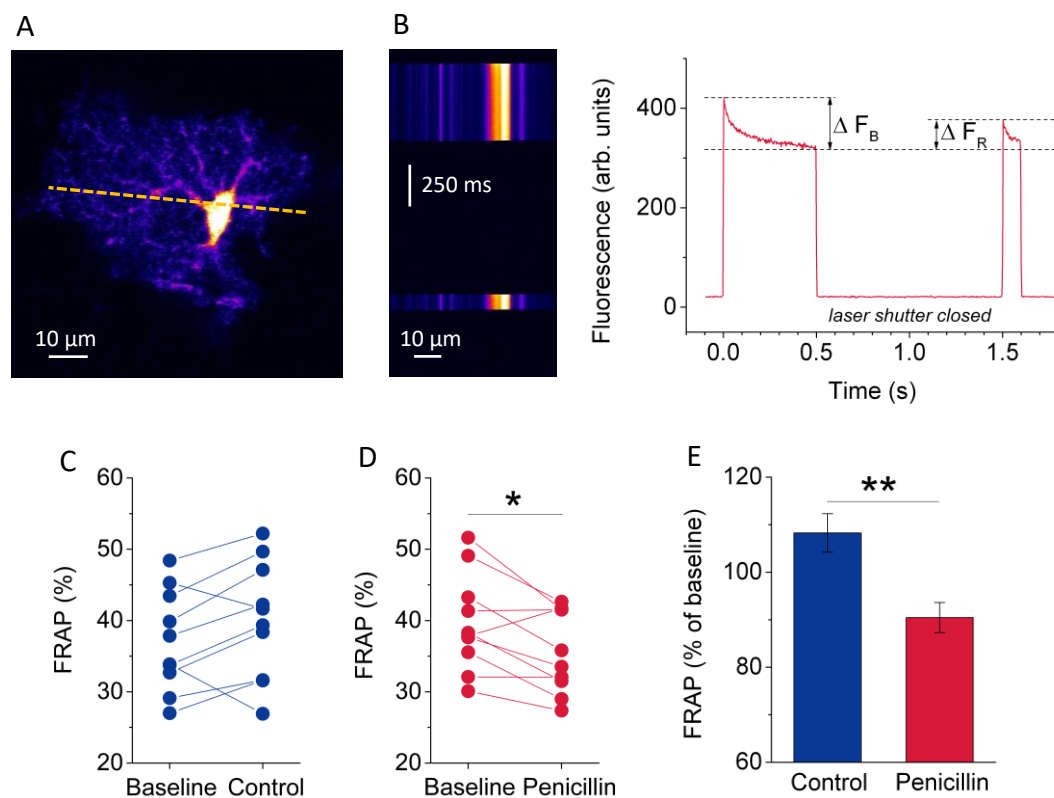


**Figure 30 Intracellular diffusion in astrocyte processes during control and epileptiform recordings.** (A) Example EGFP-expressing astrocyte with bleached region of interest (dashed line), (B) Linescan through the astrocyte (left panel) with fluorescence arbitrary units plotted over time (right panel), (C) In control recordings FRAP stayed stable over time with a slight increase ( $n = 10$ ,  $p = 0.07$ , paired-sample t-test). Under penicillin conditions FRAP was significantly reduced compared to baseline (D,  $n = 10$ ,  $p = 0.016$ , paired-sample t-test) and to control recordings (E,  $p = 0.003$ , unpaired two-sample t-test, analysis done by C. Henneberger).

### 5.3.2 Astrocyte dye coupling in different rat hippocampal regions

Alterations of the intracellular diffusion of astrocytes may not only affect a single cell. Astrocytes are extensively coupled via gap junctions (Giaume et al., 1997; Nagy and Dermietzel, 2000), which allows the exchange of metabolites and ions between cells in the gap junction-coupled network. An altered intracellular diffusion of astrocytes therefore could also have an effect on the diffusion between the cells. This could have consequences for the astrocyte-neuron communication. To assess possible functional consequences caused by astrocyte morphology changes during epileptiform activity, astrocyte dye coupling was investigated in acute rat hippocampal slices. Before investigating possible differences in astrocyte coupling under epileptiform conditions, spatial hippocampal astrocyte coupling was characterised in healthy brain tissue. For these experiments a new analytical approach was developed (Anders et al., 2014). It allowed to characterise the coupling strength of an astrocyte network independent of the frequently used and possibly biased cell counting method. The astrocyte network in the CA1 stratum radiatum (Figure 31A) could be visualized by the spread of the morphological dye Alexa 594 from the initial patched cell into their neighbouring gap junction-coupled astrocytes. The whole dye-coupled network was captured by obtaining a z-stack (Figure 31A). Figure 31B shows the patched astrocyte and its coupled neighbours filled with the morphology dye Alexa 594. The dye spreads from the initial patched cell to their neighbouring cells. This can be described by a monoexponential function. The decay constant  $\tau$  of the monoexponential function was defined as coupling length constant  $C\lambda$  and was used to quantify the coupling strength of the gap-junction coupled astrocyte network. Figure 31C shows an example plot of the cell intensities over their distances to the patched cell, where the coupling length constant  $C\lambda$  was 32.9  $\mu\text{m}$ .

To further characterize astrocyte coupling in the hippocampus, astrocyte dye coupling was compared between different brain regions. Therefore, experiments were performed in hippocampal CA1 stratum radiatum and in the molecular layer of the ventral and dorsal dentate gyrus. The mean coupling length constant of astrocyte dye-coupled networks in the CA1 stratum radiatum was  $31.1 \pm 2.5 \mu\text{m}$  ( $n = 7$ ) which was not significantly different from the mean coupling length constant measured in the dorsal and ventral molecular layer of the dorsal and ventral dentate gyrus (Figure 31D,  $28.5 \pm 2.8 \mu\text{m}$ ,  $n = 18$ ,  $p = 0.59$ , unpaired two-sample t-test). The comparison of the coupling strength between dorsal ( $\lambda = 30.1 \pm 3.9$ ) and ventral ( $\lambda = 26.9 \pm 4.3$ ) dentate gyrus also did not reveal any significant differences (Figure 31E,  $n = 9$  for both groups,  $p = 0.58$ , unpaired two-sample t-test) between the groups. These results suggest that the coupling strength of astrocyte networks neither differ between the CA1 region and the dentate nor between the dorsal and ventral hippocampus.

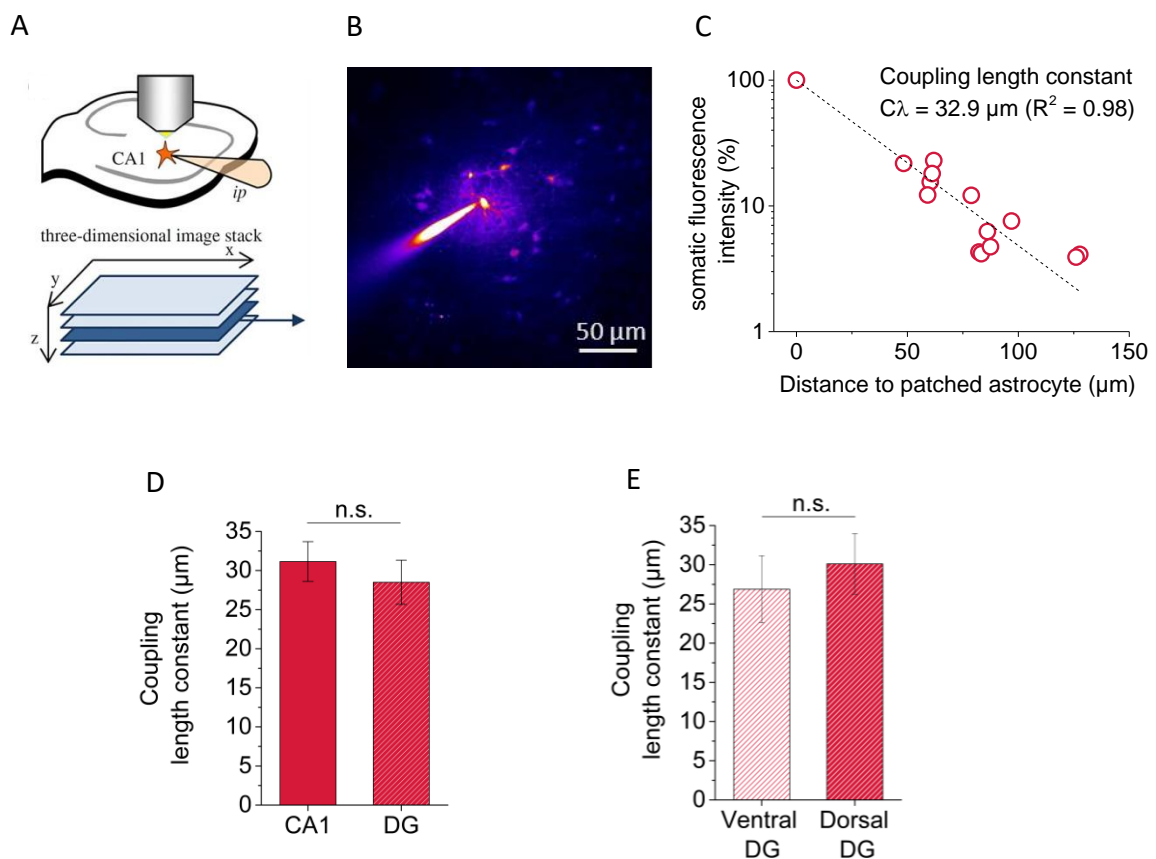


**Figure 31 Astrocyte dye coupling in different brain regions.** (A) Astrocytes were patched and filled with a morphology dye and a z-stack was obtained (adopted from (Anders et al., 2014)). The dye spreads from the patched cell into the gap-junction coupled astrocyte network (B) with a monoexponential decay (C). This decay was defined as coupling length constant  $C\lambda$ . (C) Example plot of the cell intensities of the coupled astrocytes normalized to the initial cell and dependent on their distance to the patched astrocyte. (D) Analysis of  $C\lambda$  in the CA1 stratum radiatum and the dentate gyrus revealed no difference between these brain regions ( $n = 16$  for DG,  $n = 7$  for CA1 stratum radiatum,  $p = 0.59$ , unpaired two-sample t-test) and also no differences between the molecular layer of the dentate gyrus in the ventral and dorsal hippocampus (E,  $n = 9$  for both groups,  $p = 0.58$  unpaired two-sample t-test).

To test, whether the coupling length constant resolve changes in astrocyte gap junction-coupling, astrocyte dye-coupling was measured in different temperature conditions (Anders et al., 2014). It was shown before that gap junction conductance is temperature-dependent (Bukauskas and Weingart, 1993). To reveal temperature-dependent changes in astrocyte gap-junction coupling, astrocyte networks were filled with the morphological dye Alexa Fluor 594 in room temperature (RT) and at  $34^\circ\text{C}$ . As described before, the initial cell was patched in whole-cell configuration. Image stacks were obtained 20 minutes after opening. The dye spreaded into the neighbouring coupled astrocytes, which could be described by a monoexponential function. For each coupling cloud of the different

temperature conditions, the coupling length constant  $C\lambda$  was calculated (chapter 4.2.7).  $C\lambda$  reflects the decay of the monoexponential function. Thus, a higher value for  $C\lambda$  indicates a higher fluorescence intensity at a distinct distance from the initial patched cell and thus, a higher coupling strength. To be more precise, the decay of the monoexponential fit (and thus  $C\lambda$ ) is the distance to the initial patched cell, where the fluorescence intensity remains at 36.8 % from the initial fluorescence intensity of the patched cell. Comparison of the mean  $C\lambda$  for RT ( $20.6 \pm 1.1 \mu\text{m}$ ,  $n = 5$ ) and  $34^\circ\text{C}$  ( $31.1 \pm 1.9 \mu\text{m}$ ,  $n = 7$ ) revealed a temperature-dependent increase of  $C\lambda$  of 51% (Figure 32A,  $p = 0.0011$ , unpaired two-sample t-test). To compare this result with a standard method used for the quantification of astrocyte coupling, cells were also manually counted in the same image stacks. Interestingly, with this method no temperature-dependent differences could be measured (Figure 32A, RT:  $n = 5$ ,  $48 \pm 7.9$  cells;  $34^\circ\text{C}$ :  $n = 7$ ,  $45.6 \pm 8.1$  cells,  $p = 0.83$ , unpaired two-sample t-test). Analysis of the coefficient of variation (CV) revealed high values for cell counting at RT (Figure 32B,  $\text{CV} = 0.37$ ) and at  $34^\circ\text{C}$  ( $\text{CV} = 0.47$ ). This indicates a high variability of the data, which could explain that no differences could be found. In contrast, the CV of the coupling length constants was 0.11 for RT and 0.17 for  $34^\circ\text{C}$  (Figure 32B). These data showed that the coupling length constant is a sensitive measure to quantify astrocyte coupling (Anders et al., 2014). The increase of  $C\lambda$  at  $34^\circ\text{C}$  compared to RT could be caused by a faster cytosolic diffusion of Alexa Fluor 594. To test this, the intracellular diffusivity at different temperatures (RT and  $34^\circ\text{C}$ ) was tested using fluorescence recovery after photobleaching (FRAP) in mice expressing EGFP in astrocytes under the hGFAP promotor (Nolte et al., 2001). Since EGFP is also freely moving in the cytosol, changes in the intracellular diffusion should be detectable. FRAP was measured by scanning a line across the astrocyte (Figure 32C). As described before (chapter 5.3.1) this region of interest (ROI) was bleached by increasing the laser power at the objective to 15-30 mW for 500 ms (Figure 32D). By closing the laser shutter for 1 s, intact EGFP molecules could diffuse into the bleached ROI and after reopening the laser shutter a recovery fluorescence could be measured. FRAP was calculated by the ratio of the recovered fluorescence  $\Delta F_R$  and the bleached fluorescence  $\Delta F_B$  (Figure 32D). With a higher diffusion, more intact EGFP molecules would diffuse into the ROI and a higher recovered fluorescence would be measured, which would result in a higher FRAP. Analysis revealed that FRAP was increased in  $34^\circ\text{C}$  by 28.8 % compared to RT (Figure 32E,  $n = 10$  for RT,  $n = 12$  for  $34^\circ\text{C}$ ,  $p = 0.048$ , unpaired two-sample t-test). This suggests a higher intracellular diffusion at  $34^\circ\text{C}$ , which is likely to affect the intercellular diffusion between neighbouring astrocytes and thus astrocyte dye-coupling.

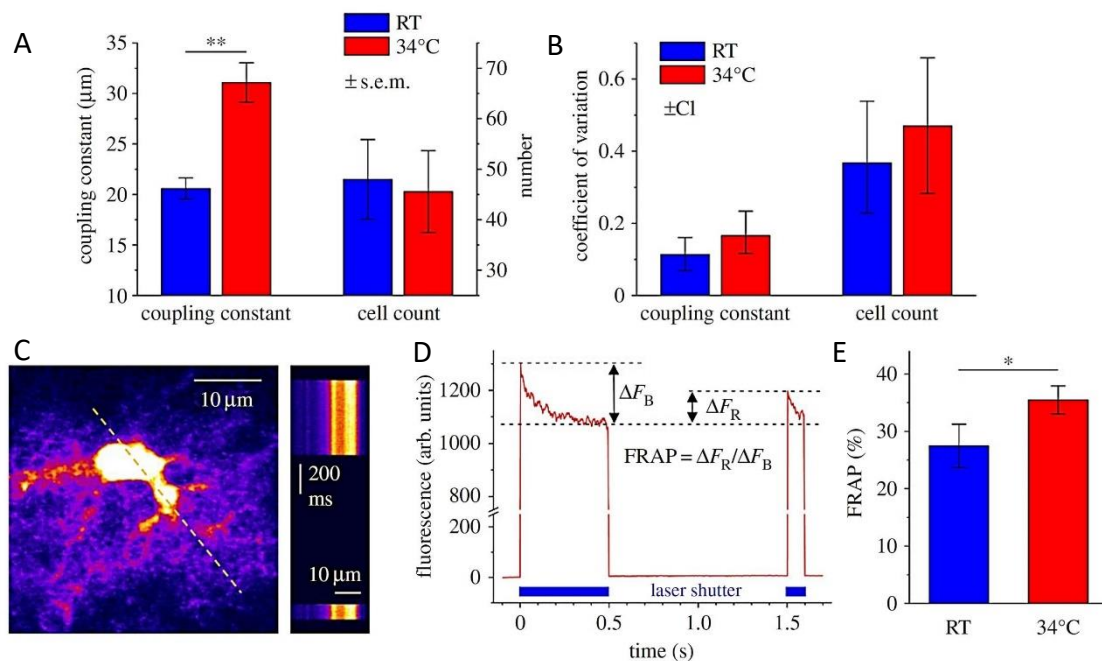


**Figure 32 Quantification of astrocyte dye coupling in the CA1 stratum radiatum.** (A) Astrocyte networks were investigated at RT (blue,  $n = 5$ ) and at 34 °C (red,  $n = 7$ ). The coupling length constant  $C\lambda$  was sensitive to temperature changes ( $p = 0.0011$ , unpaired two-sample t-test), whereas manual cell counting was not temperature-sensitive ( $p = 0.83$ , unpaired two-sample t-test). (B) The coefficients of variation indicate a lower variability of  $C\lambda$  analysis (error bars show 5 to 95 % confidence intervals, obtained by bootstrap analysis). (C) FRAP of EGFP expressing astrocytes ( $n = 10$  for RT,  $n = 12$  for 34 °C). Bleaching was induced along the dashed line by using high laser power. Intact fluorescent EGFP molecules diffuse into the bleached region resulting in recovery fluorescence  $\Delta F_R$ . (D) FRAP was quantified using the bleached fluorescence  $\Delta F_B$  and the recover fluorescence  $\Delta F_R$ ,  $FRAP = \Delta F_R / \Delta F_B$ . (E) FRAP was significantly increased at 34 °C compared to RT ( $p = 0.048$ , unpaired two-sample t-test, figure and analysis done by C. Henneberger, adapted from Anders et al., 2014).

### 5.3.3 Effect of epileptiform activity on astrocyte dye coupling

The previous experiments showed that an altered intracellular diffusion might affect astrocyte coupling. As the intracellular diffusion was altered upon induction of epileptiform activity, this could also have an effect on the diffusion between coupled astrocytes. Therefore, coupling length constants of dye-coupled astrocyte networks were measured under control and under penicillin conditions in rat hippocampal slices after baseline recordings. For these experiments the green fluorescent Alexa Fluor 488 was used as gap junction-permeable morphology dye because these data were obtained in parallel to the imaging of astrocyte morphology changes performed with the red fluorescent morphology dye Texas red dextran. Using a green and a red fluorescent dye allowed a clear separation of the two fluorescent signals. Coupling clouds were imaged at two time points, 20 minutes after cell opening as baseline value and another 20 minutes later either during control or

penicillin recordings (chapter 4.2.6). In control recordings  $C\lambda$  was  $33.3 \pm 3.2$  under baseline conditions and increased only slightly when the measurement was repeated 20 minutes later ( $35.8 \pm 3.9 \mu\text{m}$ ,  $n = 6$ ,  $p = 0.23$ , paired-sample t-test, figure 33A). In penicillin recordings the coupling length constant was  $40.3 \pm 2.7 \mu\text{m}$  under baseline conditions and not significantly different from control baseline recordings ( $p = 0.12$ ,  $n = 8$  for penicillin recordings,  $n = 6$  for control recordings, unpaired two-sample t-test, not shown). Induction of epileptiform activity by bath application of penicillin led to a significant decrease in the mean coupling length constant 20 minutes after baseline recording ( $33.4 \pm 2.4$ ,  $n = 8$ ,  $p = 0.0397$ , paired-sample t-test, figure 33B). Comparing the coupling length constants normalised to baseline of control and penicillin recordings measured at the second time point also revealed a significant difference between the two groups ( $p = 0.0205$ , unpaired two-sample t-test, figure 33C). The access resistance  $R_s$  was monitored and recorded during the entire experiment to exclude any effects of an altered dye filling into the cells on astrocyte dye-coupling according to changes in access resistance. Neither during baseline recordings nor in control or penicillin recordings 20 min later the access resistance was significantly different between control and penicillin group (baseline recordings,  $p = 0.47$ , control  $R_s = 10.1 \pm 1.0$ , penicillin  $R_s = 13.4 \pm 3.7$ ; control/penicillin recordings,  $p = 0.93$ , control  $R_s = 20.7 \pm 2.1$ , penicillin  $R_s = 20.3 \pm 3.5$ , unpaired two-sample t-test, not illustrated).

Taken together, these findings indicate that the induced astrocyte morphology changes during epileptiform activity result in a decreased intracellular diffusion, which in turn leads to a reduction in astrocyte dye-coupling. The observed decrease in astrocyte dye-coupling suggests a decrease in the intercellular diffusion between the coupled astrocytes. This could have important consequences for astrocyte function and affect the diffusion of ions and metabolites through the astrocyte network under epileptiform conditions.

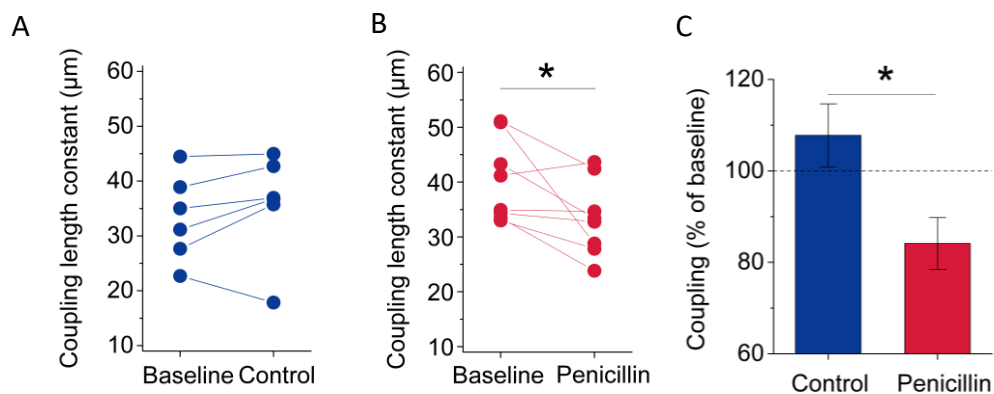


**Figure 33 Astrocyte dye coupling under control and epileptiform conditions.** (A) During control recordings the coupling length constant  $C\lambda$  stayed stable ( $n = 6$ ,  $p = 0.23$ , paired-sample t-test) whereas (B) under epileptiform conditions  $C\lambda$  was significantly reduced compared to baseline ( $n = 8$ ,  $p = 0.0397$ , paired-sample t-test) and to control recordings (C,  $p = 0.0205$ , unpaired two-sample t-test).

## 5.4 Mechanism of astrocyte morphology changes

The performed experiments revealed that peripheral astrocyte processes undergo a shrinkage after induction of epileptiform activity. These astrocyte morphology changes could be either mediated by a passive volume change through water channels or by an active restructuring of the astrocyte cytoskeleton. There is also evidence that astrocyte volume can be regulated by actin cytoskeleton pathways (Höltje et al., 2005; Ramakers and Moolenaar, 1998; Salhia et al., 2005). The experiments described in the following subchapters will clarify by which mechanism the astrocyte morphology changes were mediated after induction of epileptiform activity.

### 5.4.1 Effects of Rho Kinase inhibitor Y27632 on astrocyte morphology and epileptiform activity

To determine if restructuring of the actin cytoskeleton causes the decrease in astrocyte volume fraction after induction of epileptiform activity, the signalling pathway was investigated by using pharmacological treatment. The actin polymerisation is regulated by RhoA and its downstream effector, the RhoA associated protein kinase (ROCK; Amano et al., 2010; Riento and Ridley, 2003). Cell culture studies showed that astrocyte structure can be regulated by modulating ROCK in a manner that astrocytes start to outgrow when ROCK is inhibited (Höltje et al., 2005). Therefore, ROCK was inhibited in acute hippocampal slices by bath application of Y27632 (Figure 34) and experiments were repeated as described before (chapter 4.2.5). Spontaneous and evoked field potentials were recorded and astrocyte morphology was monitored in parallel. In the presence of 20 μM of the ROCK inhibitor astrocyte volume fraction stayed stable with  $97.5 \pm 3.5$  % of baseline also when

epileptiform activity was induced using penicillin (Figure 34A, B,  $n = 5$ ,  $p = 0.87$  compared to control, unpaired two-sample t-test). A dose-dependent effect could be observed since bath application of penicillin in the presence of  $5 \mu\text{M}$  Y27632 led to a partial but not significant change in astrocyte volume fraction with a volume fraction of  $89.5 \pm 1.2 \%$  of baseline 30 minutes after induction of epileptiform activity compared to control (Figure 34B,  $n = 5$ ,  $p = 0.12$ , unpaired two-sample t-test). In addition to astrocyte morphology changes, the epileptiform activity in the presence of the ROCK inhibitor was analysed. During bath application of penicillin slices showed a significant decrease in discharge frequency when they were exposed to the ROCK inhibitor Y27632 compared to penicillin application in the absence of Y27632 (Figure 34C, D,  $n = 19$  for penicillin,  $n = 10$  for penicillin in Y27632,  $p = 0.0004$ , unpaired two-sample t-test). Since the data showed a strong variability in discharge frequency during the washout of penicillin, the discharge probability was used as a second parameter to analyse epileptiform activity (Figure 34E). As explained before, it is the probability by which a slice shows epileptiform discharges in a distinct time period. This analysis revealed that the discharge probability is significantly decreased in slices where epileptiform activity was induced in the presence of the ROCK inhibitor. Interestingly, this was also the case after the washout of penicillin (Figure 34F,  $p = 0.0125$ , Mann Whitney U test). For statistical analysis the discharge probability in the last 40 minutes of each recording was calculated and values were averaged for each group. Mean values of discharge probability were compared statistically for recordings in absence and presence of Y27632. These results indicate that inhibiting ROCK by Y27632 prevents astrocyte morphology changes during induction of epileptiform activity, but also leads to a decreased likelihood of observing epileptiform activity.

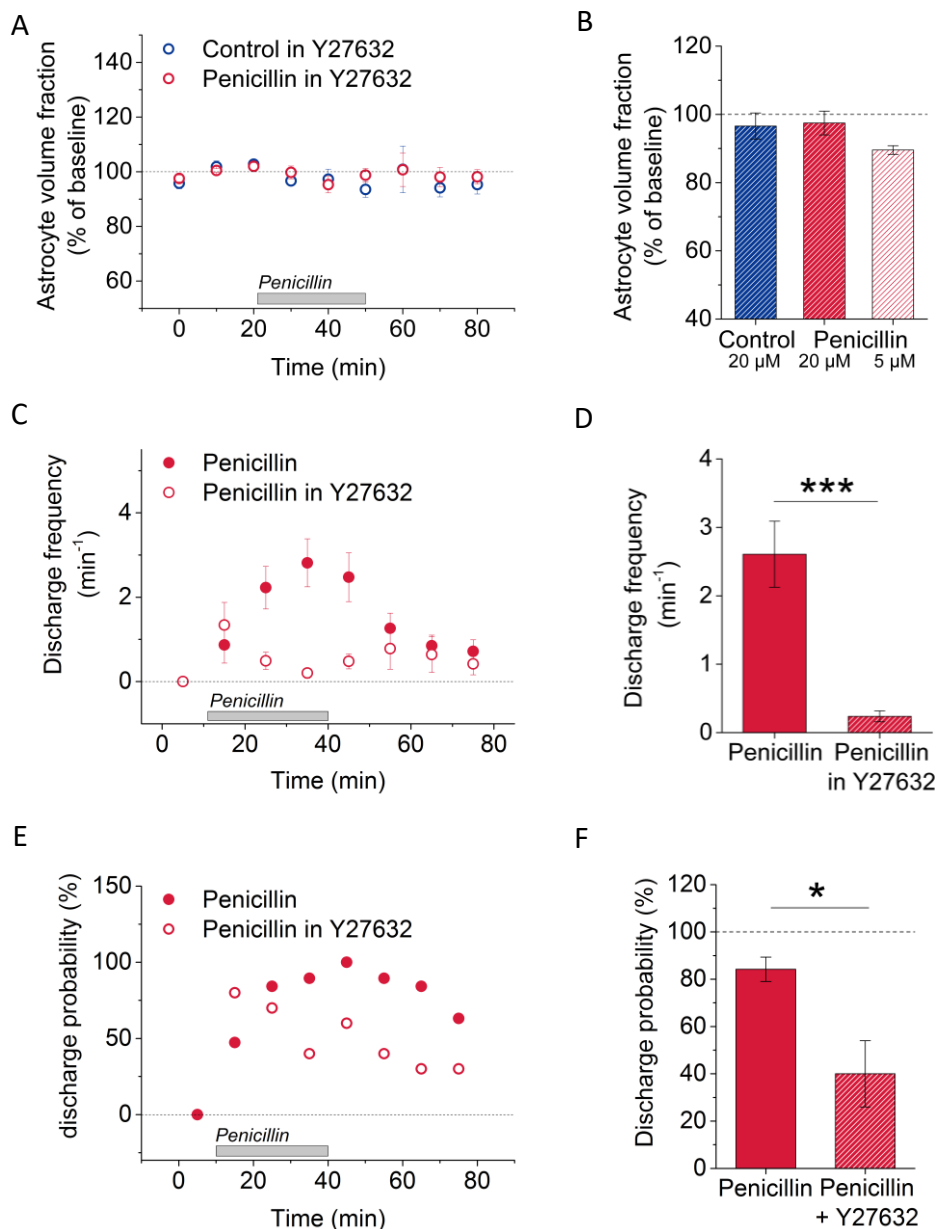


**Figure 34 Effects of ROCK inhibitor Y27632 on astrocyte morphology during induction of epileptiform activity.** (A) Time course of measured astrocyte volume fraction under control and under penicillin conditions in presence of ROCK inhibitor Y27632. (B) In presence of 20  $\mu$ M Y27632 astrocytes did not show any changes in astrocyte volume fraction ( $p = 0.87$ , unpaired two-sample t-test) upon induction of epileptiform activity and only little changes in volume fraction in presence of 5  $\mu$ M Y27632 ( $p = 0.12$ , unpaired two-sample t-test). (C) Time course of discharge frequency during penicillin application with and without Y27632 (pooled data of 20  $\mu$ M and 5  $\mu$ M). (D) The discharge frequency was significantly decreased during penicillin application in presence of Y27632 ( $p = 0.0004$ ,  $n = 19$  for penicillin,  $n = 10$  for penicillin in Y27632, unpaired two-sample t-test). (E) Discharge probability over time in slices exposed to penicillin with or without Y27632. (F) Analysis revealed also a significant reduction in discharge probability after washout of penicillin in the presence of Y27632 (20  $\mu$ M  $p = 0.0125$ , Mann Whitney U test).

To rule out any side effects of Y27632 (20 $\mu$ M) on the excitability of neurons or the synaptic transmission, different parameters under baseline conditions in presence and absence of Y27632 were analysed. The fEPSP slope recorded in the CA1 stratum radiatum in presence of Y27632 (Figure 35A, n = 5 in presence of Y27632, n = 6 in absence of Y27632, p = 0.85, unpaired two-sample t-test) as well as the fEPSP slope normalized to the fibre volley (FV) did not show any significant differences (Figure 35B, p = 0.40, unpaired two-sample t-test), although the fEPSP slope normalized to the FV tended to be decreased in presence of Y27632. This indicated that a stimulation of a similar number of axons resulted in a lower postsynaptic response. To assess the excitability of the CA1 pyramidal neurons in presence of Y27632 the population spike (ps) amplitude as well as the spike/slope coupling was analysed. No differences could be observed in the ps amplitude (Figure 35C, p = 0.88, unpaired two-sample t-test) and only a small but not significant decrease in the spike/slope coupling in the presence of Y27632 was visible (Figure 35D, right panel, p = 0.44, unpaired two-sample t-test). Thus, bath application of Y27632 did not alter neuronal excitability significantly.

Further experiments were performed to rule out any side effects of Y27632 on the neuronal inhibition (done by D. Minge). These experiments revealed that the ROCK inhibitor did not alter the penicillin-induced suppression of the inhibition (see chapter 6.2.1).

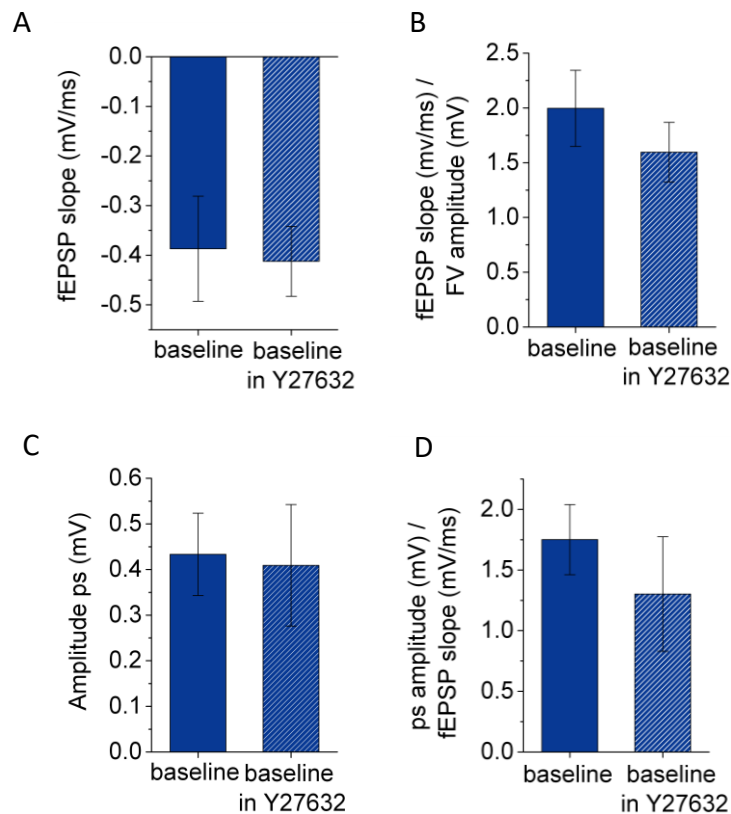


**Figure 35 Impact of the ROCK inhibitor Y27632 on the neuronal synaptic transmission and excitability in the CA1 region of the hippocampus.** (A) Y27632 (20 $\mu$ M) did not alter the fEPSP slope in baseline recordings ( $p = 0.85$ ,  $n = 5$  in presence of Y27632,  $n = 6$  in absence of Y27632, unpaired two-sample t-test). (B) The fEPSP slope normalized to the FV ( $p = 0.40$ , unpaired two-sample t-test) was also not significantly altered. (C) The baseline ps amplitude was similar in presence and absence of Y27632 ( $p = 0.88$ , unpaired two-sample t-test). (D) The spike/slope coupling was unaltered in presence of Y27632 compared to control baseline recordings ( $p = 0.44$ , unpaired two-sample t-test), although it tended to be decreased.

Until now Y27632 was bath applied. Since an effect on astrocyte morphology was observable, this drug probably entered the cell through the membrane. However, it could not be ruled out that Y27632 also entered the neuronal cytosol, thereby affecting epileptiform activity. To target astrocyte morphology more specifically, the ROCK inhibitor Y27632 (10  $\mu$ M) was added to the intracellular solution (IC) and brought into the astrocyte network via whole-cell patch clamp configuration in rat hippocampal slices. The criteria for a proper patch-clamp experiment were the same like described in chapter 5.1.2. When epileptiform activity was induced by bath application of penicillin, astrocytes filled with the ROCK inhibitor did not undergo volume fraction changes (Figure 35A,  $n = 5$ ,  $p = 0.83$  compared to control, unpaired two-sample t-test) whereas astrocytes filled with normal IC showed the described change in astrocyte volume fraction compared to control recordings (Figure 35A,  $n = 7$ ,  $p = 0.0209$ , unpaired two-sample t-test). Statistical analysis between data obtained from astrocytes with control IC and from astrocytes filled with Y27632 also

revealed a significant difference in astrocyte volume fraction 30 minutes after penicillin application (Figure 36B,  $p = 0.0175$ , unpaired two-sample t-test), whereby the volume fraction of astrocyte filled with Y27632 was similar to control recordings (Figure 36B,  $p = 0.83$ , unpaired two-sample t-test). In addition to the astrocyte morphology, also the epileptiform activity was analysed using the same parameters as described before, the discharge frequency and the discharge probability. When the ROCK inhibitor was applied intracellularly to the astrocyte by whole-cell patch-clamp configuration, the discharge frequency was decreased compared to control IC (Figure 36C), although not significantly (Figure 36D,  $n = 5$  for control IC,  $n = 6$  for IC+Y27632,  $p = 0.24$ , unpaired two-sample t-test). Plotting the discharge probability over time (Figure 36E) indicated a lower discharge probability in slices, when astrocytes were filled with the ROCK inhibitor. For statistical analysis the discharge probability of every single slice in the last 20 minutes was calculated and these values were averaged. The mean discharge probability of slices, in which astrocytes were patched in presence and absence of the ROCK inhibitor, was compared. Statistical analysis showed that the discharge probability was not significantly altered between the groups (Figure 36F,  $p = 0.22$ , Mann Whitney U test). In summary, it could be shown that modulation of astrocyte ROCK, by introducing its inhibitor into the cell, prevented astrocyte morphology changes due to induction of epileptiform activity. Although inhibiting astrocyte morphology changes lead to a trend of reduced epileptiform activity, no significant differences in epileptiform activity could be observed.

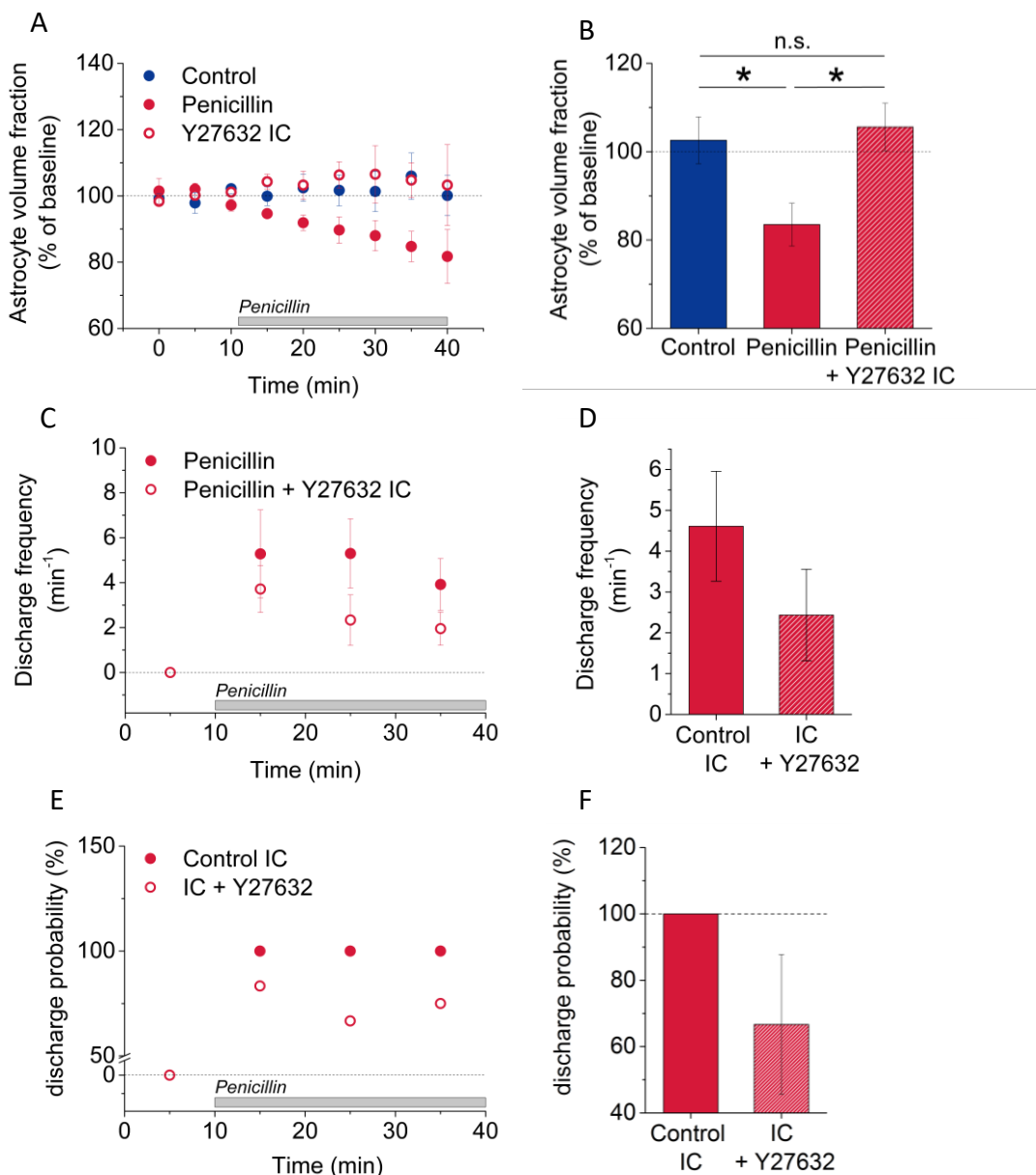


**Figure 36 Effect of astrocyte specific intracellular application of Y27632 on astrocyte morphology changes and epileptiform activity.** (A) Time course of astrocyte volume fraction in control, penicillin and with Y27632 in the patch pipette. (B) Astrocytes filled with the ROCK inhibitor Y27632 did not undergo astrocyte volume changes upon induction of epileptiform activity ( $p = 0.83$  compared to control,  $n = 5$  for control IC,  $n = 6$  for IC+Y27632, unpaired two-sample t-test). (C) Time course of discharge frequency in presence of penicillin with and without Y27632 in the patch pipette. (D) The discharge frequency tended to be decreased in slices where the astrocyte network was filled with Y27632 ( $p = 0.24$ , unpaired two-sample t-test). (E) Time course of discharge probability with control IC ( $n = 5$ ) and IC + Y27632 ( $n = 6$ ). (F) The discharge probability was not significantly decreased when Y27632 was used intracellularly by whole-cell patch-clamp recordings of astrocytes ( $p = 0.22$ , Mann Whitney U test).

### 5.4.2 Involved signalling cascade of astrocyte morphology changes

To investigate the mechanism which links epileptiform activity to the ROCK-dependent astrocyte morphology changes, pharmacological modulation of different upstream key players of the RhoA signalling was used. Two receptors were described to modulate the RhoA-ROCK pathway, the sphingosine-1-phosphate receptor (S1P) and the lysophosphatidic acid (LPA) receptor (Tönges et al., 2011). These are G protein-coupled receptors and their activation results in the transformation of RhoA-GDP to RhoA-GTP, thereby activating it. RhoA in turn leads to the activation of ROCK. S1P and LPA receptors were shown to be expressed by astrocytes (Fischer et al., 2011; Steiner et al., 2002). Astrocyte morphology changes were also shown to be regulated by cyclic adenosine monophosphate (cAMP; Ramakers and Moolenaar, 1998). The upstream regulator of cAMP is the adenylyl cyclase (AC). For activation or inhibition of AC NKH477 or SQ22536 were used, respectively. The mean volume fraction 20 to 30 minutes after application of LPA was  $93.5 \pm 2.6$  % of baseline whereas in control recordings an astrocyte volume fraction of  $99.8 \pm 4.5$  % of baseline could be measured at the same time point. Using S1P to modulate astrocyte volume fraction led to a mean volume fraction of  $95.3 \pm 3.6$  % of baseline. Control recordings for this subset of experiments were performed in the same concentration of methanol like used S1P recordings. In these conditions the measured astrocyte volume fraction during the last 10 minutes of the experiment was  $98.2 \pm 1.4$  % of baseline. Neither activation of LPA receptors nor S1P receptors displayed a significant effect on astrocyte volume fraction compared to control recordings (Control:  $n = 9$ , LPA:  $n = 6$ ,  $p = 0.31$ , unpaired two-sample t-test; Control/Methanol:  $n = 4$ , S1P:  $n = 5$ ,  $p = 0.53$ , unpaired two-sample t-test, figure 37A). To directly modulate AC two different drugs were bath applied. NKH477 was used to activate AC and SQ22532 should inhibit this cyclase. 20 to 30 minutes after application of NKH477 the astrocyte volume fraction was decreased significantly by  $14.2 \pm 3.6$  % of baseline (NKH477:  $n = 6$ , Control:  $n = 9$ ,  $p = 0.042$ , unpaired two-sample t-test, figure 37B). Application of SQ22532, in contrast, had no effect on the astrocyte volume fraction compared to control and baseline values (SQ22532:  $n = 3$ , mean astrocyte volume fraction  $94.0 \pm 4.6$  % of baseline, Control/DMSO:  $n = 2$ , mean astrocyte volume fraction  $97.1 \pm 9.5$  % of baseline,  $p = 0.76$ , unpaired two-sample t-test, figure 37B). Control recordings were performed in the same concentration of DMSO as present in SQ22532 recordings.

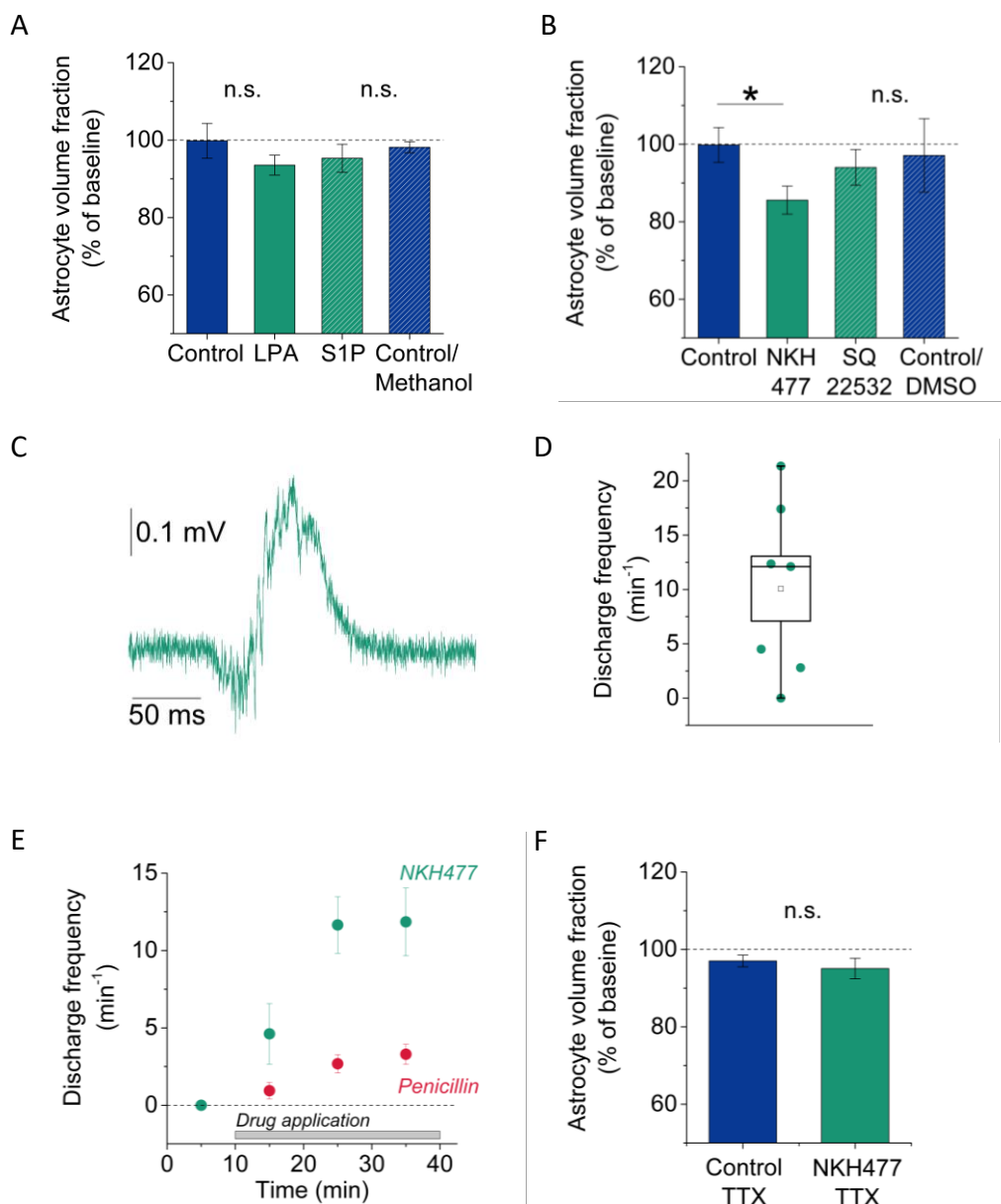


**Figure 37 Examination of possible signal cascade underlying the observed astrocyte morphological changes.**

(A) Activating LPA (Control:  $n = 9$ , LPA:  $n = 6$ ,  $p = 0.31$ , unpaired two-sample t-test) and S1P (Control/Methanol:  $n = 4$ , S1P:  $n = 5$ ,  $p = 0.53$ , unpaired two-sample t-test) receptors had no effect on astrocyte volume fraction. (B) Also bath application of SQ22532 did not affect astrocyte volume fraction (SQ22532:  $n = 3$ , Control/DMSO:  $n = 2$ ,  $p = 0.76$ , unpaired two-sample t-test), but activation of AC with NKH477 revealed a significant decrease of astrocyte volume fraction 20 to 30 minutes after start of application (NKH477:  $n = 6$ , Control:  $n = 9$ ,  $p = 0.042$ , unpaired two-sample t-test). (C) The decrease in astrocyte volume fraction was accompanied by spontaneous epileptiform discharges recorded in hippocampal CA1 stratum pyramidale. (D) The discharges occurred with a mean frequency of  $10.1 \text{ min}^{-1} \pm 2.99 \text{ min}^{-1}$  which was five to six fold higher than observed when penicillin was used (E). (F) Repeating the experiments with blocked neuronal activity revealed that NKH477 alone had no effect on astrocyte volume fraction (NKH477/TTX:  $n = 10$ , Control/TTX:  $n = 9$ ,  $p = 0.58$ , unpaired two-sample t-test).

Surprisingly, slices treated with the AC activator NKH477 developed epileptiform discharges with a similar waveform like the ones recorded from penicillin treated slices (Figure 37C) but they occurred with a 5 to 6 fold higher frequency ( $10.1 \text{ min}^{-1} \pm 2.99 \text{ min}^{-1}$ , figure 37D). To clarify whether the observed decrease in astrocyte volume fraction upon bath application of NKH477 (Figure 37B) was caused by the occurring epileptiform discharges, experiments were repeated with blocked neuronal activity by inhibiting the voltage gated sodium channels with TTX. When neuronal activity was blocked, bath application of NKH477 had no significant effect on astrocyte morphology (NKH477/TTX:  $n = 10$ , Control/TTX:  $n = 9$ ,  $p = 0.58$ , unpaired two-sample t-test, Figure 37F). In summary, modulation of the S1P and LPA receptor as well as direct inhibition of the AC had no effect on astrocyte morphology. Activation of the AC with NKH477 led to a significant decrease of astrocyte volume fraction, which was probably induced by the side effect of this drug inducing epileptiform activity.

#### **5.4.3 Proconvulsive effects of astrocyte morphology changes**

The conducted experiments have shown that a blockage of astrocyte morphology changes during induction of epileptiform activity also resulted in a reduced epileptiform activity. Furthermore, blocking neuronal activity during penicillin washout had no effect on the persistent decrease of astrocyte volume fraction (Figure 25). Thus, continuing changes in astrocyte morphology after induction of epileptiform activity did not require ongoing epileptiform discharges. This suggests that the induction of epileptiform activity is required and acts like a trigger for astrocyte morphology changes, which are then not reversible during the observed time period. This suggests, that the persistent decrease in astrocyte volume fraction could cause ongoing epileptiform activity. To understand how astrocyte morphology changes are possibly linked to ongoing epileptiform discharges, the strength of astrocyte volume fraction change as a mean of the values obtained 25 to 30 minutes within application of penicillin was correlated with the fraction of remaining discharges. For this value, the number of the remaining epileptiform discharges during the last 10 minutes of penicillin washout was normalized to the number of discharges occurred during the last 10 minutes of penicillin application. Plotting the fraction of remaining discharges over the astrocyte volume fraction change (Figure 38) revealed a significant correlation between the strength of astrocyte volume fraction decrease and the remaining fraction of discharges ( $n = 14$ ,  $p = 0.013$ , Spearman correlation,  $\rho = 0.645$ ). This indicates that the induced astrocyte morphology changes have a proconvulsive effect.

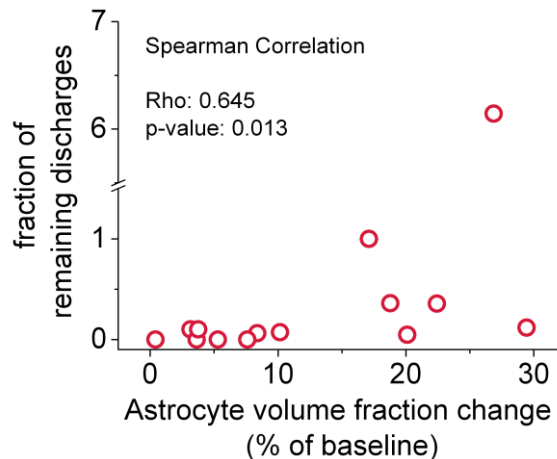


**Figure 38 Correlation between fraction of remaining discharges and strength of astrocyte volume fraction change.** Plotting the fraction of remaining discharges over the astrocyte volume fraction change revealed a positive correlation between these parameters ( $p = 0.013$ , Spearman correlation,  $\rho = 0.645$ ).

Throughout the experiments it turned out that not all astrocytes responded with a morphology change to epileptiform activity. To understand if these are only single cells not responding or if this single imaged cell represents the network response of astrocyte, epileptiform activity was analysed in slices with responding and slices with non-responding cells. Cells were chosen as responder when their morphology response was bigger than twice the standard deviation of the baseline. The time course (Figure 39A) shows that the group of non-responders stay very stable in their volume fraction whereas the responder group show a strong decrease in volume fraction. Analysing the discharge frequency revealed that slices where non-responders were imaged, developed a significant lower frequency of epileptiform discharges at the end of the recordings compared to slices where responder cells were imaged (Figure 39B, C,  $n = 8$  for non-responder,  $n = 15$  for responder,  $p = 0.0007$ , one way ANOVA RM with posthoc Fisher test) although the discharge frequency measured in the first 10 minutes did not differ in the two groups ( $p = 0.21$ , one way ANOVA RM with posthoc Fisher test). One could argue that the overall decreased epileptiform activity prevents astrocyte morphology changes. But also in measurements with very low discharge frequencies, significant volume fraction decreases could be observed, indicating that not a distinct discharge frequency is required to induce astrocyte morphology changes. This result supports the hypothesis that a decrease in astrocyte volume fraction promotes epileptiform activity and that the response of a single astrocyte represents the network morphology response of all astrocytes, which may explain the consequences for neuronal network activity.

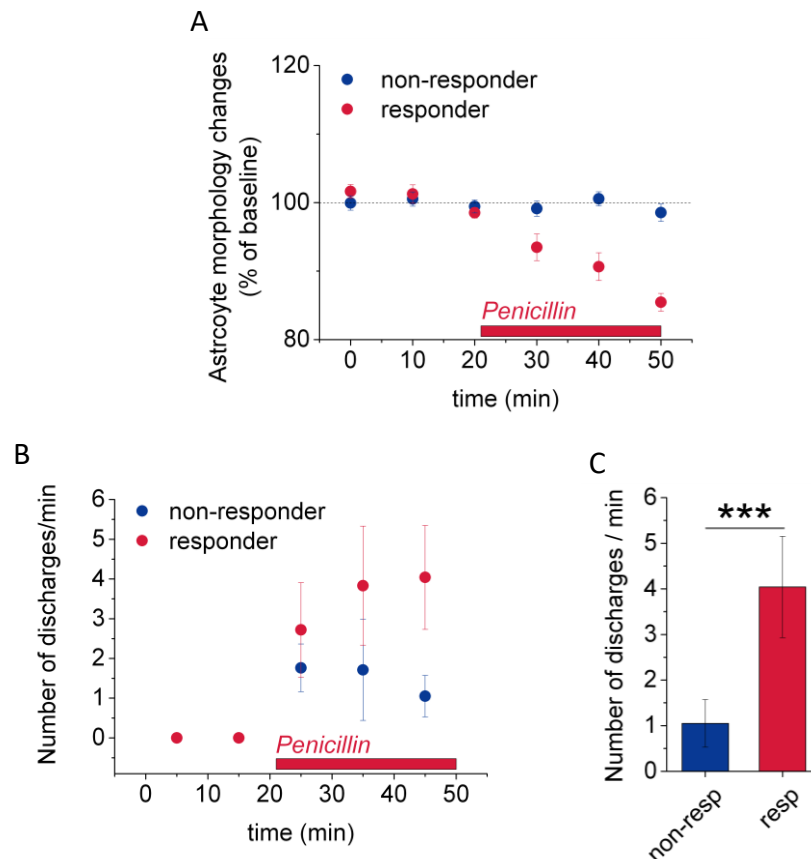


**Figure 39 Effect of morphology responder and non-responder discharge frequency.** (A) Time course of astrocyte volume fraction of responder ( $n = 15$ ) and non-responder cells ( $n = 8$ ). (B) Discharge frequency was decreased in slices where non-responder cells were imaged and differed significantly at the end of penicillin application (C,  $p = 0.007$ , one way ANOVA RM with posthoc Fisher test).

## 5.5 Mechanism linking astrocyte morphology changes to epileptiform activity

The previous experiments revealed that fine astrocyte processes shrink due to the induction of epileptiform activity. This shrinkage is mediated by alterations in the actin cytoskeleton. As a consequence of these astrocyte morphology changes a reduced intra- and intercellular diffusivity were observed. Overall, these astrocyte morphology changes appear to act proconvulsive. The following experiments should help to identify the mechanistic link, how the observed rapid astrocyte morphology changes contribute to the persistence of epileptiform activity.

### 5.5.1 Effect on synaptic transmission

Alterations in intra- and intercellular diffusion could have strong effects on all cellular processes including the basal mechanism for brain information processing, synaptic transmission. Additionally, morphology changes of the fine astrocyte processes may result

in a spatial disruption between astrocyte protrusion and neuronal synapses. As shown previously (chapter 5.2.3), neuronal morphology was not altered after induction of epileptiform activity, which suggested an increase in extracellular space. This could affect the neurotransmitter uptake by astrocytes, since the distance to the transporters and receptors has changed. In turn, the gliotransmitter supply, like for instance D-serine, could be impaired due to the altered spatial relationship between astrocyte and postsynaptic compartment. To investigate any possible effects of astrocyte morphology changes on synaptic transmission, stimulation of Schaffer collaterals was performed throughout the experiment and the slope as well as the paired pulse ratio (PPR) of the fEPSPs were analysed. In figure 40 the typical responses to single Schaffer collateral stimulation in the stratum radiatum (Figure 40A) and the stratum pyramidale (Figure 40B) are shown. Blue indicates the fEPSP during baseline recordings and red displays the fEPSP after 30 minutes penicillin application in the same slice. Stimulation occurred every 30 seconds and data were binned per minute. Although induction of epileptiform activity leads to recurrent discharges (red traces), which could be recorded in both layers of the hippocampus, the initial slopes of the signals (arrow) match perfectly (Figure 40A). The first 10 to 40 % of the signal were used as slope of the fEPSPs in the stratum radiatum. This response of the stratum radiatum was used for analysis. The fEPSP slopes recorded in CA1 stratum radiatum did not change over 80 minutes (Figure 40C) of recording and did not differ between control and penicillin treatment (Figure 40D,  $n = 6$  for both groups,  $p = 0.16$ , unpaired two-sample t-test, data points of  $t = 40 - 50$  minutes were used). Comparing the slopes in the respective phases (baseline, control/penicillin, washout) of recording revealed that the slope was unaltered in control (Figure 40E,  $p = 0.33$ , one-way ANOVA repeated measurements, RM) and in penicillin (Figure 40F,  $p = 0.69$ , one-way ANOVA RM) recordings during the entire experiment. Thus, the synaptic transmission does not seem to be altered during induction of epileptiform activity.

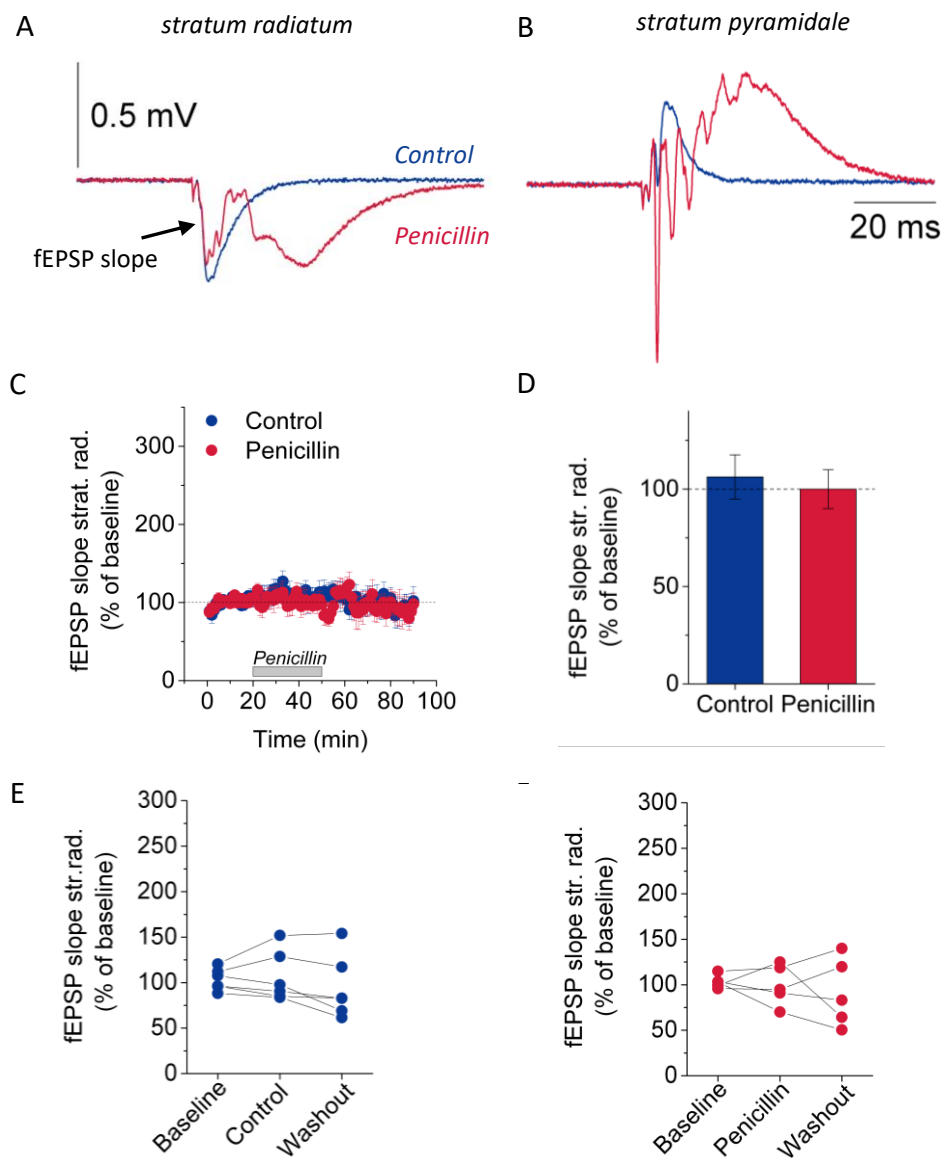


**Figure 40** Evoked fEPSPs due to Schaffer collateral stimulation recorded in the CA1 region of the hippocampus. (A) recorded fEPSPs in the CA1 stratum radiatum (blue: baseline conditions, red: during penicillin application), (B) fEPSPs recorded in parallel to (A) in the CA1 stratum pyramidale, penicillin application evoked recurrent discharges (red traces), (C) the initial slope of the signals plotted over time, which do not differ between control and penicillin recordings at time point  $t = 40 - 50$  minutes (D,  $p = 0.16$ , unpaired two-sample t-test), Paired statistics of control (E,  $n = 6$ ,  $p = 0.33$ , one-way ANOVA RM) and penicillin recordings (F,  $n = 6$ ,  $p = 0.69$ , one-way ANOVA RM) revealed that the fEPSP slope is not changing over time.

To test if the observed changes in astrocyte morphology, intra- and intercellular diffusion have any effects on presynaptic release mechanisms, the paired pulse ratio (PPR) was measured during baseline and control respectively penicillin conditions. Schaffer collaterals were stimulated with a double pulse in a subset of experiments with 50 ms interstimulus interval in rat and mouse hippocampal slices (see also chapter 4.1.4). Responses were recorded in stratum pyramidale of the CA1 region. Figure 41A shows representative fEPSPs

of mouse hippocampal slices expressing EGFP in astrocytes under the hGFAP promoter (Nolte et al., 2001) in response to the stimulation under control conditions, whereas the fEPSP responses during penicillin conditions are shown in figure 41B. Both example traces are averages of 20 single traces. Under penicillin conditions stimulation evoked recurrent discharges which had less spikes after the second stimulus. For PPR analysis the initial slope of the signal was used (chapter 4.1.4). In mice the mean PPR was  $1.33 \pm 0.23$  in control recordings and  $1.37 \pm 0.36$  in penicillin recordings under baseline conditions and not significantly different from each other ( $n = 8$  for control,  $n = 9$  for penicillin,  $p = 0.87$ , unpaired two-sample t-test, not shown). Comparing the PPR at the end of a control respectively penicillin recording with the baseline PPR revealed that the PPR was not altered neither during a control experiment (Figure 41C,  $p = 0.51$ , paired-sample t-test) nor during penicillin treatment (Figure 41D,  $p = 0.11$ , paired-sample t-test). Analysis of the mean PPRs in the last 10 minutes of an experiment showed that the PPR was not significantly altered during induction of epileptiform activity and control recordings (Figure 41E,  $p = 0.17$ , unpaired two-sample t-test). The analysis was also conducted for experiments done in rat hippocampal slices. The baseline PPR of control recordings ( $n = 8$ ) in rat hippocampal slices was with  $1.79 \pm 0.16$  not significantly different from the baseline PPR of penicillin recordings ( $n = 6$ ), which was  $2.10 \pm 2.8$  ( $p = 0.32$ , unpaired two-sample t-test). Paired analysis revealed that also in rat hippocampal slices PPR did not change over time in control recordings (Figure 41F,  $p = 0.89$ , paired-sample t-test) as well as in penicillin recordings (Figure 41G,  $p = 0.22$ , paired-sample t-test). Comparing the PPR of control and penicillin recordings at the end of an experiment showed no significant differences between the two groups (Figure 41H,  $p = 0.81$ , unpaired two-sample t-test). The observed repetitive activity after induction of epileptiform activity could mask an effect on the paired pulse ratio, since it might have affected the analysed slope. But in summary, the observed results indicate that induction of epileptiform activity using penicillin had no effect on the fEPSP slope and the PPR in the CA1 region of the hippocampus.

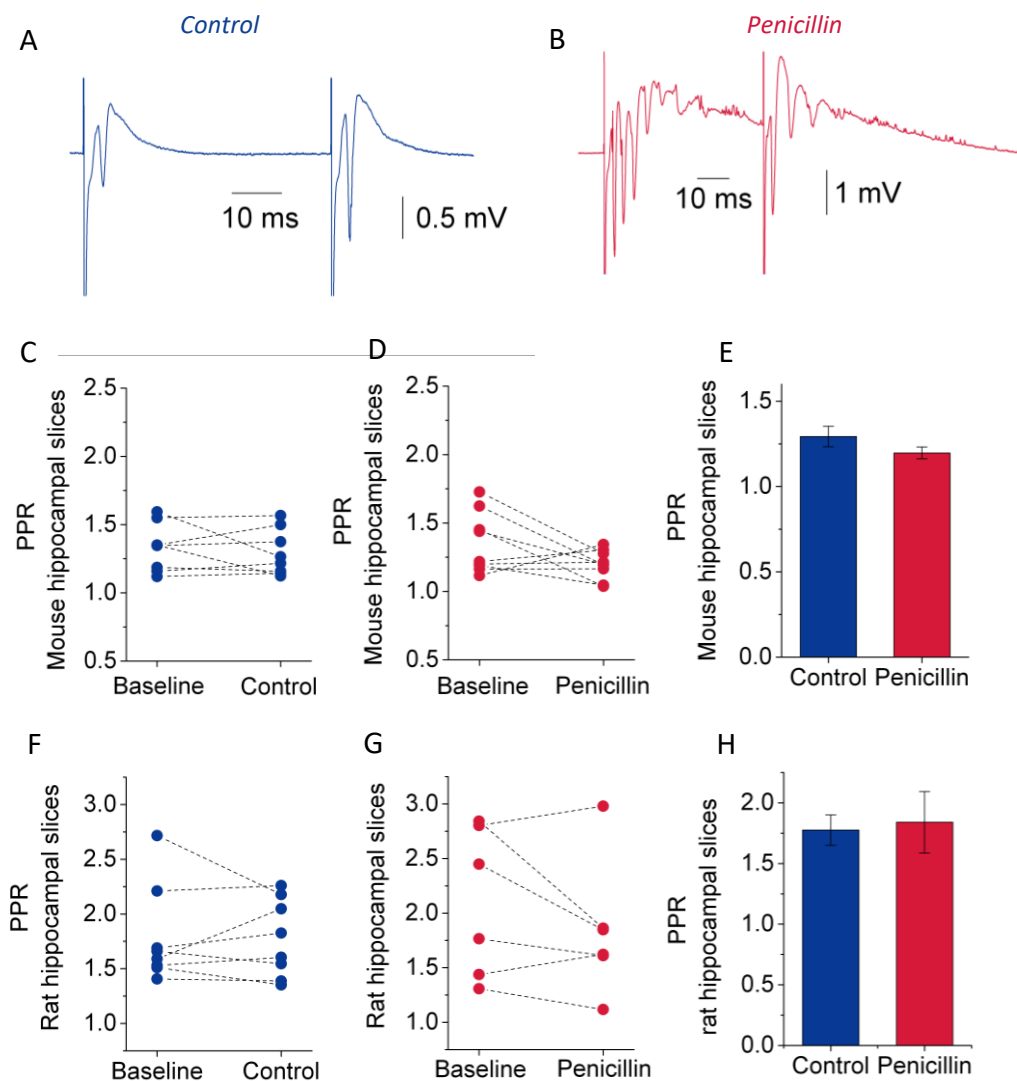


**Figure 41 Synaptic transmission during and after epileptiform activity.** (A) Typical fEPSP responses to paired pulse stimulation in slices of hGFAP-EGFP mice in control recordings and (B) in penicillin recordings. (C) The PPR in the CA1 stratum radiatum did not change over time in control ( $n = 8$ ,  $p = 0.51$ , paired-sample t-test) and (D) penicillin ( $n = 9$ ,  $p = 0.11$ , paired-sample t-test) recordings and was not significantly altered during penicillin application compared to control recordings (E,  $p = 0.17$ , unpaired two-sample t-test) and did not change over time (control:  $p = 0.33$ , penicillin:  $p = 0.69$ ). (F) In rat hippocampal slices the PPR also did not change during the experiment in control recordings ( $n = 6$ ,  $p = 0.90$ , paired-sample t-test) as well as in (G) penicillin recordings ( $n = 8$ ,  $p = 0.22$ , paired-sample t-test). (H) No significant changes could be observed comparing PPR of control and penicillin recordings ( $p = 0.81$ , unpaired two-sample t-test).

### 5.5.2 Excitability of hippocampal neurons

The results of chapter 5.2.1 revealed that epileptiform activity as well as astrocyte morphology changes persisted after washout of penicillin. To investigate how these observations are related to each other and by which mechanism astrocyte morphology changes may influence long-lasting epileptiform activity, the spike-slope coupling of

pyramidal cells was analysed. The spike-slope coupling is a measurement to describe the excitability of a cell.

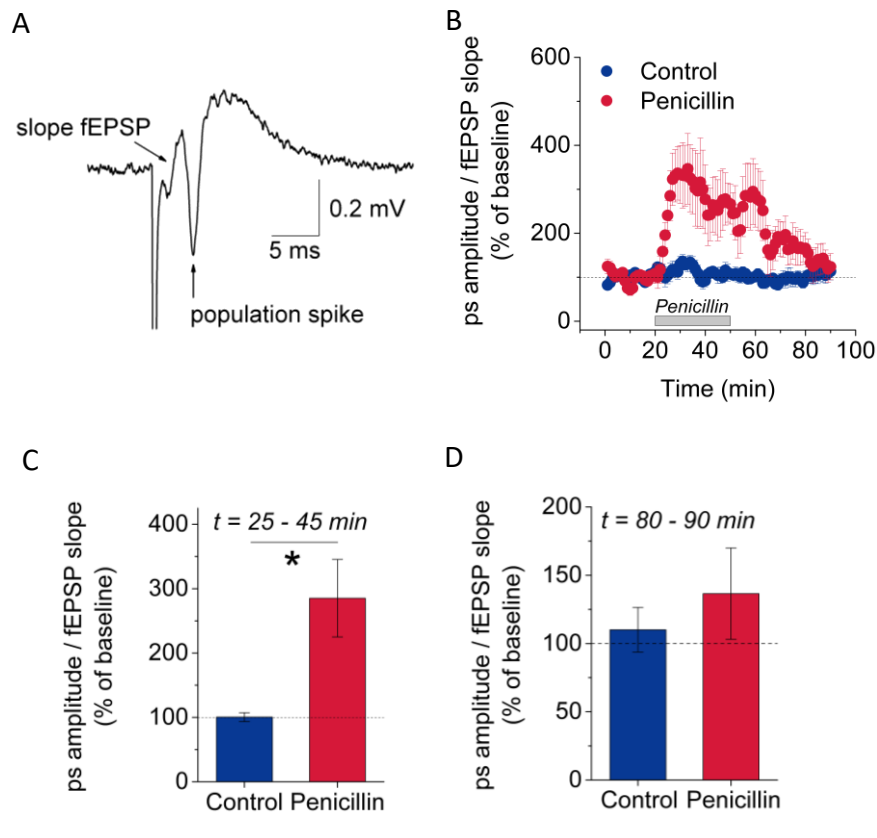


**Figure 42 Excitability of hippocampal CA1 pyramidal cells examined by analysing the spike-slope-coupling.** (A) Example fEPSP recorded in CA1 stratum pyramidale, arrows indicate the analysed parts of the signal. (B) Time course of the normalized ps amplitude / fEPSP slope ratio. (C) Induction of epileptiform activity leads to a significant increase in spike/slope coupling during penicillin application ( $p = 0.0276$ , unpaired two-sample t-test). (D) After washout of penicillin the spike/slope ratio decreased to control conditions ( $p = 0.47$ , unpaired two-sample t-test).

The amplitude of the population spike (spike) was normalised to the slope of a fEPSP (slope) in response to electrical stimulation. With this analysis the excitability of a neuronal population in different conditions can be compared independent of the strength of the synaptic stimulation. The slope of a fEPSP directly scales with the strength of the synaptic input. In contrast, the firing of a population of neurons in response to electrical stimulation depends on their firing threshold, which is modulated by different voltage-gated ion channels. For instance, former studies have suggested that activation of extrasynaptic NMDA receptors leads to a reduction of the A-type potassium current which generated an increased neuronal firing in magnocellular neurosecretory neurons (Naskar and Stern,

2014). The persistent shrinkage of astrocyte processes upon induction of epileptiform activity might lead to an activation of extrasynaptic NMDA receptors via glutamate spillover since less glia are bordering the synaptic cleft. This in turn could lead to an increased neuronal firing through the described mechanism promoting a long lasting epileptiform activity. To analyse this parameter, the evoked fEPSPs recorded during the entire experiment in the stratum pyramidale were used (Chapter 4.1.5). The amplitude of the population spike (ps) was normalized to the slope of the fEPSP as indicated in the example fEPSP trace (Figure 42A). The time course of the spike/slope coupling under control and penicillin conditions (Figure 42B) indicates that within 5 minutes of penicillin application the spike/slope coupling was strongly increased. During penicillin application (time period 25 to 45 minutes of the experiment) this increase in spike/slope coupling compared to control was significant ( $n = 6$  for control,  $n = 5$  for penicillin,  $p = 0.0276$ , unpaired two-sample t-test, Figure 42C). After washout of penicillin this ratio slowly decreased (Figure 42B, red data points) and after 40 minutes of washout the spike/slope coupling is comparable to control conditions ( $p = 0.47$  for the time period 80 to 90 minutes of the experiment, unpaired two-sample t-test, Figure 42D). Thus, the spike/slope coupling was altered in presence of penicillin, when the GABAergic transmission was inhibited. But this effect did not persist after washout of penicillin, indicating that the altered astrocyte morphology does not affect the spike/slope coupling.

### 5.5.3 Effect of astrocyte morphology changes on long-term potentiation

It was shown that hippocampal long-term potentiation (LTP) depends on the release of D-serine by astrocytes (Henneberger et al., 2010). Therefore, alterations in the spatial relationship between astrocyte processes and neuronal synapses might affect synaptic plasticity. LTP was induced after a complete experiment as indicated by the time course in figure 43A, when penicillin was completely washed out and astrocyte volume fraction was still decreased and at the same time point after a control recording when astrocyte morphology was not altered. Baseline fEPSPs were recorded in the CA1 stratum radiatum before induction of LTP by high frequency stimulation (HFS). Afterwards, single stimulation was used for another 30 minutes (see also chapter 4.1.4). Example traces (Figure 43B) before HFS (dark blue) and after HFS (light blue) indicate the potentiated response after HFS. Figure 43C displays the time course of the LTP experiment. Induction of LTP led to a short-time post-tetanic potentiation (PTP) 2-3 minutes after induction as well as to long-term potentiation (LTP) measured until 30 minutes after induction. Quantitative analysis revealed that induced LTP in slices, which underwent spontaneous epileptiform activity, did not differ from LTP recorded in control slices concerning post-tetanic potentiation ( $p = 0.99$ ,  $n = 5$  for both groups, unpaired two-sample t-test, figure 43D) and long-term

potentiation ( $p = 0.94$ , unpaired two-sample t-test, figure 43E). Thus, LTP was not affected by induction of epileptiform activity and the related astrocyte morphology changes.

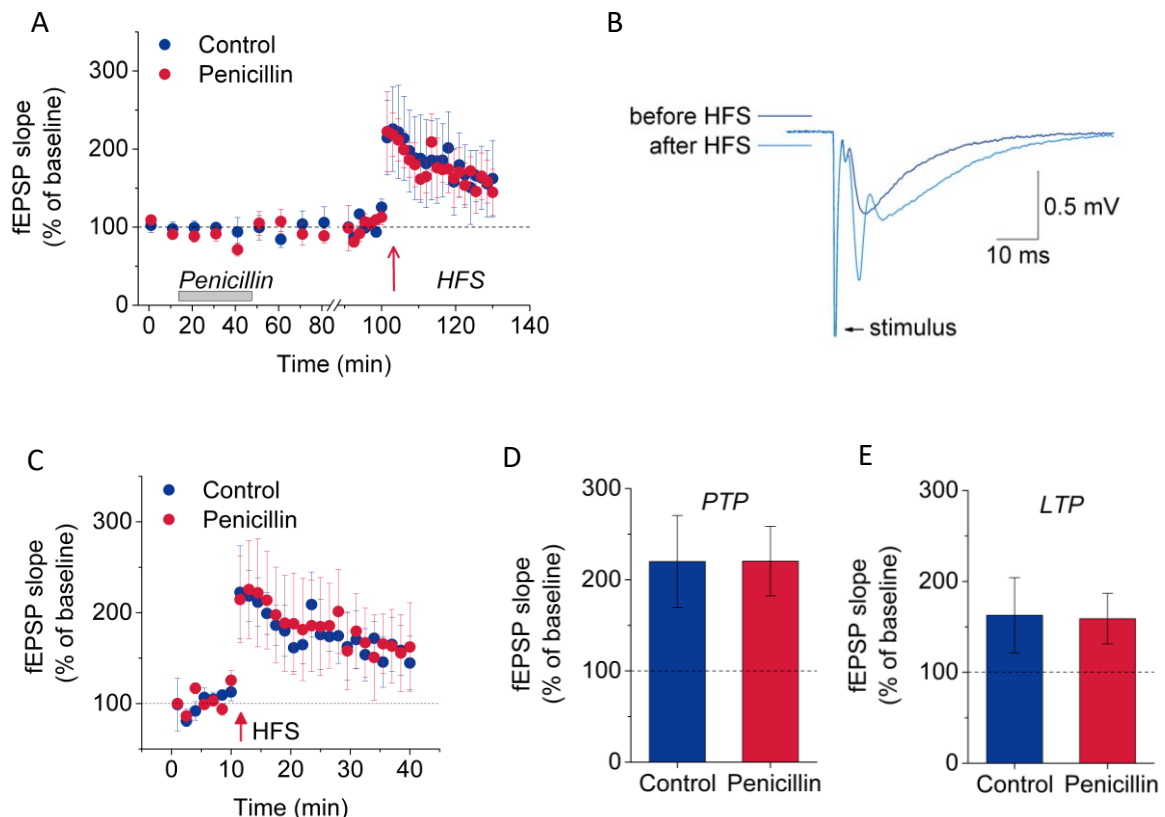


**Figure 43 Effect of previous epileptiform activity on synaptic plasticity.** (A) Timecourse of the whole experiment in control ( $n = 5$ ) and penicillin ( $n = 5$ ) conditions. (B) example traces of fEPSPs before (dark blue) and after (light blue) HFS. (C) timecourse of LTP experiment. (D) Induction of epileptiform activity did not lead to differences neither in PTP ( $p = 0.99$ , unpaired two-sample t-test) nor in LTP (E,  $p = 0.94$ , unpaired two-sample t-test).

#### 5.5.4 Effect on $K^+$ buffering

Astrocytes have been shown to play an important role in spatial  $K^+$ -buffering (Kofuji and Newman, 2004; Wallraff et al., 2006). The extensive gap junction coupling between astrocytes is thought to be an important factor for spatial  $K^+$ -buffering (Steinhäuser et al., 2012). Thus, alterations in intra- and intercellular diffusion could impair this distinct function. Impaired  $K^+$ -buffering in turn could have an effect on the extracellular  $K^+$  concentration which is believed to maintain neuronal activity on an appropriate level. An indicator for an increased resting extracellular  $K^+$  level is the membrane potential of an astrocyte since this is mainly determined by the  $K^+$  equilibrium potential in these cells (Somjen, 1975). As shown before, astrocyte coupling and their intracellular diffusion was

decreased after induction of epileptiform activity. This might impair spatial  $K^+$ -buffering, which in turn could result in ongoing epileptiform activity and thus explain the proconvulsive effect of astrocyte morphology changes. To investigate this hypothesis, the membrane potential of the patched astrocytes in rat hippocampal slices were monitored during the entire experiment by holding them in current clamp configuration (see also chapter 4.1.8). Figure 44A shows a typical field potential recording during epileptiform activity whereas the lower panel shows the astrocyte field potential recorded via the patch pipette of the astrocyte. Single spontaneous discharges (arrows) produced transient depolarisation shifts of the astrocyte membrane potential, which were caused by the transient increase in the extracellular  $K^+$  concentration due to the neuronal firing. How the astrocyte membrane potential depends on the extracellular  $K^+$  concentration is visualized in Figure 44B. Astrocyte membrane potentials were measured in ACSF with extracellular  $K^+$  concentrations of 2.5 mM ( $n = 18$ ), 5 mM ( $n = 20$ ) and 12 mM ( $n = 8$ ). At an extracellular  $K^+$  concentration of 2.5 mM the mean astrocyte resting membrane potential was  $-86.5 \pm 1.75$  mV. A  $K^+$  increase of 2.5 mM to 5mM resulted in a resting membrane potential of  $-74.2 \pm 1.33$  mV. An extracellular K concentration of 12 mM led to a strong depolarisation of astrocytes to  $-57.4 \pm 1.84$  mV. This shows, that the astrocyte resting membrane potential is very sensitive measure to capture small changes in extracellular  $K^+$  concentrations. To clarify if the spontaneous firing of the neurons generates a higher level of the resting  $K^+$  concentration in the extracellular space, the membrane potential of the astrocytes was measured in all recordings under baseline conditions and in the last 10 minutes of control or penicillin conditions when the transient depolarisations returned completely to resting membrane potential. Quantitative analysis revealed that the resting membrane potential did not differ significantly in control recordings compared to baseline (Figure 44C,  $p = 0.29$ ,  $n = 7$ , paired-sample t-test) as well as in penicillin recordings compared to baseline (Figure 44D,  $p = 0.46$ ,  $n = 7$ , paired-sample t-test). The membrane potentials recorded in astrocytes under control or penicillin conditions were also not significantly different from each other ( $p = 0.21$ ,  $n = 7$  for both groups, unpaired two-sample t-test, not shown). The results indicate that the resting extracellular  $K^+$  concentrations were not altered after induction of epileptiform activity.

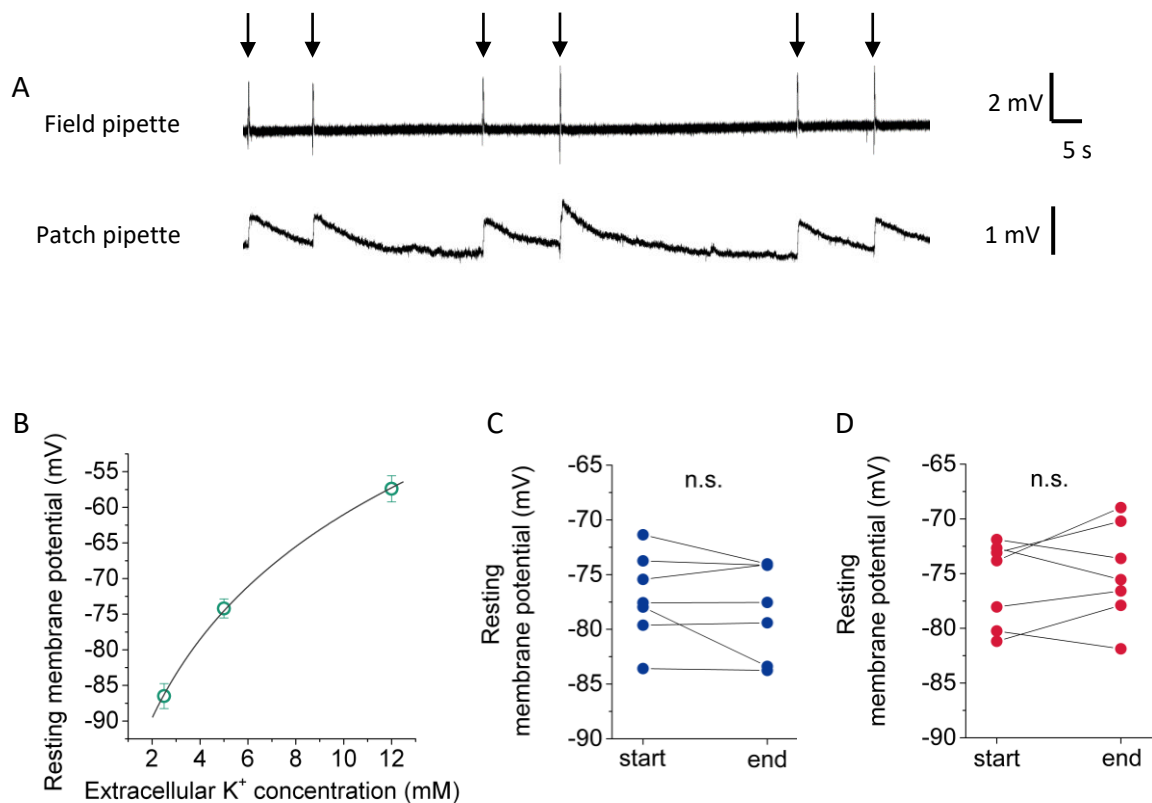


**Figure 44 Impact of astrocyte morphology changes on  $K^+$  buffering in the CA1 stratum radiatum.** (A) Upper trace shows an example field recording with epileptiform discharges, lower trace shows the membrane depolarisations of the astrocyte captured via the patch pipette in whole-cell configuration. (B) Corresponding changes in astrocyte resting membrane potential to alterations in extracellular  $K^+$  concentrations, 2.5 mM ( $n = 18$ ), 5 mM ( $n = 20$ ) and 12 mM ( $n = 8$ ) (C) The resting membrane potential did not alter between the beginning and the end of control recordings ( $p = 0.29$ ,  $n = 7$ , paired-sample t-test) and (D) did also not differ between baseline and penicillin recordings ( $p = 0.46$ ,  $n = 7$ , paired-sample t-test).

Another possible consequence of the altered astrocyte morphology upon induction of epileptiform activity was an impaired transient  $K^+$  uptake of astrocytes. To evaluate this possibility the astrocyte fEPSPs (afEPSP, Henneberger and Rusakov, 2012) were recorded after paired pulse stimulation (chapter 4.1.8). Example traces are shown in figure 45A under control and penicillin conditions. Field EPSPs were recorded in the stratum pyramidale whereas astrocytes were patched in the stratum radiatum and thus the afEPSPs were recorded there.

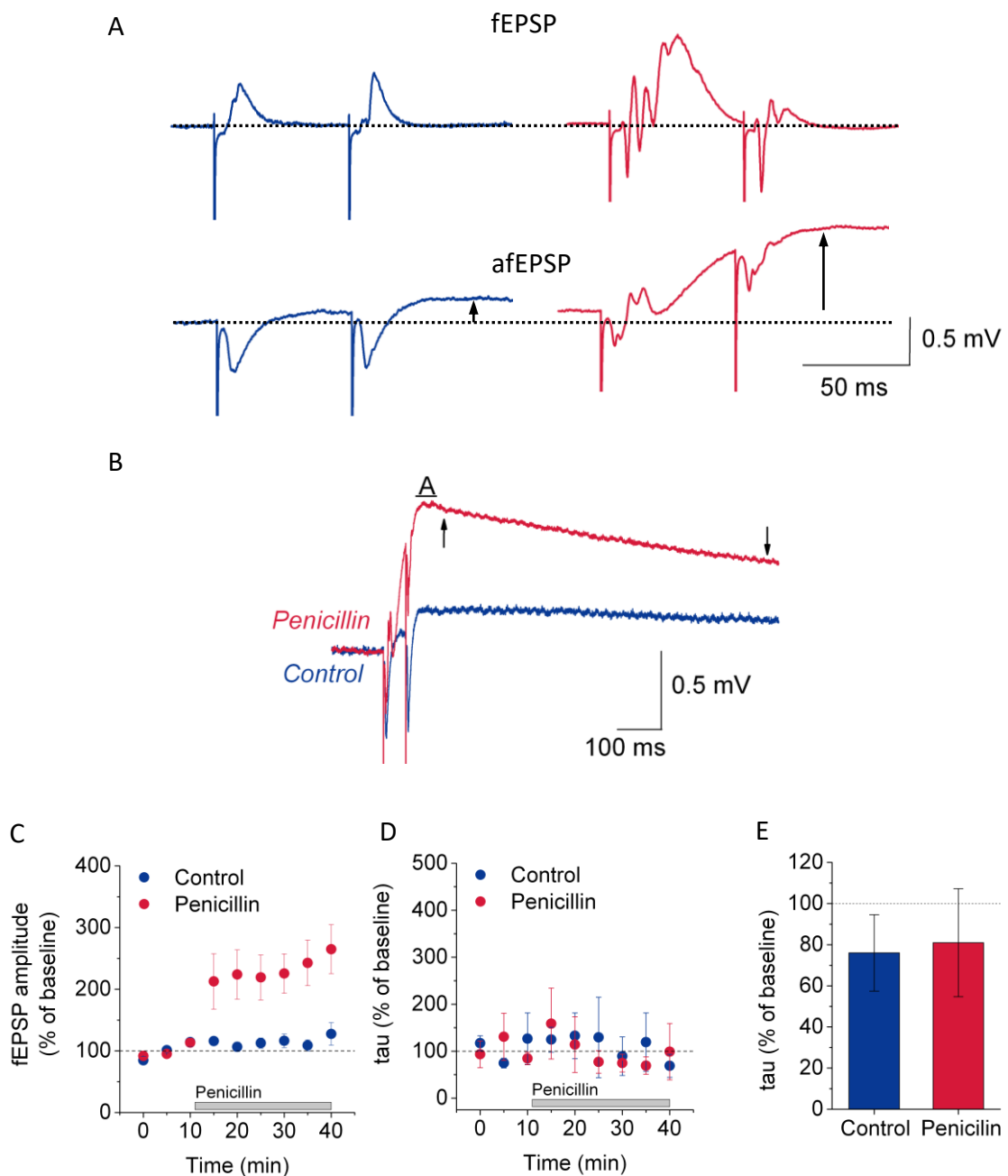


**Figure 45 Astrocyte fEPSPs in response to Schaffer collateral stimulation.** (A) Upper row: example fEPSPs in the CA1 stratum pyramidale in control and penicillin conditions, lower row: corresponding afEPSPs recorded by patching astrocytes in the CA1 stratum radiatum. (B) Example traces visualising the depolarisation of the astrocytes after stimulation in control and penicillin conditions. A (amplitude), line below indicates the region used for amplitude analysis, arrows indicate the region chosen for analysis of the decay. (C) Time course of the afEPSP amplitude showing a clear increase during penicillin application. (D) The decay of the signals is not changing over time in control and penicillin recordings. (E) No differences were found comparing the decay values of the last 10 minutes of control and penicillin experiments ( $p = 0.88$ ,  $n = 5$  for both groups, unpaired two-sample t-test).

Whereas the fEPSP signals turned back to baseline quickly, depolarisations could be observed in the aEPSPs (see arrows). Astrocyte fEPSPs consist of different phases. After paired pulse stimulation the depolarisations after the second stimulus are caused by an increase in the extracellular  $[K^+]$  (Henneberger and Rusakov, 2012). Due to the recurrent discharges occurring during penicillin application, more  $K^+$  is released into the extracellular space, which leads to higher depolarisations of the astrocyte (Figure 45A, lower red trace). For estimation of the astrocyte  $K^+$  uptake the amplitude of the depolarisation and the decay of the signal turning back to baseline (Figure 45B, arrows) were analysed (chapter 4.1.8). The time course of the depolarisation amplitude normalised to baseline (Figure 45C) showed a strong increase during penicillin application compared to control values like shown in the example trace (Figure 45B). The decay  $\tau$  of the signal, in contrast, did not change over time under control and under penicillin conditions (Figure 45D) and comparisons between control and penicillin conditions of the last 10 minutes of the experiments revealed no significant differences between these two groups (Figure 45E,  $p = 0.88$ ,  $n = 5$  for both groups, unpaired two-sample t-test). These results suggest that the  $K^+$  uptake of astrocytes is not altered during induction of epileptiform activity. Taken together, the results indicate that neither the resting nor the transient extracellular  $K^+$  levels are altered after induction of epileptiform activity. This suggests that the induced astrocyte morphology changes do not result in altered astrocyte  $K^+$  uptake or buffering.

### 5.5.5 Effect of astrocyte morphology changes on extracellular glutamate levels

An important function of astrocytes, which depend on the proximity of astrocytes protrusion and neuronal synapse, is the glutamate clearance. Astrocytes express glutamate transporters, which allow a fast transmitter clearance thereby shaping synaptic transmission (Danbolt, 2001; Murphy-Royal et al., 2015). Alterations in astrocyte structure could affect glutamate uptake, which may have consequences for neuronal activity. Thus, altered glutamate levels could also promote epileptiform activity. To investigate if glutamate uptake was impaired after induction of astrocyte morphology changes, glutamate was applied iontophoretically. It was tested, whether glutamate accumulates with the same speed in control slices and in epileptiform slices using the glutamate sensor iGluSnFR (Marvin et al., 2013) expressed in astrocytes (chapter 4.1.2). After obtaining 10 minutes of baseline recordings, penicillin was bath applied for 30 minutes or a control recording was performed, respectively. After control or penicillin recordings neuronal activity and synaptic transmission were blocked using TTX, NBQX, D-AP5 and LY341495 (chapter 4.1.2). This ensured to isolate glutamate transients independent of synaptic and epileptiform activity.

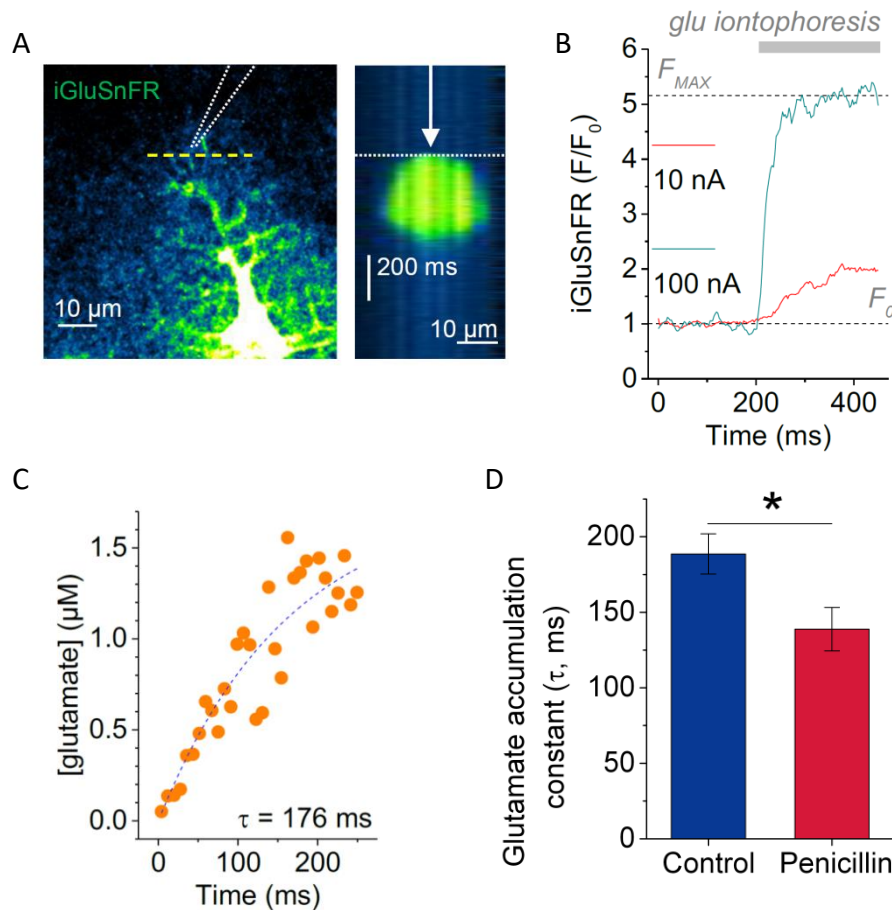


**Figure 46 Glutamate accumulation after induction of astrocyte morphology changes.** (A) Glutamate transients were evoked using glutamate iontophoresis and detected by the glutamate sensor iGluSnFR expressed by astrocytes. As ROI a line was scanned in the periphery of an astrocyte (dashed line, yellow). The right panel shows a typical response of the iGluSnFR to glutamate exposure. (B) Corresponding fluorescence profiles after glutamate application was performed with 100 nA and 10 nA currents. (C) The iGluSnFR response after 10 nA current injections was translated into glutamate concentrations and the result was fitted by a monoexponential function to obtain the time constant of glutamate accumulation. (D) Induction of astrocyte morphology changes by epileptiform activity resulted in a significantly smaller time constant of glutamate accumulation ( $n = 9$  for control,  $n = 7$  for penicillin,  $p = 0.0241$ , unpaired two-sample t-test, analysis and figure done by C. Henneberger).

Glutamate was applied iontophoretically and the glutamate levels were measured using the fluorescence response of the glutamate sensor iGluSnFR in peripheral astrocyte processes. For recording of the iGluSnFR signal a line scan through peripheral astrocytes processes was performed  $1\mu\text{m}$  away from the iontophoretic pipette (Figure 46A). Glutamate was applied with a 100 nA pulse (250 ms) to receive a saturating response, which was used to establish the maximum fluorescence ( $F_{max}$ ). A 10 nA pulse (250 ms) was used to receive a non-saturating iGluSnFR response, which was translated into the glutamate concentration (chapter 4.2.12). The corresponding fluorescence profiles are

visualised in figure 46B. The time constant of the glutamate transients was obtained by fitting the glutamate concentrations with a monoexponential function (Figure 46C). Induction of epileptiform activity resulted in a smaller time constant of glutamate accumulation compared to control recordings (Figure 46D,  $n = 9$  for control  $n = 7$  for penicillin,  $p = 0.0241$ , unpaired two-sample t-test). This result indicates that glutamate accumulated faster after induction of astrocyte morphology changes. This in turn could result in increased neuronal excitation thereby promoting ongoing epileptiform activity.

## 6. Discussion

Mesial temporal lobe epilepsy (MTLE) is the most common form of focal epilepsy in adults. It mainly originates in the hippocampus or surrounding structures. One issue of this disease is that a high fraction of up to 75% of patients suffering from this disease is resistant to anticonvulsants (Schmidt and Löscher, 2005). Often a surgical therapy is the best option since it helps the patients to become seizure free. To identify novel treatment strategies a deeper understanding of the cellular mechanism involved in the originating and progression of MTLE is required. Recent studies in the last decades showed that the physiological functions of the hippocampus do not solely depend on neuronal function, but information processing can also be modulated astrocyte-neuron interaction (for review Sofroniew and Vinters, 2010). Thus, alterations in astrocyte function may also influence neuronal signalling and thus astrocytes could be involved in the development of pathophysiological states of neurological diseases like epilepsy (Coulter and Steinhäuser, 2015; Losi et al., 2012; Seifert et al., 2010). Indeed, long-term changes of astrocytes were found in the later states of MTLE. Also, a main finding in humans and in animal models of epilepsy was that astrocytes undergo astrogliosis. This implicates altered astrocyte function, density and morphology (Pekny et al., 2014). Although it was shown that astrocyte structure is affected during the late states of epilepsy, it is not clear how early alterations in astrocyte morphology occur during the onset of epileptic seizures and to what degree they may contribute to the development of epilepsy. These possible changes in astrocyte-neuron communication during the early state of epilepsy might play a crucial role in the development of this disease and therefore could be a new approach to help developing novel therapy strategies. To this end, acute astrocyte morphology changes during induction of epileptiform activity and the related consequences on astrocyte physiology and their possible impact on the progression of epileptiform activity were investigated in this project. The results and their potential relevance for MTLE will be discussed in the following subchapters.

### 6.1 Astrocyte morphology changes rapidly during the onset of epileptiform activity

#### 6.1.1 Effects in vitro

The first aim of my work was to investigate whether astrocytes undergo acute morphology changes in response to the induction of epileptiform activity. This was done by combining electrophysiological recordings and two-photon excitation microscopy. This method allowed online monitoring of the astrocyte morphology during the onset of epileptiform

activity. Since astrocytes form contacts with neurons through their fine processes (Peters A., Palay S.L., and Webster H., 1991) it was important to capture morphology changes in these fine astrocyte branches and segments. To this end, an analysis tool was used, which captured morphology changes in the very fine astrocyte processes, the so-called astrocyte volume fraction (Medvedev et al., 2014). This analysis tool allowed to quantify astrocyte morphology changes after the onset of epileptiform activity, which has not been demonstrated before.

As an *in vitro* epilepsy model, bath application of penicillin was used (chapter 4.1.4). The penicillin model was firstly described by WALKER A et al. (1945). It was established as a classical *in vivo* and *in vitro* model for epileptiform activity (Chen et al., 1986; Dichter M. and Spencer A., 1969; Schwartzkroin and Prince, 1977). The reasons for choosing this *in vitro* epilepsy model were on one hand that reliable and frequent occurring discharges throughout application could be induced. On the other hand that only the inhibition was modulated without directly acting on NMDA receptors, which should avoid synaptic potentiation by the model itself during induction of epileptiform activity. Another advantage of penicillin is that it can also be used as an *in vivo* epilepsy model since it can be applied in many different variants like intraperitoneal, intravenous but also intracortical (Chen et al., 1986). Penicillin G sodium salt was described to act proconvulsive by inhibiting the chloride ion flux of GABA<sub>A</sub> receptors (Tsuda et al., 1994) and to induce interictal epileptiform activity when applied directly on the cat cortex *in vivo* (Dichter M. and Spencer A., 1969). The effect of penicillin on hippocampal *in vitro* preparations of guinea pigs were firstly investigated by (Schwartzkroin and Prince, 1977). They observed interictal epileptiform discharges in acute hippocampal slices with a typical shape, which could also be recorded in the current study. The shape, frequency and amplitude of the recorded interictal discharges were similar in rat and mouse hippocampal slices (Figure 22).

Interestingly, in both species the successful establishment of the *in vitro* epilepsy model required an slightly increased extracellular K<sup>+</sup> concentration to at least 4mM This is consistent with the extracellular K<sup>+</sup> concentrations used in former studies using this epilepsy model (Schwartzkroin and Prince, 1977; Schwartzkroin and Wyler, 1980). The role of K<sup>+</sup> in the used epilepsy model will be discussed later (chapter 6.3.3). Monitoring astrocyte morphology in parallel to electrophysiological recordings and analysing their volume fraction over time revealed that astrocytes showed a significant decrease of volume fraction upon induction of epileptiform activity within 10 minutes of occurrence of epileptiform discharges. This result could be obtained in rat hippocampal slices, in which astrocytes were visualized by using whole-cell patch-clamp configuration and filling them with a morphology dye but also in hGFAP-EGFP mice where astrocytes were labelled by genetic expression of EGFP (Nolte et al., 2001). These results show that the astrocyte

morphology response to epileptiform activity occurs on a very rapid time scale of minutes. It was present in two different species and was not artificially induced by the method of visualisation of the astrocytes. Astrocytes were visualized either by filling them with the morphological dye Texas red dextran (3kDa), which is due to its size unable to diffuse through gap junctions, or by using genetically expressed EGFP in hGFAP-EGFP mice. To ensure that EGFP is also freely diffusing in the cytosol, a subset of experiments were performed. EGFP-expressing astrocytes were held in cell-attached modus and pictures of the astrocyte were obtained. Subsequently, the patch configuration was switched to whole-cell configuration and the astrocyte was filled with Texas red dextran and again pictures were obtained with two-photon excitation microscopy. The volume fraction of the labelled astrocyte was analysed for the EGFP signal as well as for the Texas red dextran signal. Comparison revealed that astrocyte volume fractions monitored using either genetically expressed EGFP or gap-junction impermeable Texas red dextran showed a perfect match and a linear positive correlation (Figure 21). Thus, both dyes label the astrocyte cytosol. This indicates that using astrocytes expressing EGFP under the hGFAP promotor (Nolte et al., 2001) is a useful tool to investigate astrocyte morphology. Additionally, this suggests that the decrease in astrocyte volume fraction measured using whole-cell patch-clamp recordings is not an artefact of the whole-cell configuration.

Until now only long-term morphology changes of astrocytes were described in the late states of epilepsy (Arisi et al., 2011). In this study, astrocytes were reported to undergo astrogliosis during the chronic states of epilepsy one month after induction of status epilepticus (SE) using the pilocarpine model. In this pathophysiological state astrocytes show an altered morphology and function. Stainings with antibodies against GFAP revealed that astrocytes have an increased volume and a stronger overlap between the cells, which is maximal 10% under physiological conditions (Bushong et al., 2004; Oberheim et al., 2008). In contrast to the increasing volume observed during astrogliosis, it could be shown in the current project, that astrocytes respond with an acute decrease of astrocyte volume fraction to epileptiform activity in rat and mouse hippocampal slices. Application of penicillin during blocked neuronal activity and synaptic transmission had no effect on astrocyte morphology (Figure 24). This was an important control experiment to rule out any side effects of penicillin onto astrocyte morphology. It also indicates that the observed astrocyte morphology changes require epileptiform activity and are a consequence of the extensive neuronal firing. Astrocyte morphology changes were direct temporally linked to the onset of epileptiform activity. Epileptiform activity reached a plateau 5 to 10 minutes within penicillin application (Figure 18, Figure 22), but the maximum decrease of astrocyte volume fraction occurred 20 to 30 minutes within penicillin application (Figure 19, Figure 24). This suggests that the measured astrocyte morphology changes could be a

consequence of the induced epileptiform activity. To ensure that the observed effect is not only due to interictal epileptiform activity which reflects only a part of epileptiform activity (Fisher et al., 2014), experiments were repeated using the 0 Mg<sup>2+</sup> and bicuculline model, which was described to induce ictal and interictal activity (Gomez-Gonzalo et al., 2011) and thus may better reflect epileptic seizures occurring during epilepsy. Using this model the typical ictal and interictal activity could be reproduced in this study (Figure 23). Also in these experiments the induced epileptiform activity was accompanied by a decrease in astrocyte volume fraction (Figure 24). One possible explanation for this observation could be that although the ictal activity consisted of a neuronal firing bursts, the overall frequency at which ictal and interictal events occurred was 10 fold less than observed in the penicillin model. The distribution of the epileptiform discharges was different from the one using penicillin. Whereas the epileptiform discharges are equally distributed during penicillin application, the ictal and interictal activity using 0 Mg<sup>2+</sup> and bicuculline occurred rather in clustered than evenly distributed over time. Assuming that epileptiform activity leads to a neuronal signalling that in turn acts on astrocyte morphology, this may have led to a smaller effect on astrocyte volume fraction since there was more time for recovery between the discharges.

One interesting result appeared analysing the success rate of the different epilepsy models in the two different species rat and mouse. Application of penicillin led to epileptiform activity of 100% in male rat but only in 75% of male mice and even only 50% in female mice. Thus, there were also animals, in which no epileptiform activity at all could be induced in their hippocampal slices. The difference between male mouse and rat hippocampal slices could be explained by the used extracellular K<sup>+</sup> concentration. In general, an increased extracellular K<sup>+</sup> concentration was required to induce epileptiform activity. In rat hippocampal slices the extracellular K<sup>+</sup> concentration was 5 mM whereas in mice only 4 mM could be used, because otherwise the slices did not show stable neuronal network activity under baseline and control conditions. The higher extracellular K<sup>+</sup> concentration leads to a stronger depolarisation of the neurons due to the change in the K<sup>+</sup> equilibrium potential, which could enhance neuronal excitability. This effect might explain the differences in the success rate of induction of epileptiform activity between male rat and mouse hippocampal slices. The reason for the low chance to induce epileptiform activity in female mice is probably the altered hormone level, which was not tested here. Studies showed that female sex steroid hormones could affect neuronal excitability (Taubøll et al., 2015). For example, estrogen had proconvulsive effects when applied via injections or directly to the cortex (Logothetis et al., 1959; Marcus EM et al., 1966) whereas progesterone showed anticonvulsive effects (Reddy, 2009; Spiegel and Wycis, 1945). Since the hormone level of the used female mice was not checked, it might be possible that the

hormone fluctuations affected the neuronal excitability in these mice and thus led to a reduced success rate in developing epileptiform activity. Interestingly, it was also reported for humans that males have a higher incidence for epilepsy than women (Hauser et al., 1993; McHugh and Delanty, 2008). The strength of the astrocyte volume fraction decrease observed after induction of epileptiform activity was independent of the used sexes. Using 0  $Mg^{2+}$  and bicuculline induced epileptiform discharges in 100 % of the slices of female and male mice. In this model not only the inhibition is altered by blocking  $GABA_A$  receptors with bicuculline, but also the excitability of the neurons is increased since the NMDA receptors are not blocked by  $Mg^{2+}$ . Thus, the inhibition/excitation ratio in these slices was even more shifted towards excitation, which probably lowers the threshold for induction of epileptiform activity.

In summary, the results show that induction of epileptiform activity is accompanied by a rapid decrease in astrocyte volume fraction in a timescale of minutes. This result appears to be a robust phenomenon, since it could be shown in two different species and with two different *in vitro* models for epilepsy. This indicates that the structural changes of astrocytes are caused by pathophysiological firing of neurons and may therefore be a general response to epileptiform activity. However, since these structural changes were found in such different species like rat and mice, one could speculate that they could also occur in humans. This would need to be demonstrated by further experiments to check whether this phenomenon could be a possible target for further research concerning novel treatment therapies of MTLE.

There are two emerging questions regarding the astrocyte morphology changes. The first question is, if the decrease of astrocyte volume fraction are induced by distinct neuronal activity pattern. A reduction in astrocyte volume fraction after induction of epileptiform activity could also be observed in *in vivo* experiments (chapter 6.1.2). *In vivo* seizures often show a very diverse neuronal activity pattern. Thus it is unlikely, that a distinct activity rhythm is the cause for astrocyte morphology changes. Additionally, induction of long-term depression by regular 2 Hz stimulation over 15 minutes did not result in astrocyte morphology changes (D. Minge, unpublished data). This supports the hypothesis, that the observed structural changes of astrocytes after induction of epileptiform activity are induced by an increased neuronal firing independent of the neuronal spiking pattern.

As second point, it would be important to know, whether the astrocyte morphology changes are locally restricted to the CA1 region. All experiments were performed in the CA1 region of the hippocampus in the different species. It is not clear whether the changes in astrocyte morphology upon induction of epileptiform activity are CA1 specific or a general response of astrocytes to intense neuronal network activity independent of the brain region. To answer this question similar astrocyte morphology could be monitored and

analysed in different brain regions during induction of epileptiform activity. Additionally, the results do not show if the astrocyte morphology changes are locally restricted to the initiation site of epileptiform activity. Since field potentials were only recorded in the CA1 region of the hippocampus and the connections between dentate gyrus (DG), CA3 and CA1 region were intact in these experiments, it is not clear where the initiation site in the used penicillin model was. There is evidence that the initiation of epileptiform activity occurs in the CA3 region (Avoli et al., 1996; Chever et al., 2016; Hablitz, 1984) in acute hippocampal slices, when epileptiform activity is induced by pharmacological treatment. Thus, this might also be the case for the used penicillin model, although no studies were performed clarifying the origin of epileptiform activity using penicillin as *in vitro* model for epilepsy. Thus, the CA1 region does not need to be the initiation site of epileptiform activity in the current study. Assuming that the observed astrocyte morphology changes are a consequence of neuronal firing, it can be suggested, that they would also occur in the CA3 region or the DG. This favours the idea that astrocyte morphology changes due to epileptiform activity is not locally restricted to the initiation site but probably is at least spreading in the hippocampus and possibly also to further brain regions depending on the spread of epileptiform activity. A simple experiment to confirm this hypothesis would be to monitor astrocyte morphology in the DG, the CA3 region and the CA1 region during induction of epileptiform activity in acute hippocampal slices using penicillin application.

### **6.1.2 Astrocyte morphology changes in an *in vivo* epilepsy model**

As a first indication, if astrocyte morphology changes are relevant during epileptogenesis *in vivo* and not only a slice artefact, astrocyte volume fractions were measured in the kainate model of epilepsy (Bedner et al., 2015). To this end, juxta hippocampal injections of kainate or NaCl as a sham treatment were conducted in respectively three hGFAP promotor-controlled EGFP-expressing transgenic mice (Figure 47, done by Peter Bedner). 30 minutes after kainate or sham injection the animals were perfused and the brains were fixed in paraformaldehyde. Brains were cut and pictures were obtained with a laser scanning confocal microscope (TCS NT, Leica, figure 47, middle panel, perfusion and microscopy were done by Michel Herde). Volume fraction analysis was conducted as described before (chapter 4.2.3, done by M. Herde and C. Henneberger) and revealed that astrocytes showed a significant reduced volume fraction in kainate-treated animals compared to sham-treated animals with a stronger effect on the ipsilateral side (Figure 47, right panel,  $n = 48$  for sham ipsi,  $n = 49$  for all other groups,  $p = 0.000007$ , two way ANOVA repeated measurements (RM) with posthoc Fisher test). In detail, the volume fraction on the ipsilateral side of astrocytes in kainate treated animals was significantly decreased compared to the ipsilateral mean volume fraction of astrocytes from sham injected animals

( $p = 0.0003$ , two way ANOVA RM with posthoc Fisher test). The astrocyte volume fraction on the ipsilateral side of kainate-injected mice was also significantly reduced compared to the contralateral side of sham-injected mice ( $p = 0.000002$ , two way ANOVA RM with posthoc Fisher test). The decrease of astrocyte volume fraction was significantly stronger on the ipsilateral side of kainate-treated animals than on the contralateral side of the same group of animals ( $p = 0.0187$ , two way ANOVA RM with posthoc Fisher test). The fact that the mean volume fractions of the ipsi- and contralateral sides of sham-injected animals is not significantly different ( $p = 0.68$ , two way ANOVA RM with posthoc Fisher test), indicates that the mechanical stress by the injection itself has no influence on astrocyte morphology. Thus, the observed decrease in astrocyte volume fraction in kainate-treated animals compared to sham-treated animals is a direct effect of the excessive neuronal firing during the induced status epilepticus. Showing that the decrease in astrocyte volume fraction also occurs in an *in vivo* epilepsy model is a very important finding. It rules out that the effect on astrocyte morphology observed *in vitro* is a methodical artefact due to the *in vitro* conditions. The advantage of the used *in vivo* epilepsy model was that it reproduces the key features of chronic human MTLE (Bedner et al., 2015). To compare features of chronic human MTLE with their mouse model they observed the morphological, molecular and functional changes in their animal model and compared it with tissue from MTLE patients. They found a close match in these parameters in tissue of the two species, including astrocyte loss and impairment of astrocyte coupling. This observed similarity suggests that also the very early phase of developing epilepsy could be similar between the mouse model and humans. Thus, it can be speculated that the described effect of the reduced astrocyte volume fraction after status epilepticus could occur during human epileptogenesis and might have functional consequences for the development of chronic epilepsy.

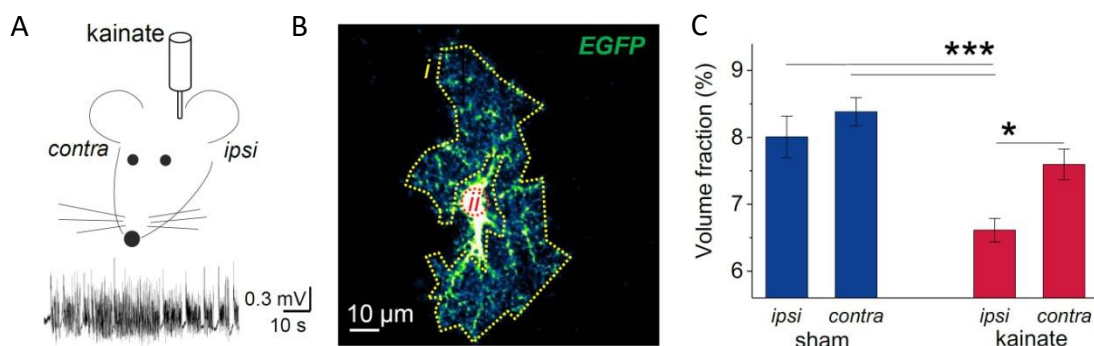


**Figure 47 Astrocyte volume fraction after kainate and sham injection.** (A) Mice were injected with kainate, which induced status epilepticus (SE) and chronic epileptic seizures. (B) Volume fraction of EGFP expressing astrocytes was estimated 30 minutes after induction of SE, (C) kainate injected mice showed a significant reduced volume fraction compared to sham injected mice with a stronger effect on the ipsilateral side ( $p = 0.000007$ , two way ANOVA RM with posthoc Fisher test, figure adopted from C. Henneberger).

### 6.1.3 Persistence of astrocyte morphology changes

To understand if the observed changes in astrocyte volume fraction due to induction of epileptiform activity are only transient events and how epileptiform activity and astrocyte morphology changes determine each other, recovery experiments were performed (chapter 5.2.1). The results showed that epileptiform activity persisted for at least 40 minutes after washout of penicillin although with a lower frequency, which was accompanied by a persistent decrease in astrocyte volume fraction (Figure 25). To clarify, whether the ongoing epileptiform activity is caused by an incomplete washout of penicillin and thus a still partial blocked inhibition, inhibitory postsynaptic currents (IPSCs) were measured during baseline, penicillin application and penicillin washout (experiments and analysis performed by D. Minge and C. Henneberger). The measured IPSCs went back to control conditions when penicillin was washout (Figure 48,  $n = 5$  for control,  $n = 10$  for penicillin,  $p = 0.30$ , unpaired two-sample t-test), although the IPSC amplitude tended to be lower. This shows that the inhibition almost completely recovered and that the ongoing epileptiform activity was probably not caused by an ongoing affected inhibition in the slice.

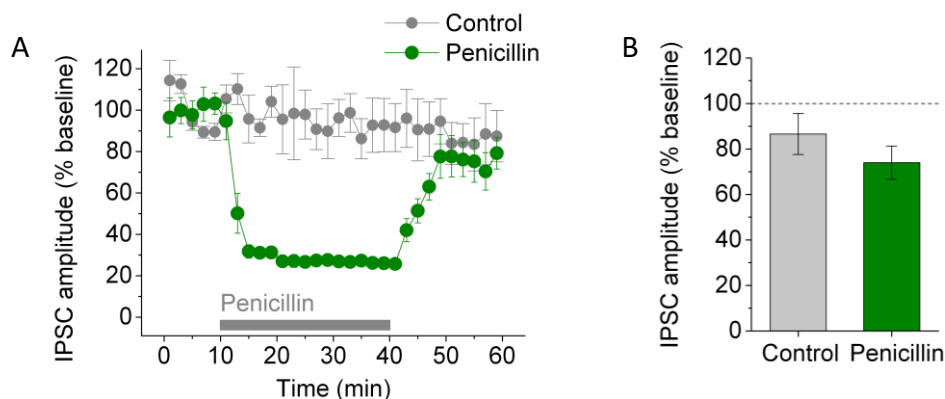


**Figure 48 IPSC amplitudes during control and penicillin recordings.** (A) Application of penicillin leads to a reduction of IPSC currents of 75%. After washout of penicillin IPSC currents recovered back to control conditions (B,  $n = 5$  for control,  $n = 8$  for penicillin,  $p = 0.30$ , unpaired two-sample t-test, Figure adapted from C. Henneberger).

Interestingly, blocking neuronal activity during penicillin washout using TTX had no effect on the persistent decrease of astrocyte volume fraction (Figure 25). Thus, persistent changes in astrocyte morphology after induction of epileptiform activity did not require ongoing epileptiform discharges. This suggests that the induction of epileptiform activity is required and acts like a trigger for astrocyte morphology changes, which are then not reversible during the observed time period. Together the findings, that epileptiform activity and astrocyte morphology changes persist, although the inhibition recovered completely, suggest that the astrocyte volume fraction decrease could cause ongoing epileptiform activity. To understand how astrocyte morphology changes are possibly linked to ongoing epileptiform activity, the strength of astrocyte volume fraction change as a mean of the values obtained 25 to 30 minutes within application of penicillin was correlated with the fraction of remaining discharges (Figure 38). Plotting the fraction of remaining discharges over the astrocyte volume fraction change revealed a significant correlation between the strength of astrocyte volume fraction decrease and the remaining fraction of discharges. This result indicates that the astrocyte morphology changes could have a proepileptic effect in the CA1 region of the hippocampus. Further on, it also shows that the morphology response of the single astrocyte probably represents a network response of these cells. Precisely, by using recording of local field potentials the signals of a population of neurons is recorded. Thus, the response of a neuronal network is recorded. Modelling of interictal activity revealed that the minimal neuronal aggregate required for an interictal discharge is 1000 to 2000 neurons (Osorio et al., 2011). If, by accident, a single astrocyte was imaged, which, for any reason, did not respond to the induced epileptiform activity, then this was unlikely to have an effect on the whole neuronal network activity. The more likely explanation might be that the response of the single astrocytes reflects the network response of the majority of astrocytes, which in turn could have an effect on neuronal network activity. The possible proepileptic effect of astrocyte morphology changes will be discussed in more detail in chapter 6.2.2.

In conclusion, this would mean that epileptiform activity triggers astrocyte morphology changes. These astrocyte restructuring in turn promotes ongoing epileptiform discharges. The persistence of epileptiform discharges was NMDA receptor-dependent (Figure 25), which was shown before using penicillin as *in vitro* epilepsy model (Watson and Lanthorn, 1990). This is probably not specific for the used epilepsy model, but rather due to the general role described for NMDA receptors in animal models of epilepsy (Ghasemi and Schachter, 2011). The NMDA receptor seem to be involved in epileptiform activity in almost all commonly used models, like the kindling model, pilocarpine, kainate-induced, or picrotoxin (Gerfin-Moser et al., 1995; Kraus et al., 1994; Lasoń et al., 1997). Further investigation revealed that the GluN2A and GluN2B subunits of the NMDA receptor play a

role in epileptogenesis. However, keeping in mind the astrocyte function and their ability to act on NMDA receptors (Henneberger et al., 2010), confirms the potential role for this cell type in the development of epilepsy (Auzmendi et al., 2008; Chen et al., 2007).

The discussed effects occurred in the acute phase of epileptiform activity. The decrease in astrocyte volume fraction and its persistence is a different morphologic behaviour of the astrocytes than described for the chronic phase of TLE. It was shown in former studies that astrocytes undergo astrogliosis during the chronic phase of epilepsy (Binder and Steinhäuser, 2006) with an increased volume and a higher overlap of their territories (Arisi et al., 2011; Oberheim et al., 2008). The time point of beginning astrogliosis during epileptogenesis is not clearly defined in literature. But probably the very acute morphology response observed in the current project and the described later emerging astrogliosis during chronic states of epilepsy are two distinct mechanisms.

Astrogliosis is observed, when the hippocampus is already in a pathophysiological condition, whereas slices developing epileptiform discharges could be in an intermediate state between physiological and pathophysiological conditions. The possible proepileptic effect caused by the strength of shrinkage of astrocyte processes (Figure 38) allows to speculate that the progression of epileptogenesis depends on the astrocyte morphology response, either epileptiform activity is promoted and the hippocampus develops a pathophysiological behaviour. Alternatively, it is suppressed and the neuronal network turns back to its physiological condition. To further investigate this hypothesis, it would be necessary to monitor epileptiform activity progression and astrocyte morphology over a longer timescale using the *in vivo* kainate model of epilepsy, for instance. Possibly this could give a new hint to explain the high variability of seizure frequency in kainate treated animals (Bedner et al., 2015).

#### **6.1.4 Characterization of astrocyte morphology changes**

To assess possible physiological and pathophysiological functions associated with the observed astrocyte morphology changes, it was necessary to characterise what kind of morphology changes occurs in the astrocyte and where these changes are localised. Analysis revealed that the observed astrocyte morphology changes occur in the periphery, in the small and medium thick astrocyte branches (Figure 26). Segmentation analysis indicated that these processes shrink (Figure 27). It is important to mention here that the astrocyte territories were not altered (unpublished data, C. Henneberger). Thus, the astrocyte had still the same territorial size, but the processes were thinned. This results in a decreased cytosol volume. The shrinkage of astrocyte processes is a different response to increased neuronal activity than described to occur during synaptic plasticity. Neuronal activation increased the motility of astrocyte processes (Haber et al., 2006). Whisker

stimulation *in vivo* (Genoud et al., 2006) and induction of LTP (Bernardinelli et al., 2014b; Perez-Alvarez et al., 2014a) led to a displacement of small astrocyte processes. Although these structural responses are different from the shrinkage of astrocyte processes after induction of epileptiform activity, it appears that astrocytes in general use structural changes as response to neuronal activation. Interestingly, they are able to respond with different morphology alterations to different neuronal activation patterns.

The volume shrinkage was not happening homogeneously but rather in the smaller processes, whereas the soma and thick branches are not changing their volume after induction of epileptiform activity (Figure 26). Since fine astrocyte branches are thought to form close contact with neurons (Medvedev et al., 2014; Špaček, 1985) it could be suggested that these astrocyte parts show a stronger morphology response because they are exposed to neuronal signalling. On the other hand, morphology changes of astrocyte protrusion near neuronal segments may have in turn important effects on neuronal function and network activity. To understand the possible functional consequences of the astrocyte morphology changes, it was important to not only investigate astrocyte morphology but also neuronal morphology. If neurons were swelling during induction of epileptiform activity in the same range like astrocyte were shrinking, the extracellular space (ECS) between the compartments and thus spatial relationship would not be altered significantly. Although, the receptor distribution might be altered due to the alterations in membrane surface. If neurons were not changing their volume upon induction of epileptiform activity, the ECS would increase, which could have functional effects on extracellular diffusion in addition to alterations in astrocyte function. Analysing dendritic morphology in the penicillin model revealed no changes in neuronal volume fraction. Additionally, the whole slice volume was calculated to check whether this parameter was changing during induction of epileptiform activity. As shown in Figure 29, the volume of the slice did not change in control or penicillin recordings during the entire experiment. Together with the result that neuronal morphology was not altered, this probably suggests, that the ECS could be increased due to the shrinkage of the astrocyte processes. Although it has to be mentioned, that a higher number of experiments is required to draw this conclusion. Another possibility to measure the extracellular space fraction is the use of tetramethylammonium ( $\text{TMA}^+$ , Nicholson and Phillips, 1981; Roitbak and Syková, 1999). Therefore,  $\text{TMA}^+$  would be applied iontophoretically in control and in penicillin treated slices.  $\text{TMA}^+$  diffusion curves can be recorded using  $\text{TMA}^+$  sensitive microelectrodes. Changes in the extracellular space could be captured by changes in  $\text{TMA}^+$  diffusion.

Keeping in mind that only small and medium sized astrocyte processes showed a morphology response, the ECS probably mainly increased at the same locations and not homogeneously in the slice. Since astrocyte-neuron interactions depend on the diffusion of

ions through the extracellular space, alterations of this compartment may have strong effects on synaptic function. For instance, neurotransmitters could escape from the synaptic cleft, when synapses are less covered by astrocytes, which could result in neurotransmitter spillover and synaptic cross talk (Asztely et al., 1997; Kullmann et al., 1996). It was also hypothesised that volume changes in the extracellular space modulate neuronal excitability (Hochman D. W., 2009). The fact that no alterations could have been observed in synaptic transmission and plasticity after induced astrocyte morphology changes (Figure 41) suggests that the possible changes in ECS either are not that strong to produce an effect on molecule diffusion or that the morphology changes are not happening directly at the synapse but rather in astrocyte processes further away. This second possibility would imply that the astrocyte volume change and the possible linked alterations in astrocyte function are mainly responsible for subsequent effects on neuronal activity.

## **6.2 Mechanism of astrocyte morphology changes and its effect on epileptiform activity**

In the following subchapters the underlying mechanism of the observed astrocyte morphology changes will be discussed. Furthermore, it will be discussed which consequences the astrocyte restructuring in turn could have on neuronal activity. It will be focussed on the bilateral neuron-astrocyte interaction in terms of acute epileptogenesis.

### **6.2.1 Restructuring of the actin cytoskeleton**

To understand the underlying mechanism of astrocyte processes shrinkage in response to induction of epileptiform activity, the proteins and molecules of the signalling pathways regulating the actin cytoskeleton were pharmacologically modulated. Culture studies have been demonstrated that astrocyte morphology is regulated by the RhoA pathway (Höltje et al., 2005; Kalman et al., 1999; Racchetti et al., 2012; Ramakers and Moolenaar, 1998). A consistent finding in literature is that RhoA activation inhibits astrocyte stellation (Ramakers and Moolenaar, 1998; Kalman et al., 1999; Perez et al., 2005; Höltje et al., 2005). The role of RhoA in astrocyte morphology changes during astrogliosis was also demonstrated. Interleukin-1beta, which is important for glial scar formation, deactivates human cultures astrocytes, which resulted in a stellate astrocyte morphology (John et al., 2004). The main downstream effector of RhoA is Rho associated coiled-coil containing protein kinase (ROCK). Inhibition of ROCK in cultured astrocytes also resulted in stellation (John et al., 2004; Racchetti et al., 2012) and increased migratory activity (Höltje et al., 2005). This indicates, that the RhoA-ROCK pathway controls astrocyte morphology. For this

reason, modulation of this pathway was used to investigate the mechanism of astrocyte morphology changes.

Pharmacological inhibition of the ROCK using bath application of Y27632 prevented the astrocyte volume decrease during induction of epileptiform activity (Figure 34) indicating that the observed astrocyte morphology changes are caused by changes in the actin cytoskeleton. This blockade could be induced by high concentrations (20  $\mu$ M) but also partially with low concentrations (5  $\mu$ M). The lower concentration was used to avoid side effects of the drug, which was shown to possibly also affect the protein kinases A and C activities at higher concentrations ([www.tocris.com](http://www.tocris.com)). Interestingly, epileptiform activity was significantly reduced in slices treated with the ROCK inhibitor. This was quantified by the discharge frequency, which was lower during penicillin application (Figure 34). However, after washout of penicillin the discharge frequency was comparable to the one observed in absence of Y27632. This result appeared, because in 2 of 6 measurements the number of discharges increased dramatically, whereas in the remaining 4 slices no further epileptiform discharges could be observed. Due to this high variability of the data, the discharge probability was analysed (chapter 4.1.5). Analysing this parameter revealed a significantly reduced epileptiform activity until the end of the experiment. Of course, the observed blockade of astrocyte morphology changes by the ROCK inhibitor could be induced by a side effect of this drug on neuronal excitation.

Analysis of basal parameters of synaptic transmission like fEPSP slope, fibre volley amplitude, spike/slope coupling (Figure 35) showed that there were no differences in baseline recordings regarding the parameters in presence and absence of Y27632. This suggests that neuronal excitation was not altered by the presence of this drug and that the changes in epileptiform activity were induced by the blockade of astrocyte morphology changes. Since an effect on astrocyte morphology was visible, possible effects of the ROCK inhibitor on neuronal morphology could not be excluded. To target astrocyte morphology more specifically, Y27632 was applied intracellularly using whole-cell patch-clamp configuration in astrocytes. The drug with a size of 320.3 Da should be distributed through the whole astrocyte network via gap junctions. In this experimental setup astrocyte morphology changes during induction of epileptiform activity could also be blocked in the presence of the ROCK inhibitor (Figure 36). Interestingly, also here the induced epileptiform activity tended to be reduced when Y27632 was present in the astrocyte network. Although no significant effect could be observed. These experiments did not only show that astrocyte structural plasticity is linked to neuronal activity, but it also provided a new tool to modulate astrocyte morphology changes.

Further investigation of the possible signal cascade linking neuronal hyperactivity to astrocyte morphology changes did not give conclusive results. As possible receptor

candidates, the sphingosine-1-phosphate receptor (S1P) and the lysophosphatidic acid receptor were investigated. These two receptors were shown to be upstream activators of ROCK (Tönges et al., 2011). These are G protein-coupled receptors and their activation results in the transformation of RhoA-GDP to RhoA-GTP, thereby activating it. RhoA in turn leads to the activation of ROCK. S1P and LPA receptors were shown to be expressed by astrocytes (Fischer et al., 2011; Steiner et al., 2002). Their activation was expected to activate RhoA and thus result in a decrease in astrocyte volume fraction. However, no significant changes in astrocyte volume fraction could be found when S1P and LPA were bath applied (Figure 37). There is also evidence that astrocyte morphology changes are cAMP-dependent (Ramakers and Moolenaar, 1998). The upstream regulator of cAMP is the adenylyl cyclase (AC). Therefore, the membrane-permeable activator NKH477 and inhibitor SQ22537 of the AC were also bath applied to modulate astrocyte morphology. Interestingly, bath application of NKH477 led to a significant decrease in astrocyte volume fraction (Figure 37), but it also resulted in epileptiform discharges. The control experiment in presence of TTX to block neuronal activity showed that NKH477 alone had no effect on astrocyte morphology. These observations confirm the link between neuronal hyperexcitability and astrocyte morphology changes, although it is not clear, by which mechanism NKH477 mediates epileptiform activity. The AC inhibitor SQ22537 had also no effect on astrocyte morphology. Thus, it could not be clarified, by which upstream pathway of RhoA/ROCK the changes in the astrocyte actin cytoskeleton were modulated. Another possible candidate would be metabotropic glutamate receptors (mGluRs). RhoA is mainly regulated by G-protein-coupled receptors. mGluRs belong to this family of receptors. The epileptiform discharges lead to a strong release of glutamate, which could activate astrocyte mGluRs (Aronica et al., 2003; Cai et al., 2000; Cormier et al., 2001; Devaraju et al., 2013; Gibbs and Bowser, 2009). Although no direct link between mGluR activation and RhoA signalling was shown yet in astrocytes, this mechanism could be a possible scenario. In neurons, among many other things, glutamate signalling induces spine growth (Kwon and Sabatini, 2011). Thus, also in astrocytes glutamatergic activation of mGluRs could induce changes in the actin cytoskeleton.

Additionally, also passive mechanisms responsible for astrocyte morphology changes were described. Aquaporin 4 (AQP4) was thought to be a crucial for inducing astrocyte morphology changes due to neuronal activation as it regulates the water influx into the astrocytes after  $K^+$  or glutamate uptake (Nagelhus and Ottersen, 2013; Song and Gunnarson, 2012). A link between astrocyte swelling and its proconvulsive effect was described by (Dudek et al., 1990). In this study a decreased extracellular space induced by changing medium osmolarity resulted in generation of epileptiform activity. However, the used method also led to neuronal swelling and thus led to a different physiology of the

neuron- astrocyte network than induced by the penicillin model, where neurons, for instance, were unaffected. In the present project it cannot be ruled out that AQP4 channels also play a role during astrocyte volume changes and that a combined effect caused by cytoskeletal alterations and water flux regulations is observed.

In any case, inhibition of ROCK appears to be sufficient to block astrocyte morphology changes during epileptiform activity. In the context of human MTLE, modulation of astrocyte morphology may thus be considered as possible treatment strategy since epileptiform activity could be reduced by controlling astrocyte morphology. To approach this aim, further experiments would be required to examine if also accompanied described changes in gap junction coupling, K<sup>+</sup> buffering, astrogliosis and hippocampal sclerosis can also be reduced by controlling astrocyte morphology changes on an early time point in epileptogenesis. A possible experimental design would be to use the *in vivo* kainate model of epilepsy in mice with a conditional knockout of astrocyte ROCK to avoid developmental alterations in the brain. The ROCK knockout should be induced before kainate injection, because the results in this study showed that astrocyte morphology changes are temporally linked to the onset of epileptiform activity. Epileptic seizures should be monitored using EEG recordings. At different time points after induction of status epilepticus (SE), astrocyte morphology, astrocyte gap junction coupling and the characteristics of hippocampal sclerosis should be examined. Possible time points for these investigations could start 30 minutes after induction of SE until the chronic phase of epilepsy nine months later. One important point would be to monitor the SE directly from the beginning. This would help to differentiate if an altered SE results in possible subsequent alterations in the development of epilepsy or if the blockade of astrocyte morphology changes cause potential differences in epileptogenesis.

### **6.2.2 Proconvulsive effect of astrocyte morphology changes**

The observed rapid astrocyte morphology changes induced by epileptiform activity could have variable effects on the further development of epileptiform activity. Alterations in astrocyte morphology accompanied with the observed decreases in intra- and intercellular diffusion could affect a number of astrocyte functions. This in turn could result in altered neuronal activity. Thereby, the overall effect of rapid astrocyte morphology changes may be pro- or antiepileptic. Several results in the current study provided evidence that the observed astrocyte volume fraction decrease has a proepileptic effect. It could be shown that the strength of the decrease is positively correlated with the fraction of remaining discharges (chapter 5.2.1). This means that slices developed a higher fraction of remaining discharges after washout of penicillin, when the strength of astrocyte volume fraction decrease was higher after induction of epileptiform activity. This result directly links the

structural change of astrocytes with ongoing epileptiform discharges. Furthermore, blocking astrocyte morphology changes either by bath application of the ROCK inhibitor Y27632 resulted in decreased epileptiform activity (chapter 5.4.1). Thus, the fine astrocyte processes could not shrink in response to epileptiform activity as they do in absence of the ROCK inhibitor. This resulted in a decreased epileptiform activity. Interestingly, the discharge probability during the first 10 minutes did not differ significantly between recordings in presence and absence of Y27632. But the further development of epileptiform activity was did not decrease significantly when Y27632 was brought into the astrocyte network. This can be possibly explained by the number of astrocytes, which receive an effective concentration of the drug. The range is probably too small to induce an effect on the whole neuronal network activity. Changes in astrocyte morphology usually started in the first 10 minutes of induction of epileptiform activity (Figure 19, Figure 24). The fact that the inhibition of the astrocyte volume fraction decrease resulted in a reduced further development of epileptiform discharges already during penicillin application suggests that astrocyte morphology changes in this model have a proepileptic effect.

To further link structural changes of astrocytes with epileptiform activity, astrocyte morphology responses were deeper analysed. Throughout the experiments it turned out that not all astrocytes responded with a morphology change to epileptiform activity. Analysing the discharge frequency revealed that slices, where astrocytes did not respond with a volume fraction decrease developed a significant lower frequency of epileptiform discharges over time compared to slices where responder cells were imaged (Figure 39), although the discharge frequency measured in the first 10 minutes did not differ in the two groups. Thus, astrocyte morphology changes were correlated with an increasing frequency of epileptiform discharges. One could argue that the overall decreased epileptiform activity (Figure 39) prevents astrocyte morphology changes. But also in measurements with very low discharge frequencies, significant volume fraction decreases could be observed, indicating that not a threshold discharge frequency is required to induce astrocyte morphology changes. This result supports the hypothesis that a decrease in astrocyte volume fraction could promote epileptiform activity and that the structural response of a single astrocyte probably represents the network morphology response of all astrocytes, which could explain the consequences for neuronal network activity.

### **6.3 Physiological and pathophysiological consequences of altered astrocyte morphology**

The observed astrocyte morphology changes due to the induction of epileptiform activity could have important effects in physiological brain function as well as on further development of epileptiform activity. To this end, the possible functional consequences of

altered astrocyte morphology were investigated and will be discussed in the following subchapters. The decrease of astrocyte volume fraction upon induction of epileptiform activity could be observed in rat hippocampal slices where astrocytes were visualized by filling them with the morphological dye Texas red dextran (3kDa) as well as in hGFAP-EGFP mice, in which astrocytes expressed EGFP endogenously (Nolte et al., 2001). In both species the application of 4 mM penicillin led to reliable epileptiform discharges with an interictal shape. Frequency and amplitude were similar in rat and mice, although in mice both parameters tended to be lower. Thus, with this protocol it was possible to induce the same type of epileptiform activity. The observed subsequent decrease in astrocyte volume fraction was also comparable between the two different method conditions. Due to the similar results in these different experimental conditions, it appears valid to perform subsequent experiments in the two species and to arrive at an overall result from these different experiments.

### **6.3.1 Effects on intracellular and intercellular diffusion**

As described before (chapter 5.2.2) the observed astrocyte morphology changes are a volume fraction decrease and are caused by a shrinkage of the fine and medium-sized processes. As mentioned previously, the astrocyte territory was not altered after induction of epileptiform activity. Thus, the volume fraction decrease was caused by a thinning of astrocyte processes. A very basic cellular mechanism modulating and regulating cell function is the intracellular diffusion which probably might be affected by an altered cytosolic volume of astrocyte processes. Fluorescence recovery after photobleaching (FRAP) can be used as indicator to measure intracellular diffusion (Meyvis et al., 1999). Using a high laser power a region of interest, which included the soma, thick and fine branches of EGFP-expressing astrocytes, was bleached and after closing the laser shutter intact fluorescent EGFP molecules could diffuse back into the bleached region. The recovery fluorescence caused by the back-diffusing EGFP molecules was captured when reopening the shutter (chapter 4.2.8). In this set of experiments it was expected that due to the decreased volume of astrocyte processes also the diffusivity of EGFP was reduced, which should be observable by calculating FRAP. The speed by which molecules can diffuse through processes, but also the number of fluorescent molecules that can enter the ROI in the same time depend on the diameter of the processes. The obtained results confirmed this expectation. Analysis of FRAP experiments revealed that after induction of epileptiform activity, FRAP was decreased in contrast to control recordings where FRAP was not significantly altered compared to baseline (chapter 5.3.1). Since the significant changes in astrocyte volume fraction occurred in the fine and medium sized branches, almost no volume changes were found in thick branches and the soma upon induction of epileptiform

activity (Figure 26) it can be suggested that the observed reduction of FRAP in penicillin treated slices is probably caused by diffusion changes in the fine and medium sized branches due to their strong volume changes. Thus, it could be possible that the intracellular astrocyte diffusion was decreased as a consequence of the astrocyte fine and medium-sized processes shrinkage during epileptiform activity. The intracellular diffusion is an important factor, since the diffusion of signalling molecules to the membrane or the propagation of  $\text{Ca}^{2+}$  waves in astrocytes depends on the intracellular diffusivity. Thus, an alteration could affect a number of cellular mechanisms and have functional consequences in the brain information processing.

Astrocytes are extensively coupled via gap junctions (Giaume et al., 2010; Gutnick et al., 1981; Kuffler et al., 1966). The key functions of this so-called astrocyte syncytium include on the one hand metabotropic support of neurons (Rouach et al., 2008) and on the other hand spatial buffering of  $\text{K}^+$  (Wallraff et al., 2006). The efficacy of functional astrocyte networks might also depend on the diffusion of metabolites and ions through the gap junctions. A decrease in intracellular diffusion could also result in a reduced intercellular diffusion. Thus, ions and metabolites will be transported slower and the efficacy of the astrocyte network could be impaired. If this was the case, then astrocyte coupling should be reduced in slices treated with penicillin and developing epileptiform activity. As an indicator for astrocyte coupling a new analysis tool was used for this project (Anders et al., 2014). Astrocyte dye coupling was investigated in different hippocampal regions and during induction of epileptiform activity. As parameter the coupling length constant  $C\lambda$  was used. In cooperation with Daniel Minge and Stephanie Griemsmann the coupling length constant of astrocyte networks was investigated in room temperature and in  $34^\circ\text{C}$  and compared to results obtained by standard cell counting. Using cell counting as parameter no temperature-dependent differences could be observed in astrocyte dye coupling. In contrast, the coupling length constant captured significant temperature-dependent differences in astrocyte dye coupling of the same astrocyte clouds as used for cell counting (Figure 32). The coefficient of variation was much smaller for the coupling length constant compared to cell counting, suggesting a lower variability in coupling length constant than in cell counts. This shows that using the coupling length constant is a more sensitive measure to capture changes in astrocyte gap junction coupling. It also has the advantage to be an objective measure in contrast to manual cell counting, which has the disadvantage of a potential subjective bias during visualisation and analysis.

To investigate if an altered intracellular diffusion of the morphological dye was causing the temperature-dependent changes in astrocyte dye coupling, FRAP experiments were used. FRAP was performed in astrocytes expressing EGFP, which is membrane impermeable and freely diffusing in the cytosol. Indeed, an increase in FRAP and thus in intracellular

diffusivity could be found (Figure 32). The temperature-dependent increase of  $C\lambda$  was 51%, whereas the increase in FRAP was 28.8%. Further analysis and modelling of astrocyte dye-coupling revealed, that temperature-dependent changes in intracellular diffusivity could only partly explain the increase in astrocyte dye-coupling (Anders et al., 2014). Although (Ogata and Kosaka, 2002) observed a dorso-ventral gradient in number of coupled astrocytes in the molecular layer of the dentate gyrus, the analysis of the coupling length constants in these regions revealed no significant differences. Also no differences in coupling length constant between the CA1 region and the DG could be found, indicating that the astrocyte dye coupling is homogenous in the hippocampus.

With this newly-established method for quantification of astrocyte coupling, possible changes on astrocyte dye coupling after induction of epileptiform activity were investigated. Interestingly, induction of epileptiform activity resulted in a significantly reduced dye-coupling (chapter 5.3.3). A possible reason for this reduction could be the decrease in intracellular diffusivity. Alternatively it could be caused by alterations in protein expression of the connexins (Cx) 43 and 30 or phosphorylation of the Cx43 (Solan and Lampe, 2014), from which astrocyte gap junctions in the hippocampus are built (Giaume et al., 2010; Wallraff et al., 2006). The time period of 30 minutes would be probably too short to alter protein expression levels. However, western blot analysis of control slices and epileptiform slices was performed (Figure 49, Western blot performed by Tushar Deshpande). The results showed that neither the protein expression level of Cx43 and 30 ( $N = 4$ ,  $n = 8$ ,  $p = 0.87$  for Cx 43,  $p = 0.46$  for Cx30, unpaired two-sample t-test) nor the phosphorylation of Cx43, which was shown to have 3 different phosphorylation forms (P0, P1, P2), were altered upon induction of epileptiform activity ( $p = 0.47$  for P0,  $p = 0.88$  for P1,  $p = 0.83$  for P2, unpaired two-sample t-test). Each different phosphorylation form includes the phosphorylation at several different sites of the connexin (Solan and Lampe, 2009). Different phosphorylation patterns could possibly not be resolved by analysing the three phosphorylation forms of Cx43. The alterations in astrocyte dye coupling could be caused by many alterations of gap junction coupling, including the number, the localisation, the open probability and the conductance of gap junctions. However, although these possible changes were not investigated, the decreased intracellular diffusivity could also be a reason for the decreased astrocyte gap junction coupling. It is reasonable to suggest, that if the dye diffusion through the astrocytic network is impaired, also diffusion of molecules like  $K^+$  or  $Ca^{2+}$  or metabolites will be affected.

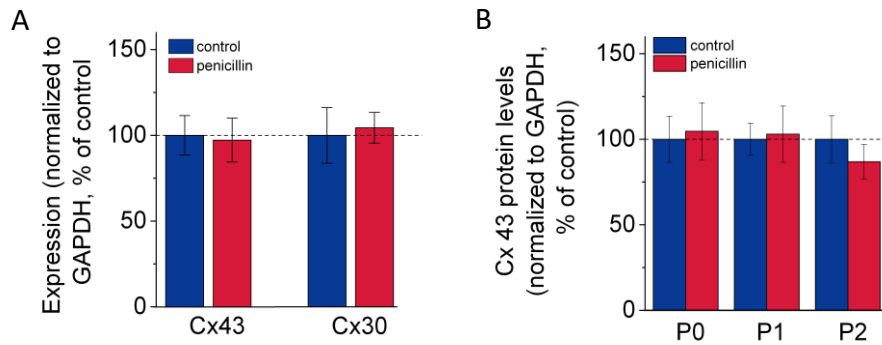


**Figure 49 Connexin expression levels and phosphorylation states after induction of epileptiform activity.** (A) The protein expression levels of Cx43 and 30 were not altered after induction of epileptiform activity ( $N = 4$ ,  $n = 8$ ,  $p = 0.87$  for Cx 43,  $p = 0.46$  for Cx30, unpaired two-sample t-test). (B) The phosphorylation states of Cx43 are also not affected upon induction of epileptiform activity ( $n = 8$ ,  $p = 0.47$  for P0,  $p = 0.88$  for P1,  $p = 0.83$  for P2, unpaired two-sample t-test).

In general, the finding that astrocyte coupling is reduced 30 minutes after induction of epileptiform activity is very interesting in terms of the progression of epilepsy in MTLE. It was described that in the *in vivo* kainate model of epilepsy, which mimics several key features of human MTLE, astrocyte coupling was reduced 4 hours after kainate injection by ca. 50% (Bedner et al., 2015). In addition, astrocytes in sclerotic tissue of patients suffering from chronic MTLE were completely uncoupled. Thus, the uncoupling of astrocyte networks seems to be a key feature in the development of epilepsy and the data obtained from the penicillin model indicate that the astrocyte uncoupling starts immediately after induction of epileptiform activity and is possibly a consequence of the astrocyte volume decrease and the accompanied change in intracellular diffusion. Former studies demonstrated that mice lacking Cx43 and 30, also showed an impaired  $K^+$  buffering as well as lower thresholds for developing epileptiform seizures (Wallraff et al., 2006). Thus, astrocyte uncoupling could promote epileptogenesis. Although this topic is under debate, since there is also evidence that inhibition of the astrocyte gap junction coupling could have anticonvulsive effects (Rouach et al., 2008). The metabolic support of neurons is done by astrocytes which transport metabolites from the blood vessels to the neurons (Rouach et al., 2008) and decreased gap junction coupling would lead an impaired neuronal energy supply.

Additionally,  $Ca^{2+}$  waves were reported to propagate through the astrocyte network enhancing neuronal synchronisation and spread of ictal activity (Gomez-Gonzalo et al., 2011), which would also be impaired by a decreased astrocyte gap junction coupling and thus would be anticonvulsive. One possible explanation, which combines these results, could be that the astrocyte network can act pro- and anticonvulsive at the same time. In a focal seizure, an impaired  $K^+$  buffering due to a decreased coupling strength would favour

epileptiform seizures at this focal point since  $K^+$  would accumulate in the extracellular space. At the same time  $Ca^{2+}$  waves through the astrocyte network promoting neuronal synchronisation would also be impaired and the seizures would not be able to spread that far. Thus, epileptiform seizures would be enhanced, but only at a focal point. One study is supporting this idea of the involvement of astrocyte coupling into network synchronisation (Chever et al., 2016), although the underlying mechanism is not clear. They showed that connected astrocytes coordinated neuronal activity bursts over large regions, whereas mice with disconnected astrocyte networks showed less severe seizures than control mice, although with higher frequency.

In addition to investigating the coupling strength of astrocyte networks in the hippocampus, it was also found that coupling was anisotropic in the CA1 stratum radiatum (Anders et al., 2014). Astrocytes located close to the stratum pyramidale showed a preferential dye diffusion in parallel to the pyramidal layer, whereas astrocytes distal to the pyramidal layer were coupled perpendicular to the cell layer. In line with that, it was found that EGFP-expressing astrocytes showed an elongated morphology into the same direction perpendicular to the CA1 stratum pyramidale (Anders et al., 2014). Similar results in astrocyte coupling anisotropy have been shown before (Nixdorf-Bergweiler et al., 1994). The orientated morphology could promote a directional anisotropic coupling under physiological conditions. When the astrocyte volume fraction and gap junction coupling are reduced after induction of epileptiform activity, the anisotropy of the coupling and thus the directional diffusion through the network could be altered. This may have strong consequences for other brain regions since this might affect neuronal network signalling in the CA1 region, which is the major output of the hippocampus (Andersen et al., 2006).

In summary, the induced alterations in astrocyte coupling during epileptogenesis can have pro- and antiepileptic consequences, which could be important not only for the initiation point of epileptiform activity, but also for the spreading of epileptic discharges in the brain.

### **6.3.2 Synaptic transmission**

Astrocytes have been shown to play an important role in neuronal synaptic transmission, since they are able to shape it by fast glutamate uptake via the glutamate transporters GLAST and GLT1 (Lehre and Danbolt, 1998; Murphy-Royal et al., 2015; for review Danbolt, 2001), but they are also able to modulate synaptic transmission via NMDA receptor co-agonist supply (Henneberger et al., 2010). Thus the observed altered astrocyte morphology after induction of epileptiform activity could have consequences for the neuronal synaptic transmission. Measuring and analysing the fEPSP slope and the paired pulse ratio (PPR) showed that these two parameters were not affected by induction of epileptiform activity and the accompanied astrocyte morphology changes (Figure 41), indicating that neither

presynaptic nor postsynaptic mechanisms were influenced during that time period. Analysis revealed that small and medium-sized astrocytes branches were shrinking with an initial volume fraction below 50%. Significant alterations could be expected in the excitability of neurons since the inhibition was blocked by penicillin application. This was measured using the spike/slope coupling (chapter 4.1.5). Indeed, during penicillin application the spike/slope coupling was significantly increased (Figure 42), indicating a lower firing threshold of neurons to a similar stimulation input.

However, assuming that induction of epileptiform activity leads to a shrinkage of peripheral astrocyte processes and thus less glial coverage of the synapse, it was hypothesized that this might lead to glutamate spillover thereby activating extrasynaptic NMDA receptors. Former studies indicated a possible involvement of extrasynaptic NMDA receptors on neuronal excitation (Naskar and Stern, 2014). Following the study of Naskar and Stern (2014) activation of extrasynaptic NMDA receptors leads to inhibition of the A-type  $K^+$  current and thus increases neuronal excitability. Since the observed astrocyte morphology changes persist after penicillin washout and inhibition was almost completely recovered (Figure 48), this mechanism could have underlain the ongoing epileptiform activity and link the astrocyte morphology changes to neuronal excitability. After washout of penicillin the spike/slope coupling turned back to control conditions, showing that neuronal excitability was not altered persistently concerning this parameter. This does not mean that neuronal excitability is not altered at all. Although the study of Naskar and Stern (2014) was performed in hypothalamic magnocellular neurosecretory cells, the result suggests that the induced astrocyte morphology changes did not lead to an altered neuronal excitability over a longer time period via glutamate spillover and subsequent activation of extrasynaptic NMDA receptors.

Another possible parameter, which could have been affected by alterations in astrocyte morphology, was synaptic plasticity. Many studies have been demonstrated an astrocyte involvement in synaptic plasticity (Henneberger et al., 2010; Ota et al., 2013) and even showed structural changes of astrocyte processes in response to neuronal activation and plasticity (Henneberger et al., 2008; Bernardinelli et al., 2014b; Perez-Alvarez et al., 2014a). Alterations in the spatial relationship between astrocyte processes and neuronal compartment due to astrocyte morphology changes could therefore also affect synaptic plasticity. To examine this hypothesis, long-term potentiation (LTP), a distinct form of synaptic plasticity, was induced at the end of an experiment after penicillin was washed out for 40 minutes. However, astrocytes still showed their altered morphology (Figure 25). No changes in comparison to control recordings could be observed neither in post-tetanic potentiation (PTP) nor in LTP. These results indicate that astrocyte function concerning synaptic transmission and plasticity was not altered when their morphology was changed

after induction of epileptiform activity. LTP is thought to be the underlying mechanism of memory consolidation. It was described that patients suffering from TLE also show impairments of memory consolidation in the chronic phase of this disease (Giovagnoli and Avanzini, 1999; Helmstädter, 2002). The observation that LTP was not altered in the used penicillin model could be caused by the fact that changes in synaptic strength including LTP and long-term depression (LTD) reflect the number of functional AMPA receptors (Zheng et al., 2015; for review Malinow and Malenka, 2002). Thus, the AMPA receptor dependent synaptic signalling does not seem to be affected by the astrocyte morphology changes induced by epileptiform activity. In contrast, NMDA receptor activity could play an important role, since epileptiform discharges disappeared immediately in presence of the NMDA receptor blocker APV.

### 6.3.3 K<sup>+</sup> buffering during induction of epileptiform activity

One main function of astrocytes is their ability to regulate the extracellular K<sup>+</sup> concentration thereby modulating the basal neuronal activity level. In terms of neuronal hyperexcitability this astrocyte function could play an important role during epileptogenesis. High extracellular levels of 10 to 12 mM of K<sup>+</sup> were reported to occur *in vivo* after seizures (Heinemann and Dieter Lux, 1977). Indeed, altered astrocyte K<sup>+</sup> homeostasis was shown in the chronic phase of temporal lobe epilepsy (Bedner et al., 2015; Bordey and Sontheimer, 1998; Hinterkeuser et al., 2000; Steinhäuser et al., 2012). Balancing neuronal activity by regulating the extracellular K<sup>+</sup> concentration is thought to be dependent on two distinct mechanisms: K<sup>+</sup> uptake and spatial K<sup>+</sup> buffering. Whereas K<sup>+</sup> uptake is mainly mediated by the Na<sup>+</sup> / K<sup>+</sup> ATPase, Na<sup>+</sup>-K<sup>+</sup>-Cl<sup>-</sup> cotransporters and K<sup>+</sup> channels (D'Ambrosio et al., 2002; Kofuji and Newman, 2004; Ransom et al., 2000), spatial K<sup>+</sup> buffering is regulated by the difference between the astrocyte membrane potential and the local K<sup>+</sup> equilibrium potential (Orkand, 1986). Due to their strong gap junction-dependent coupling to neighbouring astrocytes building an astrocyte syncytium, it is believed that astrocytes redistribute K<sup>+</sup> from sites with high extracellular K<sup>+</sup> concentrations through the astrocyte network to sites with low extracellular K<sup>+</sup> concentrations. The observed changes in astrocyte morphology as well as the related alterations in intra- and intercellular diffusion (chapter 5.3) could have affected both mechanisms. If the hypothesis was valid that the extracellular space expands after the induction of epileptiform activity (chapter 6.1.4,) this increase in extracellular space could have functional consequences. The morphology changes in the small astrocyte processes near neuronal compartments could have led to a K<sup>+</sup> accumulation in the extracellular space due to its increase and the shrinkage of the astrocyte could result in lower cytosolic space such, that less K<sup>+</sup> could be taken up. An accumulation of K<sup>+</sup> in the extracellular space leads to changes in the K<sup>+</sup> equilibrium

potential and thus to membrane depolarisations of neurons and astrocytes. Depolarised neurons in turn could promote epileptic seizures. Measuring changes in the astrocyte membrane potential (Chapter 5.5.4) during induction of epileptiform activity was used to estimate if the resting extracellular  $K^+$  concentrations were increased after observed astrocyte morphology changes. Surprisingly, no changes in the resting astrocyte membrane potential and thus in the extracellular resting  $K^+$  concentration could be found (Figure 44). As described, all experiments were performed in 4 mM KCl in mouse hippocampal slices respectively 5mM KCl in rat hippocampal slices, which are slightly increased concentrations for KCl, since the physiological values are 2 - 3 mM.

To understand if the transient  $K^+$  uptake itself was affected after induction of epileptiform activity, the astrocyte field potential (afEPSP) was measured after Schaffer collateral (SC) stimulation (chapter 5.5.4). The measured amplitude of the afEPSP scales with the neuronal fEPSP. When paired pulse stimulation is used this amplitude is also caused by the transient increase in  $[K^+]_{ex}$  due to the neuronal response to stimulation (Henneberger and Rusakov, 2012b). During penicillin application the amplitude was significantly increased which is caused by the neuronal response with recurrent activity and thus, a higher  $K^+$  release from neurons into the extracellular space. The decay afterwards is mainly caused by decreasing extracellular  $K^+$  levels back to baseline. This was not altered during penicillin application compared to baseline and compared to control recordings. Since, amongst others, the decrease of extracellular  $K^+$  levels is caused by astrocyte  $K^+$  uptake, these data could suggest that the astrocyte  $K^+$  uptake was not affected by the observed morphology changes. No data were obtained after washout of penicillin, which could be an interesting time point to examine possible alterations in astrocyte  $K^+$  uptake.

Another subset of experiments was performed to investigate  $K^+$  transients after induction of epileptiform activity (performed by B. Breithausen). By using  $K^+$ -sensitive microelectrodes, the extracellular  $K^+$  concentration can be directly measured. To enable a comparison between control and penicillin recordings, experiments were designed as follows. Spontaneous and evoked field potentials were recorded in the CA1 stratum pyramidale of rat hippocampal slices in an interface chamber (Figure 50A). Schaffer collaterals were stimulated throughout the experiment every 30 seconds. Epileptiform activity was induced by bath application of 4 mM penicillin, which reliably induced epileptiform discharges (Figure 50B). Penicillin was washed out after 30 minutes and synaptic activity was blocked simultaneously using D-AP5 and NBQX to inhibit NMDA and AMPA receptors, respectively. Synaptic activity was also blocked after control recordings. This enabled a comparison between control and penicillin recordings, because with intact synaptic transmission the extracellular  $K^+$  levels would differ in penicillin recordings due to the increased neuronal activation. As shown previously, the astrocyte morphology changes

persisted after washout of penicillin for at least 40 minutes. Thus,  $K^+$  transients could be recorded when astrocyte morphology was unaltered and when astrocyte volume fraction was decreased, respectively. To measure extracellular  $K^+$  transients  $K^+$ -sensitive microelectrodes were used. To compare these transients after control and penicillin recordings, a high frequency stimulation was done after synaptic transmission was completely blocked and  $K^+$  transients were recorded (Figure 50C, upper panel). The recorded  $K^+$  transients were normalised to the fibre volley (Figure 50C, arrows) to exclude artificial effects by differences in stimulation intensity. As readout the maximal amplitude was used. No differences in the amplitude (Figure 50D, control:  $1.1 \pm 0.1$  mM/mV,  $n=4$ ; penicillin:  $1.3 \pm 0.1$  mM/mV,  $n = 4$ ,  $p = 0.47$ , unpaired two-sample t-test) between control and penicillin recordings could be found.

Taken together, these data suggest that neither the astrocyte  $K^+$  uptake nor the spatial  $K^+$  buffering is affected, when astrocyte morphology was altered after induction of epileptiform activity. In contrast to the findings of Bedner et al. (2015) and Wallraff et al. (2006), this would mean that a decrease in astrocyte coupling of ca. 15 % is not sufficient to result in an impaired  $K^+$  buffering. This could rely on a non-linear relationship between these two parameters. In addition, in the study of Wallraff et al. (2006) developmental effects on astrocyte coupling could not be ruled out, because they used a conventional knockout of Cx43 and 30. Furthermore, they recorded the  $K^+$  transients in the CA1 stratum lacunosum moleculare, which could be important when astrocyte  $K^+$  buffering is investigated. One possible explanation could be that  $K^+$  is buffered via an alternative pathway. For the described model here, an increased extracellular  $K^+$  level after astrocyte morphology changes appears not to be the reason for the observed proepileptic action. However, the increased extracellular  $K^+$  concentration was a critical point for the successful induction of epileptiform discharges. In presence of lower  $[K^+]_{ex}$  no epileptiform activity could be induced. This indicates that the extracellular  $K^+$  concentration has a crucial role during epileptogenesis.

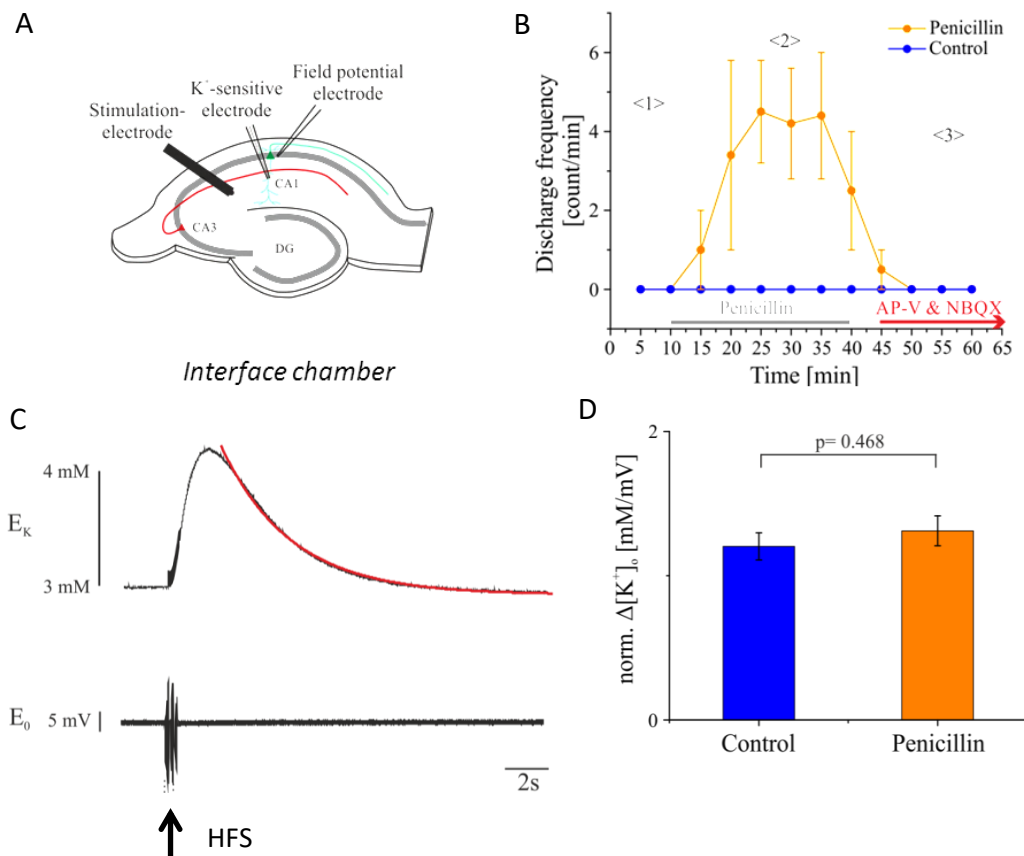


**Figure 50 Recording of extracellular  $K^+$  transients using  $K^+$  sensitive microelectrodes.** (A) Schematic of hippocampal slice used in an interface chamber. Schaffer collaterals were stimulated and evoked and spontaneous field potentials were recorded in the CA1 stratum pyramidale.  $K^+$  transients were recorded in the stratum radiatum. (B) Epileptiform activity was induced by bath application of penicillin. During penicillin synaptic transmission was blocked using D-AP5 and NBQX. (C) After synaptic activity was blocked,  $K^+$  transients were recorded due to high frequency stimulation (HFS). (D) The amplitude of the  $K^+$  transients was not significantly different between control and penicillin recordings (control:  $1.1 \pm 0.1$  mM/mV,  $n = 4$ ; penicillin:  $1.3 \pm 0.1$  mM/mV,  $n = 4$ ,  $p = 0.47$ , unpaired two-sample t-test, experiments, analysis and figure done by B. Breithausen).

### 6.3.4 Extracellular glutamate levels after induction of astrocyte morphology changes

The results of the present study suggested that the induced astrocyte morphology changes might have a proepileptic effect and could be the cause for the persistence of epileptiform activity. The link between the decrease in astrocyte volume fraction and ongoing epileptiform activity was not clear yet. As possible candidate, glutamate levels were investigated. In addition to  $K^+$  buffering, astrocytes were also reported to play an important role for glutamate clearance out of the extracellular space. The rapid binding of glutamate by astrocyte glutamate transporters (GLT1) has been shown to control synaptic transmission and neuronal excitability (Tanaka et al., 1997; Lehre and Danbolt, 1998;

Murphy-Royal et al., 2015). An altered glutamate metabolism was also described for MTL patients, where higher glutamate levels and bigger glutamate transients after seizures were described (Cavus et al., 2005; Coulter and Eid, 2012; During and Spencer, 1993). Changes in astrocyte morphology might affect the glutamate levels at the synapse since the presence of GLT-1 could be altered by the cytoskeletal changes in astrocytes after induction of epileptiform activity. GLT1 were described to be highly mobile and an activity dependent diffusion on the astrocyte membrane towards and away from the synapse was shown to be a possible mechanism to shape synaptic transmission (Murphy-Royal et al., 2015). The altered astrocyte morphology in combination with the decreased intracellular diffusion might also have an impact on the transporter diffusion at the membrane and in turn could reduce the availability of GLT1 to bind glutamate. There is also evidence that astrocyte modulate synaptic transmission via outgrowth of astrocyte protrusions into the synaptic cleft to increase the presence of glutamate transporters within the synaptic cleft thereby decreasing synaptic transmission through glutamate binding (Pannasch et al., 2014). Decrease in astrocyte volume after induction of epileptiform activity might interfere with this function allowing more glutamate molecules to activate postsynaptic glutamate receptors and thus an increased neuronal activation.

To investigate if alterations in astrocyte morphology induced by epileptiform activity affect the extracellular glutamate levels, the glutamate sensor iGluSnFR was used (Marvin et al., 2013). This sensor was expressed by astrocytes after virus injection of AAV.GFAP.iGluSnFR. Glutamate was applied iontophoretically in the periphery of astrocytes after control or penicillin recordings. Before glutamate application, neuronal activity and synaptic transmission was blocked using TTX, D-AP5 and NBQX. Metabotropic glutamate receptors were also inhibited using LY341495. This allowed the comparison of control and penicillin treated slices, because otherwise remaining epileptiform activity could mask possible effects in glutamate levels. Interestingly, analysing the iGluSnFR signal revealed a faster rise time of the iGluSnFR signal. This means that a higher glutamate concentration could be measured after the same iontophoretic application of glutamate in penicillin treated slices compared to control slices.

It can be concluded from previous experiments that astrocyte volume fraction was decreased after induction of epileptiform activity and that this decrease persisted even during blocked neuronal activity, because this could be shown before (Figure 25). Thus, the altered astrocyte morphology resulted in a faster extracellular glutamate accumulation compared to control recordings, where astrocyte morphology was unaltered.

The underlying mechanism of this faster glutamate accumulation could rely on the mechanism of astrocyte glutamate uptake. This is accompanied by the uptake of Na<sup>+</sup> ions (Rose and Ransom, 1997; for review Danbolt, 2001). Astrocyte Na<sup>+</sup> transients were

reported to occur time-locked to epileptiform activity in hippocampal slices (Karus et al., 2015). The increase of astrocyte cytosolic  $\text{Na}^+$  levels was demonstrated to change the driving forces for the glutamate uptake (Karus et al., 2015). Induction of epileptiform activity results in a decrease of astrocyte volume fraction accompanied with a reduction of intra- and intercellular diffusivity. This could result in a stronger accumulation of  $\text{Na}^+$  in the astrocyte cytosol during the uptake of glutamate caused by the lower cytosolic volume. Also the propagation of  $\text{Na}^+$  away from the small astrocyte processes and through the astrocyte network could be impaired by the reduced diffusivity. It was demonstrated that locally generated  $\text{Na}^+$  transients propagate through the astrocyte network (Langer and Rose, 2009). Since less glutamate can be taken up by the astrocyte, iontophoretic application of this neurotransmitter would result in a faster accumulation. An increase in cytosolic  $\text{Na}^+$  could have diverse effects on astrocyte function, which in turn could have anti- and proepileptic effects. For instance, it could reverse the GABA uptake and release it, which could have an antiepileptic effect. Since an overall proepileptic effect was observed by induction of rapid astrocyte morphology changes in this study, the possible proepileptic actions of this mechanism will be discussed.

The faster glutamate accumulation could act on NMDA receptors, thereby amplifying neuronal activity. Persistent epileptiform discharges were shown to be NMDA receptor-dependent in this study. The increased glutamate levels caused by rapid astrocyte morphology changes could be the reason for ongoing epileptiform activity by increasing NMDA receptor activity. As described previously altered glutamate levels were reported to be involved in the development of epilepsy (Cavus et al., 2005; Coulter and Eid, 2012; During and Spencer, 1993). There is also evidence that NMDA receptors play a crucial role during the development of epilepsy (Gerfin-Moser et al., 1995; Kraus et al., 1994; Lasoń et al., 1997). The observed rapid astrocyte morphology changes leading to faster glutamate accumulations might be the underlying mechanism linking these observations. Thus, rapid astrocyte morphology changes and the accompanied alterations in intra- and intercellular diffusion might therefore be crucial for the further development of epileptiform activity.

Another possibility for a proepileptic effect of an astrocyte  $\text{Na}^+$  accumulation is an indirect excitatory feedback loop. A  $\text{Na}^+$  increase can also result in a reversal of the  $\text{Na}^+/\text{Ca}^{2+}$  exchanger. This would lead to a  $\text{Ca}^{2+}$  increase in astrocytes. This in turn could lead to glutamate or D-serine release from astrocytes (Henneberger et al., 2010, 2012; Parpura et al., 1994; Takata et al., 2011), thereby creating an excitatory feedback loop. An increased probability of  $\text{Ca}^{2+}$  transients in astrocytes was observed when epileptiform activity with ictal and interictal events was induced (Fellin et al., 2006), whereas a later study indicated that only ictal activity resulted in somatic  $\text{Ca}^{2+}$  transients in astrocytes (Gomez-Gonzalo et al., 2011). The authors also confirmed the proepileptic effects of astrocyte  $\text{Ca}^{2+}$  signalling

showing that buffering intracellular  $\text{Ca}^{2+}$  using the  $\text{Ca}^{2+}$  chelator BAPTA resulted in reduced ictal activity. The mechanism, by which the faster glutamate accumulation, induced by rapid astrocyte morphology changes, promotes epileptiform activity, is not clear yet. But the results suggest that the early onset of epileptogenesis induces rapid astrocyte morphology changes, which result in a faster glutamate accumulation thereby supporting ongoing epileptiform activity.

## 6.4 Conclusion

The current project gave novel insights concerning the involvement of astrocyte morphology in the acute development of epileptiform activity. It could be shown that astrocytes respond with a robust structural change to epileptiform activity on a timescale of minutes under *in vitro* and *in vivo* conditions. Astrocyte processes shrinkage is triggered by the onset of epileptiform activity and is mediated by restructuring of the actin cytoskeleton. In turn, the decrease in astrocyte volume fraction results in a decreased intra- and intercellular diffusion and has an overall proepileptic effect. This proepileptic action of rapid astrocyte morphology changes could not be explained by changes in astrocyte  $\text{K}^+$  buffering. Instead, it is likely mediated by the fast accumulation of glutamate, which could result in an increased neuronal excitation. These results show that astrocyte morphology changes in terms of epileptiform activity occur on a very rapid time scale. Furthermore, during this early onset of epileptiform activity astrocyte morphology changes appear to be able to modulate the development of ongoing epileptiform activity. Thus, astrocyte morphology changes could play a crucial role during epileptogenesis.

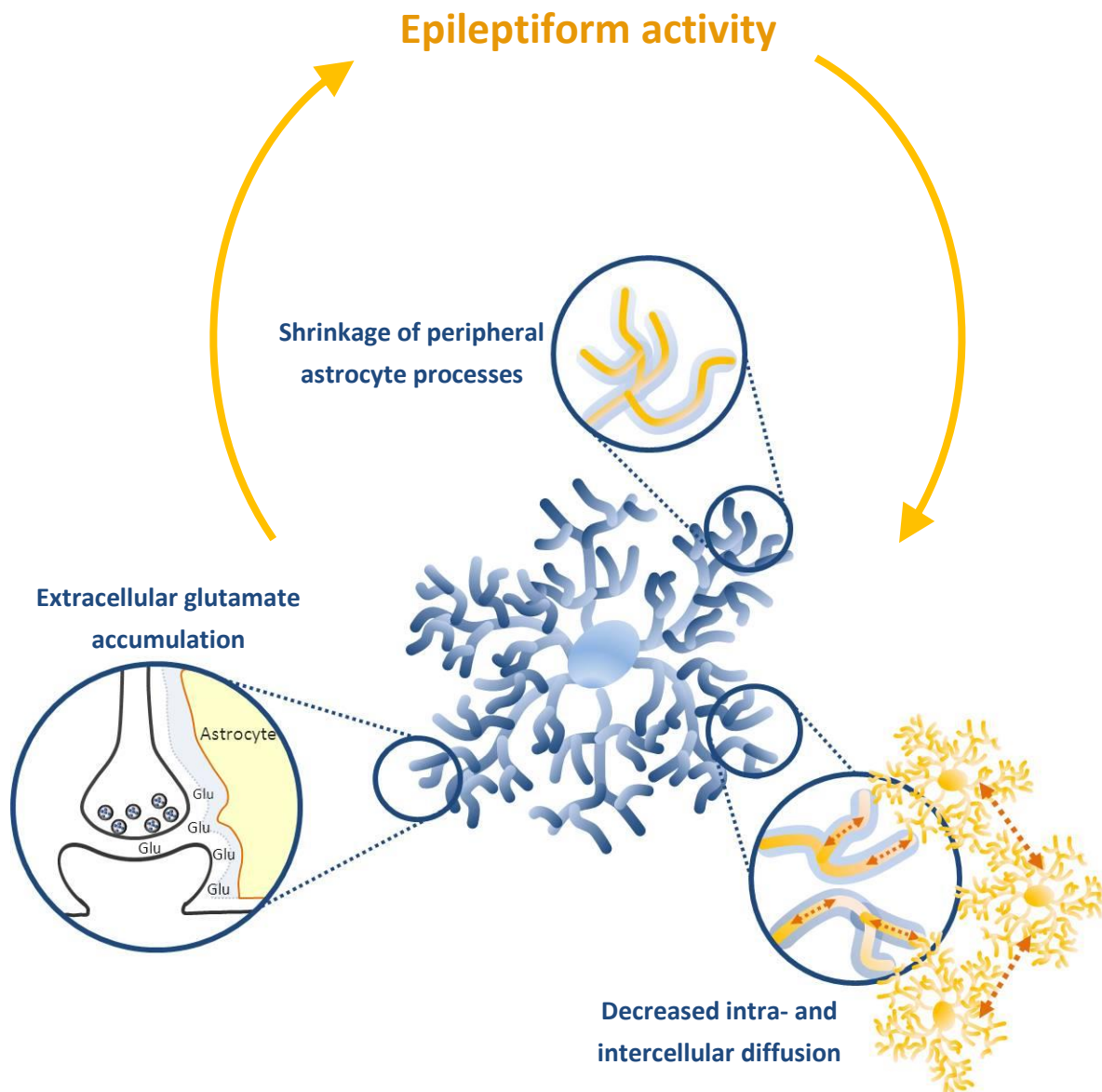


**Figure 51 The role of rapid astrocyte morphology changes in epileptogenesis.** Epileptiform activity results in changes in astrocyte morphology and function. Blue indicates the astrocyte morphology under physiological conditions. Yellow visualises the observed changes. Induction of epileptiform activity leads to a shrinkage of peripheral astrocyte processes. This is accompanied by a decreased intracellular diffusion and a reduced astrocyte coupling. After induction of astrocyte morphology changes, a faster accumulation of extracellular glutamate could be recorded. This is a potential reason for the overall proepileptic effect of astrocyte morphology changes.

## 7. Summary

In the past decades astrocytes have been demonstrated to play an important role in physiological brain processes but also neurodegenerative diseases. Their characteristic morphology allows them to closely contact neurons. The close proximity of astrocyte peripheral processes and neuronal compartments enables astrocytes to modulate synaptic transmission and neuronal activity. Changes in this spatial relationship could therefore result in alterations of neuronal activity, which could also be of pathophysiological relevance. Indeed, astrocyte structural and associated functional changes were observed in the late states of epilepsy implying a potential crucial role of astrocytes in epileptogenesis. How early these astrocyte morphology changes occur and to what degree they may contribute to the development of epilepsy is yet unknown.

The present study aimed to investigate *i)* if and on which timescale astrocyte morphology is altered after induction of acute epileptiform activity, *ii)* which mechanism mediates structural changes of astrocytes and *iii)* what the functional consequences of astrocyte morphology changes are and if they contribute to the development of epileptiform activity. Combining electrophysiological recordings and two-photon excitation fluorescence microscopy revealed novel results concerning the involvement of astrocyte morphology in the acute development of epileptiform activity. It could be shown that astrocytes respond with a robust structural change to epileptiform activity on a timescale of minutes *in vitro* and *in vivo* in different species. This morphology change could be described as shrinkage of peripheral astrocyte processes. Astrocyte processes shrinkage was triggered by the onset of epileptiform activity and did not require ongoing epileptiform activity. By modulating the ROCK pathway it could be demonstrated that these astrocyte morphology changes are ROCK dependent, suggesting a potential involvement of the actin cytoskeleton. As a functional consequence, a decreased astrocyte intra- and intercellular diffusion was observed. Interestingly, the induced astrocyte morphology changes had an overall proepileptic effect. This proepileptic action of rapid astrocyte morphology changes could not be explained by changes in astrocyte K<sup>+</sup> buffering. Instead, it was likely mediated by faster accumulation of glutamate, which could result in an amplification of neuronal excitation.

These results indicate that astrocyte morphology changes occur on a very rapid time scale after induction of epileptiform activity and are mediated by a fast cytoskeletal restructuring. These astrocyte morphology changes support persistent epileptiform activity. In conclusion, this study provides evidence that astrocyte morphology changes could play a crucial role early during epileptogenesis.

## 8. Perspectives

The current study demonstrated an important role of astrocyte morphology and function during the acute onset of epileptiform activity. The potential mechanisms linking the reciprocal action of neuronal activity and astrocyte morphology changes could be demonstrated. These results raised new questions, which could be clarified by future experiments

It could be shown that astrocyte morphology changes are mediated by the Rho associated coiled coil protein kinase (ROCK), which probably resulted in a cytoskeleton rearrangement. It is not clear, which astrocyte receptor is targeted by neuronal activity thereby mediating astrocyte cytoskeletal restructuring. Using further pharmacological treatment could be a possible way to identify the upstream signaling and receptors responsible for astrocyte cytoskeletal alterations.

There is evidence that astrocytes respond to neuronal activity with structural changes. This was not only shown in the current study in response to epileptiform activity, but also in former studies, which demonstrated astrocyte restructuring upon physiological stimuli (Haber et al., 2006; Bernardinelli et al., 2014b; Perez-Alvarez et al., 2014b). To understand if astrocyte morphology changes are a consequence of neuronal activity or if they are able to initiate alterations in synaptic transmission or neuronal excitability, experimental control of astrocyte morphology, for instance inducing astrocyte retraction or stellation, would be from great advantage. To modulate astrocyte morphology, one could alter the the levels of RhoA, a direct upstream effector of ROCK, in astrocytes or introduce altered forms of RhoA, like dominant-negative or constitutive active forms, using astrocyte specific virus injections. Another possibility is to knock down astrocyte ROCK by viral injection of small interfering RNA. In comparison to a ROCK knockout mouse line, this method has the advantage that developmental effects can be avoided. By controlling astrocyte morphology, its role in physiological and pathophysiological cellular mechanisms could be investigated thereby understanding the general function of astrocyte structure in, for instance, learning and memory or neurodegenerative diseases.

In the current study, it could not be clarified if there are also changes in extracellular space volume after induction of epileptiform activity. This is an important parameter, since former studies demonstrated the impact of the extracellular space on neuronal activity (Dudek et al., 1990; Hochman D. W., 2009). The extracellular space fraction can be measured using tetramethylammonium ( $\text{TMA}^+$ , Nicholson and Phillips, 1981; Roitbak and Syková, 1999). Therefore,  $\text{TMA}^+$  would be applied iontophoretically in control and in penicillin treated slices.  $\text{TMA}^+$  diffusion curves can be recorded using  $\text{TMA}^+$  sensitive microelectrodes. Changes in the extracellular space could be captured by changes in  $\text{TMA}^+$  diffusion. Understanding, how the extracellular space is altered after induction of astrocyte

morphology changes, would help to identify the link between the astrocyte restructuring and ongoing epileptiform activity. In line with this, it is required to test, whether the hypothesis is correct that the observed faster glutamate accumulation is caused by an astrocyte  $\text{Na}^+$  accumulation. Intracellular  $\text{Na}^+$  levels under control and under epileptiform conditions could be measured using the  $\text{Na}^+$  sensitive dye SBFI in astrocytes. To determine a causal role of astrocyte  $\text{Na}^+$  levels for the induction of epileptiform activity, the intracellular  $\text{Na}^+$  levels would need to be controlled by a  $\text{Na}^+$  buffer, for instance. With this controlled intracellular  $\text{Na}^+$  concentration in astrocytes the probability of inducing epileptiform activity could be investigated.

As a long-term perspective, it would be interesting to investigate whether astrocyte morphology is a potential target for the treatment of epilepsy. As a first step the role of astrocyte morphology changes in *in vivo* epilepsy models should be further investigated. For instance, the kainate model could be used, which was shown to mimic human temporal lobe epilepsy (TLE, Bedner et al., 2015). Astrocyte morphology changes could be blocked by using a mouse line with a constitutive knockout of ROCK or a knockdown of ROCK by virus injection as described previously. The typical characteristics of the development of chronic epilepsy in this model, like impairment of astrocyte coupling, hippocampal sclerosis, astrogliosis or granular cell dispersion, should be investigated at different time points after kainate injection. This would clarify if astrocyte morphology changes at a very early time point of epileptogenesis are required for the development of chronic epilepsy.

## 9. References

- Akdogan, I., and Yonguc, N.G. (2011). Experimental Epilepsy Models and Morphologic Alterations of Experimental Epilepsy Models in Brain and Hippocampus (Intech Open Access Publisher).
- Allen G, Barnard H, McColl R, and et al (2007). Reduced hippocampal functional connectivity in alzheimer disease. *Arch. Neurol.* 64, 1482–1487.
- Amano, M., Nakayama, M., and Kaibuchi, K. (2010). Rho-Kinase/ROCK: A Key Regulator of the Cytoskeleton and Cell Polarity. *Cytoskelet. Hoboken Nj* 67, 545–554.
- Amaral, D.G., Scharfman, H.E., and Lavenex, P. (2007). The dentate gyrus: fundamental neuroanatomical organization (dentate gyrus for dummies). *Prog. Brain Res.* 163, 3–22.
- Anders, S., Minge, D., Griemsmann, S., Herde, M.K., Steinhäuser, C., and Henneberger, C. (2014). Spatial properties of astrocyte gap junction coupling in the rat hippocampus. *Philos. Trans. R. Soc. Lond. B Biol. Sci.* 369, 20130600.
- Andersen, P., Sundberg, S.H., Sveen, O., and Wigström, H. (1977). Specific long-lasting potentiation of synaptic transmission in hippocampal slices. *Nature* 266, 736–737.
- Andersen, P., Morris, R., Amaral, D., Bliss, T., and O’Keefe, J. (2006). *The Hippocampus Book* (Oxford University Press).
- Anderson, C.M., and Swanson, R.A. (2000). Astrocyte glutamate transport: review of properties, regulation, and physiological functions. *Glia* 32, 1–14.
- Araque, A., Parpura, V., Sanzgiri, R.P., and Haydon, P.G. (1999). Tripartite synapses: glia, the unacknowledged partner. *Trends Neurosci.* 22, 208–215.
- Arisi, G.M., Ruch, M., Foresti, M.L., Mukherjee, S., Ribak, C.E., and Shapiro, L.A. (2011). Astrocyte Alterations in the Hippocampus Following Pilocarpine-induced Seizures in Aged Rats. *Aging Dis.* 2, 294–300.
- Aronica, E., Gorter, J.A., Ijlst-Keizers, H., Rozemuller, A.J., Yankaya, B., Leenstra, S., and Troost, D. (2003). Expression and functional role of mGluR3 and mGluR5 in human astrocytes and glioma cells: opposite regulation of glutamate transporter proteins. *Eur. J. Neurosci.* 17, 2106–2118.
- Arruda, F., Cendes, F., Andermann, F., Dubeau, F., Villemure, J.G., Jones-Gotman, M., Poulin, N., Arnold, D.L., and Olivier, A. (1996). Mesial atrophy and outcome after amygdalohippocampectomy or temporal lobe removal. *Ann. Neurol.* 40, 446–450.
- Asztely, F., Erdemli, G., and Kullmann, D.M. (1997). Extrasynaptic glutamate spillover in the hippocampus: dependence on temperature and the role of active glutamate uptake. *Neuron* 18, 281–293.

- Auzmendi, J., González, N., and Girardi, E. (2008). The NMDAR Subunit NR2B Expression is Modified in Hippocampus after Repetitive Seizures. *Neurochem. Res.* *34*, 819–826.
- Avoli, M., Barbarosie, M., Lücke, A., Nagao, T., Lopantsev, V., and Köhling, R. (1996). Synchronous GABA-Mediated Potentials and Epileptiform Discharges in the Rat Limbic System In Vitro. *J. Neurosci.* *16*, 3912–3924.
- Balestrino, M., and Somjen, G.G. (1986). Chlorpromazine protects brain tissue in hypoxia by delaying spreading depression-mediated calcium influx. *Brain Res.* *385*, 219–226.
- Bear, M.F. (1995). Mechanism for a sliding synaptic modification threshold. *Neuron* *15*, 1–4.
- Bear, M.F., and Abraham, W.C. (1996). Long-term depression in hippocampus. *Annu. Rev. Neurosci.* *19*, 437–462.
- Bedner, P., and Steinhäuser, C. (2014). Crucial Role for Astrocytes in Epilepsy. In *Pathological Potential of Neuroglia*, V. Parpura, and A. Verkhratsky, eds. (Springer New York), pp. 155–186.
- Bedner, P., Dupper, A., Hüttmann, K., Müller, J., Herde, M.K., Dublin, P., Deshpande, T., Schramm, J., Häussler, U., Haas, C.A., et al. (2015). Astrocyte uncoupling as a cause of human temporal lobe epilepsy. *Brain* *138*, 1208–1222.
- Ben-Ari, Y., and Lagowska, J. (1978). [Epileptogenic action of intra-amygdaloid injection of kainic acid]. *Comptes Rendus Hebd. Séances Académie Sci. Sér. Sci. Nat.* *287*, 813–816.
- Bernardinelli, Y., Muller, D., and Nikonenko, I. (2014a). Astrocyte-Synapse Structural Plasticity. *Neural Plast.* *2014*.
- Bernardinelli, Y., Randall, J., Janett, E., Nikonenko, I., König, S., Jones, E.V., Flores, C.E., Murai, K.K., Bochet, C.G., Holtmaat, A., et al. (2014b). Activity-Dependent Structural Plasticity of Perisynaptic Astrocytic Domains Promotes Excitatory Synapse Stability. *Curr. Biol.* *24*, 1679–1688.
- Binder, D.K., and Steinhäuser, C. (2006). Functional changes in astroglial cells in epilepsy. *Glia* *54*, 358–368.
- Binder, D.K., Yao, X., Zador, Z., Sick, T.J., Verkman, A.S., and Manley, G.T. (2006). Increased seizure duration and slowed potassium kinetics in mice lacking aquaporin-4 water channels. *Glia* *53*, 631–636.
- Binder, D.K., Nagelhus, E.A., and Ottersen, O.P. (2012). Aquaporin-4 and epilepsy. *Glia* *60*, 1203–1214.
- Bingman, V.P., Salas, C., and Rodriguez, F. (2009). Evolution of the Hippocampus. In *Encyclopedia of Neuroscience*, M.D. Binder, N. Hirokawa, and U. Windhorst, eds. (Springer Berlin Heidelberg), pp. 1356–1360.

- Bliss, T.V.P., and Lømo, T. (1973). Long-lasting potentiation of synaptic transmission in the dentate area of the anaesthetized rabbit following stimulation of the perforant path. *J. Physiol.* *232*, 331–356.
- Blümcke, I., Thom, M., Aronica, E., Armstrong, D.D., Bartolomei, F., Bernasconi, A., Bernasconi, N., Bien, C.G., Cendes, F., Coras, R., et al. (2013). International consensus classification of hippocampal sclerosis in temporal lobe epilepsy: A Task Force report from the ILAE Commission on Diagnostic Methods. *Epilepsia* *54*, 1315–1329.
- Bordey, A., and Sontheimer, H. (1998). Properties of human glial cells associated with epileptic seizure foci. *Epilepsy Res.* *32*, 286–303.
- Bukauskas, F.F., and Weingart, R. (1993). Temperature dependence of gap junction properties in neonatal rat heart cells. *Pflüg. Arch. Eur. J. Physiol.* *423*, 133–139.
- Burgess, N., Maguire, E.A., and O'Keefe, J. (2002). The human hippocampus and spatial and episodic memory. *Neuron* *35*, 625–641.
- Bushong, E.A., Martone, M.E., Jones, Y.Z., and Ellisman, M.H. (2002). Protoplasmic astrocytes in CA1 stratum radiatum occupy separate anatomical domains. *J. Neurosci. Off. J. Soc. Neurosci.* *22*, 183–192.
- Bushong, E.A., Martone, M.E., and Ellisman, M.H. (2004). Maturation of astrocyte morphology and the establishment of astrocyte domains during postnatal hippocampal development. *Int. J. Dev. Neurosci.* *22*, 73–86.
- Cai, Z., Schools, G.P., and Kimelberg, H.K. (2000). Metabotropic glutamate receptors in acutely isolated hippocampal astrocytes: Developmental changes of mGluR5 mRNA and functional expression. *Glia* *29*, 70–80.
- Cajal y Ramón, S. (1909). *Histologie du système nerveux de l'homme & des vertébrés* (Paris : Maloine).
- Carmignoto, G., and Haydon, P.G. (2012). Astrocyte calcium signaling and epilepsy. *Glia* *60*, 1227–1233.
- Cavanagh, J.B., and Meyer, A. (1956). Aetiological aspects of Ammon's horn sclerosis associated with temporal lobe epilepsy. *Br. Med. J.* *2*, 1403–1407.
- Cavazos, J.E., Das, I., and Sutula, T.P. (1994). Neuronal loss induced in limbic pathways by kindling: evidence for induction of hippocampal sclerosis by repeated brief seizures. *J. Neurosci. Off. J. Soc. Neurosci.* *14*, 3106–3121.
- Cavus, I., Kasoff, W.S., Cassaday, M.P., Jacob, R., Gueorguieva, R., Sherwin, R.S., Krystal, J.H., Spencer, D.D., and Abi-Saab, W.M. (2005). Extracellular metabolites in the cortex and hippocampus of epileptic patients. *Ann. Neurol.* *57*, 226–235.
- Chapman, A.G. (1998). Glutamate receptors in epilepsy. *Prog. Brain Res.* *116*, 371–383.

- Chaudhry, F.A., Schmitz, D., Reimer, R.J., Larsson, P., Gray, A.T., Nicoll, R., Kavanaugh, M., and Edwards, R.H. (2002). Glutamine Uptake by Neurons: Interaction of Protons with System A Transporters. *J. Neurosci.* 22, 62–72.
- Chen, C.-J., Ou, Y.-C., Lin, S.-Y., Liao, S.-L., Huang, Y.-S., and Chiang, A.-N. (2006). I-Glutamate activates RhoA GTPase leading to suppression of astrocyte stellation. *Eur. J. Neurosci.* 23, 1977–1987.
- Chen, Q., He, S., Hu, X.-L., Yu, J., Zhou, Y., Zheng, J., Zhang, S., Zhang, C., Duan, W.-H., and Xiong, Z.-Q. (2007). Differential roles of NR2A- and NR2B-containing NMDA receptors in activity-dependent brain-derived neurotrophic factor gene regulation and limbic epileptogenesis. *J. Neurosci. Off. J. Soc. Neurosci.* 27, 542–552.
- Chen, R.-C., Huang, Y.-H., and How, S.-W. (1986). Systemic penicillin as an experimental model of epilepsy. *Exp. Neurol.* 92, 533–540.
- Chever, O., Dossi, E., Pannasch, U., Derangeon, M., and Rouach, N. (2016). Astroglial networks promote neuronal coordination. *Sci Signal* 9, ra6-ra6.
- Collingridge, G.L., Kehl, S.J., and McLennan, H. (1983). Excitatory amino acids in synaptic transmission in the Schaffer collateral-commissural pathway of the rat hippocampus. *J. Physiol.* 334, 33–46.
- Cooper, C.E., Cope, M., Elwell, C.E., and Delpy, D.T. (2009). Bicuculline-induced seizures: a challenge for optical and biochemical modeling of the cytochrome oxidase CuA NIRS signal. *Adv. Exp. Med. Biol.* 645, 129–134.
- Cope, D.W., Di Giovanni, G., Fyson, S.J., Orbán, G., Errington, A.C., Lőrincz, M.L., Gould, T.M., Carter, D.A., and Crunelli, V. (2009). Enhanced tonic GABAA inhibition in typical absence epilepsy. *Nat. Med.* 15, 1392–1398.
- Cormier, R.J., Mennerick, S., Melbostad, H., and Zorumski, C.F. (2001). Basal levels of adenosine modulate mGluR5 on rat hippocampal astrocytes. *Glia* 33, 24–35.
- Correale, J., and Farez, M.F. (2015). The Role of Astrocytes in Multiple Sclerosis Progression. *Front. Neurol.* 6.
- Coulter, D.A., and Eid, T. (2012). Astrocytic regulation of glutamate homeostasis in epilepsy. *Glia* 60, 1215–1226.
- Coulter, D.A., and Steinhäuser, C. (2015). Role of Astrocytes in Epilepsy. *Cold Spring Harb. Perspect. Med.* 5, a022434.
- Curia, G., Longo, D., Biagini, G., Jones, R.S.G., and Avoli, M. (2008). The pilocarpine model of temporal lobe epilepsy. *J. Neurosci. Methods* 172, 143–157.
- Curtis de, M., and Avanzini, G. (2001). Interictal spikes in focal epileptogenesis. *Prog. Neurobiol.* 63, 541–567.

- Curtis de, M., Jefferys, J.G.R., and Avoli, M. (2012). Interictal Epileptiform Discharges in Partial Epilepsy: Complex Neurobiological Mechanisms Based on Experimental and Clinical Evidence. In Jasper's Basic Mechanisms of the Epilepsies, J.L. Noebels, M. Avoli, M.A. Rogawski, R.W. Olsen, and A.V. Delgado-Escueta, eds. (Bethesda (MD): National Center for Biotechnology Information (US)), p.
- D'Ambrosio, R., Gordon, D.S., and Winn, H.R. (2002). Differential Role of KIR Channel and Na<sup>+</sup>/K<sup>+</sup>-Pump in the Regulation of Extracellular K<sup>+</sup> in Rat Hippocampus. *J. Neurophysiol.* *87*, 87–102.
- Danbolt, N.C. (2001). Glutamate uptake. *Prog. Neurobiol.* *65*, 1–105.
- Debanne, D., Guérineau, N.C., Gähwiler, B.H., and Thompson, S.M. (1996). Paired-pulse facilitation and depression at unitary synapses in rat hippocampus: quantal fluctuation affects subsequent release. *J. Physiol.* *491*, 163–176.
- Demarque, M., Villeneuve, N., Manent, J.-B., Becq, H., Represa, A., Ben-Ari, Y., and Aniksztejn, L. (2004). Glutamate transporters prevent the generation of seizures in the developing rat neocortex. *J. Neurosci. Off. J. Soc. Neurosci.* *24*, 3289–3294.
- Derkach, V., Barria, A., and Soderling, T.R. (1999). Ca<sup>2+</sup>/calmodulin-kinase II enhances channel conductance of alpha-amino-3-hydroxy-5-methyl-4-isoxazolepropionate type glutamate receptors. *Proc. Natl. Acad. Sci. U. S. A.* *96*, 3269–3274.
- Devaraju, P., Sun, M.-Y., Myers, T.L., Lauderdale, K., and Fiocco, T.A. (2013). Astrocytic group I mGluR-dependent potentiation of astrocytic glutamate and potassium uptake. *J. Neurophysiol.* *109*, 2404–2414.
- Dichter M., and Spencer A. (1969). Penicillin-induced interictal discharges from the Cat hippocampus. I. Characteristics and topographical features. *J. Neurophysiol.* *32*, 649–662.
- Dotd, H.-U., and Zieglgänsberger, W. (1990). Visualizing unstained neurons in living brain slices by infrared DIC-videomicroscopy. *Brain Res.* *537*, 333–336.
- Donald O. Hebb (1949). *The Organization of Behavior: A Neuropsychological Theory* (Lawrence Erlbaum Associates Inc).
- Dong, Z., Bai, Y., Wu, X., Li, H., Gong, B., Howland, J.G., Huang, Y., He, W., Li, T., and Wang, Y.T. (2013). Hippocampal long-term depression mediates spatial reversal learning in the Morris water maze. *Neuropharmacology* *64*, 65–73.
- Dube, C., Chen, K., Eghbal-Ahmadi, M., Brunson, K., Soltesz, I., and Baram, T.Z. (2000). Prolonged Febrile Seizures in the Immature Rat Model Enhance Hippocampal Excitability Long Term. *Ann. Neurol.* *47*, 336–344.
- Dudek, F.E., Obenaus, A., and Tasker, J.G. (1990). Osmolality-induced changes in extracellular volume alter epileptiform bursts independent of chemical synapses in the rat: importance of non-synaptic mechanisms in hippocampal epileptogenesis. *Neurosci. Lett.* *120*, 267–270.

- During, M.J., and Spencer, D.D. (1993). Extracellular hippocampal glutamate and spontaneous seizure in the conscious human brain. *Lancet Lond. Engl.* *341*, 1607–1610.
- Eid, T., Thomas, M.J., Spencer, D.D., Rundén-Pran, E., Lai, J.C.K., Malthankar, G.V., Kim, J.H., Danbolt, N.C., Ottersen, O.P., and de Lanerolle, N.C. (2004). Loss of glutamine synthetase in the human epileptogenic hippocampus: possible mechanism for raised extracellular glutamate in mesial temporal lobe epilepsy. *Lancet Lond. Engl.* *363*, 28–37.
- Engel, J. (1996). Excitation and inhibition in epilepsy. *Can. J. Neurol. Sci. J. Can. Sci. Neurol.* *23*, 167–174.
- Englot, D.J., and Blumenfeld, H. (2009). Consciousness and epilepsy: why are complex-partial seizures complex? *Prog. Brain Res.* *177*, 147–170.
- Enoki, R., Hu, Y., Hamilton, D., and Fine, A. (2009). Expression of Long-Term Plasticity at Individual Synapses in Hippocampus Is Graded, Bidirectional, and Mainly Presynaptic: Optical Quantal Analysis. *Neuron* *62*, 242–253.
- Fellin, T., Gomez-Gonzalo, M., Gobbo, S., Carmignoto, G., and Haydon, P.G. (2006). Astrocytic Glutamate Is Not Necessary for the Generation of Epileptiform Neuronal Activity in Hippocampal Slices. *J. Neurosci.* *26*, 9312–9322.
- Feng, G., Mellor, R.H., Bernstein, M., Keller-Peck, C., Nguyen, Q.T., Wallace, M., Nerbonne, J.M., Lichtman, J.W., and Sanes, J.R. (2000). Imaging Neuronal Subsets in Transgenic Mice Expressing Multiple Spectral Variants of GFP. *Neuron* *28*, 41–51.
- Fischer, I., Alliod, C., Martinier, N., Newcombe, J., Brana, C., and Pouly, S. (2011). Sphingosine Kinase 1 and Sphingosine 1-Phosphate Receptor 3 Are Functionally Upregulated on Astrocytes under Pro-Inflammatory Conditions. *PLOS ONE* *6*, e23905.
- Fisher, R.S., Scharfman, H.E., and deCurtis, M. (2014). How Can We Identify Ictal and Interictal Abnormal Activity? *Adv. Exp. Med. Biol.* *813*, 3–23.
- Freneau, R.T., Kam, K., Qureshi, T., Johnson, J., Copenhagen, D.R., Storm-Mathisen, J., Chaudhry, F.A., Nicoll, R.A., and Edwards, R.H. (2004). Vesicular glutamate transporters 1 and 2 target to functionally distinct synaptic release sites. *Science* *304*, 1815–1819.
- French, J.A., Williamson, P.D., Thadani, V.M., Darcey, T.M., Mattson, R.H., Spencer, S.S., and Spencer, D.D. (1993). Characteristics of medial temporal lobe epilepsy: I. Results of history and physical examination. *Ann. Neurol.* *34*, 774–780.
- Freund, T. f., and Buzsáki, G. (1996). Interneurons of the hippocampus. *Hippocampus* *6*, 347–470.
- Fukunaga, K., Stoppini, L., Miyamoto, E., and Muller, D. (1993). Long-term potentiation is associated with an increased activity of Ca<sup>2+</sup>/calmodulin-dependent protein kinase II. *J. Biol. Chem.* *268*, 7863–7867.

- Fyhn, M., Molden, S., Witter, M.P., Moser, E.I., and Moser, M.-B. (2004). Spatial Representation in the Entorhinal Cortex. *Science* 305, 1258–1264.
- Genoud, C., Quairiaux, C., Steiner, P., Hirling, H., Welker, E., and Knott, G.W. (2006). Plasticity of Astrocytic Coverage and Glutamate Transporter Expression in Adult Mouse Cortex. *PLoS Biol.* 4.
- Gerfin-Moser, A., Grogg, F., Rietschin, L., Thompson, S.M., and Streit, P. (1995). Alterations in glutamate but not GABAA receptor subunit expression as a consequence of epileptiform activity in vitro. *Neuroscience* 67, 849–865.
- Ghasemi, M., and Schachter, S.C. (2011). The NMDA receptor complex as a therapeutic target in epilepsy: a review. *Epilepsy Behav.* 22, 617–640.
- Giaume, C., Taberner, A., and Medina, J.M. (1997). Metabolic trafficking through astrocytic gap junctions. *Glia* 21, 114–123.
- Giaume, C., Koulakoff, A., Roux, L., Holcman, D., and Rouach, N. (2010). Astroglial networks: a step further in neuroglial and gliovascular interactions. *Nat. Rev. Neurosci.* 11, 87–99.
- Gibbs, M.E., and Bowser, D.N. (2009). Astrocytes and Interneurons in Memory Processing in the Chick Hippocampus: Roles for G-Coupled Protein Receptors, GABA(B) and mGluR1. *Neurochem. Res.* 34, 1712–1720.
- Giovagnoli, A.R., and Avanzini, G. (1999). Learning and memory impairment in patients with temporal lobe epilepsy: relation to the presence, type, and location of brain lesion. *Epilepsia* 40, 904–911.
- Gloveli, T., Albrecht, D., and Heinemann, U. (1995). Properties of low Mg<sup>2+</sup> induced epileptiform activity in rat hippocampal and entorhinal cortex slices during adolescence. *Brain Res. Dev. Brain Res.* 87, 145–152.
- Goddard, G.V. (1967). Development of epileptic seizures through brain stimulation at low intensity. *Nature* 214, 1020–1021.
- Gomez-Gonzalo, M., Losi, G., Brondi, M., Uva, L., Sulis-Sato, S., De Curtis, M., Ratto, G.M., and Carmignoto, G. (2011). Ictal but not interictal epileptic discharges activate astrocyte endfeet and elicit cerebral arteriole responses. *Front. Cell. Neurosci.* 5, 8.
- Gosejacob, D., Dublin, P., Bedner, P., Hüttmann, K., Zhang, J., Tress, O., Willecke, K., Pfrieger, F., Steinhäuser, C., and Theis, M. (2011). Role of astroglial connexin30 in hippocampal gap junction coupling. *Glia* 59, 511–519.
- Gregory, R.P., Oates, T., and Merry, R.T. (1993). Electroencephalogram epileptiform abnormalities in candidates for aircrew training. *Electroencephalogr. Clin. Neurophysiol.* 86, 75–77.
- Griemsmann, S., Höft, S.P., Bedner, P., Zhang, J., Staden, E. von, Beinhauer, A., Degen, J., Dublin, P., Cope, D.W., Richter, N., et al. (2015). Characterization of Panglial Gap Junction

Networks in the Thalamus, Neocortex, and Hippocampus Reveals a Unique Population of Glial Cells. *Cereb. Cortex* 25, 3420–3433.

Gutnick, M.J., Connors, B.W., and Ransom, B.R. (1981). Dye-coupling between glial cells in the guinea pig neocortical slice. *Brain Res.* 213, 486–492.

Haber, M., Zhou, L., and Murai, K.K. (2006). Cooperative Astrocyte and Dendritic Spine Dynamics at Hippocampal Excitatory Synapses. *J. Neurosci.* 26, 8881–8891.

Hablitz, J.J. (1984). PicROTOXIN-induced epileptiform activity in hippocampus: role of endogenous versus synaptic factors. *J. Neurophysiol.* 51, 1011–1027.

Hafting, T., Fyhn, M., Molden, S., Moser, M.-B., and Moser, E.I. (2005). Microstructure of a spatial map in the entorhinal cortex. *Nature* 436, 801–806.

Halassa, M.M., and Haydon, P.G. (2010). Integrated Brain Circuits: Astrocytic Networks Modulate Neuronal Activity and Behavior. *Annu. Rev. Physiol.* 72, 335–355.

Halassa, M.M., Fellin, T., Takano, H., Dong, J.-H., and Haydon, P.G. (2007). Synaptic islands defined by the territory of a single astrocyte. *J. Neurosci. Off. J. Soc. Neurosci.* 27, 6473–6477.

Hauser, W.A., Annegers, J.F., and Kurland, L.T. (1993). Incidence of Epilepsy and Unprovoked Seizures in Rochester, Minnesota: 1935–1984. *Epilepsia* 34, 453–458.

Heinemann, U., and Dieter Lux, H. (1977). Ceiling of stimulus induced rises in extracellular potassium concentration in the cerebral cortex of cat. *Brain Res.* 120, 231–249.

Heller, J.P., and Rusakov, D.A. (2015). Morphological plasticity of astroglia: Understanding synaptic microenvironment. *Glia* 63, 2133–2151.

Helmstädter, C. (2002). Effects of chronic epilepsy on declarative memory systems. B.-P. in *B. Research*, ed. (Elsevier), pp. 439–453.

Henneberger, C., and Rusakov, D.A. (2012). Monitoring local synaptic activity with astrocytic patch pipettes. *Nat. Protoc.* 7, 2171–2179.

Henneberger, C., Medvedev, N., Stuart, M. G., and Rusakov, D. A. (2008). LTP induction changes the morphology of astrocytes in the CA1 region of the hippocampus in vitro. (Washington DC), p.

Henneberger, C., Papouin, T., Oliet, S.H.R., and Rusakov, D.A. (2010). Long-term potentiation depends on release of d-serine from astrocytes. *Nature* 463, 232–236.

Henneberger, C., Bard, L., and Rusakov, D.A. (2012). d-Serine: A key to synaptic plasticity? *Int. J. Biochem. Cell Biol.* 44, 587–590.

Heuser, K., Eid, T., Lauritzen, F., Thoren, A.E., Vindedal, G.F., Taubøll, E., Gjerstad, L., Spencer, D.D., Ottersen, O.P., Nagelhus, E.A., et al. (2012). Loss of perivascular Kir4.1

potassium channels in the sclerotic hippocampus of patients with mesial temporal lobe epilepsy. *J. Neuropathol. Exp. Neurol.* *71*, 814–825.

Hinterkeuser, S., Schröder, W., Hager, G., Seifert, G., Blümcke, I., Elger, C.E., Schramm, J., and Steinhäuser, C. (2000). Astrocytes in the hippocampus of patients with temporal lobe epilepsy display changes in potassium conductances. *Eur. J. Neurosci.* *12*, 2087–2096.

Hochman D. W. (2009). Changes in the extracellular space as a modulator of excitability and epileptogenicity. In *Basic Epilepsy Research*, (Oxford: Academic Press), pp. 946–953.

Höltje, M., Hoffmann, A., Hofmann, F., Mucke, C., Grosse, G., Van Rooijen, N., Kettenmann, H., Just, I., and Ahnert-Hilger, G. (2005). Role of Rho GTPase in astrocyte morphology and migratory response during in vitro wound healing. *J. Neurochem.* *95*, 1237–1248.

Hsu, M.S., Seldin, M., Lee, D.J., Seifert, G., Steinhäuser, C., and Binder, D.K. (2011). Lamina-specific and developmental expression of aquaporin-4 in the mouse hippocampus. *Neuroscience* *178*, 21–32.

Hubbard, J.A., Hsu, M.S., Seldin, M.M., and Binder, D.K. (2015). Expression of the Astrocyte Water Channel Aquaporin-4 in the Mouse Brain. *ASN NEURO* *7*.

İnan, S.Y., and Büyükafşar, K. (2008). Antiepileptic effects of two Rho-kinase inhibitors, Y-27632 and fasudil, in mice. *Br. J. Pharmacol.* *155*, 44–51.

Ishizuka, N., Cowan, W.M., and Amaral, D.G. (1995). A quantitative analysis of the dendritic organization of pyramidal cells in the rat hippocampus. *J. Comp. Neurol.* *362*, 17–45.

Javidan, M., and Javidan, M. (2012). Electroencephalography in Mesial Temporal Lobe Epilepsy: A Review, *Electroencephalography in Mesial Temporal Lobe Epilepsy: A Review. Epilepsy Res. Treat.* *2012*, *2012*, e637430.

Jefferys, J.G.R. (1999). Hippocampal sclerosis and temporal lobe epilepsy: cause or consequence? *Brain* *122*, 1007–1008.

John, G.R., Chen, L., Riviaccio, M.A., Melendez-Vasquez, C.V., Hartley, A., and Brosnan, C.F. (2004). Interleukin-1beta induces a reactive astroglial phenotype via deactivation of the Rho GTPase-Rock axis. *J. Neurosci. Off. J. Soc. Neurosci.* *24*, 2837–2845.

Johnson, J.W., and Ascher, P. (1987). Glycine potentiates the NMDA response in cultured mouse brain neurons. *Publ. Online* 05 Febr. 1987 Doi101038325529a0 *325*, 529–531.

Kalman, D., Gomperts, S.N., Hardy, S., Kitamura, M., and Bishop, J.M. (1999). Ras Family GTPases Control Growth of Astrocyte Processes. *Mol. Biol. Cell* *10*, 1665–1683.

Kandel, E., and Schwartz, J. (2013). *Principles of Neural Science, Fifth Edition* (McGraw Hill Professional).

- Karus, C., Mondragão, M.A., Ziemens, D., and Rose, C.R. (2015). Astrocytes restrict discharge duration and neuronal sodium loads during recurrent network activity. *Glia* 63, 936–957.
- Katzman, R. (1976). Maintenance of a constant brain extracellular potassium. *Fed. Proc.* 35, 1244–1247.
- Kentros, C. (2006). Hippocampal place cells: the “where” of episodic memory? *Hippocampus* 16, 743–754.
- Kettenmann, H., and Ransom, B.R. (2013). *Neuroglia* (OUP USA).
- Khalilov, I., Khazipov, R., Esclapez, M., and Ben-Ari, Y. (1997). Bicuculline induces ictal seizures in the intact hippocampus recorded in vitro. *Eur. J. Pharmacol.* 319, R5-6.
- Kharatishvili, I., and Pitkänen, A. (2010). Association of the severity of cortical damage with the occurrence of spontaneous seizures and hyperexcitability in an animal model of posttraumatic epilepsy. *Epilepsy Res.* 90, 47–59.
- King, D., and Spencer, S. (1995). Invasive electroencephalography in mesial temporal lobe epilepsy. *J. Clin. Neurophysiol. Off. Publ. Am. Electroencephalogr. Soc.* 12, 32–45.
- Kofuji, P., and Newman, E.A. (2004). Potassium Buffering in the Central Nervous System. *Neuroscience* 129, 1045–1056.
- Kohara, K., Pignatelli, M., Rivest, A.J., Jung, H.-Y., Kitamura, T., Suh, J., Frank, D., Kajikawa, K., Mise, N., Obata, Y., et al. (2014). Cell type-specific genetic and optogenetic tools reveal hippocampal CA2 circuits. *Nat. Neurosci.* 17, 269–279.
- Köhling, R., Vreugdenhil, M., Bracci, E., and Jefferys, J.G.R. (2000). Ictal Epileptiform Activity Is Facilitated by Hippocampal GABAA Receptor-Mediated Oscillations. *J. Neurosci.* 20, 6820–6829.
- Kourdougli, N., Varpula, S., Chazal, G., and Rivera, C. (2015). Detrimental effect of post Status Epilepticus treatment with ROCK inhibitor Y-27632 in a pilocarpine model of temporal lobe epilepsy. *Front. Cell. Neurosci.* 9, 413.
- Kraus, J.E., Yeh, G.C., Bonhaus, D.W., Nadler, J.V., and McNamara, J.O. (1994). Kindling induces the long-lasting expression of a novel population of NMDA receptors in hippocampal region CA3. *J. Neurosci.* 14, 4196–4205.
- Kuffler, S.W., Nicholls, J.G., and Orkand, R.K. (1966). Physiological properties of glial cells in the central nervous system of amphibia. *J. Neurophysiol.* 29, 768–787.
- Kullmann, D.M., Erdemli, G., and Asztély, F. (1996). LTP of AMPA and NMDA receptor-mediated signals: evidence for presynaptic expression and extrasynaptic glutamate spill-over. *Neuron* 17, 461–474.

- Kwon, H.-B., and Sabatini, B.L. (2011). Glutamate induces de novo growth of functional spines in developing cortex. *Nature* 474, 100–104.
- Langer, J., and Rose, C.R. (2009). Synaptically induced sodium signals in hippocampal astrocytes in situ. *J. Physiol.* 587, 5859–5877.
- Lansford, R., Bearman, G., and Fraser, S.E. (2001). Resolution of multiple green fluorescent protein color variants and dyes using two-photon microscopy and imaging spectroscopy. *J. Biomed. Opt.* 6, 311–318.
- Larsen, B.R., Assentoft, M., Cotrina, M.L., Hua, S.Z., Nedergaard, M., Kaila, K., Voipio, J., and MacAulay, N. (2014). Contributions of the Na<sup>+</sup>/K<sup>+</sup>-ATPase, NKCC1, and Kir4.1 to hippocampal K<sup>+</sup> clearance and volume responses. *Glia* 62, 608–622.
- Lasoń, W., Turchan, J., Przewłocki, R., Machelska, H., Łabuz, D., and Przewłocka, B. (1997). Effects of pilocarpine and kainate-induced seizures on N-methyl-d-aspartate receptor gene expression in the rat hippocampus. *Neuroscience* 78, 997–1004.
- Lau, C.G., and Zukin, R.S. (2007). NMDA receptor trafficking in synaptic plasticity and neuropsychiatric disorders. *Nat. Rev. Neurosci.* 8, 413–426.
- Leclercq, K., and Kaminski, R.M. (2015). Genetic background of mice strongly influences treatment resistance in the 6 Hz seizure model. *Epilepsia* 56, 310–318.
- Lee, H.S., Ghetti, A., Pinto-Duarte, A., Wang, X., Dziewczapolski, G., Galimi, F., Huitron-Resendiz, S., Piña-Crespo, J.C., Roberts, A.J., Verma, I.M., et al. (2014). Astrocytes contribute to gamma oscillations and recognition memory. *Proc. Natl. Acad. Sci.* 111, E3343–E3352.
- Lehre, K.P., and Danbolt, N.C. (1998). The Number of Glutamate Transporter Subtype Molecules at Glutamatergic Synapses: Chemical and Stereological Quantification in Young Adult Rat Brain. *J. Neurosci.* 18, 8751–8757.
- Lehre, K.P., and Rusakov, D.A. (2002). Asymmetry of glia near central synapses favors presynaptically directed glutamate escape. *Biophys. J.* 83, 125–134.
- Lein, E.S., Callaway, E.M., Albright, T.D., and Gage, F.H. (2005). Redefining the boundaries of the hippocampal CA2 subfield in the mouse using gene expression and 3-dimensional reconstruction. *J. Comp. Neurol.* 485, 1–10.
- Levy, L.M., Warr, O., and Attwell, D. (1998). Stoichiometry of the Glial Glutamate Transporter GLT-1 Expressed Inducibly in a Chinese Hamster Ovary Cell Line Selected for Low Endogenous Na<sup>+</sup>-Dependent Glutamate Uptake. *J. Neurosci.* 18, 9620–9628.
- Logothetis, J., Harner, R., Morrell, F., and Torres, F. (1959). The role of estrogens in catamenial exacerbation of epilepsy. *Neurology* 9, 352–352.
- Lorente de Nó (1934). Studies on the structure of the cerebral cortex. II. Continuation of the study of the ammonic system. *J Psychol Neurol* 113–177.

- Losi, G., Cammarota, M., and Carmignoto, G. (2012). The Role of Astroglia in the Epileptic Brain. *Front. Pharmacol.* *3*.
- Lothman, E.W., and Somjen, G.G. (1975). Extracellular potassium activity, intracellular and extracellular potential responses in the spinal cord. *J. Physiol.* *252*, 115–136.
- Lüscher, C., and Malenka, R.C. (2012). NMDA Receptor-Dependent Long-Term Potentiation and Long-Term Depression (LTP/LTD). *Cold Spring Harb. Perspect. Biol.* *4*.
- Maccaferri, G., and Lacaille, J.-C. (2003). Interneuron Diversity series: Hippocampal interneuron classifications--making things as simple as possible, not simpler. *Trends Neurosci.* *26*, 564–571.
- Malarkey, E.B., and Parpura, V. (2008). Mechanisms of glutamate release from astrocytes. *Neurochem. Int.* *52*, 142–154.
- Malenka, R.C., and Bear, M.F. (2004). LTP and LTD: an embarrassment of riches. *Neuron* *44*, 5–21.
- Malinow, R., and Malenka, R.C. (2002). Ampa Receptor Trafficking and Synaptic Plasticity. *Annu. Rev. Neurosci.* *25*, 103–126.
- Marcus EM, Watson C, and Goldman PL (1966). Effects of steroids on cerebral electrical activity: Epileptogenic effects of conjugated estrogens and related compounds in the cat and rabbit. *Arch. Neurol.* *15*, 521–532.
- Marsan, C.A., and Zivin, L.S. (1970). Factors related to the occurrence of typical paroxysmal abnormalities in the EEG records of epileptic patients. *Epilepsia* *11*, 361–381.
- Martinez-Hernandez, A., Bell, K.P., and Norenberg, M.D. (1977). Glutamine synthetase: glial localization in brain. *Science* *195*, 1356–1358.
- Marvin, J.S., Borghuis, B.G., Tian, L., Cichon, J., Harnett, M.T., Akerboom, J., Gordus, A., Renninger, S.L., Chen, T.-W., Bargmann, C.I., et al. (2013). An optimized fluorescent probe for visualizing glutamate neurotransmission. *Nat. Methods* *10*, 162–170.
- Mayer, M.L., Westbrook, G.L., and Guthrie, P.B. (1984). Voltage-dependent block by Mg<sup>2+</sup> of NMDA responses in spinal cord neurones. *Nature* *309*, 261–263.
- McHugh, J.C., and Delanty, N. (2008). Chapter 2 Epidemiology and Classification of Epilepsy: Gender Comparisons. *B.-I.R. of Neurobiology*, ed. (Academic Press), pp. 11–26.
- McKenna, M.C. (2007). The glutamate-glutamine cycle is not stoichiometric: Fates of glutamate in brain. *J. Neurosci. Res.* *85*, 3347–3358.
- McKhann II, G.M., Wenzel, H.J., Robbins, C.A., Sosunov, A.A., and Schwartzkroin, P.A. (2003). Mouse strain differences in kainic acid sensitivity, seizure behavior, mortality, and hippocampal pathology. *Neuroscience* *122*, 551–561.

- McNamara, J.O. (1984). Kindling: An animal model of complex partial epilepsy. *Ann. Neurol.* *16*, S72–S76.
- Medvedev, N., Popov, V., Henneberger, C., Kraev, I., Rusakov, D.A., and Stewart, M.G. (2014). Glia selectively approach synapses on thin dendritic spines. *Philos. Trans. R. Soc. Lond. B Biol. Sci.* *369*, 20140047.
- Meldrum, B.S. (1994). The role of glutamate in epilepsy and other CNS disorders. *Neurology* *44*, S14-23.
- Meyer, A., and Beck, E. (1955). The hippocampal formation in temporal lobe epilepsy. *Proc. R. Soc. Med.* *48*, 457–462.
- Meyvis, T.K.L., Smedt, S.C.D., Oostveldt, P.V., and Demeester, J. (1999). Fluorescence Recovery After Photobleaching: A Versatile Tool for Mobility and Interaction Measurements in Pharmaceutical Research. *Pharm. Res.* *16*, 1153–1162.
- Minelli, A., DeBiasi, S., Brecha, N.C., Zuccarello, L.V., and Conti, F. (1996). GAT-3, a High-Affinity GABA Plasma Membrane Transporter, Is Localized to Astrocytic Processes, and It Is Not Confined to the Vicinity of GABAergic Synapses in the Cerebral Cortex. *J. Neurosci.* *16*, 6255–6264.
- Mody, I., Lambert, J.D., and Heinemann, U. (1987). Low extracellular magnesium induces epileptiform activity and spreading depression in rat hippocampal slices. *J. Neurophysiol.* *57*, 869–888.
- Moody Jr., W.J., Futamachi, K.J., and Prince, D.A. (1974). Extracellular potassium activity during epileptogenesis. *Exp. Neurol.* *42*, 248–263.
- Moraga-Amaro, R., Jerez-Baraona, J.M., Simon, F., and Stehberg, J. (2014). Role of astrocytes in memory and psychiatric disorders. *J. Physiol. Paris* *108*, 240–251.
- Morris, R. (1984). Developments of a water-maze procedure for studying spatial learning in the rat. *J. Neurosci. Methods* *11*, 47–60.
- Morris, R.G.M., Garrud, P., Rawlins, J.N.P., and O’Keefe, J. (1982). Place navigation impaired in rats with hippocampal lesions. *Nature* *297*, 681–683.
- Mothet, J.-P., Parent, A.T., Wolosker, H., Brady, R.O., Linden, D.J., Ferris, C.D., Rogawski, M.A., and Snyder, S.H. (2000). d-Serine is an endogenous ligand for the glycine site of the N-methyl-d-aspartate receptor. *Proc. Natl. Acad. Sci. U. S. A.* *97*, 4926–4931.
- Mu, Y., and Gage, F.H. (2011). Adult hippocampal neurogenesis and its role in Alzheimer’s disease. *Mol. Neurodegener.* *6*, 85.
- Mulkey, R.M., and Malenka, R.C. (1992). Mechanisms underlying induction of homosynaptic long-term depression in area CA1 of the hippocampus. *Neuron* *9*, 967–975.

- Murphy-Royal, C., Dupuis, J.P., Varela, J.A., Panatier, A., Pinson, B., Baufreton, J., Groc, L., and Oliet, S.H.R. (2015). Surface diffusion of astrocytic glutamate transporters shapes synaptic transmission. *Nat. Neurosci. advance online publication*.
- Nabavi, S., Fox, R., Proulx, C.D., Lin, J.Y., Tsien, R.Y., and Malinow, R. (2014). Engineering a memory with LTD and LTP. *Nature* *511*, 348–352.
- Nagelhus, E.A., and Ottersen, O.P. (2013). Physiological Roles of Aquaporin-4 in Brain. *Physiol. Rev.* *93*, 1543–1562.
- Nagy, J.I., and Dermietzel, R. (2000). Gap junctions and connexins in the mammalian central nervous system. B.-A. in M. and C. Biology, ed. (Elsevier), pp. 323–396.
- Nagy, J.I., Patel, D., Ochalski, P.A., and Stelmack, G.L. (1999). Connexin30 in rodent, cat and human brain: selective expression in gray matter astrocytes, co-localization with connexin43 at gap junctions and late developmental appearance. *Neuroscience* *88*, 447–468.
- Nash, M.S., Schell, M.J., Atkinson, P.J., Johnston, N.R., Nahorski, S.R., and Challiss, R.A.J. (2002). Determinants of Metabotropic Glutamate Receptor-5-mediated Ca<sup>2+</sup> and Inositol 1,4,5-Trisphosphate Oscillation Frequency. Receptor density versus agonist concentration. *J. Biol. Chem.* *277*, 35947–35960.
- Naskar, K., and Stern, J.E. (2014). A functional coupling between extrasynaptic NMDA receptors and A-type K<sup>+</sup> channels under astrocyte control regulates hypothalamic neurosecretory neuronal activity. *J. Physiol.* *592*, 2813–2827.
- Navarrete, M., Perea, G., Fernandez de Sevilla, D., Gómez-Gonzalo, M., Núñez, A., Martín, E.D., and Araque, A. (2012). Astrocytes mediate in vivo cholinergic-induced synaptic plasticity. *PLoS Biol.* *10*, e1001259.
- Navarrete, M., Perea, G., Maglio, L., Pastor, J., Sola, R.G. de, and Araque, A. (2013). Astrocyte Calcium Signal and Gliotransmission in Human Brain Tissue. *Cereb. Cortex* *23*, 1240–1246.
- Nave, K.-A., and Ehrenreich, H. (2014). Myelination and oligodendrocyte functions in psychiatric diseases. *JAMA Psychiatry* *71*, 582–584.
- Neher, E., and Sakmann, B. (1976). Single-channel currents recorded from membrane of denervated frog muscle fibres. *Nature* *260*, 799–802.
- Nicholson, C., and Phillips, J.M. (1981). Ion diffusion modified by tortuosity and volume fraction in the extracellular microenvironment of the rat cerebellum. *J. Physiol.* *321*, 225–257.
- Nixdorf-Bergweiler, B.E., Albrecht, D., and Heinemann, U. (1994). Developmental changes in the number, size, and orientation of GFAP-positive cells in the CA1 region of rat hippocampus. *Glia* *12*, 180–195.

- Nolte, C., Matyash, M., Pivneva, T., Schipke, C.G., Ohlemeyer, C., Hanisch, U.-K., Kirchhoff, F., and Kettenmann, H. (2001). GFAP promoter-controlled EGFP-expressing transgenic mice: A tool to visualize astrocytes and astrogliosis in living brain tissue. *Glia* 33, 72–86.
- Nowak, L., Bregestovski, P., Ascher, P., Herbet, A., and Prochiantz, A. (1984). Magnesium gates glutamate-activated channels in mouse central neurones. *Nature* 307, 462–465.
- Numberger, M., and Draguhn, A. (1996). Patch-Clamp-Technik (Spektrum Akademischer Verlag).
- Oberheim, N.A., Wang, X., Goldman, S., and Nedergaard, M. (2006). Astrocytic complexity distinguishes the human brain. *Trends Neurosci.* 29, 547–553.
- Oberheim, N.A., Tian, G.-F., Han, X., Peng, W., Takano, T., Ransom, B., and Nedergaard, M. (2008). Loss of Astrocytic Domain Organization in the Epileptic Brain. *J. Neurosci.* 28, 3264–3276.
- Oberheim, N.A., Takano, T., Han, X., He, W., Lin, J.H.C., Wang, F., Xu, Q., Wyatt, J.D., Pilcher, W., Ojemann, J.G., et al. (2009). Uniquely hominid features of adult human astrocytes. *J. Neurosci. Off. J. Soc. Neurosci.* 29, 3276–3287.
- Oberheim, N.A., Goldman, S.A., and Nedergaard, M. (2012). Heterogeneity of Astrocytic Form and Function. *Methods Mol. Biol. Clifton NJ* 814, 23–45.
- Ogata, K., and Kosaka, T. (2002). Structural and quantitative analysis of astrocytes in the mouse hippocampus. *Neuroscience* 113, 221–233.
- O’Keefe, J. (1976). Place units in the hippocampus of the freely moving rat. *Exp. Neurol.* 51, 78–109.
- O’Keefe, J. (1979). A review of the hippocampal place cells. *Prog. Neurobiol.* 13, 419–439.
- O’Keefe, J., and Nadel, L. (1978). *The Hippocampus as a Cognitive Map* (Oxford University Press).
- Oliet, S.H.R., Piet, R., and Poulain, D.A. (2001). Control of Glutamate Clearance and Synaptic Efficacy by Glial Coverage of Neurons. *Science* 292, 923–926.
- Olsen, M.L., and Sontheimer, H. (2008). Functional implications for Kir4.1 channels in glial biology: from K<sup>+</sup> buffering to cell differentiation. *J. Neurochem.* 107, 589–601.
- Orkand, R.K. (1986). Introductory Remarks: Glial-Interstitial Fluid Exchange. *Ann. N. Y. Acad. Sci.* 481, 269–272.
- Orkand, R.K., Nicholls, J.G., and Kuffler, S.W. (1966). Effect of nerve impulses on the membrane potential of glial cells in the central nervous system of amphibia. *J. Neurophysiol.* 29, 788–806.

- Ortinski, P.I., Dong, J., Mungenast, A., Yue, C., Takano, H., Watson, D.J., Haydon, P.G., and Coulter, D.A. (2010). Selective induction of astrocytic gliosis generates deficits in neuronal inhibition. *Nat. Neurosci.* *13*, 584–591.
- Osorio, I., Zaveri, H.P., Frei, M.G., and Arthurs, S. (2011). *Epilepsy: The Intersection of Neurosciences, Biology, Mathematics, Engineering, and Physics* (CRC Press).
- Ota, Y., Zanetti, A.T., Hallock, R.M., Ota, Y., Zanetti, A.T., and Hallock, R.M. (2013). The Role of Astrocytes in the Regulation of Synaptic Plasticity and Memory Formation. *Neural Plast. Neural Plast.* *2013*, *2013*, e185463.
- Ouyang, Y., Kantor, D., Harris, K.M., Schuman, E.M., and Kennedy, M.B. (1997). Visualization of the Distribution of Autophosphorylated Calcium/Calmodulin-Dependent Protein Kinase II after Tetanic Stimulation in the CA1 Area of the Hippocampus. *J. Neurosci.* *17*, 5416–5427.
- Pan, E., and Stringer, J.L. (1996). Influence of osmolality on seizure amplitude and propagation in the rat dentate gyrus. *Neurosci. Lett.* *207*, 9–12.
- Panatier, A., and Oliet, S.H.R. (2006). Neuron-glia interactions in the hypothalamus. *Neuron Glia Biol.* *2*, 51–58.
- Panatier, A., Theodosis, D.T., Mothet, J.-P., Touquet, B., Pollegioni, L., Poulain, D.A., and Oliet, S.H.R. (2006). Glia-derived D-serine controls NMDA receptor activity and synaptic memory. *Cell* *125*, 775–784.
- Pannasch, U., and Rouach, N. (2013). Emerging role for astroglial networks in information processing: from synapse to behavior. *Trends Neurosci.* *36*, 405–417.
- Pannasch, U., Freche, D., Dallérac, G., Ghézali, G., Escartin, C., Ezan, P., Cohen-Salmon, M., Benchenane, K., Abudara, V., Dufour, A., et al. (2014). Connexin 30 sets synaptic strength by controlling astroglial synapse invasion. *Nat. Neurosci.* *17*, 549–558.
- Parpura, V., Basarsky, T.A., Liu, F., Jeftinija, K., Jeftinija, S., and Haydon, P.G. (1994). Glutamate-mediated astrocyte-neuron signalling. *Nature* *369*, 744–747.
- Parri, H.R., Gould, T.M., and Crunelli, V. (2001). Spontaneous astrocytic Ca<sup>2+</sup> oscillations in situ drive NMDAR-mediated neuronal excitation. *Nat. Neurosci.* *4*, 803–812.
- Pasti, L., Volterra, A., Pozzan, T., and Carmignoto, G. (1997). Intracellular calcium oscillations in astrocytes: a highly plastic, bidirectional form of communication between neurons and astrocytes in situ. *J. Neurosci. Off. J. Soc. Neurosci.* *17*, 7817–7830.
- Pekny, M., and Pekna, M. (2014). Astrocyte Reactivity and Reactive Astroglia: Costs and Benefits. *Physiol. Rev.* *94*, 1077–1098.
- Pekny, M., Wilhelmsson, U., and Pekna, M. (2014). The dual role of astrocyte activation and reactive gliosis. *Neurosci. Lett.* *565*, 30–38.

- Perego, C., Vanoni, C., Bossi, M., Massari, S., Basudev, H., Longhi, R., and Pietrini, G. (2000). The GLT-1 and GLAST glutamate transporters are expressed on morphologically distinct astrocytes and regulated by neuronal activity in primary hippocampal cocultures. *J. Neurochem.* *75*, 1076–1084.
- Perez, E.L., Lauritzen, F., Wang, Y., Lee, T.-S.W., Kang, D., Zaveri, H.P., Chaudhry, F.A., Ottersen, O.P., Bergersen, L.H., and Eid, T. (2012). Evidence for astrocytes as a potential source of the glutamate excess in temporal lobe epilepsy. *Neurobiol. Dis.* *47*, 331–337.
- Perez, V., Bouschet, T., Fernandez, C., Bockaert, J., and Journot, L. (2005). Dynamic reorganization of the astrocyte actin cytoskeleton elicited by cAMP and PACAP: a role for phosphatidylinositol 3-kinase inhibition. *Eur. J. Neurosci.* *21*, 26–32.
- Perez-Alvarez, A., Navarrete, M., Covelo, A., Martin, E.D., and Araque, A. (2014a). Structural and Functional Plasticity of Astrocyte Processes and Dendritic Spine Interactions. *J. Neurosci.* *34*, 12738–12744.
- Perez-Alvarez, A., Navarrete, M., Covelo, A., Martin, E.D., and Araque, A. (2014b). Structural and functional plasticity of astrocyte processes and dendritic spine interactions. *J. Neurosci. Off. J. Soc. Neurosci.* *34*, 12738–12744.
- Peters A., Palay S.L., and Webster H. (1991). *The Fine Structure of the Nervous system: The Cells and Their Processes* (New York: Oxford University Press).
- Petzold, G.C., Albeanu, D.F., Sato, T.F., and Murthy, V.N. (2008). Coupling of neural activity to blood flow in olfactory glomeruli is mediated by astrocytic pathways. *Neuron* *58*, 897–910.
- Porter, J.T., and McCarthy, K.D. (1996). Hippocampal astrocytes in situ respond to glutamate released from synaptic terminals. *J. Neurosci. Off. J. Soc. Neurosci.* *16*, 5073–5081.
- Pyapali, G.K., Sik, A., Penttonen, M., Buzsaki, G., and Turner, D.A. (1998). Dendritic properties of hippocampal CA1 pyramidal neurons in the rat: intracellular staining in vivo and in vitro. *J. Comp. Neurol.* *391*, 335–352.
- Racchetti, G., D’Alessandro, R., and Meldolesi, J. (2012). Astrocyte Stellation, a Process Dependent on Rac1 Is Sustained by the Regulated Exocytosis of Enlargeosomes. *Glia* *60*, 465–475.
- Ramakers, G.J.A., and Moolenaar, W.H. (1998). Regulation of Astrocyte Morphology by RhoA and Lysophosphatidic Acid. *Exp. Cell Res.* *245*, 252–262.
- Ransom, C.B., and Sontheimer, H. (1995). Biophysical and pharmacological characterization of inwardly rectifying K<sup>+</sup> currents in rat spinal cord astrocytes. *J. Neurophysiol.* *73*, 333–346.

- Ransom, C.B., Ransom, B.R., and Sontheimer, H. (2000). Activity-dependent extracellular K<sup>+</sup> accumulation in rat optic nerve: the role of glial and axonal Na<sup>+</sup> pumps. *J. Physiol.* 522, 427–442.
- Rappold, P.M., and Tieu, K. (2010). Astrocytes and Therapeutics for Parkinson's Disease. *Neurother. J. Am. Soc. Exp. Neurother.* 7, 413–423.
- Reddy, D.S. (2009). The Role of Neurosteroids in the Pathophysiology and Treatment of Catamenial Epilepsy. *Epilepsy Res.* 85, 1–30.
- Riento, K., and Ridley, A.J. (2003). ROCKs: multifunctional kinases in cell behaviour. *Nat. Rev. Mol. Cell Biol.* 4, 446–456.
- Robel, S., and Sontheimer, H. (2016). Glia as drivers of abnormal neuronal activity. *Nat. Neurosci.* 19, 28–33.
- Roitbak, T., and Syková, E. (1999). Diffusion barriers evoked in the rat cortex by reactive astrogliosis. *Glia* 28, 40–48.
- Rose, C.R., and Ransom, B.R. (1997). Gap junctions equalize intracellular Na<sup>+</sup> concentration in astrocytes. *Glia* 20, 299–307.
- Rosso, L., Pierson, P.M., Golfier, C., Peteri-Brunbäck, B., Deroanne, C., Van Obberghen-Schilling, E., and Mienville, J.-M. (2007). Pituicyte stellation is prevented by RhoA- or Cdc42-dependent actin polymerization. *Cell. Mol. Neurobiol.* 27, 791–804.
- Rouach, N., Koulakoff, A., Abudara, V., Willecke, K., and Giaume, C. (2008). Astroglial metabolic networks sustain hippocampal synaptic transmission. *Science* 322, 1551–1555.
- Ryan, L., Cox, C., Hayes, S.M., and Nadel, L. (2008). Hippocampal Activation during Episodic and Semantic Memory Retrieval: Comparing Category Production and Category Cued Recall. *Neuropsychologia* 46, 2109–2121.
- Salhia, B., Rutten, F., Nakada, M., Beaudry, C., Berens, M., Kwan, A., and Rutka, J.T. (2005). Inhibition of Rho-Kinase Affects Astrocytoma Morphology, Motility, and Invasion through Activation of Rac1. *Cancer Res.* 65, 8792–8800.
- Sander, J.W., and Shorvon, S.D. (1996). Epidemiology of the epilepsies. *J. Neurol. Neurosurg. Psychiatry* 61, 433–443.
- Satoh, J., Tabunoki, H., Yamamura, T., Arima, K., and Konno, H. (2007). Human astrocytes express aquaporin-1 and aquaporin-4 in vitro and in vivo. *Neuropathol. Off. J. Jpn. Soc. Neuropathol.* 27, 245–256.
- Savchenko, V.L., Nikonenko, I.R., Skibo, G.G., and McKanna, J.A. (1997). Distribution of microglia and astrocytes in different regions of the normal adult rat brain. *Neurophysiology* 29, 343–351.

- Scemes, E., and Spray, D.C. (1998). Increased intercellular communication in mouse astrocytes exposed to hyposmotic shocks. *Glia* 24, 74–84.
- Schauwecker, P.E. (2011). The relevance of individual genetic background and its role in animal models of epilepsy. *Epilepsy Res.* 97, 1–11.
- Schiller, J., Schiller, Y., and Clapham, D.E. (1998). NMDA receptors amplify calcium influx into dendritic spines during associative pre- and postsynaptic activation. *Nat. Neurosci.* 1, 114–118.
- Schindelin, J., Rueden, C.T., Hiner, M.C., and Eliceiri, K.W. (2015). The ImageJ ecosystem: An open platform for biomedical image analysis. *Mol. Reprod. Dev.* 82, 518–529.
- Schmidt, D., and Löscher, W. (2005). Drug Resistance in Epilepsy: Putative Neurobiologic and Clinical Mechanisms. *Epilepsia* 46, 858–877.
- Schousboe, A., Bak, L.K., and Waagepetersen, H.S. (2013). Astrocytic Control of Biosynthesis and Turnover of the Neurotransmitters Glutamate and GABA. *Front. Endocrinol.* 4, 102.
- Schwartzkroin, P.A. (1994). Role of the hippocampus in epilepsy. *Hippocampus* 4, 239–242.
- Schwartzkroin, P.A., and Prince, D.A. (1977). Penicillin-induced epileptiform activity in the hippocampal in vitro preparation. *Ann. Neurol.* 1, 463–469.
- Schwartzkroin, P.A., and Wyler, A.R. (1980). Mechanisms underlying epileptiform burst discharge. *Ann. Neurol.* 7, 95–107.
- Scolding, N.J. (1999). Glial Cells: Their Role in Behaviour. *Brain* 122, 1599–1600.
- Scoville, W.B., and Milner, B. (1957). LOSS OF RECENT MEMORY AFTER BILATERAL HIPPOCAMPAL LESIONS. *J. Neurol. Neurosurg. Psychiatry* 20, 11–21.
- Seeburg, P.H., Burnashev, N., Köhr, G., Kuner, T., Sprengel, R., and Monyer, H. (1995). The NMDA receptor channel: molecular design of a coincidence detector. *Recent Prog. Horm. Res.* 50, 19–34.
- Seifert, G., Hüttmann, K., Binder, D.K., Hartmann, C., Wyczynski, A., Neusch, C., and Steinhäuser, C. (2009). Analysis of Astroglial K<sup>+</sup> Channel Expression in the Developing Hippocampus Reveals a Predominant Role of the Kir4.1 Subunit. *J. Neurosci.* 29, 7474–7488.
- Seifert, G., Carmignoto, G., and Steinhäuser, C. (2010). Astrocyte dysfunction in epilepsy. *Brain Res. Rev.* 63, 212–221.
- Sharma, A.K., Reams, R.Y., Jordan, W.H., Miller, M.A., Thacker, H.L., and Snyder, P.W. (2007). Mesial Temporal Lobe Epilepsy: Pathogenesis, Induced Rodent Models and Lesions. *Toxicol. Pathol.* 35, 984–999.

- Shi, S.H., Hayashi, Y., Petralia, R.S., Zaman, S.H., Wenthold, R.J., Svoboda, K., and Malinow, R. (1999). Rapid spine delivery and redistribution of AMPA receptors after synaptic NMDA receptor activation. *Science* *284*, 1811–1816.
- Smith, S.J.M. (2005). EEG in the diagnosis, classification, and management of patients with epilepsy. *J. Neurol. Neurosurg. Psychiatry* *76*, ii2-ii7.
- Sofroniew, M.V., and Vinters, H.V. (2010). Astrocytes: biology and pathology. *Acta Neuropathol. (Berl.)* *119*, 7–35.
- Solan, J.L., and Lampe, P.D. (2009). Connexin 43 Phosphorylation – Structural Changes and Biological Effects. *Biochem. J.* *419*, 261–272.
- Solan, J.L., and Lampe, P.D. (2014). Specific Cx43 phosphorylation events regulate gap junction turnover in vivo. *FEBS Lett.* *588*, 1423–1429.
- Somjen, G.G. (1975). Electrophysiology of Neuroglia. *Annu. Rev. Physiol.* *37*, 163–190.
- Somjen, G.G. (1979). Extracellular Potassium in the Mammalian Central Nervous System. *Annu. Rev. Physiol.* *41*, 159–177.
- Song, Y., and Gunnarson, E. (2012). Potassium Dependent Regulation of Astrocyte Water Permeability Is Mediated by cAMP Signaling. *PLoS ONE* *7*.
- Špaček, J. (1985). Three-dimensional analysis of dendritic spines. *Anat. Embryol. (Berl.)* *171*, 245–252.
- Spiegel, E., and Wycis, H. (1945). Anticonvulsant effects of steroids. *J. Lab. Clin. Med.* *30*, 947–953.
- Steiner, M.R., Urso, J.R., Klein, J., and Steiner, S.M. (2002). Multiple astrocyte responses to lysophosphatidic acids. *Biochim. Biophys. Acta BBA - Mol. Cell Biol. Lipids* *1582*, 154–160.
- Steinhäuser, C., Seifert, G., and Bedner, P. (2012). Astrocyte dysfunction in temporal lobe epilepsy: K<sup>+</sup> channels and gap junction coupling. *Glia* *60*, 1192–1202.
- Stevens, E.R., Esguerra, M., Kim, P.M., Newman, E.A., Snyder, S.H., Zahs, K.R., and Miller, R.F. (2003). D-serine and serine racemase are present in the vertebrate retina and contribute to the physiological activation of NMDA receptors. *Proc. Natl. Acad. Sci.* *100*, 6789–6794.
- Straughan, D.W., Neal, M.J., Simmonds, M.A., Collins, G.G., and Hill, R.G. (1971). Evaluation of bicuculline as a GABA antagonist. *Nature* *233*, 352–354.
- Strohschein, S., Hüttmann, K., Gabriel, S., Binder, D.K., Heinemann, U., and Steinhäuser, C. (2011). Impact of aquaporin-4 channels on K<sup>+</sup> buffering and gap junction coupling in the hippocampus. *Glia* *59*, 973–980.

- Sweatt, J.D. (1999). Toward a Molecular Explanation for Long-Term Potentiation. *Learn. Mem.* *6*, 399–416.
- Takata, N., Mishima, T., Hisatsune, C., Nagai, T., Ebisui, E., Mikoshiba, K., and Hirase, H. (2011). Astrocyte Calcium Signaling Transforms Cholinergic Modulation to Cortical Plasticity In Vivo. *J. Neurosci.* *31*, 18155–18165.
- Taketo, M., Schroeder, A.C., Mobraaten, L.E., Gunning, K.B., Hanten, G., Fox, R.R., Roderick, T.H., Stewart, C.L., Lilly, F., and Hansen, C.T. (1991). FVB/N: an inbred mouse strain preferable for transgenic analyses. *Proc. Natl. Acad. Sci. U. S. A.* *88*, 2065–2069.
- Tanaka, K., Watase, K., Manabe, T., Yamada, K., Watanabe, M., Takahashi, K., Iwama, H., Nishikawa, T., Ichihara, N., Kikuchi, T., et al. (1997). Epilepsy and exacerbation of brain injury in mice lacking the glutamate transporter GLT-1. *Science* *276*, 1699–1702.
- Taubøll, E., Sveberg, L., and Svalheim, S. (2015). Interactions between hormones and epilepsy. *Seizure* *28*, 3–11.
- Thom, M. (2014). Review: Hippocampal sclerosis in epilepsy: a neuropathology review. *Neuropathol. Appl. Neurobiol.* *40*, 520–543.
- Tole, S., Christian, C., and Grove, E.A. (1997). Early specification and autonomous development of cortical fields in the mouse hippocampus. *Development* *124*, 4959–4970.
- Tönges, L., Koch, J.C., Bähr, M., and Lingor, P. (2011). ROCKing regeneration: Rho kinase inhibition as molecular target for neurorestoration. *Front. Mol. Neurosci.* *4*, 39.
- Traub, R.D., Jefferys, J.G., and Whittington, M.A. (1994). Enhanced NMDA conductance can account for epileptiform activity induced by low Mg<sup>2+</sup> in the rat hippocampal slice. *J. Physiol.* *478*, 379–393.
- Traynelis, S.F., and Dingledine, R. (1988). Potassium-induced spontaneous electrographic seizures in the rat hippocampal slice. *J. Neurophysiol.* *59*, 259–276.
- Tsuda, A., Ito, M., Kishi, K., Shiraishi, H., Tsuda, H., and Mori, C. (1994). Effect of penicillin on GABA-gated chloride ion influx. *Neurochem. Res.* *19*, 1–4.
- Tsurui, H., Nishimura, H., Hattori, S., Hirose, S., Okumura, K., and Shirai, T. (2000). Seven-color fluorescence imaging of tissue samples based on Fourier spectroscopy and singular value decomposition. *J. Histochem. Cytochem. Off. J. Histochem. Soc.* *48*, 653–662.
- Turski, W.A., Cavalheiro, E.A., Bortolotto, Z.A., Mello, L.M., Schwarz, M., and Turski, L. (1984). Seizures produced by pilocarpine in mice: a behavioral, electroencephalographic and morphological analysis. *Brain Res.* *321*, 237–253.
- Tuunanen, J., and Pitkänen, A. (2000). Do seizures cause neuronal damage in rat amygdala kindling? *Epilepsy Res.* *39*, 171–176.

- VanLandingham, K.E., Heinz, E.R., Cavazos, J.E., and Lewis, D.V. (1998). Magnetic resonance imaging evidence of hippocampal injury after prolonged focal febrile convulsions. *Ann. Neurol.* *43*, 413–426.
- Ventura, R., and Harris, K.M. (1999). Three-Dimensional Relationships between Hippocampal Synapses and Astrocytes. *J. Neurosci.* *19*, 6897–6906.
- Verkhatsky, A., Olabarria, M., Noristani, H.N., Yeh, C.-Y., and Rodriguez, J.J. (2010). Astrocytes in Alzheimer's disease. *Neurother. J. Am. Soc. Exp. Neurother.* *7*, 399–412.
- Virchow, R. (1858). *Die Cellularpathologie in ihrer Begründung auf physiologische und pathologische Gewebelehre: zwanzig Vorlesungen, gehalten während der Monate Februar, März und April 1858 in Pathologischen Institute zu Berlin* (Berlin: Verlag von August Hirschwald ...).
- Volterra, A., Liaudet, N., and Savtchouk, I. (2014). Astrocyte Ca<sup>2+</sup> signalling: an unexpected complexity. *Nat. Rev. Neurosci.* *15*, 327–335.
- Walker, M.C. (2015). Hippocampal Sclerosis: Causes and Prevention. *Semin. Neurol.* *35*, 193–200.
- Wallraff, A., Köhling, R., Heinemann, U., Theis, M., Willecke, K., and Steinhäuser, C. (2006). The Impact of Astrocytic Gap Junctional Coupling on Potassium Buffering in the Hippocampus. *J. Neurosci.* *26*, 5438–5447.
- Walz, W. (2000). Role of astrocytes in the clearance of excess extracellular potassium. *Neurochem. Int.* *36*, 291–300.
- Watson, G.B., and Lanthorn, T.H. (1990). NMDA Receptor antagonists attenuate a portion of the penicillin-induced epileptiform burst. *Brain Res. Bull.* *24*, 765–768.
- Weiker, A.E., and Johnson, H.C. (1945). Convulsive factor in commercial penicillin. *Arch. Surg.* *50*, 69–73.
- Wieser, H.-G., and ILAE Commission on Neurosurgery of Epilepsy (2004). ILAE Commission Report. Mesial temporal lobe epilepsy with hippocampal sclerosis. *Epilepsia* *45*, 695–714.
- Wilhelmsson, U., Li, L., Pekna, M., Berthold, C.-H., Blom, S., Eliasson, C., Renner, O., Bushong, E., Ellisman, M., Morgan, T.E., et al. (2004). Absence of Glial Fibrillary Acidic Protein and Vimentin Prevents Hypertrophy of Astrocytic Processes and Improves Post-Traumatic Regeneration. *J. Neurosci.* *24*, 5016–5021.
- Williamson, P.D., French, J.A., Thadani, V.M., Kim, J.H., Novelly, R.A., Spencer, S.S., Spencer, D.D., and Mattson, R.H. (1993). Characteristics of medial temporal lobe epilepsy: II. Interictal and ictal scalp electroencephalography, neuropsychological testing, neuroimaging, surgical results, and pathology. *Ann. Neurol.* *34*, 781–787.
- Witcher, M.R., Kirov, S.A., and Harris, K.M. (2007). Plasticity of perisynaptic astroglia during synaptogenesis in the mature rat hippocampus. *Glia* *55*, 13–23.

- Witcher, M.R., Park, Y.D., Lee, M.R., Sharma, S., Harris, K.M., and Kirov, S.A. (2010). Three-Dimensional Relationships Between Perisynaptic Astroglia and Human Hippocampal Synapses. *Glia* 58, 572–587.
- Wolosker, H., Blackshaw, S., and Snyder, S.H. (1999). Serine racemase: A glial enzyme synthesizing d-serine to regulate glutamate-N-methyl-d-aspartate neurotransmission. *Proc. Natl. Acad. Sci.* 96, 13409–13414.
- Yang, T., Zhou, D., and Stefan, H. (2010). Why mesial temporal lobe epilepsy with hippocampal sclerosis is progressive: Uncontrolled inflammation drives disease progression? *J. Neurol. Sci.* 296, 1–6.
- Zerangue, N., and Kavanaugh, M.P. (1996). Flux coupling in a neuronal glutamate transporter. *Nature* 383, 634–637.
- Zhang, J., Wang, H., Ye, C., Ge, W., Chen, Y., Jiang, Z., Wu, C., Poo, M., and Duan, S. (2003). ATP released by astrocytes mediates glutamatergic activity-dependent heterosynaptic suppression. *Neuron* 40, 971–982.
- Zheng, N., Jeyifous, O., Munro, C., Montgomery, J.M., and Green, W.N. (2015). Synaptic activity regulates AMPA receptor trafficking through different recycling pathways. *eLife* 4.
- Zimmermann, T. (2005). Spectral imaging and linear unmixing in light microscopy. *Adv. Biochem. Eng. Biotechnol.* 95, 245–265.

## List of Figures

<b>Figure 1</b>	Schematic of hippocampal slice and its intrinsic connections. ....	3
<b>Figure 2</b>	Interictal and ictal activity recorded using EEG recordings from a patient suffering from left MTLE. ....	8
<b>Figure 3</b>	Astrocyte structure in the mouse hippocampus. ....	12
<b>Figure 4</b>	Astrocytes are extensively coupled via gap junctions. ....	14
<b>Figure 5</b>	Calcium transients of hippocampal human astrocyte. ....	16
<b>Figure 6</b>	Electrophysiological setup. ....	31
<b>Figure 7</b>	Analysis of spike slope coupling. ....	34
<b>Figure 8</b>	Typical epileptiform discharge induced by bath application of penicillin. ....	35
<b>Figure 9</b>	Example traces of astrocyte field potentials recorded after paired pulse stimulation. ....	39
<b>Figure 10</b>	Examples of fluorescent astrocytes. ....	41
<b>Figure 11</b>	Definition of the astrocyte volume fraction. ....	41
<b>Figure 12</b>	Image processing for segmentation analysis. ....	43
<b>Figure 13</b>	Visualisation of astrocyte coupling in the CA1 stratum radiatum of the hippocampus. ....	44
<b>Figure 14</b>	FRAP experiments. ....	46
<b>Figure 15</b>	Emission spectra of GFP and YFP. ....	48
<b>Figure 16</b>	Schematic for calculation of possible slice volume changes. ....	49
<b>Figure 17</b>	Example of glutamate imaging using the glutamate sensor iGluSnFR. ....	50
<b>Figure 18</b>	Induction of epileptiform activity in the CA1 region of rat hippocampal slices. ....	54
<b>Figure 19</b>	Astrocyte volume fraction decreases upon induction of epileptiform activity in rat hippocampal slices. ....	56
<b>Figure 20</b>	Three-dimensional reconstruction of astrocyte fragments with adjacent synapses. ....	57
<b>Figure 21</b>	Astrocyte volume fractions of EGFP labelled astrocytes and subsequently filled with Texas red dextran. ....	59
<b>Figure 22</b>	Induction of epileptiform activity in mouse hippocampal slices. ....	60
<b>Figure 23</b>	Induction of epileptiform activity by bath application of 0 Mg <sup>2+</sup> and bicuculline. ....	62
<b>Figure 24</b>	Astrocyte volume fraction changes upon induction of epileptiform activity with penicillin. ....	64
<b>Figure 25</b>	Persistence of epileptiform activity and morphology changes. ....	68

---

<b>Figure 26</b> Astrocyte morphology changes induced by induction of epileptiform activity occur in the periphery in thin and medium-sized processes.....	69
<b>Figure 27</b> Segmentation analysis of astrocyte processes under control and penicillin conditions.....	71
<b>Figure 28</b> Neuronal morphology changes during induction of epileptiform activity. ....	73
<b>Figure 29</b> Slice volume under control and penicillin conditions.....	74
<b>Figure 30</b> Intracellular diffusion in astrocyte processes during control and epileptiform recordings. ....	75
<b>Figure 31</b> Astrocyte dye coupling in different brain regions. ....	77
<b>Figure 32</b> Quantification of astrocyte dye coupling in the CA1 stratum radiatum. ....	79
<b>Figure 33</b> Astrocyte dye coupling under control and epileptiform conditions. ....	81
<b>Figure 34</b> Effects of ROCK inhibitor Y27632 on astrocyte morphology during induction of epileptiform activity.....	83
<b>Figure 35</b> Impact of the ROCK inhibitor Y27632 on the neuronal synaptic transmission and excitability in the CA1 region of the hippocampus.....	85
<b>Figure 36</b> Effect of astrocyte specific intracellular application of Y27632 on astrocyte morphology changes and epileptiform activity.....	87
<b>Figure 37</b> Examination of possible signal cascade underlying the observed astrocyte morphological changes. ....	89
<b>Figure 38</b> Correlation between fraction of remaining discharges and strength of astrocyte volume fraction change. ....	91
<b>Figure 39</b> Effect of morphology responder and non-responder discharge frequency.....	92
<b>Figure 40</b> Evoked fEPSPs due to Schaffer collateral stimulation recorded in the CA1 region of the hippocampus. ....	94
<b>Figure 41</b> Synaptic transmission during and after epileptiform activity. ....	96
<b>Figure 42</b> Excitability of hippocampal CA1 pyramidal cells examined by analysing the spike-slope-coupling. ....	97
<b>Figure 43</b> Effect of previous epileptiform activity on synaptic plasticity. ....	99
<b>Figure 44</b> Impact of astrocyte morphology changes on K <sup>+</sup> buffering in the CA1 stratum radiatum.....	101
<b>Figure 45</b> Astrocyte fEPSPs in response to Schaffer collateral stimulation.....	102
<b>Figure 46</b> Glutamate accumulation after induction of astrocyte morphology changes. .	104
<b>Figure 47</b> Astrocyte volume fraction after kainate and sham injection. ....	113
<b>Figure 48</b> IPSC amplitudes during control and penicillin recordings.....	113
<b>Figure 49</b> Connexin expression levels and phosphorylation states after induction of epileptiform activity.....	125

**Figure 50** Recording of extracellular  $K^+$  transients using  $K^+$  sensitive microelectrodes. .. 131

**Figure 51** The role of rapid astrocyte morphology changes in epileptogenesis. .... 135

## List of Tables

<b>Table 1:</b> Chemicals.....	24
<b>Table 2:</b> Coordinates for stereotactic injections .....	29
<b>Table 3:</b> p-values of the volume fraction change of astrocyte segments dependent on their initial volume fraction. ....	69

## Abbreviations

[K <sup>+</sup> ] <sub>ex</sub>	extracellular K <sup>+</sup> concentration
AAV	adeno-associated virus
AC	adenylyl cyclase
ACSF	artificial cerebrospinal fluid
AD	analogue digital
afEPSP	astrocyte field excitatory postsynaptic potential
AMPA	α-amino-3-hydroxy-5-methyl-4-isoxazolepropionic acid
AQP4	aquaporin 4
ATP	adenosine triphosphat
CA	cornu ammonis
CaMKII	Ca <sup>2+</sup> /calmodulin-dependent protein kinase II
cAMP	cyclic adenosine monophosphate
CFP	cyan fluorescence protein
C <sub>m</sub>	membrane capacitance
Cx	connexin
Cλ	coupling length constant
D-AP5	DL-2-amino-5-phosphonovaleric acid
DG	dentate gyrus
DIC	differential interference contrast
DMSO	dimethylsulfoxid
EC	entorhinal cortex
ECS	extracellular space
EEG	electroencephalography
EGFP	enhanced green fluorescent protein
EM	electron microscopy
EPSP	excitatory postsynaptic potentials
fEPSP	field excitatory postsynaptic potential
FRAP	fluorescence recovery after photobleaching
FV	fibre volley
FVB	friend leukemia virus B
GABA	γ-aminobutyric acid
GDH	glutamate dehydrogenase
GFAP	glial fibrillary acidic protein
GLAST	glutamate aspartate transporter
GLT1	glutamate transporter 1

---

GPCR	G protein-coupled receptor
GS	glutamine synthetase
GTP	Guanosine-5'-triphosphate
HFS	high-frequent stimulation
HS	hippocampal sclerosis
i.p.	intraperitoneal
IC	intracellular solution
iGluSnFR	intensity-based glutamate sensing fluorescent reporter
IP3	inositol-1,4,5-trisphosphate
IPSC	inhibitory postsynaptic current
$K_d$	dissociation constant
KMS	Potassium methanesulfonate
LPA	lysophosphatidic acid
LTD	long-term depression
LTP	long-term potentiation
MAPK	mitogen-activated protein kinases
mGluR	metabotropic glutamate receptor
MTLE	mesial temporal lobe epilepsy
NA	numerical aperture
NBQX	2,3-dihydroxy-6-nitro-7-sulfamoyl-benzo[f]quinoxaline-2,3-dione
NMDA	N-methyl-D-aspartate
p	postnatal day
PAG	mitochondrial phosphate-activated glutaminase
PKC	protein kinase C
PMT	photomultiplier tubes
PPR	paired pulse ratio
ps	population spike
PTP	post-tetanic potentiation
$R_i$	input resistance
ROCK	Rho associated protein kinase
ROI	region of interest
$R_s$	access resistance
RT	room temperature
S1P	sphingosine-1-phosphate
SC	Schaffer collaterals
SE	status epilepticus
SR-B	sulforhodamine B

TCA	tricarboxylic acid
TLE	temporal lobe epilepsy
TMA <sup>+</sup>	tetramethylammonium
TR	Texas Red dextran 3kDa
TTX	Tetrodotoxin
VF	volume fraction
YFP	yellow fluorescent protein

## Acknowledgements

First of all, I would like to thank my supervisor Professor Dr. Christian Henneberger for giving me the opportunity to work in his laboratory on this interesting topic for my PhD thesis. I am very thankful for his support over the years, his great scientific guidance and for arousing my enthusiasm about astrocytes.

I would like to thank Professor Dr. Gerhard von der Emde for being the second referee of the examination committee and for his support since my first steps in neuroscience.

Additionally, I would like to thank Professor Dr. Michael Hofmann and Professor Dr. Klaus Mohr for being part of my thesis committee and for their time and efforts reviewing my thesis.

My sincere thanks go to Professor Dr. Steinhäuser for his support and fruitful scientific discussions.

I would like to thank PD Dr. Gerald Seifert for his help in animal breeding and interesting scientific discussions. Thomas Erdmann deserves a great thank for his organisatoy support. I also want to thank PD Dr. Ronald Jabs for interesting discussions on this project.

My special thanks go to Michel, Daniel, Kirsten, Björn and Anne for spending their time and their effort supporting this project. I also appreciate the days and retreats, where we had a great time together.

Of course, I would like to thank my colleagues Aline, Camille, Julia, Tushar, Magda, Delaware, Stefan, Steffi, Eva, Ines and Silke for creating a helpful and friendly atmosphere, good conversations, soccer betting, motivation and a wonderful time together.

Finally, my deepest thanks go to my parents and Christian for their mental support, their patience and constant encouragement throughout the years.

## Erklärung

Hiermit versichere ich, dass diese Dissertation von mir selbst und ohne unerlaubte Hilfe angefertigt worden ist. Es wurden keine anderen als die angegebenen Hilfsmittel verwendet. Ferner erkläre ich, dass die vorliegende Arbeit an keiner anderen Hochschule als Dissertation eingereicht worden ist.

Bonn, den 13.10.2016

Stefanie Anders